



**UNIVERSITÀ
DI PARMA**



A JOINT DOCTORAL THESIS

**University of Tunis El Manar
University of Parma**

Thesis Submitted for obtaining the Degree of Doctor in Geology

Laboratories: Sedimentary Basins and Petroleum Geology LR18ES07 (FST, UTM) & Hydrogeology (UP, Italy)

Hydro-geochemical modeling of Hajeb Layoun-Jelma basin (Central Tunisia)

Defended on 18/02/2022

By Miss Soumaia AOUITI

Front of the jury composed by

Mr. Fetheddine Melki	Professor	UTM, FST	Chairman
Mrs. Mounira Zammouri	Professor	UTM, FST	Supervisor
Mr. Fulvio Celico	Professor	UP, Italy	Supervisor
Mrs. Emma Petrella	Professor	UP, Italy	Reviewer
Mr. Mohamed fethi Ben Hamouda	Professor	CNSTN	Reviewer
Mr. Alessandro Chelli	Professor	UP, Italy	Examiner

Academic year 2021-2022

Résumé

Les eaux souterraines sont la principale source d'eau dans le monde entier et spécialement dans les régions arides et semi-arides. Le bassin de Hajeb Layoun-Jelma est la principale source d'approvisionnement en eau pour la région de Sidi Bouzid et de Sfax. Au cours des dernières décennies, la pollution est considérée comme un problème commun des eaux souterraines qui représente une menace grave et nuisible pour les ressources en eau.

Dans ce contexte, ce travail a eu lieu. Le bassin de Hajeb Layoun-Jelma est le site choisi dans ce travail afin de garantir son approvisionnement en eau qualitativement et quantitativement. Cette recherche vise à réaliser une vision géochimique des deux principaux aquifères, à mettre en œuvre un mode numérique de contrôle du bassin et à évaluer la vulnérabilité à la pollution de l'aquifère peu profond à l'aide de différents modèles ; modèle indexé et modèle de simulation.

Les principaux objectifs de l'étude hydrochimique des eaux souterraines sont de déterminer les origines de la chimie de l'eau et d'évaluer la qualité des eaux souterraines à des fins de boisson et d'irrigation.

Vingt huit échantillons d'eau ont été prélevés en 2017 (période humide), à la fois dans les aquifères peu profonds et profonds, et analysés pour différents paramètres physico-chimiques (température, pH, CE, salinité, Na^+ , Ca^{2+} , K^+ , Mg^{2+} , Cl^- , HCO_3^- , et SO_4^{2-}). La nappe phréatique montre une salinité élevée dans la plupart des échantillons d'eau (93% > 1 g.l⁻¹). L'aquifère profond a une salinité modérée (21% des échantillons dépassant 1 g.l⁻¹).

Les résultats montrent que la minéralisation de l'eau des deux aquifères est contrôlée par la dissolution des carbonates / gypse et l'évaporation de l'eau. L'évaluation de la qualité de l'eau potable montre que 100% et 57% d'eau extrêmement pauvre pour les échantillons peu profonds et profonds, respectivement, qui coïncident avec le type d'eau Na-Cl. L'évaluation de la qualité de l'eau pour les utilisations d'irrigation indique que les échantillons peu profonds montrent une qualité inférieure à celle des échantillons profonds et a révélé que la majorité des échantillons dans le bassin de Hajeb Layoun-Jelma ne sont pas appropriés pour les utilisations d'irrigation.

L'estimation du taux de recharge a été réalisée en utilisant la méthode multicritère. Les résultats montrent que les aquifères peu profonds et profonds reçoivent un taux de recharge moyen, à partir des précipitations, d'environ 31,5 mm / an (infiltration : 15%) et 34 mm / an (infiltration : 16,2%), respectivement.

Le modèle numérique a été développé en utilisant le code Modflow, sous le logiciel GMS. Le système de modèle hydrodynamique a permis d'estimer la distribution de la conductivité hydraulique. Il a également permis d'estimer l'effet du prélèvement sur l'évolution du bassin par deux scénarios de pompage (2019-2050) (Sc1 : taux de pompage constants, Sc2 : taux de pompage doublé) et un scénario climatique. Les modèles hydrodynamiques montrent la diminution continue de la piezométrie des deux nappes après 30 ans.

L'évaluation de la vulnérabilité des eaux souterraines de l'aquifère peu profond du bassin de Hajeb Layoun Jelma a été réalisée en utilisant à la fois des modèles intrinsèques et de simulation. Le modèle DRASTIC a été utilisé comme outil intrinsèque pour identifier les zones sensibles à la contamination de l'aquifère peu profond. Les cartes de vulnérabilité indiquent que les classes de vulnérabilité dominantes sont la classe basse (55%) suivie de la classe modérée (43%) dans le modèle de pesticides et les classes « faibles » (86%) dans le modèle standard. Seul 1% de la zone d'étude est caractérisée par une forte vulnérabilité à la contamination par les pesticides. La superposition des cartes DRASTIC standard et pesticides avec la carte d'occupation des sols montre qu'une grande partie des zones agricoles est située dans la zone caractérisée par une vulnérabilité « élevée » à « modérée ». L'étude suggère que ces cartes « DRASTIQUES » peuvent être un outil précieux pour les autorités locales pour la gestion des eaux souterraines et de l'utilisation des terres.

Le code MTDMS est utilisé pour évaluer le transport des sels dans la nappe phréatique. Les résultats du modèle de transport du sel montrent que le processus de salinisation affecte les zones proches des montagnes dans la partie nord. La concentration du sel est liée à la superficie irriguée. Ces enquêtes pourraient constituer une base pour les décideurs de la gestion des ressources en eau et permettre de prévenir les risques de pollution.

Mots clés : Géochimie, Recharge, Vulnérabilité, Modélisation des écoulements souterrains, Modélisation des transports, Bassin de Hajeb Layoun Jelma, Centre de la Tunisie.

Abstract

Groundwater is the main water source in all the world and especially in the arid and semi-arid regions. The Hajeb Layoun Jelma basin is the principal source of water supply for Sidi Bouzid and Sfax region. In the last decades, pollution is considered a common groundwaters problem, representing a severe and harmful threat to the water resources.

In this context, this work has been taken place. The Hajeb Layoun-Jelma basin is the selected site. The main objectifs is to provide its actual water quality and quantity situation. This research aims to perform a geochemical view of the two principal aquifers, implement a numerical mode to control the basin, and assess the vulnerability to the shallow aquifer's pollution using different models.

The groundwater hydrochemistry study's main objectives are to determine the water chemistry origins and assess the groundwater suitability for drinking and irrigation purposes. Twenty-eight water samples were collected in 2017 (wet period) from shallow and deep aquifers and analyzed for different physicochemical parameters (temperature, pH, EC, salinity, Na^+ , Ca^{2+} , K^+ , Mg^{2+} , Cl^- , HCO_3^- , and SO_4^{2-}). The shallow aquifer shows high salinity in most water samples (93% $> 1 \text{ g.l}^{-1}$). The deep aquifer has moderate salinity (21% of samples exceeding 1 g.l^{-1}).

The results show that both aquifers' water mineralization is controlled by the dissolution of carbonates/gypsum and water evaporation. The drinking water quality assessment shows that 100% and 57% extremely poor water for the shallow and the deep samples, respectively, coincide with the Na-Cl water type. The water quality evaluation for irrigation uses indicates that the shallow samples show quality less than the deep one and revealed that most samples in the Hajeb Layoun-Jelma basin are not appropriate for irrigation uses.

The recharge rate estimation was made using the multi-criteria method. The results show that the shallow and the deep aquifer receive an average recharge rate, from rainfall, about 31.5 mm/year (infiltration: 15%) and 34 mm/year (16.2%), respectively.

The numerical model was developed using Modflow code under GMS software. The hydrodynamic model system permitted to estimate the hydraulic conductivity distribution. It also allowed estimating abstraction's effect on the water table evolution by two pumping scenarios (2019-2050) (Sc1: constant pumping rates, Sc2: doubled pumping rates). The hydrodynamic models show the continuous water table decrease after 30 years.

The groundwater vulnerability assessment of the shallow aquifer of Hajeb Layoun Jelma basin was made using both intrinsic and simulation models. The DRASTIC model was used as intrinsic tool for identifying the susceptible zones to contamination for the shallow aquifer. The vulnerability maps indicated that the dominant vulnerability classes are a low class (55%) followed by the moderate class (43 %) in the pesticide model and the “low” classes (86 %) in the standard model. A high vulnerability characterizes only 1 % of the study area to pesticide contamination. The superposition of the standard and the pesticide DRASTIC maps with the land use map shows that many agricultural zones are located in the area characterized by “high” to “moderate “vulnerability. The study suggests that these “DRASTIC” maps can be a valuable tool for local authorities for groundwater and land use management.

MTDMS is used to evaluate the transport of salts in the shallow aquifer. The salt transport model results show that the salinization process affects the areas close to the north part's mountains. The high salinity concentration is related to the irrigated area.

These investigations could constitute a basis for decision-makers for water resources management and prevent pollution risks.

Key words: Geochemistry, Recharge, Vulnerability, Groundwater flow modeling, Transport modeling, Hajeb Layoun Jelma basin, Central Tunisia.

Sommario

Le acque sotterranee sono la principale fonte di acqua in tutto il mondo e specialmente nelle regioni aride e semiaride. Il bacino di Hajeb Layoun Jelma è la principale fonte di approvvigionamento idrico per la regione di Sidi Bouzid e Sfax. Negli ultimi decenni l'inquinamento è considerato un problema comune delle acque sotterranee che rappresenta una grave e dannosa minaccia per le risorse idriche.

In questo contesto si è svolto questo lavoro. Il bacino Hajeb Layoun-Jelma è il sito selezionato in questo lavoro al fine di fornire la sua reale situazione di qualità e quantità dell'acqua. Questa ricerca si propone di eseguire una caratterizzazione geochimica dei due principali acquiferi, di implementare modalità numeriche per il controllo del bacino e di valutare la vulnerabilità all'inquinamento della falda acquifera superficiale utilizzando diversi modelli : il modello indicizzato ed il modello di simulazione. Gli obiettivi principali dello studio di idrochimica delle acque sotterranee è sono determinare l'origine chimica dell'acqua e valutare l'idoneità delle acque sotterranee per scopi potabili e irrigui. Nel 2017 (periodo umido) sono stati raccolti 28 campioni di acqua da acquiferi sia bassi che profondi, e analizzati per diversi parametri fisico-chimici (temperatura, pH, EC, salinità, Na^+ , Ca^{2+} , K^+ , Mg^{2+} , Cl^- , HCO_3^- , e SO_4^{2-}). La falda acquifera poco profonda mostra un'elevata salinità nella maggior parte dei campioni di acqua (93% > 1 g.l⁻¹). La falda acquifera profonda ha una salinità moderata (21% dei campioni superiore a 1 g.l⁻¹). I risultati mostrano che la mineralizzazione dell'acqua di entrambe le falde acquifere è controllata dalla dissoluzione di carbonati/gesso e dall'evaporazione dell'acqua. La valutazione della qualità dell'acqua potabile mostra che il 100% ed il 57% di acqua estremamente scarsa per i campioni poco profondi e profondi, rispettivamente, che coincidono con il tipo di acqua Na-Cl. La valutazione della qualità dell'acqua per usi irrigui indica che i campioni superficiali mostrano una qualità inferiore a quelli profondi e ha rivelato che la maggior parte dei campioni nel bacino di Hajeb Layoun-Jelma non sono adatti per usi irrigui.

La stima del tasso di ricarica è stata effettuata utilizzando il metodo multicriterio. I risultati mostrano che l'acquifero superficiale e quello profondo ricevono, rispettivamente, un tasso di ricarica medio dalla pioggia di circa 31,5 mm / anno (infiltrazione: 15%) e 34 mm / anno (infiltrazione: 16,2%).

Il modello numerico è stato sviluppato utilizzando il codice Modflow, sotto il software GMS. Il sistema modello idrodinamico ha permesso di stimare la distribuzione della

conducibilità idraulica. Ha inoltre consentito di stimare l'effetto dell'estrazione sull'evoluzione della falda freatica mediante due scenari di pompaggio (2019-2050) (Sc1: velocità di pompaggio costanti, Sc2: velocità di pompaggio raddoppiate). I modelli idrodinamici mostrano il continuo decremento della falda freatica dopo 30 anni.

La valutazione della vulnerabilità delle acque sotterranee della falda acquifera poco profonda del bacino di Hajeb Layoun Jelma è stata realizzata utilizzando modelli sia intrinseci che simulati. Il modello DRASTIC è stato utilizzato come strumento intrinseco per identificare le zone suscettibili alla contaminazione per l'acquifero poco profondo. Le mappe di vulnerabilità hanno indicato che le classi di vulnerabilità dominanti sono la classe bassa (55%) seguita dalla classe moderata (43%) nel modello dei pesticidi e dalle classi "basse" (86%) nel modello standard. Solo l'1% dell'area di studio è caratterizzata da un'elevata vulnerabilità alla contaminazione da pesticidi. La sovrapposizione delle mappe DRASTIC standard e dei fitofarmaci con la mappa dell'uso del suolo mostra che gran parte delle zone agricole si trovano nell'area caratterizzata da vulnerabilità da "alta" a "moderata". Lo studio suggerisce che queste mappe "DRASTIC" possono essere uno strumento prezioso per le autorità locali per la gestione delle acque sotterranee e del suolo.

MTDMS viene utilizzato per valutare il trasporto di sali negli acquifero studiato. I risultati del modello di trasporto del sale mostrano che il processo di salinizzazione interessa le aree vicine alle montagne nella parte nord. La concentrazione di sali è correlata all'area irrigata. Queste indagini potrebbero costituire una base per i decisori per la gestione delle risorse idriche e consentire la prevenzione dei rischi di inquinamento.

Parole chiave: Geochimica, ricarica, vulnerabilità, modellazione del flusso delle acque sotterranee, modellizzazione dei trasporti, bacino di Hajeb Layoun Jelma, Tunisia centrale.

ملخص

المياه الجوفية هي مصدر المياه الرئيسي في جميع أنحاء العالم وخاصة في المناطق القاحلة وشبه القاحلة. يعتبر حوض حاجب العيون جلمة المصدر الرئيسي لإمدادات المياه لمنطقة سيدي بوزيد وصفافس. في العقود الماضية، كان التلوث يعتبر مشكلة مياه جوفية شائعة، ويمثل تهديدًا خطيرًا وضارًا لموارد المياه.

في هذا السياق، تم تنفيذ هذا العمل. حوض حاجب العيون - جلمة هو الموقع المختار لتوفير نوعية وكمية المياه الفعلية. يهدف هذا البحث إلى إجراء نظرة جيوكيميائية لخزانات المياه الجوفية الرئيسية، وتنفيذ وضع رقمي للتحكم في الحوض، وتقييم مدى التعرض لتلوث طبقة المياه الجوفية الضحلة باستخدام نماذج مختلفة.

تتمثل الأهداف الرئيسية لدراسة الكيمياء المائية للمياه الجوفية في تحديد أصول كيمياء المياه وتقييم ملاءمة المياه الجوفية لأغراض الشرب والري. تم جمع ثمانية وعشرين عينة من المياه في عام 2017 (الفترة الرطبة) من طبقات المياه الجوفية الضحلة والعميقة وتم تحليلها وفقًا لمعايير فيزيائية كيميائية مختلفة (درجة الحرارة، ودرجة الحموضة، والتوصيل، والملوحة، Na^+ ، Ca^{2+} ، K^+ ، Mg^{2+} ، Cl^- ، HCO_3^- ، SO_4^{2-}) يُظهر الخزان الجوفي الضحل نسبة ملوحة عالية في معظم عينات المياه ($93\% < 1g/l$). يحتوي الخزان الجوفي العميق على درجة ملوحة معتدلة (21% من العينات التي تزيد عن $1g/l$).

أظهرت النتائج أن تمعدن المياه في كل من الخزانات الجوفية يتم التحكم فيه عن طريق إذابة الكربونات / الجبس وتبخر الماء. يُظهر تقييم جودة مياه الشرب أن 100% و 57% مياه رديئة للغاية للعينات الضحلة والعميقة، على التوالي، تتطابق مع نوع الماء كلوريد الصوديوم. يشير تقييم جودة المياه لاستخدامات الري إلى أن العينات الضحلة تظهر جودة أقل من تلك العميقة وكشف أن معظم العينات في حوض حاجب العيون - جلمة ليست مناسبة لاستخدامات الري.

تم تقدير معدل التغذية باستخدام طريقة المعايير المتعددة. أظهرت النتائج أن طبقة المياه الجوفية الضحلة والعميقة تتلقى معدل تغذية متوسط، من الأمطار، حوالي 31.5 مم / سنة (تسرب: 15%) و 34 مم / سنة (16.2%) على التوالي.

تم تطوير النموذج العددي باستخدام كود Modflow ضمن برنامج GMS. يسمح نظام النموذج الهيدروديناميكي بتقدير توزيع الموصلية الهيدروليكية. كما سمح بتقدير تأثير السحب على تطور منسوب المياه من خلال سيناريوهين ضخ (Sc1: 2050-2019) (معدلات الضخ الثابتة، $Sc2$: معدلات الضخ المزوجة). تُظهر النماذج الهيدروديناميكية انخفاض منسوب المياه المستمر بعد 30 عامًا. تم إجراء تقييم قابلية تعرض المياه الجوفية للخزان الجوفي الضحل لحوض حاجب العيون جلمة باستخدام نماذج جوهريّة ونماذج محاكاة. تم استخدام نموذج DRASTIC كأداة جوهريّة لتحديد المناطق المعرضة للتلوث لطبقة المياه الجوفية الضحلة. أشارت خرائط الضعف إلى أن فئات الضعف السائدة هي فئة منخفضة (55%) تليها الفئة المتوسطة (43%) في نموذج مبيدات الآفات والفئات "المنخفضة" (86%) في النموذج القياسي. تتميز نسبة 1% فقط من منطقة الدراسة بالتلوث بمبيدات الآفات بدرجة عالية من التعرض. يظهر تراكم المعيار وخرائط DRASTIC للمبيدات مع خريطة استخدام الأراضي أن العديد من المناطق الزراعية تقع في المنطقة التي تتميز بضعف "مرتفع" إلى "متوسط". تقترح الدراسة أن هذه الخرائط "DRASTIC" يمكن أن تكون أداة قيمة للسلطات المحلية لإدارة المياه الجوفية واستخدام الأراضي.

يستخدم MTDMS لتقييم انتقال الأملاح في طبقات المياه الجوفية المدروسة. تظهر نتائج نموذج نقل الملح أن عملية التملح تؤثر على المناطق القريبة من جبال الجزء الشمالي.

يرتبط تركيز الأملاح بالمنطقة المروية. يمكن أن تشكل هذه التحقيقات أساسًا لصانعي القرار لإدارة موارد المياه ومنع مخاطر التلوث.

الكلمات المفتاحية: الجيوكيمياء، التغذية، الضعف، نمذجة تدفق المياه الجوفية، نمذجة النقل، حوض حاجب العيون جلمة، وسط تونس.

—Dedications—

This modest work is dedicated to my beloved family:

My mother "Mabrouka" and father "Ali"

&

My lovely sister "Emna"

&

My Brothers "Abdallah", "Mahmoud" and "Abdelkarim"

&

My sister and brother in law: "Malika" and "Naim"

&

To my lovely nieces "Chahed", "Ayat", "Myriam" and "Balkis"

&

My sweet nephew "Tamim"

Soumaya Aouiti

—Acknowledgements—

After more than five years of starting this thesis, it is my pleasure to sit down in front of my computer to thank everyone who has participated directly or indirectly and contributed in one way or another in developing this work and writing this manuscript.

I would never have been able to finish my dissertation without my two supervisors' guidance, help from my professors, and support from my family.

I am grateful to my supervisor, **Pr. Mounira Zammouri**, professor at the Faculty of Sciences of Tunis (University of Tunis El Manar), for her leadership, availability, helpful corrections, discussion and especially her great human qualities.

My thanks are also extended to my supervisor, **Pr. Fulvio Celico**, professor at the University of Parma, for offering me the opportunity to do my research at his laboratory and for all of their guidance through this process: discussion, ideas, and feedback has been invaluable and also his great human qualities.

Special thanks are due to **Mrs. Fadoua Hamzaoui-Azaza**, assistant professor at the Faculty of Science Tunis (University of Tunis El Manar), for her great help, who mentored me in learning about water geochemistry, and patiently corrected my writing and scientifically supported my research.

I also express all my acknowledgments to **Mr. Fetheddine Melki**, professor at the Faculty of Sciences of Tunis (University of Tunis El Manar), for his great help.

I also express all my acknowledgments to **Mr. Monji Hamdi**, hydrogeologist engineer at the water resources division of Sidi Bouzid (CRDA Sidi Bouzid). I express my gratitude for his scientific help and his assistance during my water sampling collection.

My thanks are also extended to **Mr. Walid Weslati**, associate professor at the Faculty of Science of Tunis, for his help and assistance, in the laboratory, during the samples' analysis.

Special thanks are due to **Mrs. Emma Petrella**, professor at the University of Parma, for her great help and let me assist in his interesant course at the University of Parma for 4 months. Also, for accepting to review this work.

I also express all my acknowledgements to **Mr. Mohamed Fethi ben Hamouda**, Professor at National Center for Nuclear Sciences and Technologies (CNSTN Sidi thabet), for accepting to review this thesis.

I am also grateful to all the jury members for accepting to review this work, the chair **Prof. Fetheddine Melki**, the examiners **Prof. Ismail Chenini** and **Prof. Alessandro Chelli**.

I am also thankful to **Mrs. Alexandra Feo**, professor at the University of Parma, for their logistic assistance, especially her great human qualities. I also express my acknowledgments to **Mr. Andrea Zanini**, professor at the University of Parma; I express my gratitude for his scientific and logistic help.

I would like to thank my colleagues at the University of Parma, **Pietro**, and **Edoardo**, where I shared the same office during my Parma stay.

Special thanks are also due to **Mrs. Rosaria Bileti**, an Italian professor at the Italian cultural institute, to learn Italian.

Special thanks due to all my friends at the University of Tunis El Manar. I am thankful to my **family and all my friends** for their support.

Soumaya Aouiti

—Table of content—

Résumé -----	2
Abstract -----	4
Sommario -----	6
ملخص -----	8
List of figures -----	17
List of tables -----	21
Abbreviations -----	22
Introduction -----	23
1. Background -----	23
2. Problematic -----	24
3. Objectives -----	25
4. Methodology-----	25
Part 1 Study area overview -----	28
Chapter I : General presentation -----	29
I. Geographic setting-----	29
II. Climatic setting-----	31
1. Rainfall -----	31
2. Temperature -----	37
3. Humidity -----	38
4. Wind speed-----	39
5. Evaporation -----	40
6. Insolation-----	40
7. Bioclimatic zone -----	41
III. Hypsometry and geomorphology-----	43
1. Digital Elevation Model (DEM)-----	43
2. Hillshade -----	44
3. Slope -----	44
IV. Hydrological characterization-----	45
1. Hydrological network -----	45
2. Runoff -----	46
V. Soil description-----	46

VI.	Land use description-----	47
VII.	Population evolution-----	48
Chapter II: Geological and structural setting -----		49
I.	Introduction-----	49
II.	Geological setting-----	51
1.	Geologic map-----	51
2.	Stratigraphy-----	53
III.	Structural setting-----	60
1.	Anticlines-----	61
2.	Syncline of Hajeb Layoun-Jelma-----	64
3.	Faults-----	64
Chapter III: Hydrogeology of the study area-----		66
I.	Introduction-----	66
II.	Aquifers structuration-----	66
III.	Geometric characterization of the reservoir layers-----	68
1.	Geometry of aquifers-----	68
2.	Top/ Bottom of aquifers-----	74
IV.	HJB aquifers characterization-----	75
1.	Transmissivity (T)-----	75
2.	Permeability (K)-----	75
3.	Storage coefficient-----	76
V.	Groundwater abstraction evolution-----	76
1.	Shallow aquifer-----	77
2.	Beglia aquifer (Serrevallian)-----	77
3.	Hayet Mineral water-----	79
4.	Ain Ghrab aquifer (Aquitania)-----	79
5.	Cretaceous aquifer (Aptian)-----	80
VI.	Groundwater regime and piezometric contour lines-----	81
1.	Historic data-----	81
2.	Flow direction-----	85
VII.	HJB's water distribution for the Sfax region-----	86
VIII.	Groundwater Recharge-----	87

IX.	Springs discharge -----	89
X.	Hydrochemical characterization of HJB-----	89
1.	Salinity evolution -----	90
2.	Nitrate evolution -----	90
XI.	Conclusion -----	91
Part 2 Materials and Methods-----		93
Chapter I: Geo-database elaboration -----		94
I.	Data gathering and analysis -----	94
1.	Maps data -----	94
2.	Punctual data-----	94
II.	Geographical information system -----	95
Chapter II: Geochemical characterization -----		97
I.	Introduction-----	97
II.	Samples collection and analysis -----	99
III.	Hydrochemical characterization -----	101
1.	Conventional methods-----	101
2.	Origin of mineralization-----	101
3.	Multivariate statistical analysis -----	101
4.	Geochemical modeling-----	102
IV.	Water quality assessment -----	102
1.	Drinking use -----	102
2.	Irrigation suitability assessment -----	105
Chapter III: Recharge estimation and groundwater flow modeling of HJB-----		107
I.	Introduction-----	107
II.	Groundwater recharge estimation -----	108
1.	Introduction -----	108
2.	Mapping of the groundwater potential recharge-----	108
3.	Recharge estimation -----	111
4.	Geographic information system and model builder-----	112
5.	Conclusion -----	113
III.	Groundwater modeling of HJB -----	113
1.	Design steps of a hydrogeological model -----	113

2.	GMS software -----	117
3.	Flow modeling approach of HJB -----	117
4.	Conclusion -----	121
Chapter IV: Vulnerability mapping and Contaminant transport modeling-----		122
I.	Introduction-----	122
II.	Groundwater vulnerability assessment using the indexed method-----	124
1.	Description of the DRASTIC model -----	124
2.	Determination of DRASTIC parameters -----	124
3.	Sensitivity analysis -----	130
4.	GIS and model builder -----	131
5.	Conclusion -----	131
III.	Modeling of pollutant transport-----	132
1.	Introduction-----	132
2.	Theoretical description of the pollutant transport process -----	132
3.	Description of MT3DMS model of HJB -----	135
4.	Conclusion -----	136
Part 3 Results and discussions-----		137
Chapter I: Geochemical characterization -----		138
I.	Hydrochemical data -----	138
II.	Groundwater mineralization processes -----	139
1.	Correlation of parameters-----	139
2.	Identification of water–rock interaction -----	141
III.	Hydrochemical water type-----	143
IV.	Aqueous geochemical modeling-----	145
VII-	Saturation of carbonate minerals-----	145
VIII-	Saturation of carbonate minerals-----	146
V.	Multivariate Statistical Analyses -----	148
VI.	Water quality -----	150
1.	Drinking use -----	150
2.	Irrigation purposes -----	155
3.	WILCOX and USSL classification-----	155
4.	Irrigation Water Quality Index (IWQI)-----	158

VII.	Regional hydro-geochemical conceptual model of HJB -----	159
VIII.	Discussion -----	161
IX.	Conclusion -----	162
Chapter II: Recharge estimation and groundwater flow modeling of HJB -----		163
I.	Recharge estimation -----	163
1.	Thematic maps -----	163
2.	Groundwater recharge zones -----	166
3.	Recharge estimation -----	168
4.	Conclusion -----	169
II.	Groundwater modeling -----	169
1.	Boundary conditions -----	169
2.	Calibration results in steady state -----	171
3.	Transient state -----	173
4.	Predictive simulations to the year 2050 -----	176
5.	Conclusion -----	177
Chapter III: Vulnerability mapping and Contaminant transport modeling -----		179
I.	Intrinsic model -----	179
1.	Mapping the thematic layers -----	179
2.	Mapping of the DRASTIC vulnerability (Standard and pesticide) -----	181
3.	Sensitivity of the DRASTIC model -----	181
4.	Conclusions -----	184
II.	Contaminant transport modeling using MT3DMS -----	185
1.	Introduction -----	185
2.	Model structure and boundary conditions -----	185
3.	Results of calibration -----	186
4.	Conclusion -----	189
Conclusions -----		190

List of figures

Figure 1. Water in Earth (USGS 2010)	23
Figure 2. Flow chart showing the methodology adopted in this study	27
Figure 3. Geographic location of the study area (a) location of HJB in Tunisia (b) the governments occupied by HJB and (c) boundary of the HJB	30
Figure 4. Location of the rain gauge stations in Hajeb Layoun-Jelma basin.....	31
Figure 5. Annual rainfall (from 1968 to 2017) at the seven rain gauge stations in HJB	32
Figure 6. Average of annual rainfall (in mm) for the period 1968-2017 in HJB.....	33
Figure 7. (a) Diagramme of the monthly rainfall in HJB (b)Pie chart of the monthly rainfall percentage in HJB	34
Figure 8 Diagramme of the Standard deviation of the mean monthly values rainfall in HJB.....	35
Figure 9. Repartition of seasonal rainfall in Hajeb Layoun-Jelma basin.....	35
Figure 10. The standardized precipitation index (SPI) at the seven rain gauge stations in HJB: (a) Hajeb Layoun, (b) Cebala, (c) Negada, (d) Oum Ladham, (e) Jelma Her, (f) Jelma Agro, and (g) Jbel Mrhilla.....	37
Figure 11. Monthly average temperature (°C) during the period (1972-2016)	38
Figure 12. Monthly average humidity (%) for 45 years (INM 1972-2016)	39
Figure 13. Monthly average of wind speed in HJB (INM 1972-2016)	39
Figure 14. Monthly evaporation (mm) during the period (1972-2016).....	40
Figure 15. Monthly average of insolation (hour/month)	41
Figure 16. Emberger's climatogram for Hajeb Layoun-Jelma basin.....	42
Figure 17. (a) DEM of the study area (b) 3d view of the study area	43
Figure 18. Hillshade map of the study area	44
Figure 19. Slope map of the study area	45
Figure 20. The hydrological network of the study area.....	46
Figure 21. Soil map of Hajeb Layoun Jelma basin.....	47
Figure 22. Land use map of HJB extracted from the agriculture map obtained from Regional Direction of Agriculture Development of Sidi bouzid (CRDA-Sidi bouzid).....	48
Figure 23. Structural zonation of Tunisia and location of the study area.....	51
Figure 24. Geologic map of Hajeb Layoun-Jelma basin	52
Figure 25. Correlation of lithostratigraphic units of the Early Cretaceous in Central Tunisia (M'Rabet 1981 in Allouche 1997).....	55
Figure 26. Synthetic log of the late Cretaceous series in the Hajeb Layoun-Jelma basin	56
Figure 27. Synthetic log of the Cenozoic series	59
Figure 28. (a)The Saouef formation exposed at the surface near the Mghilla moutain (b) The Beglia formation exposed at the surface (pictures were taken in Jun 2019).....	60
Figure 29. Structural map of the main deformations in central Tunisia (Zouaghi 2008)	61
Figure 30. NW-SE cross-section through Mghilla mountain	62
Figure 31. Geological map of Lessouda moutain (Matmati et al., 1992).....	62
Figure 32. NW-SE cross-section through Zaouia mountain.....	64
Figure 33. Localisation of deep and shallow wells and the various cross section effected in Hajeb Layoun-Jelma basin.....	69

Figure 34. Cross-section A-A' (NW-SE) showing the principal aquifers in HJB.....	71
Figure 35. Cross-section B-B' showing the principal aquifers, in HJB, in a NE-SW direction.....	72
Figure 36. Cross-section C-C' showing the closing of the HJB in the southern-east part	73
Figure 37. Cross-section D-D' showing the closing of the HJB in the south part.....	74
Figure 38. Multi-cross sections showing the lateral variation of the thickness of the different layers	75
Figure 39. Abstraction and resources of HJB during the period 1973-2018	76
Figure 40. Evolution of the shallow aquifer abstraction and its number of wells	77
Figure 41. Evolution of the deep aquifer abstraction and the number of wells	78
Figure 42. The different uses sectors of the Beglia deep aquifer (DGRE 2017).....	78
Figure 43. Evolution of the Hayet mineral water abstraction.....	79
Figure 44. Evolution of the Ain Ghrab aquifer abstraction and the number of wells	80
Figure 45. Evolution of the Aptian aquifer abstraction	80
Figure 46. Location of the piezometers controlling the shallow aquifer	81
Figure 47. The shallow water table decline in four selected piezometers: (a) well n°27, (b) Pz 21, (c) Pz 20 and (d) Pz 24.....	82
Figure 48. Location of the six piezometers controlling the Beglia aquifer	83
Figure 49. The evolution of the piezometric level of the deep aquifer at six selected piezometers: (a) Pz1 (Hadjeb), (b) Pz2 (Ben Mrad), (c) Pz3 (Zoghmar), (d) Pz4 (Hadjeb ville), (e) Pz5 (Ghedir Gaied) and (f) Pz10 (Chastel bis)	84
Figure 50. Piezometer map of the shallow aquifer	85
Figure 51. Piezometer map of the deep aquifer	86
Figure 52. Distribution of HJB's water to Sfax	87
Figure 53. Fluctuation of the shallow piezometric level in response to the rainfall (at piezometers: (a) Pz Felta, (b) Pz 21, (c) Pz 20 and (d) Pz18) in the period January 2005 - December 2009	88
Figure 54. Fluctuation of the deep piezometric level (at piezometers: (a) Pz 1, (b) Pz 2, (c) Pz 4 and (d) Pz10) in the period January 2005 - December 2009.....	88
Figure 55. Evolution of the springs discharge in HJB.....	89
Figure 56. Flow chart showing the methodology applied in the HJB's water evaluation.....	99
Figure 57. water samples location	100
Figure 58. Flow chart showing the methodology adopted in this study	109
Figure 59. Inter-relationship between the multiple influencing factors of the recharge process.....	110
Figure 60. Structure of model builder used to generate the potential groundwater maps of Hajeb Layoun Jelma aquifers.....	112
Figure 61. Flow chart of the groundwater flow modeling process (Reilly 2001)	114
Figure 62. Plan view of the site to be modeled (a) shallow aquifer and (b) deep aquifer	119
Figure 63. Flow chart of the methodology used for the shallow aquifer vulnerability evaluation.....	125
Figure 64. Spatial distribution of salinity: (a): Deep and (b): shallow aquifer. The map was plotted using the IDW method.	139
Figure 65. Gibbs' diagrams of the shallow and deep aquifers of HJB: (a) ratio I vs. TDS and (b) ratio II vs. TDS	142
Figure 66. (a) Plot of SO ₄ ²⁻ against Ca ²⁺ , (b) Plot of Na ⁺ against Cl ⁻ , (c) Plot of Na ⁺ against (Ca ⁺⁺ +Mg ⁺) and (d): Plot of (HCO ₃ ⁻ + SO ₄ ²⁻) against (Ca ²⁺ +Mg ²⁺) in meq/l in shallow and deep aquifer water samples	143
Figure 67. (a) Piper diagram and (b) Chadha diagram of the shallow samples.....	144

Figure 68. (a) Piper diagram and (b) Chadha diagram of the deep samples.....	145
Figure 69. Plot of (a) $[Ca] + HCO_3^-$ vs SI calcite (b) $[Ca] + [HCO_3^-] + Mg$ vs SI dolomite	146
Figure 70. Plot of (a) $[Na] + [Cl]$ vs SI halite (b) $[Ca] + [SO_4]$ vs SI anhydrite (b) $[Ca] + [SO_4]$ vs SI gypsum.....	147
Figure 71. Box plots of saturation index for several mineral (a) shallow (b) deep samples	148
Figure 72. Projection of the variables in the first, second and third factorial plan (Principal component analysis): (a) including all shallow and springs samples in HJB and (b): Deep samples in HJB.....	149
Figure 73. Comparison of major ions concentration (in mg/l) and physical parameters in HJB with WHO standards and Tunisian norms (NT 09-14): (a) pH, (b) EC ($\mu S/cm$), (c) K^+ , (d) Ca^{2+} , (e) Mg^{2+} , (f) Na^+ , (g) SO_4^{2-} , (h) HCO_3^- and (i) Cl^-	151
Figure 74. Comparison of the results of the WQI, ImpWQI and EWQI indices using the WHO standard (a) shallow aquifer (b) deep aquifer.....	153
<i>Figure 75. Distribution of the three indices (ImpWQI, EWQI and WQI) based on WHO standard in (a) deep aquifer and (b) shallow aquifer.....</i>	154
Figure 76. (a) Sodium percentage Vs EC values plot for water quality classification (Wilcox diagram 1955) and (b) USSL classification of HJB samples	156
Figure 77. Results of IWQI in the study area.....	158
Figure 78. 3D Hydrogeochemical conceptual model	160
Figure 79. The five factors controlling the recharge potentiality; (a) slope gradient map (in %), (b) lithology map, (c) soil type map, (d) land use/ land cover and map (e) drainage density map	165
Figure 80. Map of Recharge zones in the HJB	166
Figure 81. Potential recharge map of the shallow aquifer	167
Figure 82. Potential recharge map of the deep aquifer	167
Figure 83. potential recharge map of the under-flow aquifers	168
Figure 84. Coverages of the (a) shallow aquifer, (b) deep aquifer	170
Figure 85 . Grid of the shallow aquifer	170
Figure 86. Grid of the deep aquifer	171
Figure 87. Comparison diagram between the calculated piezometric levels and the measured in steady state (a) shallow aquifer (b) deep aquifer	172
Figure 88. Calculated piezometric maps in the steady state; (a) Shallow aquifer, (b): Deep aquifer (piezometric contour lines in meters).	172
Figure 89. Comparison of the evolution of the calculated and measured hydraulic head in some selected shallow piezometers	174
Figure 90. Comparison of the evolution of the calculated and measured hydraulic head in some selected deep piezometers	175
Figure 91. The spatial distribution of rating for the Static parameters ((a) Topography and (b) Soil media) and the Dynamic parameters ((c) water table depth, (d) Net recharge, (e) Aquifer media, (f) vadose zone and (g) hydraulic conductivity) of the shallow aquifer.....	180
Figure 92. Drastic vulnerability maps: (a) Standard and (b) pesticide	181
Figure 93. Drastic map using the effective weight: (a) Standard DRASTIC and (b) Pesticide DRASTIC.....	183
Figure 94. Spatial distribution of measured salinity (in g/l) in four selected years (a) 1999, (b) 2006, (c) 2013 and (d) 2019	186
Figure 95. Comparison between salinity observed and calculated values in 1999 (initial condition)	187

Figure 96. Spatial distribution of calculated salinity (in g/l) in initial condition (1999).....	188
Figure 97. Correlation between the calculated and the measured concentration of salinity (g/l) in the transient state.....	189

List of tables

Table 1 Classification of the standardized precipitation index (SPI) (Mckee et al. 1993)	36
Table 2 Diagram showing the different aquifers of HJB	68
Table 3 Total decline of water table in deep aquifer during the period 1973-2018.....	84
Table 4 Evolution of salinity (g/l) between 1996 and 2006, in selected wells, for different uses (Irrigation and drinking) (DGRE 1996-2006)	90
Table 5 Evolution of nitrates concentration (mg/l) in selected shallow and deep wells between 1996 and 2015	91
Table 6 Classification of groundwater quality based on WQI, EWQI and ImpWQI	105
Table 7 Parameter limiting values for qi computing (Ayers and Westcot 1985)	106
Table 8 Effect of factor influencing relative rates and score for each five-potential factor	111
Table 9 Rates classification based on recharge intensity (Haouchine et al., 2011)	111
Table 10 Groundwater recharge potential zones and infiltration percentages (FAO 1967)	112
Table 11 Diagram showing the conceptual model of HJB	118
Table 12 Hydrodynamic characteristics of HJB aquifer (deduced from pumping tests) (Kochel 1980)	120
Table 13 Sources of data used for the production of the DRASTIC model	125
Table 14 Drastic parameters: range, rating and weight value for the study area (Standard and Pesticide Drastic) (Aller et al., 1987)	126
Table 15 Intervals and ratings of the recharge and the three parameters that control it based on the Piscopo method (2001).....	128
Table 16 Drastic range and its vulnerability class (Civita 1994).....	130
Table 17 Statistical summary of the physical and chemical parameters of HJB samples (Ionic contents in mg/l).....	138
Table 18 Pearson correlation matrix of HJB, (a): Shallow wells/Springs, (b): Deep wells, bold indicates significant 50%.....	140
Table 19 Variance explained by the first three principal components.....	148
Table 20 Classification of shallow and deep samples quality based on the three Indices (EWQI, WQI and ImpWQI)	152
Table 21 Correlation between the various water quality indices (ImpWQI, EWQI and WQI) and physico-chemical parameters for the deep and shallow aquifer.....	153
Table 22 Irrigation quality indices of Hajeb Layoun-Jelma aquifers	157
Table 23 Classifications and characteristics of general IWQI.....	158
Table 24 Ranges and its areas of the five factors controlling the recharge potentiality	164
Table 25 Recharge estimation of the HJB's aquifers.....	168
Table 26 The calculated water balance of the HJB aquifer system, in steady state.....	173
Table 27 The calculated water balance of the HJB aquifer system, in transient state	176
Table 28 The calculated water balance of the HJB aquifer system, in 2050	177
Table 29 Statistical summary of Drastic parameters	182
Table 30 Correlation matrix.....	182
Table 31 Statistics of single parameter sensitivity analysis.....	183
Table 32 Statistics of map removal sensitivity analysis	183
Table 33 Statistical summary of one map removal sensitivity analysis	184

Abbreviations

HJB : Hajeb Layoun-Jelma Basin

CRDA : Commissariat Régional au Développement Agricole

DEM : Digital Elevation Model

DGRE : Direction Générale des Ressources en Eaux

DRASTIC: Depth to water; net Recharge, Aquifer media, Soil media, Topography, Impact of the vadose zone and hydraulic Conductivity

EC: Electrical Conductivity

ETP: Evapotranspiration

GIS: Geographic Information System

MH: Magnesium Hazard

MT3DMS: Modular Three-Dimensional Multispecies Transport Model for Simulation of Advection, Dispersion, and Chemical Reactions of Contaminants in Groundwater Systems.

ne: Effective porosity

P: Precipitation

PI: Permeability Index

Pz: Piezometer

SAR: Sodium Adsorption Ratio

SI: Saturation Index

TH: Total Hardness

UTM: Universal Transverse Mercator

WHO: World Health Organization

WQI: Water Quality Index

NT: National standard

INS: National Institute of Statistics

SONEDE: National Water Supply and Distribution Company

LU/LC: Land Use/Land Cover

GMS : Groundwater Modeling System

Introduction

1. Background

Water is the principal component in the Earth that supports the life of all living. It could be found in various forms linked to the climatic conditions. Liquid form is mainly located in oceans, seas, lakes, rivers, and groundwater. Solid form of the water is snow, ice and glaciers and the gas form are as vapor. The Earth's water is like an eye drop, of our planet, with about 1385 Km of diameter (USGS 2010) (Figure 1). Just 2.5% of this water is freshwater. The most significant percent of freshwater is occupied in glaciers and icecaps.

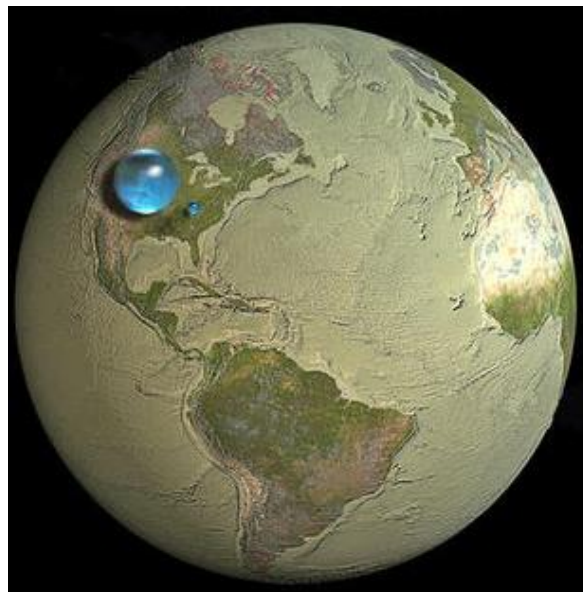


Figure 1. Water in Earth (USGS 2010)

The vital water reserves for our life's sustainability, specifically in the semi-arid and arid region, is included in groundwaters, which present 30.1% of freshwater and 0.75% of the total Earth's water (Gleick 1993). Groundwater supports all types of uses; human health, economic development, and ecological diversity (Celico et al. 2000; Jha et al. 2006; Hamzaoui-Azaza et al. 2020).

In Africa and specifically in Tunisia, groundwater is practically the primary water source in many regions, water resources' sustainable management has crucial importance. The Hajeb Layoun-Jelma basin (HJB), the subject of this thesis, is located in central Tunisia. It is extending for over 1380 km², which corresponds to 0.8% of the national territory and has about

172,003 inhabitants (INS 2014), which correspond to approximately 1.54% of the Tunisian population and which was 50,306 inhabitants in 1972 (Koschel 1980).

Several works on the Hajeb Layoun-Jelma basin has focused mainly on the hydrogeological and hydrochemical aspects. The first hydrogeological study on HJB, “Etude hydrogéologique de la nappe de Hajeb El Aioun-Jelma-Ouled Asker,” was made by Koschel (1980) and it is a detailed analysis of hydrogeological characteristics of both shallow and deep aquifer. The research “Modèle de simulation des nappes de Hajeb El Aioun-Jelma-Ouled Asker” (Zammouri 1988) aimed to develop a hydrodynamic model (transient state 1973-1986) and established a scenario for the groundwater management until the year 1995. Jallalia (2015) studied the Hajeb Layoun-Jelma basin using different approaches such as the geophysical approach to determine the basin’s geometry and the geochemistry aspect to provide information concerning groundwater origin, the geochemical characteristics of the two main reservoirs of the aquifer system of HJB.

2. Problematic

Access to safe drinking water is a human right (United Nations 1977). Nowadays, groundwater is threatened by severe problems caused by natural/ anthropogenic factors, such as extensive agricultural activities, marine intrusion, population growth, and industrial development (Zammouri et al. 2013). This factor engendered a degradation in the quality and the quantity of groundwater in many countries (Ameur et al. 2016; Adimalla 2019; Mnassri et al. 2018; Ligavha-Mbelengwa et al. 2020). Water quality has a strong relationship with health risk (Ricolfi et al. 2020). Hence, it is essential to safeguard the quantity and the quality of water resources.

In the Hajeb Layoun Jelma basin, the population growth (more than three times) plays a substantial effect on the water request. It has a significant impact on water resources (Aouiti et al. 2021a, b). The HJB aquifer system is important to both the southern and the central part of Tunisia. The deep aquifer water is transported to the Sfax city, located 180 km away from the HJB. During the last decades, the HJB presented a development of agriculture activities based on the uses of fertilizers and pesticides to improve agricultural production. This development has affected significantly pressure on groundwater resources: the water extraction increases for both aquifers (shallow and deep aquifer) from 14.8×10^6 in 1973 to 58.45×10^6 m³ in 2018 with almost 2328 shallow wells and 137 deep wells (DGRE 1973–2018a). These

human activities have put increasing pressure on the groundwater quality and quantity of these aquifers (Aouiti et al. 2021a).

3. Objectives

This thesis focus on the hydrogeological and the geochemical analysis of the two main aquifers of the Hajeb Layoun-Jelma basin: the shallow aquifer and the first deep aquifer (Begli formation). The Hajeb Layoun-Jelma basin is considered the main source of drinking water for many regions (Sidi Bouzid, Kairouan, Kasserine, and Sfax) and has been pumped since the early 1970s. The shallow aquifer is generally used for irrigation purposes. The first deep aquifer is transported by the National Water Supply and Distribution Company (S.O.N.E.D.E) to the Sidi Bouzid and Sfax region used for drinking purposes.

The main objectives of the present thesis are to:

- ✓ Synthesize the previous studies (climatic, geological, structural, and hydrogeological) and delimited the principal aquifers.
- ✓ Identify the processes and the geochemical factors that govern the variation of the water's parameters of Hajeb Layoun Jelma basin (temperature, pH, electrical conductivity and major elements), assess the groundwater quality of Hajeb Layoun Jelma basin's two principal aquifers and map out the areas of groundwater unsuitable/ suitable for drinking and irrigation purposes.
- ✓ Estimate the groundwater recharge and input it in the numerical model that describes the HJB's aquifers' hydrodynamic functioning.
- ✓ Develop management scenarios of water resources in HJB to predict the aquifers' hydrodynamic response in the face of anthropogenic factors.
- ✓ Delineate the susceptible zones to groundwater contamination using the DRASTIC method.
- ✓ Create a transport model simulating salinity concentration evolution along the shallow aquifer from the sources (irrigation area and Graa) to predict their impact.

4. Methodology

As present in the below flow chart (**Figure 2**), the first step was consecrated to define state of the art by collecting the necessary data and synthesize the previous studies to understand the various context of the study area (climatic, soil, LU/LC, geology and hydrogeology). The study area has been the subject of several research studies (Koschel 1980; Zammouri 1988; Smida 2008; Jallalia et al. 2015; Thebti et al. 2018).

In the second step, in February 2017, a groundwater sampling was effectuated. The hydrogeochemical work was achieved to identify the groundwater chemistry using the conventional methods and the water-rock interaction process (Gibbs 1970; Mnassri et al. 2018). The comparison of water's parameters with the national and international standards of drinking as well as the computing of several indices, to assess their suitability for drinking and irrigation purposes, such as : Water Quality Index (Ghouili et al. 2018; Asadi et al. 2020), improved water quality index (Zhang et al. 2020), entropy water quality index (Wu et al. 2011; Islam et al. 2017), total Hardness, Electrical conductivity, Percent sodium, Alkalinity hazard, Magnesium hazard, Permeability index and Kelley ratio.

The third step is to estimate the recharge rate, using the multi-criteria method, to introduce it in the hydrodynamic model. For the Hajeb Layoun Jelma basin, the established groundwater flow model was created in both steady and transient state using ModFlow code in GMS software. ModFlow code was used to reconstruct the studied aquifers' hydrodynamic model in steady (1973) and the transient state (1974-2019). The manual calibration is performed by adjusting the hydrodynamic parameters. The calibrated groundwater flow model over the period 1974-2019 is used to forecast the aquifer's behavior in the long-term (until 2050).

The groundwater vulnerability assessment has recently become a vital environmental management tool. The last step is sacred to study the vulnerability of HJB using both the contaminant transport simulations and the index system approach. The vulnerability index approach is worldwide used. There are various index systems for groundwater vulnerability mapping such as : DRASTIC (Aller et al. 1987), SINTACS (Civita and De Maio 1997), GOD (Foster 1987), AVI (Stempvoort et al. 1993), PI (Goldscheider et al. 2000), and GLA (Hölting et al. 1995). Among all these indices, DRASTIC is the most used by hydrogeologists (Babiker et al. 2005; Bazimenyera and Tang 2008; Shakoor et al. 2020). It has seven parameters: depth to water table (D), recharge (R), aquifer type (A), soil type (S), topography (T), the impact of vadose zone (I) and conductivity (C). The vulnerability index is computed based on the weighted sum of ratings of the seven parameters.

The DRASTIC indexed model was used to assess the shallow aquifer's quality vulnerability. The transport models were used to determine the quantitative vulnerability using MT3DMS code (Zheng and Wang 1999) in GMS software.

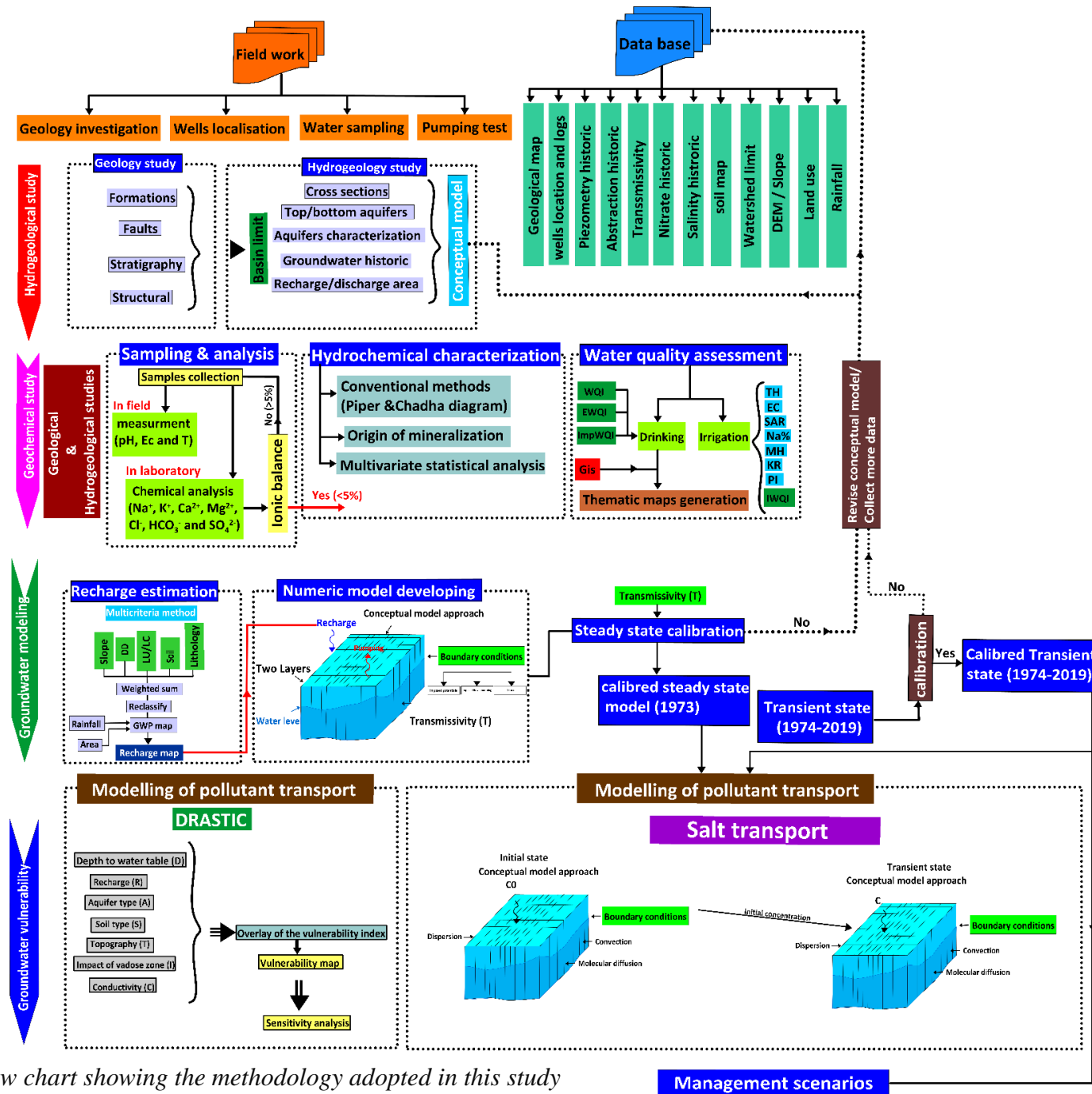


Figure 2. Flow chart showing the methodology adopted in this study

Part 1 Study area overview

Chapter I General presentation

Chapter II Geological and structural setting

Chapter III Hydrogeology of the study area

«Au commencement, il n'y avait que la géologie, qui, à son tour à engendrer toutes les sciences»

Mc Michael Batsu Iyele

Chapter I : General presentation

I. Geographic setting

The Hajeb Layoun-Jelma basin (HJB) is located in the Northeast part of central Tunisia (**Figure 3a**). It is, approximately, located between $x = 35^{\circ}00'00''$, $y = 8^{\circ}30'00''$ and $x = 35^{\circ}30'00''$, $y = 9^{\circ}00'00''$. Three economically underdeveloped regions cover the study area: Hajeb Layoun, Jelma, and Sbeitla, which belong to three different governments: Kairouan, Sidi bouzid and Kasserine.

The study area covers an area equal to 1350 km^2 . The majority of the HJB is in the Sidi Bouzid government, which occupied an area equal to 900 km^2 (**Figure 3b**). The HJB is located at an elevation ranging from 234 to 1384 m. It presents a wide NE-SW directed syncline around by various mountains; it is bordered to the North by the Labaeith mountain, to the South by the Hamra mountain, to the East by the Zaouia-Roua mountain, to the West by the Mrhilla mountain, to South-East by the Lessouda mountain and the South-West by the Koumine mountain (**Figure 3c**).

The study area has a semi-arid climate; January present the coldest month (mean temperature $\approx 11.8^{\circ}\text{C}$), and the hottest is August (mean temperature $\approx 29.4^{\circ}\text{C}$). The mean annual rainfall in the Hajeb Layoun-Jelma basin, over the period 1968–2017, is equal to 241.8 mm.

Four main rivers cross the study area: The Zeroud river, the Zerga river, the Hatab river, and the Jelma river, which are ephemeral. This study's two aquifers interest are the shallow Quaternary aquifer and the first deep aquifer that coincide with the Beglia formation. The water of HJB is used for irrigation practices and drinking supply for three regions (Sidi Bouzid, Kairouan, and Kasserine). The National Water Supply and Distribution Company (S.O.N.E.D.E) transports the water of the HJB to Sfax, which is used for drinking purposes.

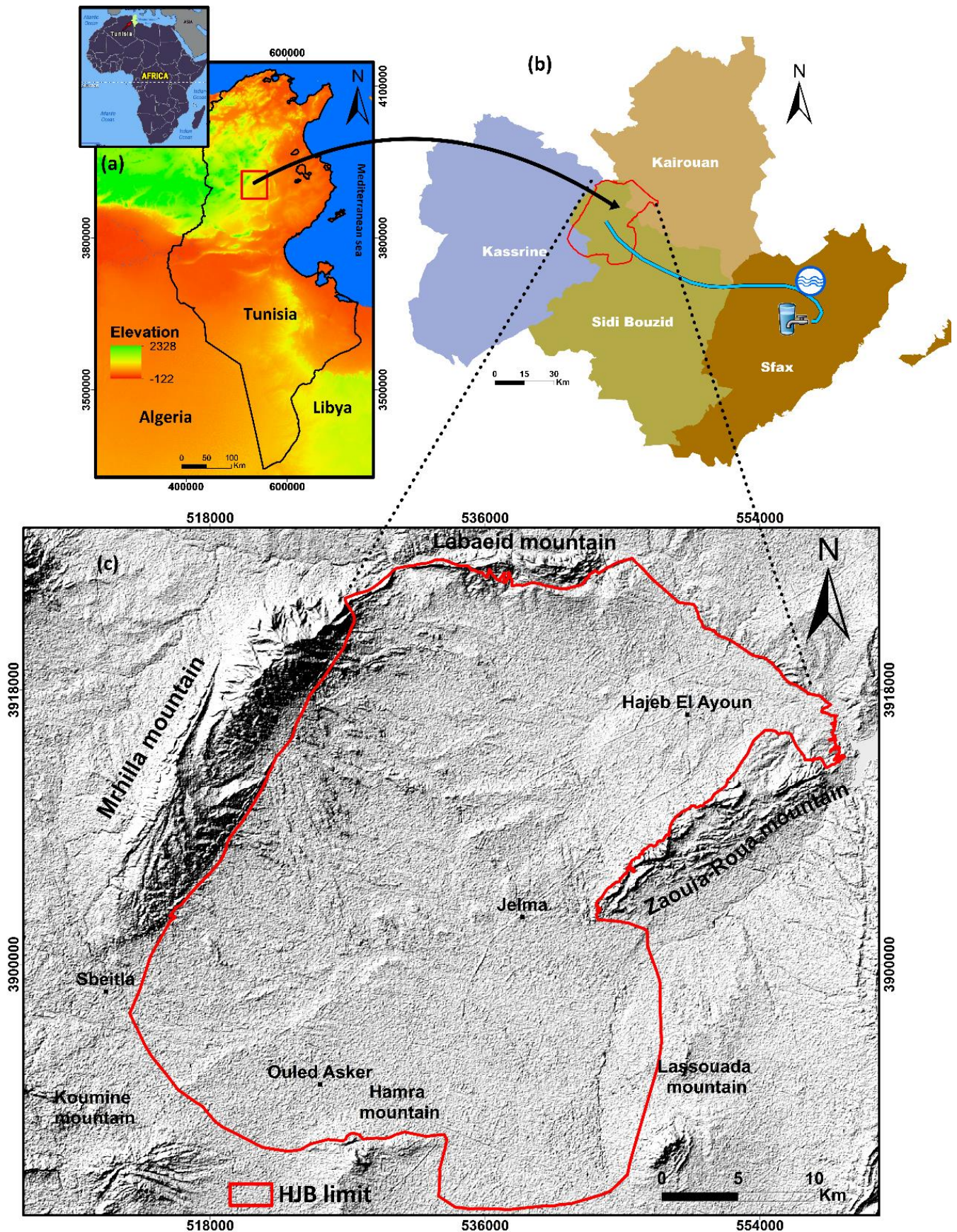


Figure 3. Geographic location of the study area (a) location of HJB in Tunisia (b) the governments occupied by HJB and (c) boundary of the HJB

II. Climatic setting

The climatic analysis is an essential step in the hydrogeological study since it presents a primordial component in the hydrological cycle. It is the source of water at an aquifer. The HJB is situated on the Tunisian steppes. The climatic components influence this study area; the North's temperate and the hot pre-saharan component at the south part. The climate component comprises various elements: the rainfall, the temperature and the evaporation, wind speed and relative humidity.

1. Rainfall

For this analysis, the data used are collected from seven rain gauge stations (Hajeb Layoun, Cebala, Negada, Oum Ladham, Jelma Her, Jelma Agro and Jbel Mrhilla) covered a period from 1968 to 2017 with daily measurement (DGRE 1968-2017). **Figure 4** shows the location of the seven rain gauge stations in HJB. The rainfall data of 50-year (**Appendix 1**) show some missing values caused by the technical problems (**Figure 5**). The measured values indicate an average of inter-annual rainfall in all the stations equal to 241.8 mm/year.

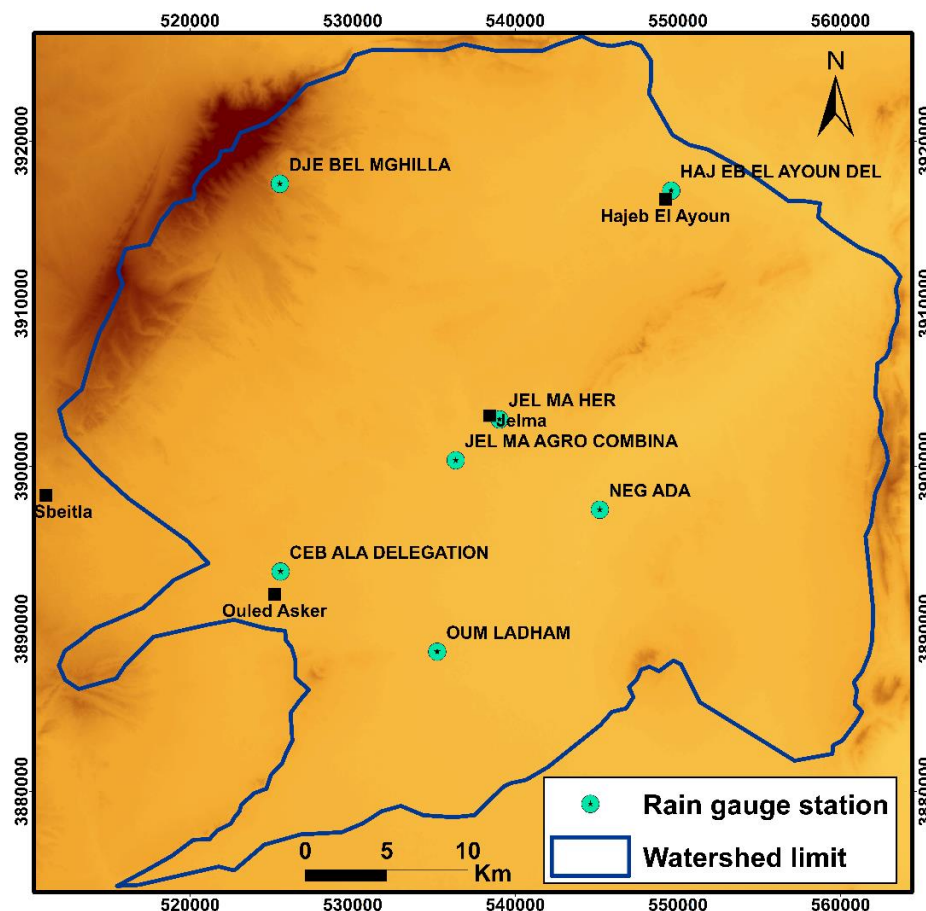


Figure 4. Location of the rain gauge stations in Hajeb Layoun-Jelma basin

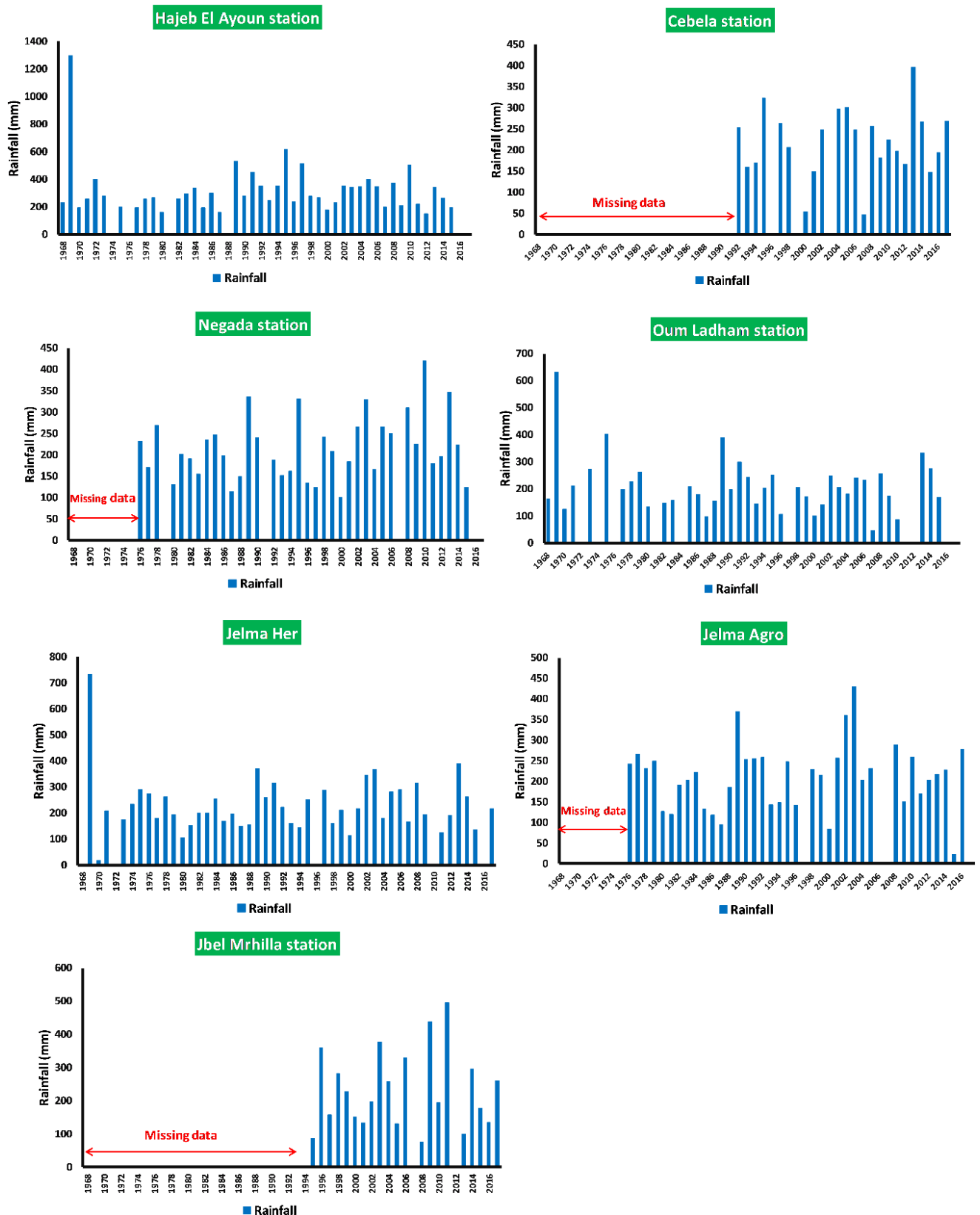


Figure 5. Annual rainfall (from 1968 to 2017) at the seven rain gauge stations in HJB

1.1 Yearly variation

The rainfall measured at the seven stations (**Figure 5**) was used to calculate the average annual precipitation (**Figure 6**). It shows an irregular general trend with an exceptional year (1969), which corresponds to flood events with an average yearly rainfall equal to 886.4 mm (**Figure 6**). For the other years, except the year 1969, the average annual rainfall fluctuates between a minimum of 110.3 mm and a maximum of 399.9 mm. As shown in **Figure 6**, the significant years in deficit, which indicate an annual rainfall less than the inter-annual average (241.8 mm), are 1970, 1980, 1987, 1993, 2000, 2007, and 2015 minimum rainfall equal to 110.3 mm registered in 1970. With rains more than the inter-annual average (241.8 mm), the primary surplus years are 1972, 1989 and 2003, with a maximum rainfall equal to 399.9 mm registered in 1972 (**Figure 6**).

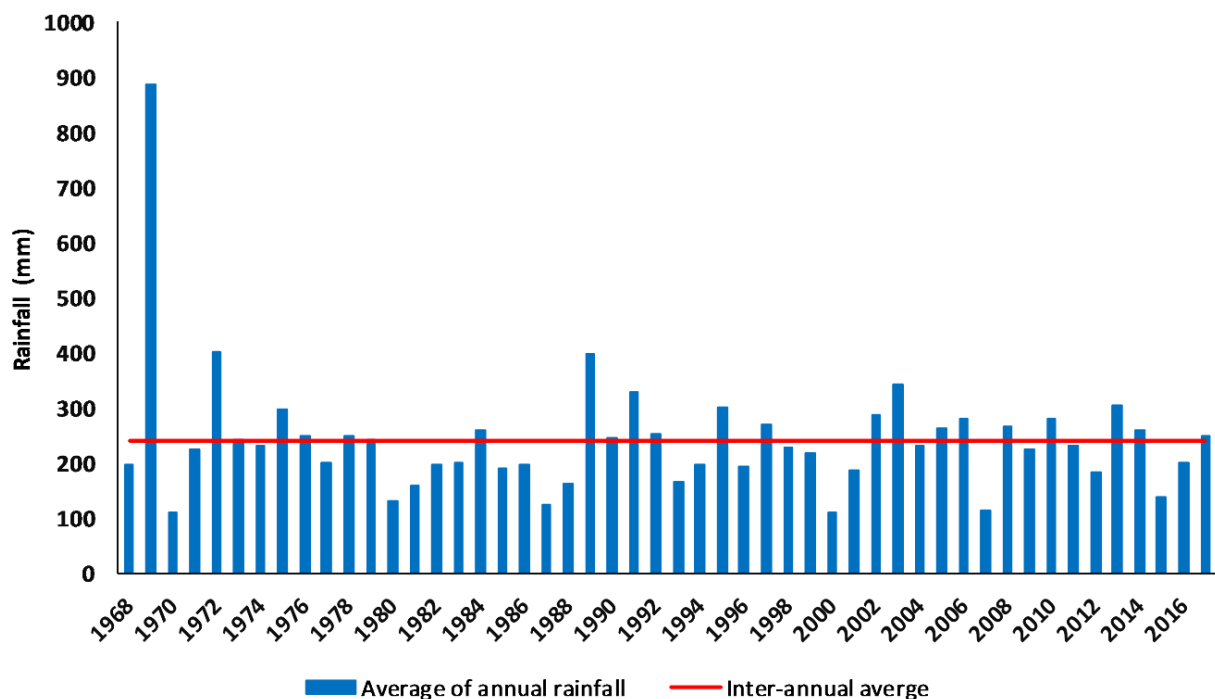


Figure 6. Average of annual rainfall (in mm) for the period 1968-2017 in HJB

1.2 Monthly variation

The monthly rainfall analysis of the seven rain gauge stations previously mentioned indicates that the monthly rain variation presents a decreased general trend from September to August. The month of November shows the rainier month with an average value of 66 mm (**Figure 7a**), and it presents 27% of the total average annual rainfall (**Figure 7b**). The lowest rainfall is shown in August with a value of 0 mm.

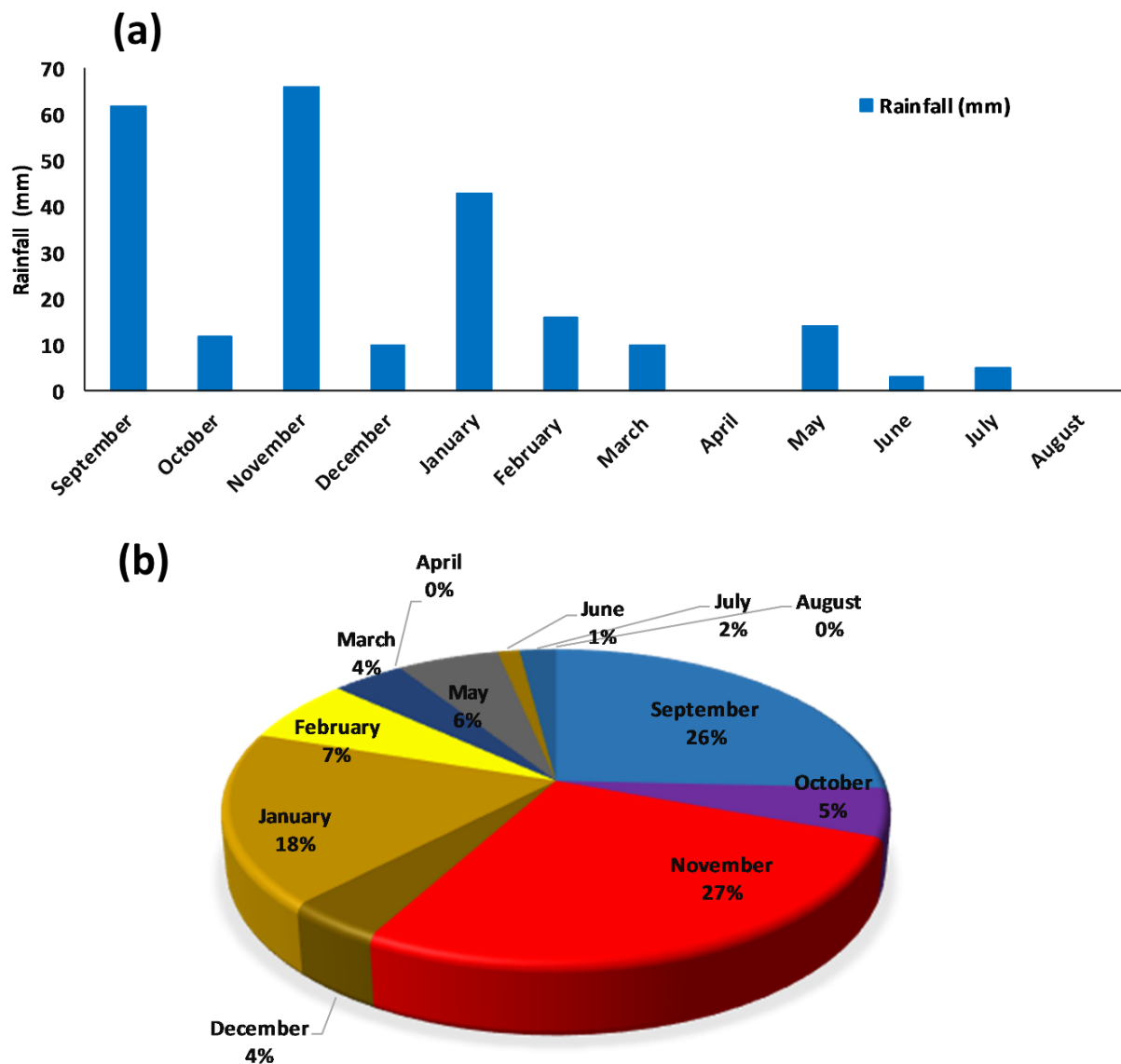


Figure 7. (a) Diagramme of the monthly rainfall in HJB (b) Pie chart of the monthly rainfall percentage in HJB

The standard deviation associated to these mean monthly values, from 1968 to 2017, indicates that the rainfall presents a mainly deviation of 15 mm from November to august (**Figure 8**). The month of September and October present the high deviation which the standard deviation of monthly rainfall indicate value of 43.36 and 71.88, respectively. These high values are due to the flood event which has been take place in 1969 with exceptual rainfall in September and October equal to 324.36 mm and 508.1 mm, respectively. The standard deviation associated to these mean monthly values, without take the year 1969 into consideration, indicate values in September and October equal to 11.72 mm and 6.22 mm, respectively.

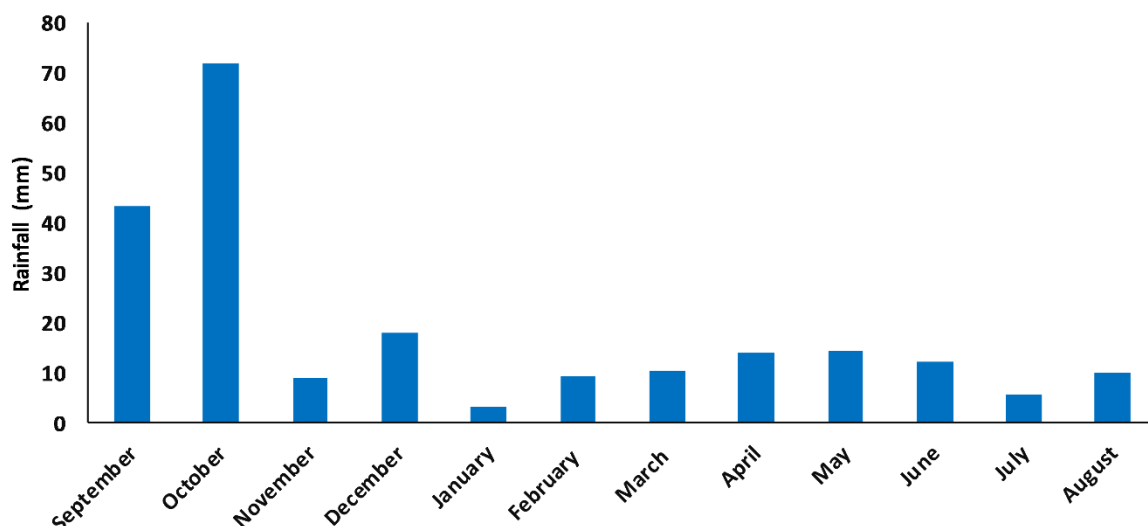


Figure 8 Diagramme of the Standard deviation of the mean monthly values rainfall in HJB

1.3 Seasonal variation

The analysis of seasonal rainfall of the seven rain gauge stations for the period from 1968 to 2017 is shown in the pie chart (Figure 9); it indicates that the rainiest season is the autumn (September, October and November) (58%) followed by the winter (December, January and February) with a percentage equal to 29%. The spring (March, April and May) is less rainy. It contributes to the annual rainfall by 10%. The summer (June, July and August) presents the low rainiest season with 3%.

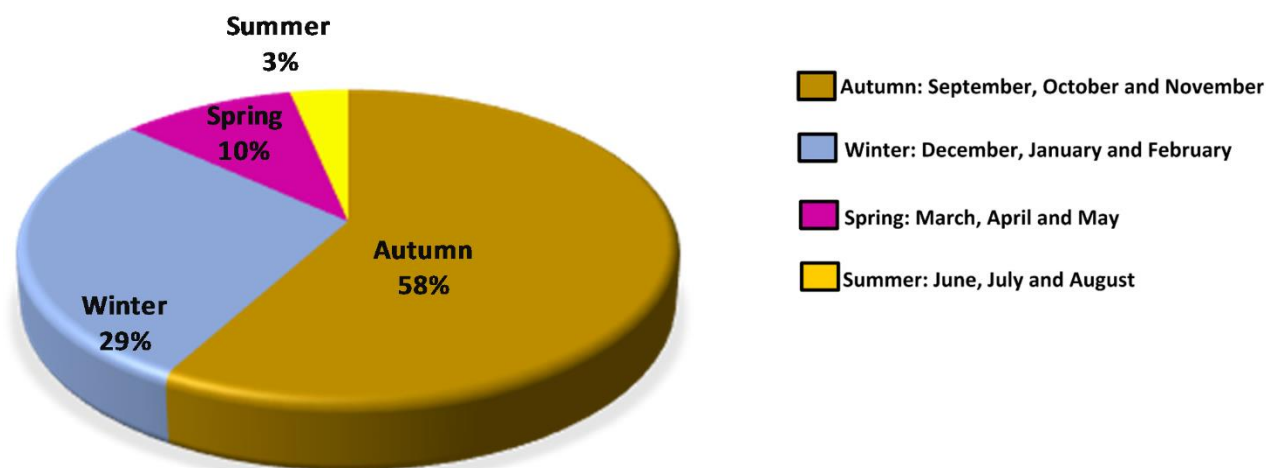


Figure 9. Repartition of seasonal rainfall in Hajeb Layoun-Jelma basin

1.1. Standardized precipitation index (SPI)

For showing the precipitation's yearly variation, we have used the standardized precipitation index (SPI) given by McKee et al. (1993) and defines the severity of the drought. The SPI is calculated as follow:

$$SPI = \frac{Xi - Xm}{Si} \quad (\text{Eq 1})$$

With Xi: cumulative rainfall

Xm: Average rainfall

Si: standard deviation

The SPI was classified according to table 1.

Table 1 Classification of the standardized precipitation index (SPI) (Mckee et al. 1993)

Range SPI	Class
SPI>2	Extremely wet
1.5 to 1.99	Very wet
1.0 to 1.49	Moderate wet
-0.99 to 0.99	Near normal
-1.0 to -1.49	Moderately dry
-1.5 to -1.99	Severely dry
<-2	Extremely dry

The SPI was calculated for the seven rain gauge stations of Hajeb Layoun-Jelma basin for 50 years (from 1968 to 2017). In the period 1968-2017, most years are characterized by “Near normal class “, with $-0.99 < SPI < 0.99$. The year 1969, which corresponds to a flood event (annual rainfall equal to 886.4 mm), indicates $SPI > 2$, showing an extremely wet class. As show in **Figure 10**; the major surplus years indicate a “very wet” to “Moderate wet” class. The main years in deficit, with rainfall less than the inter-annual average, indicate a “moderately dry” to “extremely dry” class (**Figure 10**).

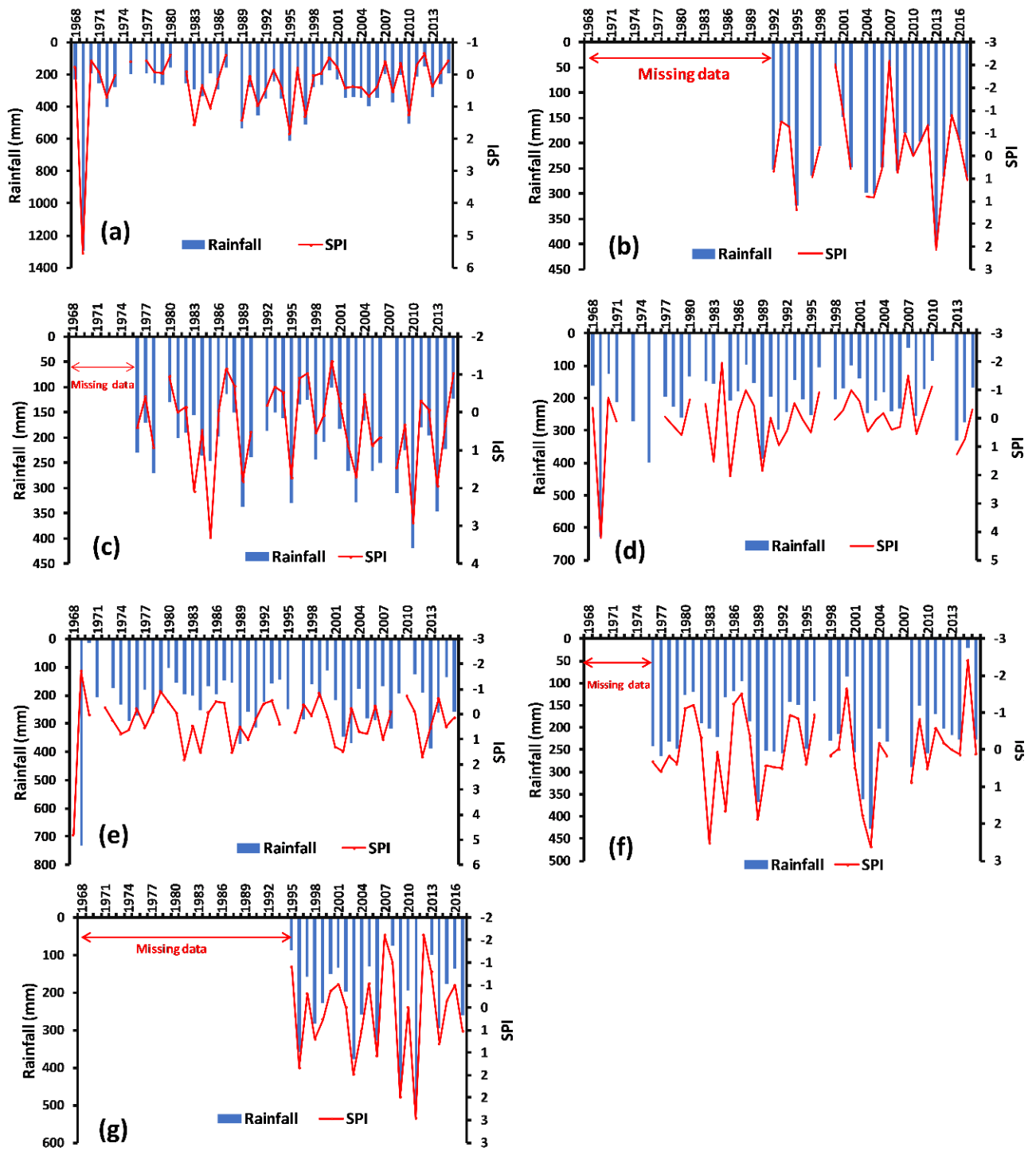


Figure 10. The standardized precipitation index (SPI) at the seven rain gauge stations in HJB: (a) Hajeb Layoun, (b) Cebala, (c) Negada, (d) Oum Ladham, (e) Jelma Her, (f) Jelma Agro, and (g) Jbel Mrhilla

2. Temperature

The temporal variation in temperature depends on latitude, altitude, terrain, vegetation, etc. These factors influence the daily, monthly or annual thermal amplitudes.

The temperature in the Hajeb Layoun Jelma basin is based on monthly data collected from INM at three stations (Kairouan, Sidi Bouzid and Sbeitla) covered a period from 1972 to 2016.

Figure 11 shows an apparent spatial variation in temperature between the different regions, materialized by a decrease in temperature from North to South. Low values are recorded in Sbeitla (extreme South-West), and high temperatures characterize the neighboring areas of Kairouan (extreme North-Est) and Sidi Bouzid. The thermal regime, in the entire study area, shows an alternation of two seasons with strong contrasts, the month of January and December record the low-temperature values (8 to 13°C) while June, July and August have high values (27 to 30°C) (INM 1972-2016).

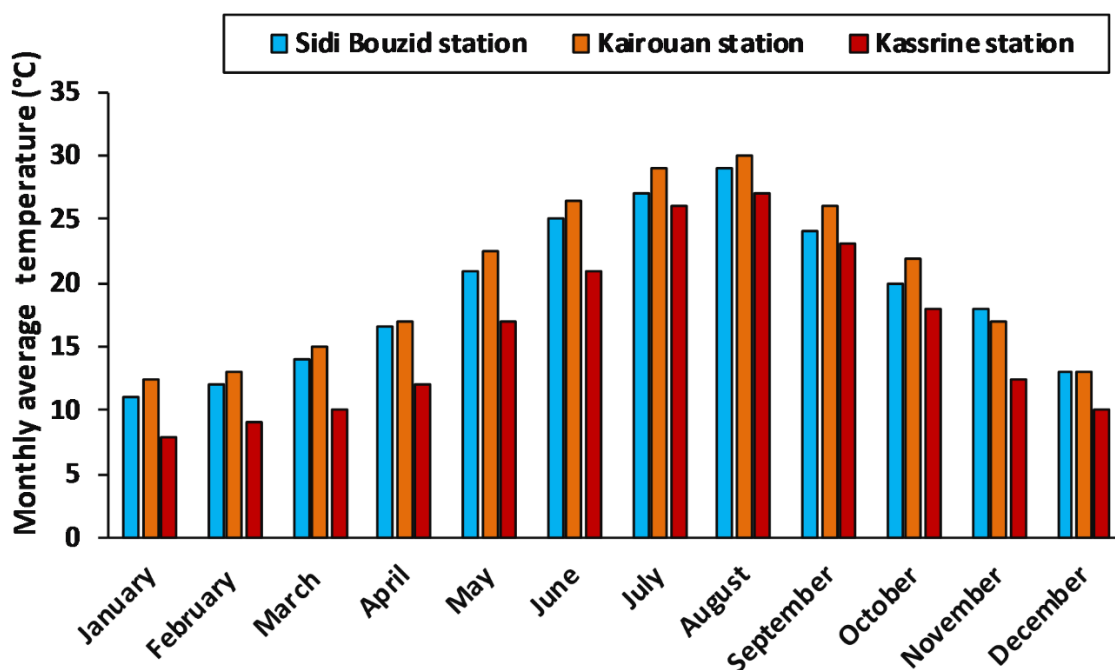


Figure 11. Monthly average temperature (°C) during the period (1972-2016)

3. Humidity

The air's relative humidity, commonly noted ϕ , corresponds to the ratio of the partial pressure of the water vapour contained in the air to the saturated vapour pressure at the same temperature. Relative humidity depends primarily on-air temperature, atmospheric pressure and continentality. It increases during thunderstorms and falls abruptly under the effect of Sirocco (Saidi 2006; Smida 2008).

Based on averages of the two stations (Sidi Bouzid and Kairouan) for the period 1972-2016, this climate parameter is highly variable in space and time (**Figure 12**). Indeed, the wet

period (RH more than 50%) extends over nine months of the year between September and May. July is the driest month with a rate of 47%.

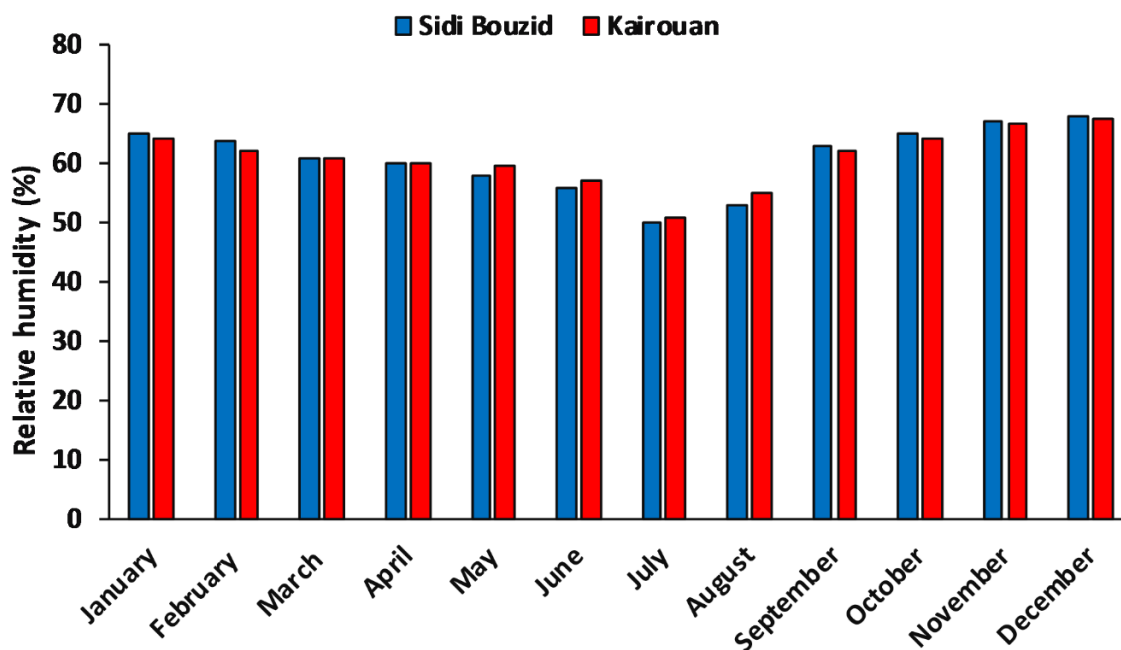


Figure 12. Monthly average humidity (%) for 45 years (INM 1972-2016)

4. Wind speed

The HJB is fairly windy, with the wind blowing most frequently from the North, North-West, and South-West. This wind is characterized by both speed and frequency. It increases in winter and spring and decreases in summer (Figure 13). The warm and dry winds are from the South, with an average of 30-40 days/year (INM 1972-2016).

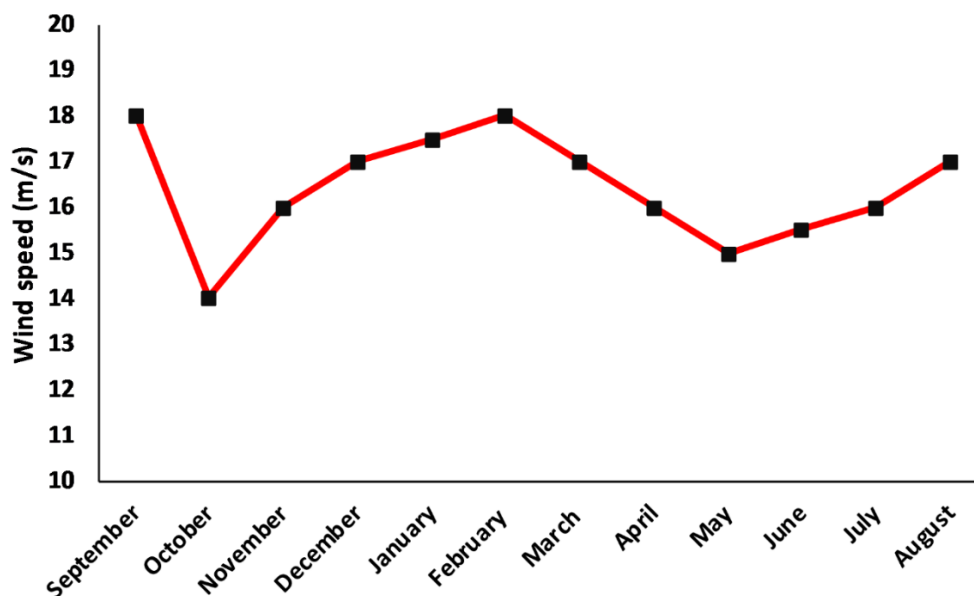


Figure 13. Monthly average of wind speed in HJB (INM 1972-2016)

5. Evaporation

The evaporation (Etp) constitutes a complex climatic component. It depends on several parameters : the thermohygrometric context (air temperature, relative humidity), the insolation and factors relating to the soil-plant system (the type of plant, the extension of the evaporation surface, the rate of plant cover) (Dassi [2004](#); Smida [2008](#)).

In the Hajeb Layoun-Jelma basin, the Etp values measurements were made using the sheltered evaporimeter instrument (“*Piche*” type). During the 1972-2016 period, the measurements carried out show an irregularity in the variation of the evaporation rate (INM [1972-2016](#)) with an interannual average of 1577 mm in the Sidi Bouzid station and 1450 mm in Kairouan station ([Figure 14](#)). For the Sidi Bouzid station, the average monthly variations recorded a minimum of 94 mm in November and a maximum of 186 mm in August. For the Kairouan station, the month of January recorded a minimum of 56 mm and the month of July records a maximum of 254 mm.

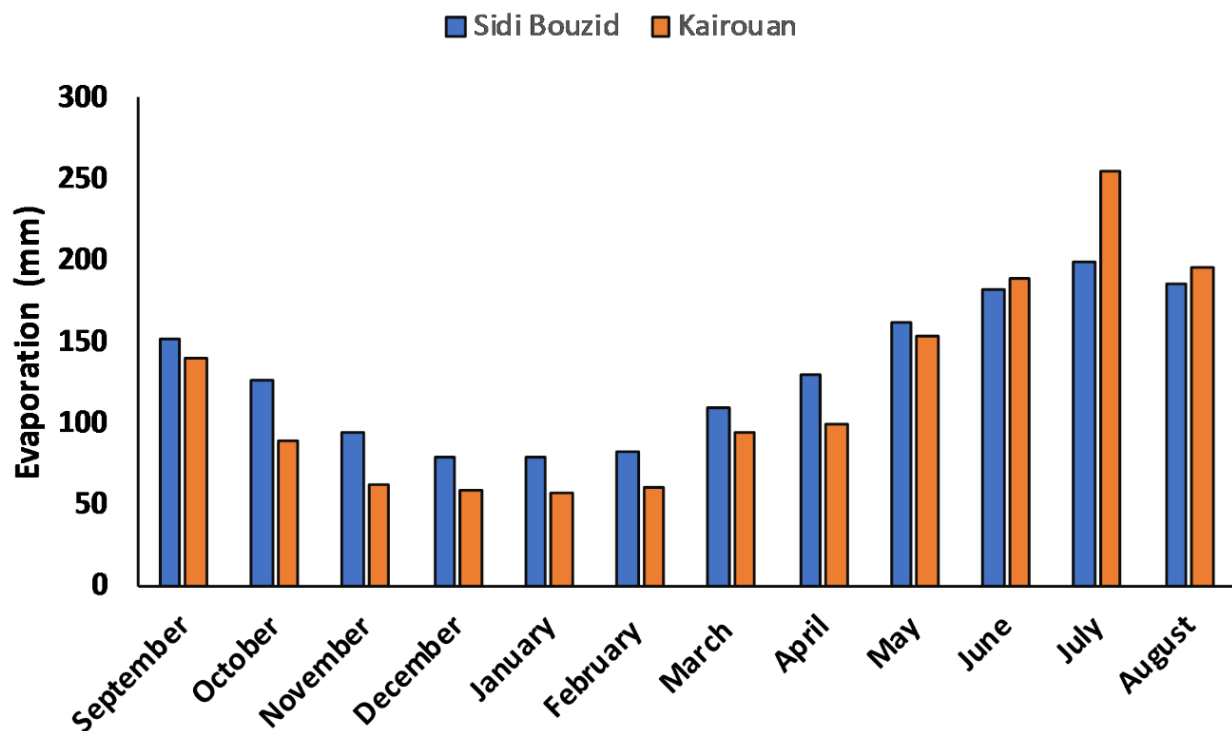


Figure 14. Monthly evaporation (mm) during the period (1972-2016)

6. Insolation

Insolation is the major component of climate; air temperature, moisture and evaporation at the soil surface are all influenced by global radiation (Dassi [2004](#)). The duration of the insolation depends on the variable orbital parameters and the cyclic activity of the Sun.

Insolation varies according to the Earth's latitude, depending on the Earth's sphere. Factors that reduce insolation include cloudiness, brown, fog and dust (Dassi 2004).

The Hajeb Layoun Jelma basin is characterized by a maximum of 340 hours during July; the minimum of insolation is measured during December with 195 hours in the station of Sidi Bouzid (Figure 15).

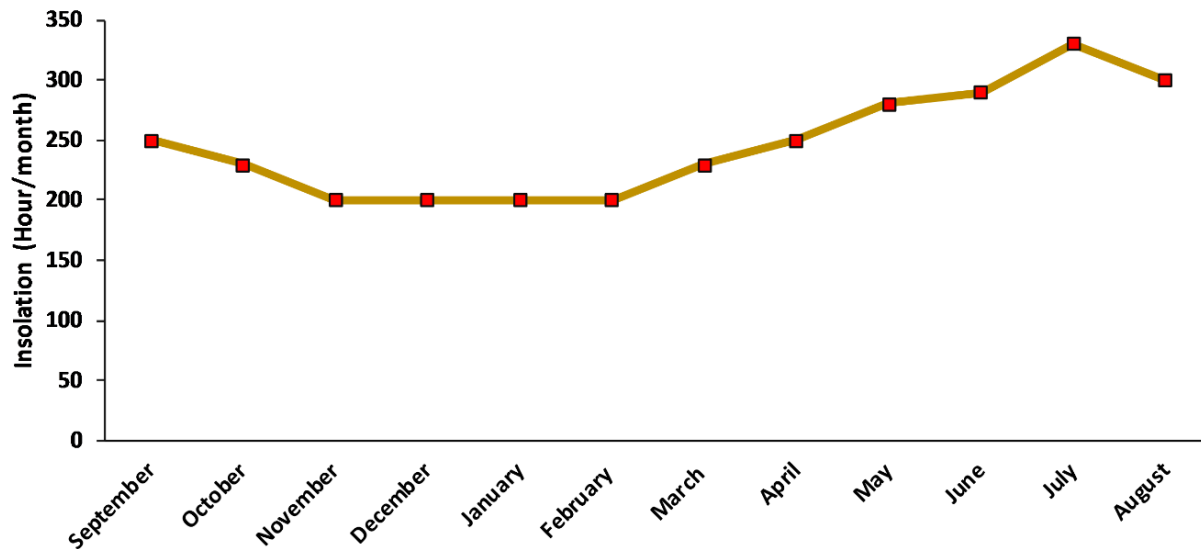


Figure 15. Monthly average of insolation (hour/month)

7. Bioclimatic zone

Emberger's bioclimatic index (Emberger 1955) was used to identify the Hajeb Layoun-Jelma basin's bioclimatic zone. The Emberger's bioclimatic index is calculated using the following formula:

$$Q = 2000 \times \frac{P}{M^2 - m^2} \quad (\text{Eq 2})$$

With P: Average annual rainfall (in mm)

M: Average of maximums temperature of the hottest month (in kelvin)

m: Average of minimums temperature of the coldest month (in kelvin)

The calculated Emberger's index, for the Hajeb Layoun-Jelma, is equal to 50.1. After projection, in the Emberger's climatogram, the classification indicates that the Hajeb Layoun-Jelma basin is characterized by a « Lower semi-arid climate » (Figure 16).

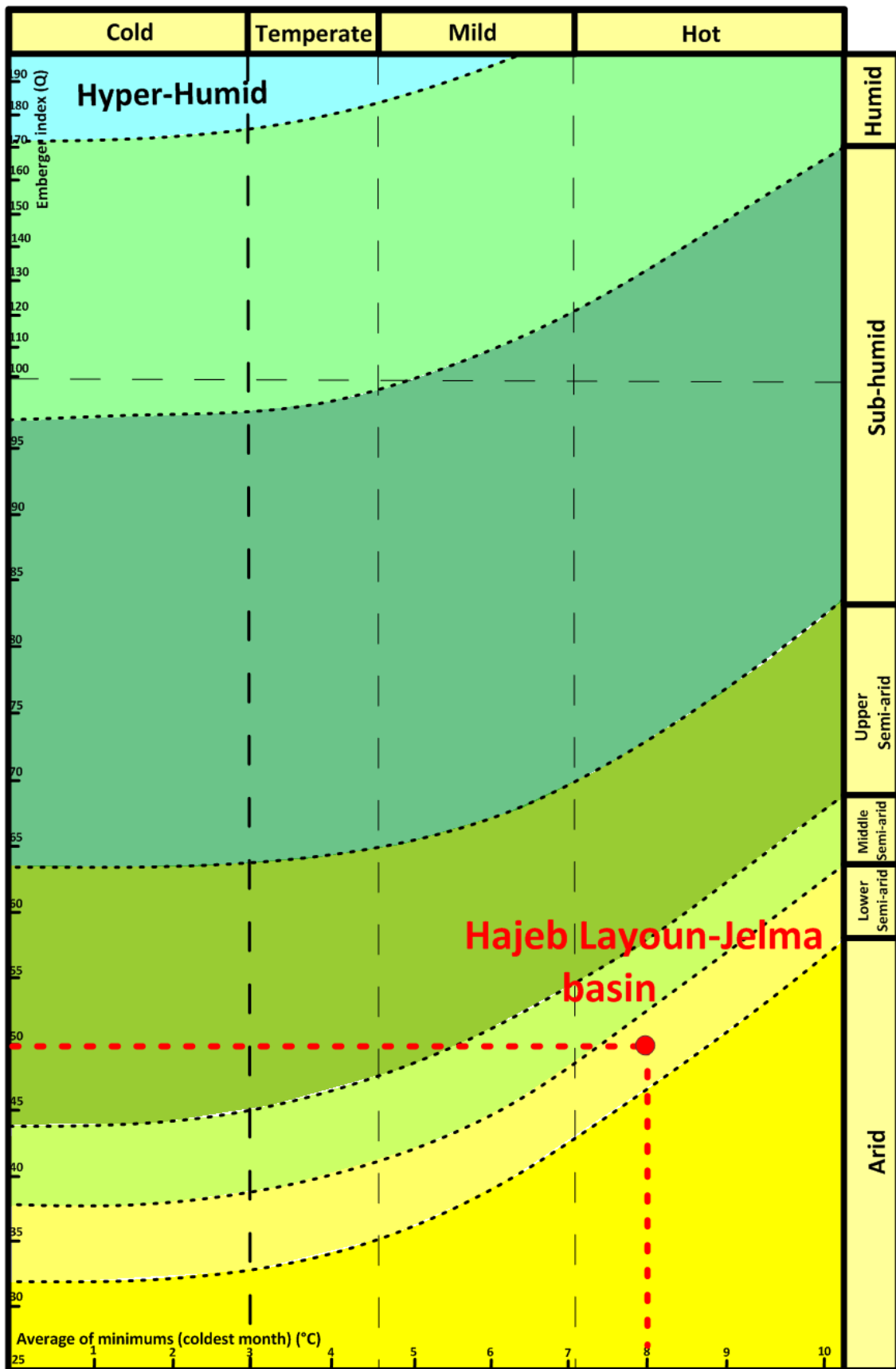


Figure 16. Emberger's climatogram for Hajeb Layoun-Jelma basin

III. Hypsometry and geomorphology

1. Digital Elevation Model (DEM)

The Hajeb Layoun Jelma basin's surface elevation varies from 234 m to 1384 m in Mrhilla mountain. The majority of the study area is at an altitude between 234 to 700 m (Figure 17).

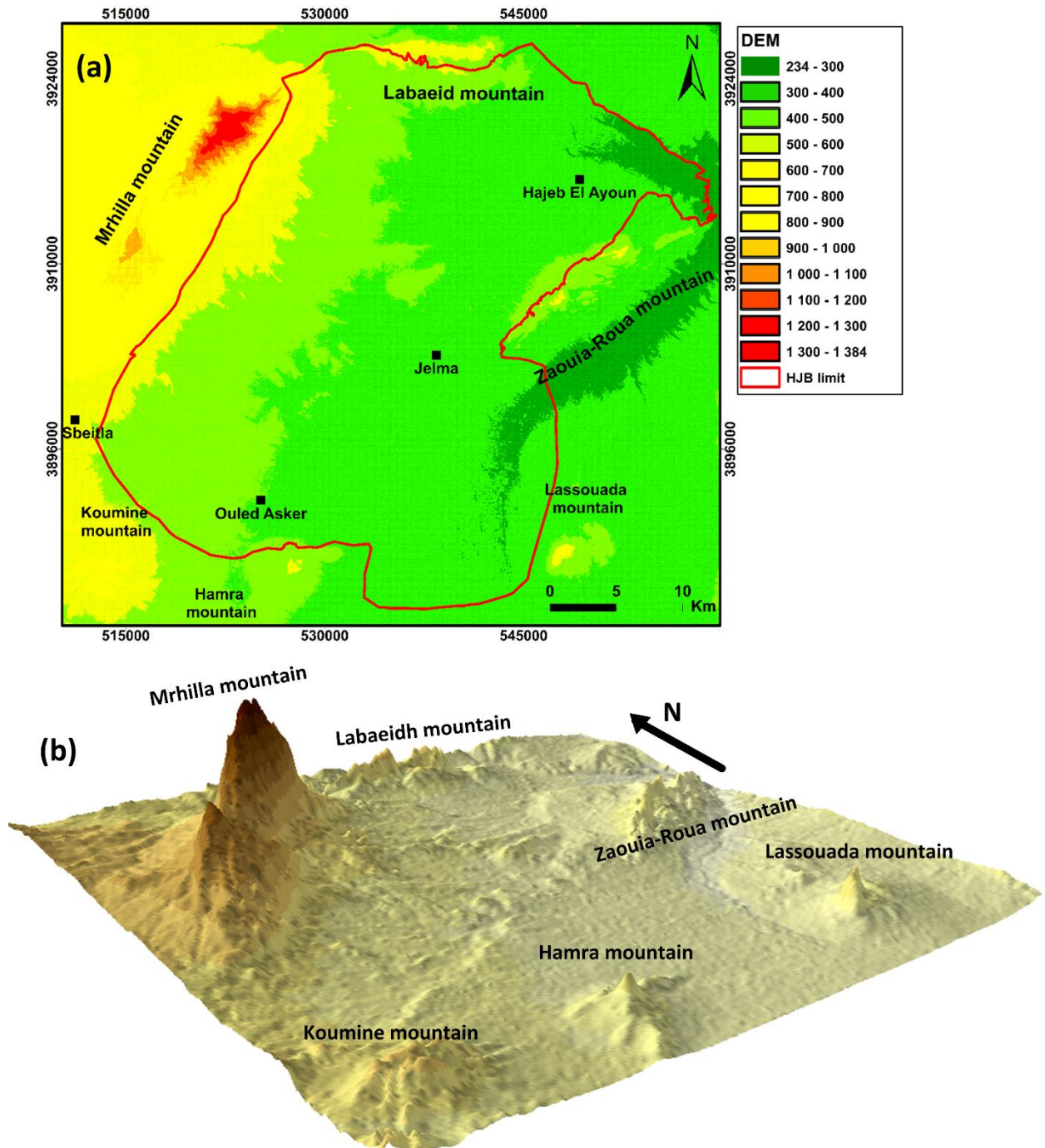


Figure 17. (a) DEM of the study area (b) 3d view of the study area

2. Hillshade

The hillshade map is a useful tool to visualize the study area's geomorphology aspect. The hillshade map of the Hajeb Layoun Jelma basin (**Figure 18**) was derived from the DEM map using ArcGIS software. The created shading patterns help us to discern both elevation and form.

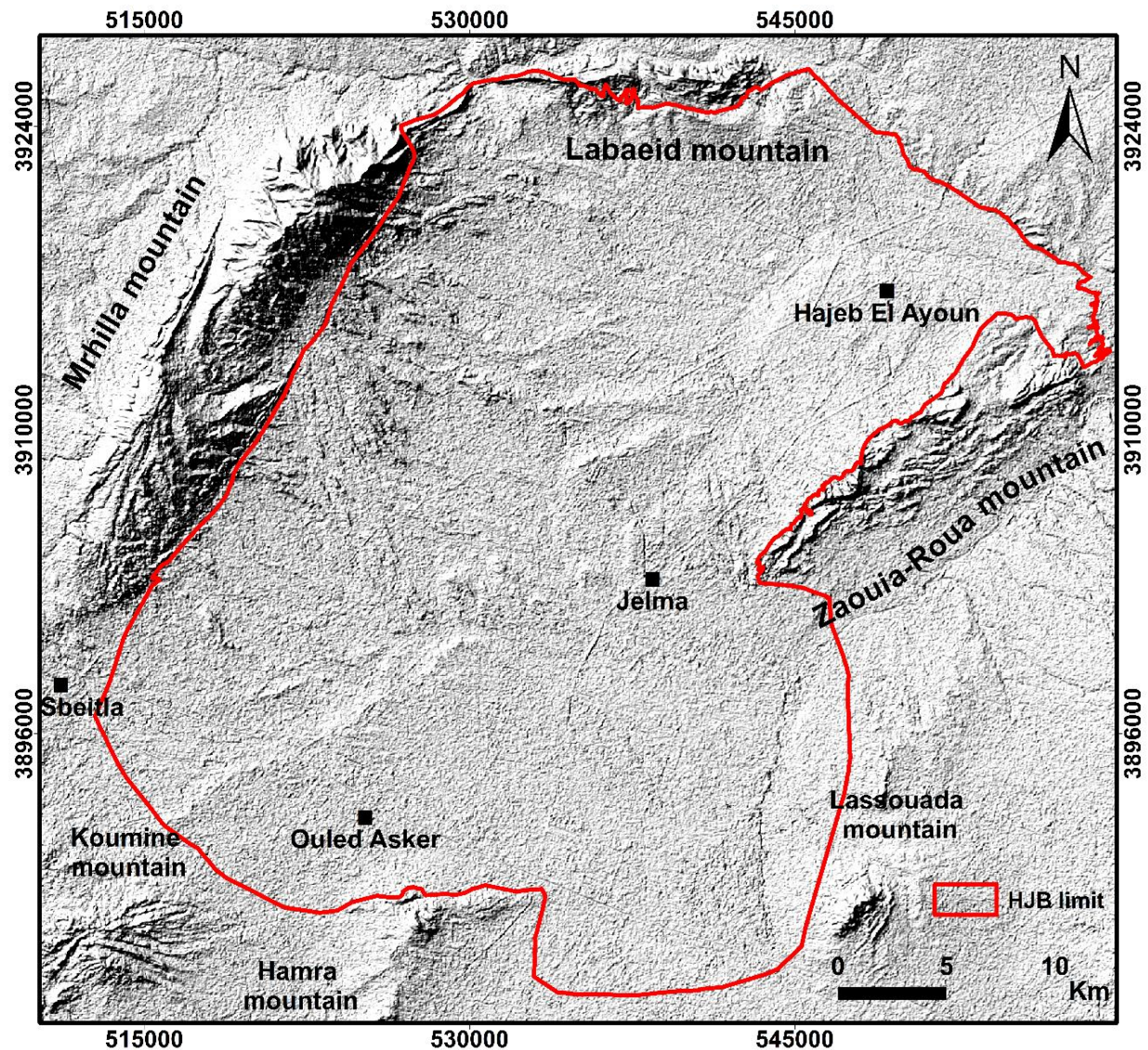


Figure 18. Hillshade map of the study area

3. Slope

The slope map of the Hajeb Layoun Jelma basin was derived from DEM using ArcGIS software. The study area contains different relief types; we distinguish mountains with a slope of more than 25° , the syncline of HJB is characterized by a slope between 0 and 5° . The study area has about 90% with a slope of less than 5° (**Figure 19**).

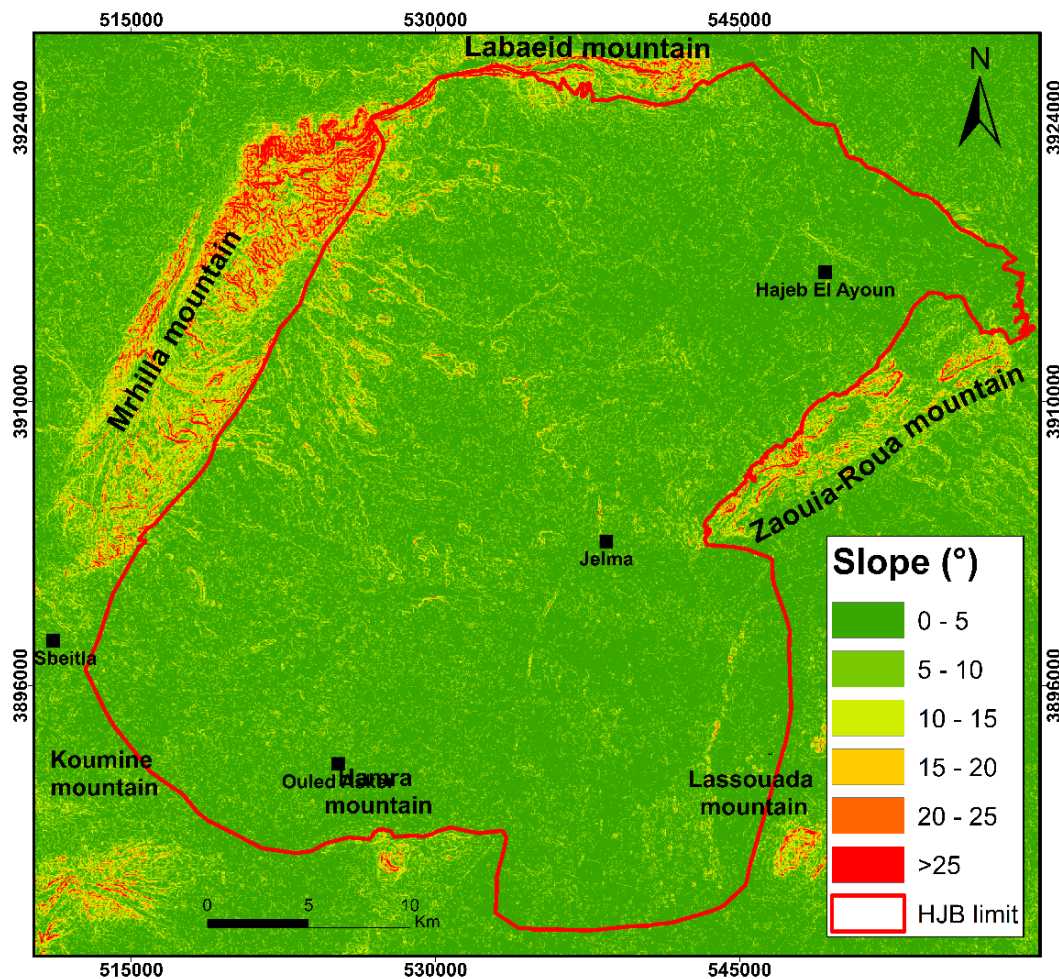


Figure 19. Slope map of the study area

IV. Hydrological characterization

1. Hydrological network

The Hajeb Layoun-Jelma basin is characterized by a very dense hydrographical network formed by a first-order network grouping the main rivers such as the Sbeitla river, Zerga river and Zéroud river (Figure 20). This main network is supplied by a second-order network formed by ravines and secondary rivers descending from the region's main mountains (Figure 20). At the northern part of the basin, we can see the El Htab river, which extends over 100 km in length and drains an area of 2900 km². It arises from the Zéroud river and gives rise to several tributaries. The most important tributary is that of the Zerga river, formed of several fan-shaped branches (El Oglâ, Dhissa, Lisilia, etc.). It covers an area of 260 km² and drains the southern flank of Labaeid mountain and the northern part of Mghilla mountain. As for the south branch of the basin, it is more spread out than the northern one. We distinguish the Sbeitla river as the main river draining an area of 260 km².

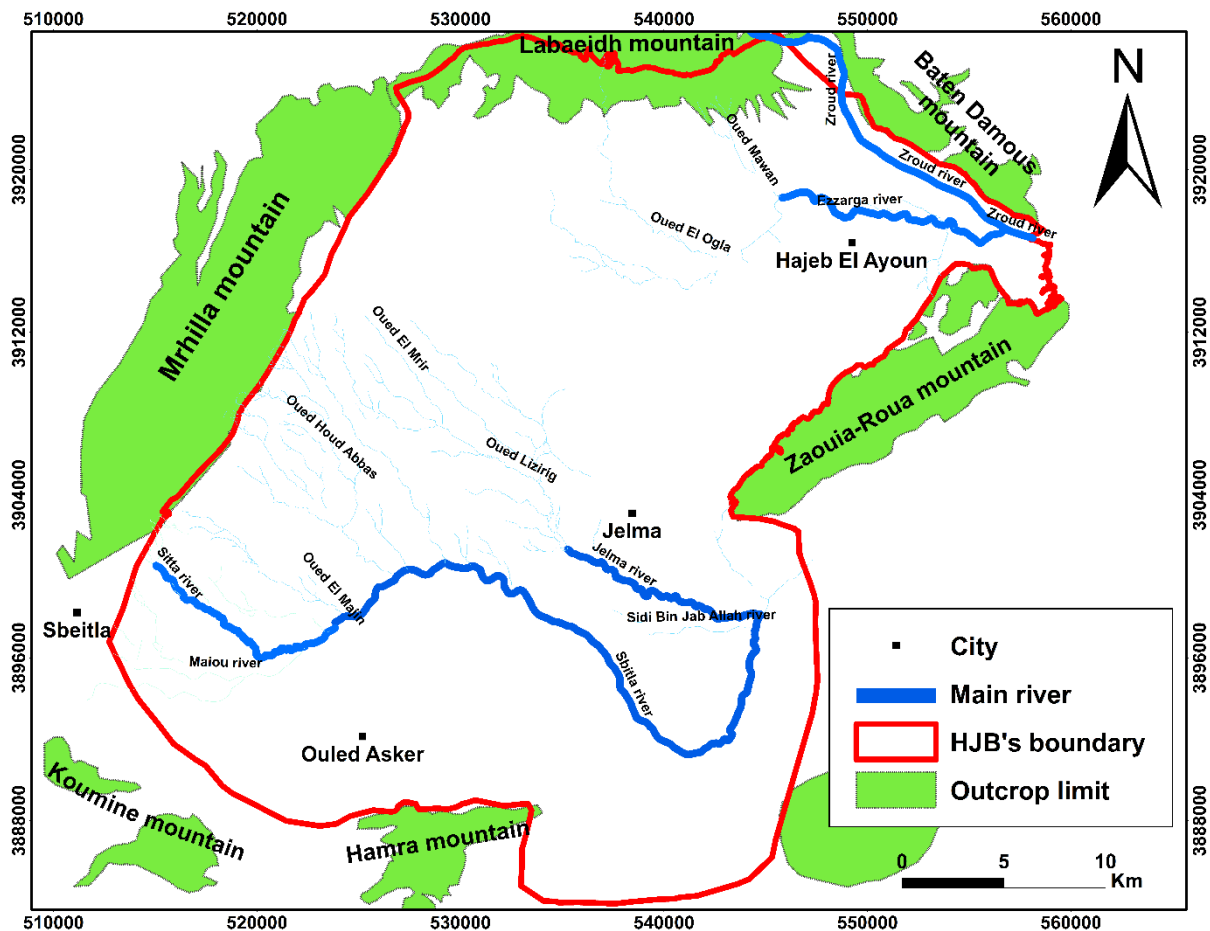


Figure 20. The hydrological network of the study area

2. Runoff

In central Tunisia, groundwater recharge is linked to the concentration of rainfall in the hydrographic network. The runoff threshold depends on several factors and varies with the season, soil moisture and downpours intensity. In the study area, runoff is triggered by rainfall more significant than 8 mm / h in winter and spring, greater than 15 mm / h in summer and autumn. (Koschel 1980).

The runoff was calculated by the D.G.R.E formula gives a runoff value equal to 6.5 mm/year.

The D.G.R.E formula is as follow:

$$Lr = 3.63 \times 10^{-6} (P)^{2.65} \quad (\text{Eq 3})$$

Where P is the annual rainfall (mm) and *Lris* the runoff (mm/year)

V. Soil description

The soil type of an area indicates the groundwater holding capacity and infiltration. The

study area is mainly underlined by sand, Sandy loam, clay sand, loamy sand, Clay loam and clay. **Figure 21** shows that a significant part of the study area is covered by clay loam (743 km²), which indicates a moderate potentiality of groundwater recharge.

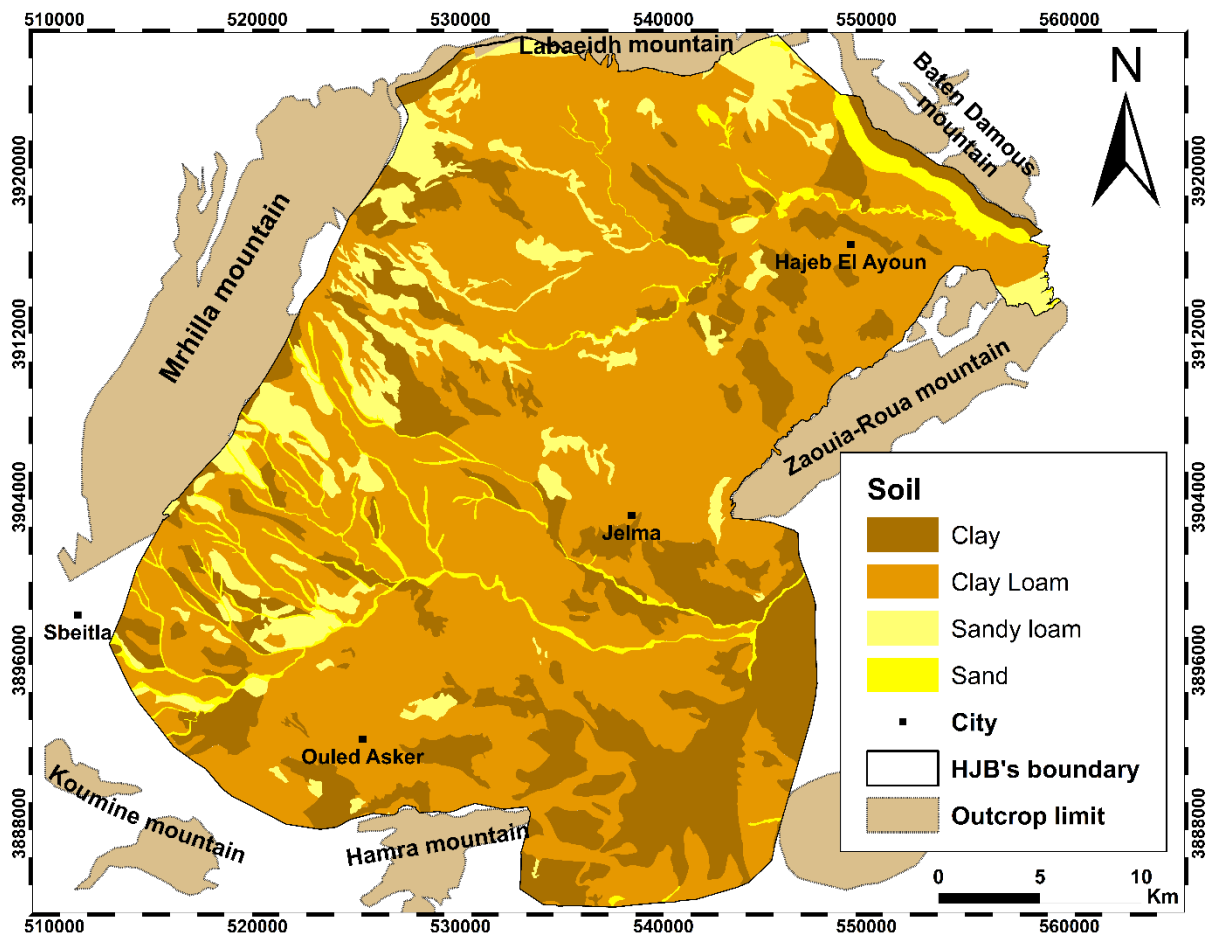


Figure 21. Soil map of Hajeb Layoun Jelma basin

VI. Land use description

The land use/land cover (LU/LC) map of Hajeb Layoun-Jelma basin, published by DGRE in 2004, shows that the primary type of agriculture is the irrigated and non-irrigated annual crops of olive (**Figure 22**), these types of crops need high amounts of water with the use of huge quantities of fertilizers as well as to increase production, which influences on groundwater quality. Urban areas are also a potential source of pollution, in fact the non-treated sewage rejected, by the ONAS (National Sanitation Office), in the natural environment of Hajeb Layoun-Jelma basin, which is estimated to an average of 400 m³ by day (DGRE 2017), can have a long-term influence on groundwater resources.

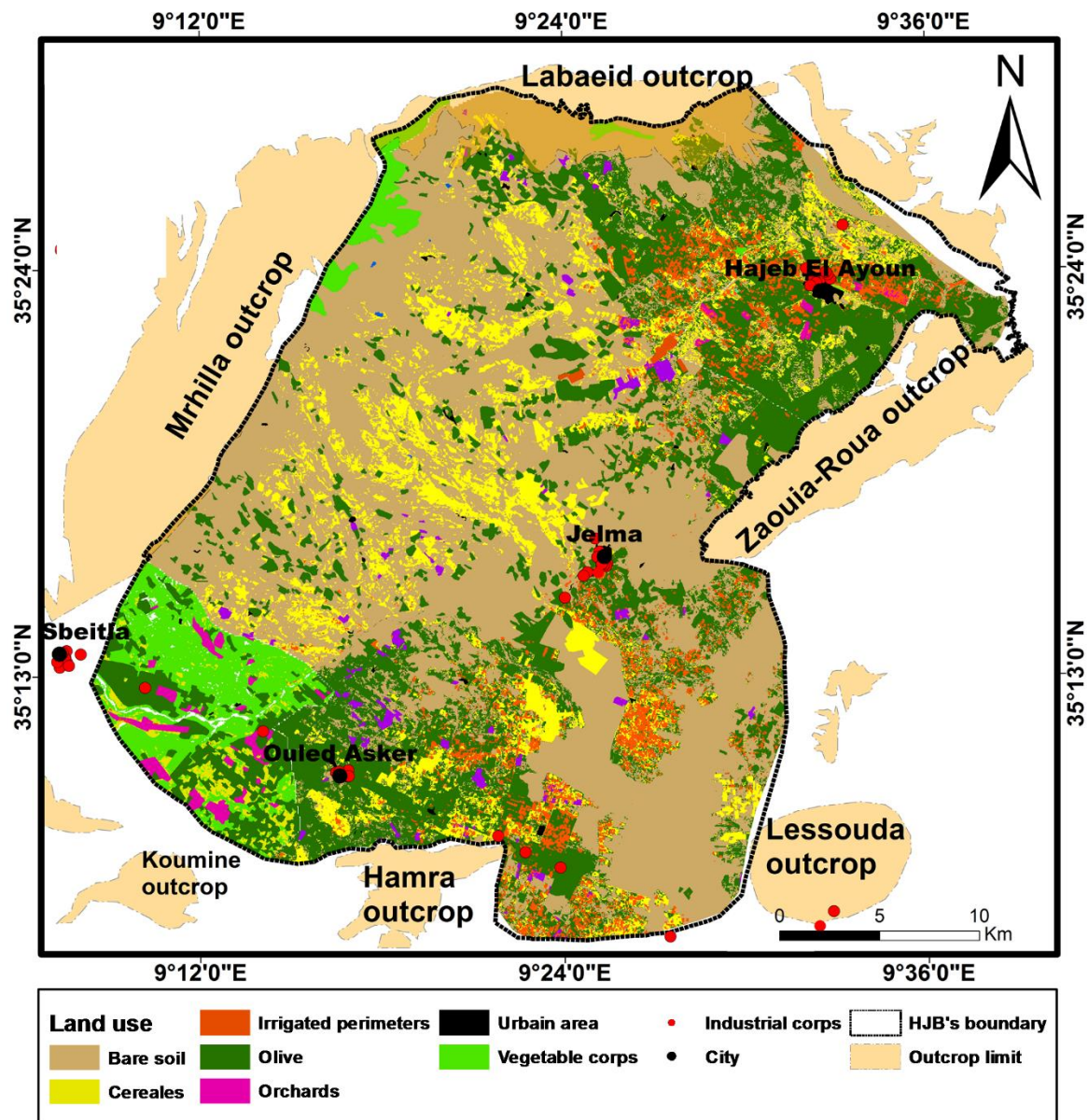


Figure 22. Land use map of HJB extracted from the agriculture map obtained from Regional Direction of Agriculture Development of Sidi bouzid (CRDA-Sidi bouzid)

VII. Population evolution

The HJB has about 172.003 inhabitants (INS [2014](#)), which corresponds to approximately 1.54% of the Tunisian population and which was 50,306 inhabitants in 1972 (Koschel [1980](#)). The population growth (more than three times) plays a strong effect on the water request and has a significant impact on water resources.

Chapter II: Geological and structural setting

I. Introduction

The convergence of the African Plate and the Eurasian plate gives rise to compressive stresses leading to the formation of the Maghrebids at the North and the Atlas chain at the South. The Tunisian Atlas is the eastern extension of the Atlas chain which stretches from Morocco to Tunisia. The Atlas zone constitutes the alpine edge of the African continent. The South Atlas accident, which extends over 2000 km from Agadir to Gabes, separate the Atlas chain from the Saharan platform.

Tunisia is composed of different structural zones (**Figure 23**) distinguished by their lithological and structural proprieties:

- ✚ **The Tellian domain** is characterized by the allochthonous units (thrust sheets) formed by the Numidian unit and Tellian units and individualized para-autochthonous units at the front of the thrust sheets defining an area dominated by characteristic clay series deposits of the Tunisian furrow type.
- ✚ **The Atlas domain** occupies the majority part of Tunisia. It forms the extension of the Algerian Saharan Atlas (Zargouni **1985**) and ends at the North-South axis level. We distinguish from North to South:
 - **The Northern Atlas**: Folds structures of NE-SW directions form it. Two main accidents of kilometers across this domain: Teboursouk-El Alia accident and Zaghouan fault (Turki **1985**).
 - **The Central Atlas**: is formed by anticlines, elongated in a direction between N40 and N60, separated by wide synclines (Turki **1985**, Zouaghi **2008**). This structural domain is characterized by NW-SE trending Mio-Plio-Quaternary infill collapse (Chihi **1984**; Ben Ayed, **1986**; Chihi et Ben Ayed **1991**; Boukadi et Zargouni **1991**; Boukadi **1994**). Various geological investigation shows that most Atlas folds are associated with upward movements of salt (Zargouni **1985**; Ben Ayed **1986**; Boukadi **1994**; Bédir **1995**; Zouari **1995**).
 - **The Southern Atlas**: Folds characterize this zone with E-W direction and shear corridors delimited by accidents of direction from E-W to N140 (Bouaziz **1995**).
- ✚ **The North-South axis**: is a break in the basement that played out during the different tectogenic phases (Burrolet **1956**). This accident acted as a stopper against which the Atlas

folds collided. Several works have been interested in this morphostructural unit study to construct its chronostratigraphic history (Abbes 1983; Haller 1983; Ouali 1984; Boukadi 1994, Rabhi 1999; Abbes 2004; Ouali 2007; Zouaghi 2008). The East of the “North-South axis” is individualized by the “eastern platform” which marked by folds with a large radius of curvature, major faults in the same direction as the Atlas structures and grabens (Haller 1983; Touati 1985; Bédir 1995; Khomsi et al 2004).

- ✚ The Saharan platform: Is characterized by a landscape dominated by a tabular series with the collapse of the eastern block known as the Jeffara plain with a major fault in the N160 direction. Several angular unconformities in the geological series indicate an active geodynamic history (Bouaziz 1995).
- ✚ The pelagian block: It is a stable platform and slowly subsident during the Secondary. The facies, recognized by some boreholes, are of the open sea neritic type with a preponderance of carbonate sediments (Burolet and Byramjee 1974). On the other hand, during the Cenozoic, subsidence becomes more active and allows the accumulation of powerful series. Tectonic deformations recognized in depth by seismic data (Haller 1983; Bedir and Bobier 1987) have three major directions: N45, N100-120 and N160-180. These mobile zones, at several geological and tectonically complex epochs, delimit vast areas with little or no deformation.
- ❖ The Hajeb Layoun-Jelma basin located in the north-east central part of Tunisia and it, approximately, located between $x = 35^{\circ} 00' 00''$, $y = 8^{\circ} 30' 00''$, and $x = 35^{\circ} 30' 00''$, $y = 9^{\circ} 00' 00''$. It belongs to the Atlassic chain and precisely the “Central Atlas” (Figure 23). The HJB is a wide NE-SW directed syncline filled by Tertiary and Quaternary deposits closed by anticlines cored by Lower Cretaceous units (Koschel 1980; Castany 1982; El Ghali 1993; Boukadi 1994; Abbes 2004). It is bordered to the North by the Labaeith mountain, to the South by the Hamra mountain, to the East by the Zaouia-Roua mountain, to the West by the Mrhilla mountain, to south-east by the Lessouda mountain, and to the south-west by the Koumine mountain.

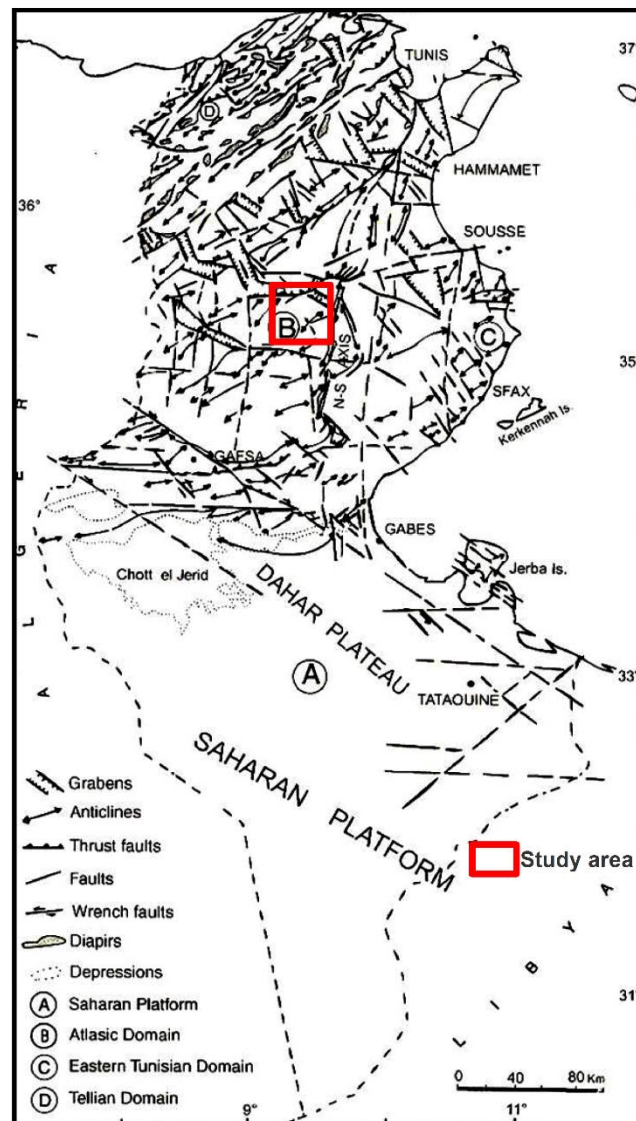


Figure 23. Structural zonation of Tunisia (Bouaziz et al.2002) and location of the study area

II. Geological setting

1. Geologic map

The geological map of the Hajeb Layoun Jelma basin (**Figure 24**) was created, using ArcGis, by the assembling of six geologic maps with scale 1/50.000 (Sbiba (Archamault et al. **1951**), Trozza (Ghali and Batik **1922**), Mghilla (Archamault et al. **1949**), Hajeb Layoun (Archamault et al. **1947**), Sbeitla (Kadri and Ben Haj Ali **1993**) and Lassouada (Matmati et al. **1992**) and the digitization of the different deposits.

The geological series in the HJB is from Triassic to Quaternary with the missing of the Jurassic series, outcrops delimiting the Hajeb Layoun Jelma basin were the subject of several studies (Burollet **1956** ; Khessibi **1978**; Gassara **1980**; Koschel **1980**; El Ghali **1993**; Amouri **1994**; Zouari **1998**; Ayadi **2002**; Abbes **2004**; Ouali **2007**; Zouaghi **2008** , etc.)

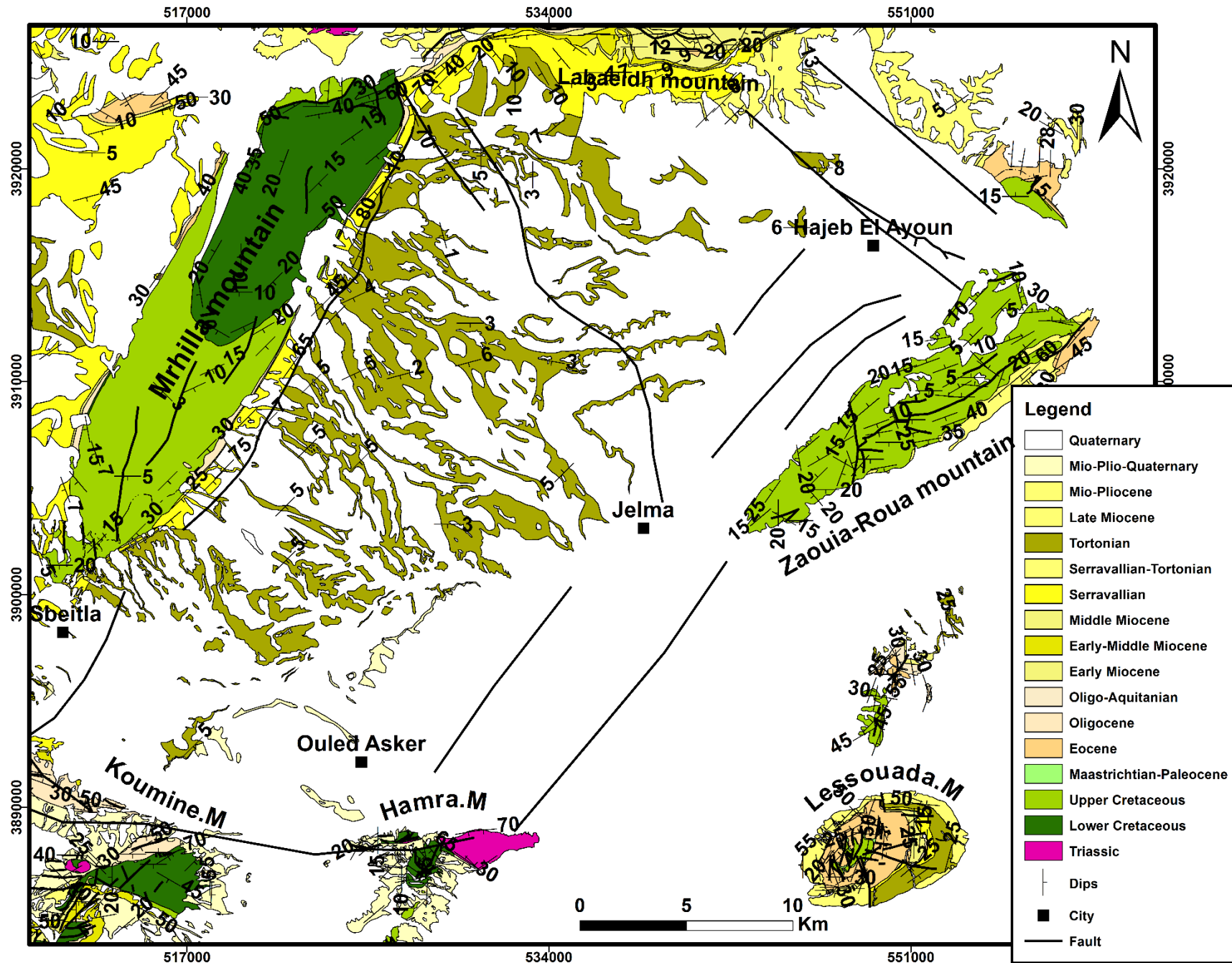


Figure 24. Geologic map of Hajeb Layoun-Jelma basin

2. Stratigraphy

2.1.Mesozoic

a. Triassic

The Triassic levels present the oldest deposits in the study area and also in all the central Tunisia. It is designed by the formation namely “*Rheouis*”. It is exposed at the surface, in HJB, in three locations: North of Mrhilla mountain (Kodiat El Halfa), Hamra and Labaeith mountains (Castany 1956). In central Tunisia, the Rheouis formation is composed by a huge evaporitic mass affected by various folds (Burolet 1956). The most significant Triassic deposits are manifested in the North of the study area (Kodiat El Halfa); it is composed by massive gypsum with rare beds of dolomites, dolomitic limestone in platelets, sandstones alternating with dolomite beds and green sandy clays (Castany 1956).

b. Jurassic

The previous stratigraphical works (Burolet 1956; Farhat 1978; Kessibi 1978; Gassara 1980; Koschel 1980; Mansouri 1980; Mamou 1981; Amouri 1994; Bédir 1995; Allouche 1997; Hajjem 1999; Ouda 2000; Abbes 2004; Dassi 2004; Tanfous 2007; Tanfous et al. 2010) demonstrated the missing of the Jurassic series in central Tunisia, except in the N-S axis. The Jurassic series coincides with the “*Nara*” formation (Burolet 1956). It shows a constant lithological composition formed by three layers: a marno-carbonate layer comprising between two dolomitic masses, corresponding to the three members (lower, middle and upper) of the Nara formation (Burolet 1956).

c. Cretaceous

The Jurassic-Cretaceous passage is included in the “*Sidi khalif*” formation (Burolet 1956). The Cretaceous deposits are widespread in the study area and throughout central Tunisia, located in the mega-anticlinal's core. The sedimentary distribution of Cretaceous deposits in Tunisia central and southern is marked by a lateral and vertical variation of the facies, associated with bevels and hiatuses, which are linked to erosion and /or non-deposits (Burolet 1956; Chihi 1984 1995; M'Rabet 1981; Zargouni 1985; Turki 1985; Ben Ayed 1986; Boukadi 1994; Bédir 1995; Zouari 1995; Bouaziz 1995; Dlala 1995; Rabhi 1999; Abbes 2004; Ouali 2007).

c.1. Early cretaceous

The early cretaceous is composed from the chotts to Kairouan (from the bottom to the top) by (Figure 25): (i) **Sidi Khalif Fm**, (ii) **Meloussi Fm**, (iii) **Boudinar Fm**, (iv) **Bouhedma Fm**, (v) **Sidi Yaïch** and **Orbata Fm** (it's equivalent: **Serdj Fm**).

The early cretaceous deposits in HJB is composed of the following formations:

- ✚ The “**Sidi Khalif**” formation (Tithonian-Berriasian) is located in Mghilla mountain. It is formed in the basal part by marl-carbonate sequences. In the top part, it is formed by gypsiferous clays and bioclastic limestones with sandstone intercalations (Bédir 1995; Abbes 2004).
- ✚ The “**Meloussi**” formation (Valanginian-Hauterivian) followed the Sidi Khalif formation without apparent discontinuity. It is an alternation of sandbanks, sandstone clays, dolomites or dolomitic limestones. It shows an average thickness of about 950 m at Jebel Mghilla (M'Rabet 1981; Zouaghi 2008).
- ✚ The “**Bouhedma**” formation (Late Hauterivian-Early Barremian) has an average thickness of 250 m at Mghilla mountain (Dassi 2004). M'Rabet (1981) has subdivided it into three terms: The lower term predominantly argillaceous with sandstone and carbonate levels of low thickness. The middle term consists of an alternation of limestones, dolomites, sandstones and clays and an upper-term carbonate.
- ✚ The “**Sidi Yaïch**” formation (middle Barremian) is formed of white sands. Its top part intercalates silty clays and limestones with an average thickness of between 30 and 120 m (Benzarti 2002).
- ✚ The “**Serdj**” formation (Aptian) is characterized in the Mghilla sector by alternating carbonates, dolomitic levels with sandstone intercalations and having average thicknesses of around 125 m (M'Rabet 1981; Zghal 1994; Benzarti 2002). The complete albian series appears only in the northern part of Mghilla mountain and more precisely in the Koudiat El Beida region. It is presented as thickened series with about 1400 m and a succession of limestone beds and clayey marls (Jallalia 2015).

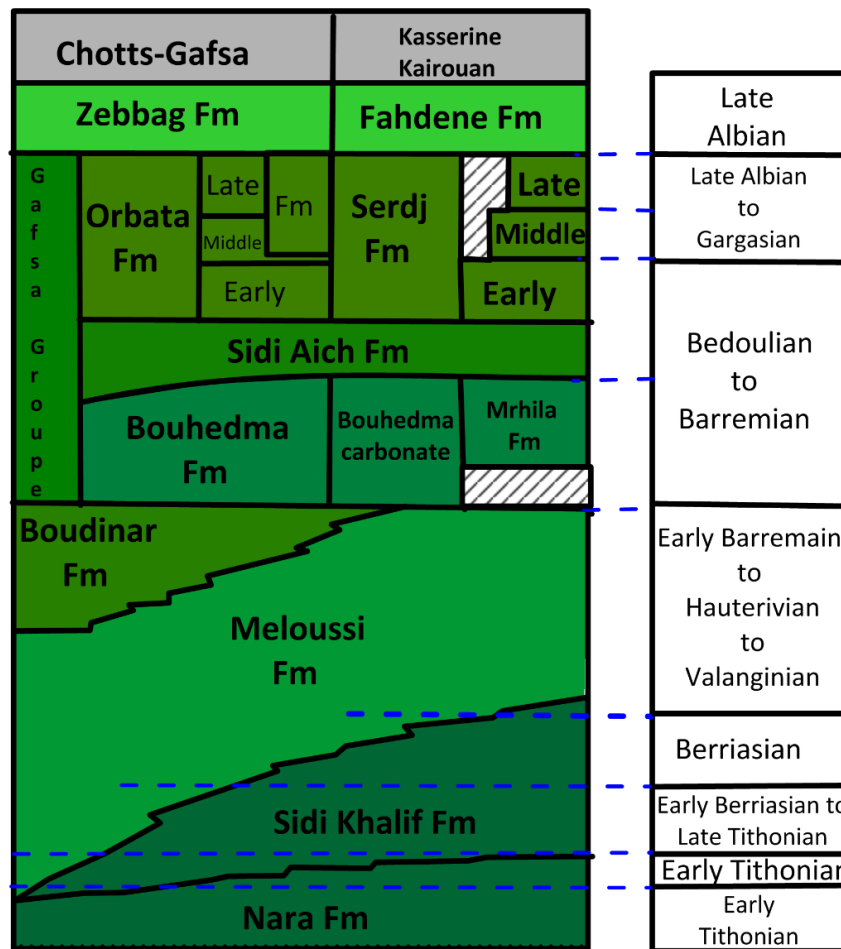


Figure 25. Correlation of lithostratigraphic units of the Early Cretaceous in Central Tunisia (M'Rabet 1981 in Allouche 1997)

c.2. Late cretaceous

The late cretaceous is composed, from the bottom to the top, by (i) The “**Zebbag**” formation (Albo-Cenomanian), (ii) The “**Aleg**” formation (Turono-Santonian) and “**Abiod**” formation (Campano-Maastrichtian) (Figure 26).

Touir et al. (1989) was defined, at the level of Mghilla mountain, five major sedimentary sequences:

- 1) The Vraconian (late Albian) sequence is formed by three lithological groups: The lower set is mainly marl-limestone with big ammonites (4 m). The average set shows 25 m of clays with foraminifera, ostracods, echinoid debris and lamellibranchs. The upper set is formed by a thick bed of sandstone dolomitic (5 m) (Touir et al. 1989).
- 2) The Cenomanian sequence also shows three sets: The lower setting is made up of 70 m of clay with decimetric beds of clay limestones. Then comes a hundred meters of oyster marl. Finally, the upper unit that formed by alternating marl-limestone take place.

- 3) The lower to middle Turonian sequence shows a variable thickness (5 to 10m). It is formed by foraminiferous marls with a few beds of fossiliferous limestone lined with a hardened surface.
- 4) The upper to middle Turonian sequence has varying thicknesses between 30 and 70 m. Green marls form it with argillaceous intercalations with limestone beds of metric thickness. These limestones are crowned, at the top, by a hardened surface testifying to an emersion at the end of the Turonian.
- 5) The fifth sequence is absent on the eastern flank of the Mghilla mountain. Tourir et al. (1989) subdivided it into three distinct lithological groups. The lower set is attributed to the late Santonian to basal Campanian. Clays form it with intercalations of clayey limestones with some foraminifera. The average complex is of Campanian age. It is made up of a succession of clayey limestone banks topped by a limestone slab rich in foraminifera. Finally, the upper unit of the Campanian-Maastrichtian age is formed by siliceous dolomites.

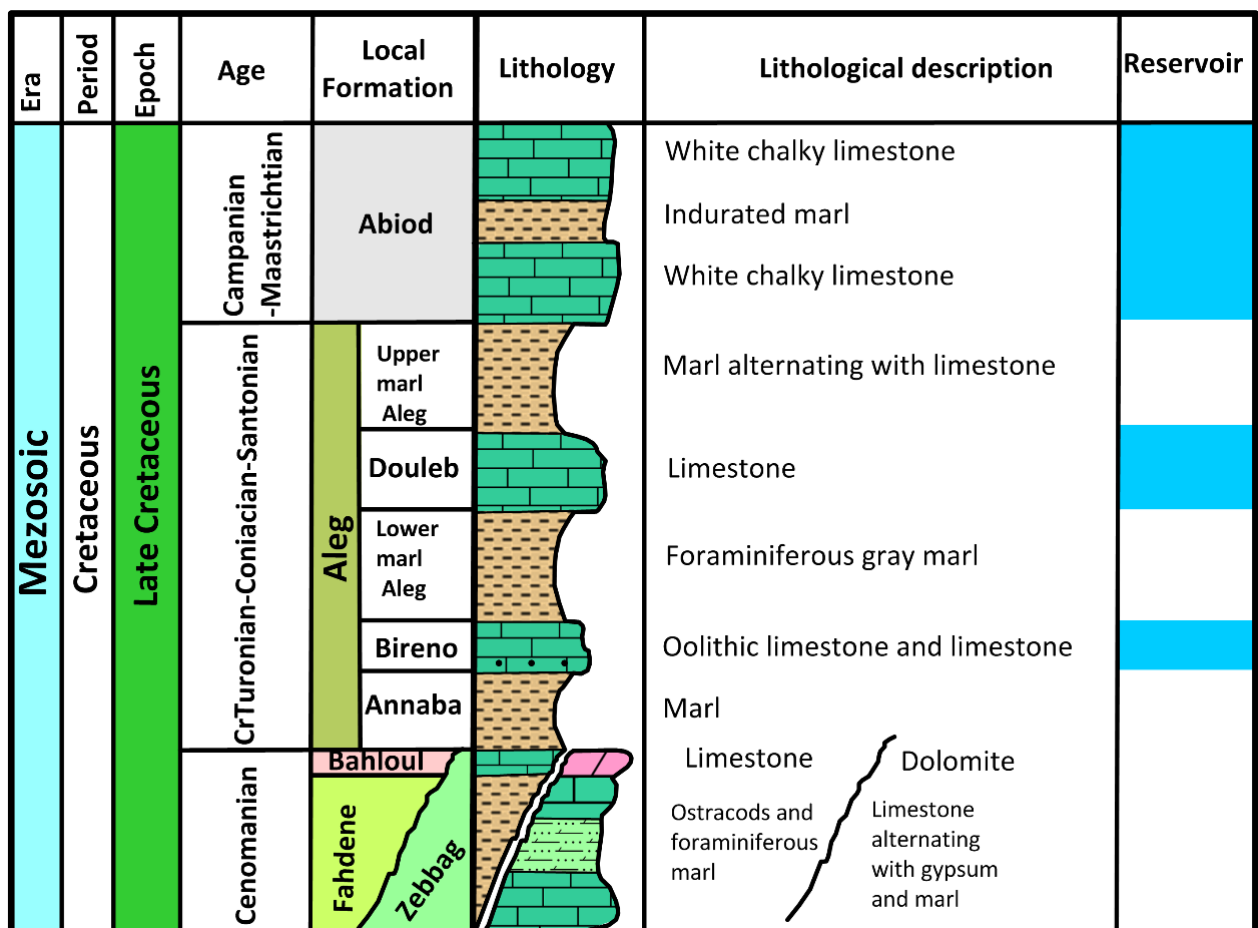


Figure 26. Synthetic log of the late Cretaceous series in the Hajeb Layoun-Jelma basin

2.2.Cenozoic

The Cenozoic series are visible along with the structure of Labaeid mountain and Mghilla mountain (**Figure 24**), and they are composed of several formations (**Figure 27**).

a. Paleogene

The Paleogene series are composed, from the bottom to the top, by: (i) the “**El Haria**” formation (Paleocene), the “**Métlaoui group**” and the “**Souar**” formation with its equivalents (Chérahil and Djebes) (Eocene) and ends with the Oligocene deposits (El Ghali **1993**).

a.1. Paleocene

According to Burolet (**1956**), in central Tunisia, the Upper Maastrichtian and the Paleocene correspond to an essentially clayey series called “**El Haria**” formation.

Based on Burolet (**1956**), the El Haria formation present a regressive mega-sequence formed by two sequences: One of an argillaceous nature and which evolves towards the top with alternations of clayey limestone and beige marls of Maastrichtian age, the other is of Paleocene age. The limit between these two sequences is materialized by a sedimentary discontinuity corresponding to a non-deposit gap from the Upper to Terminal Maastrichtian and the Lower Paleocene.

In the Mghilla and Labaeid mountain, the El Haria formation is absent. The limestone bar of the Abiod formation is covered by lumachellic limestones of the Lutetian (Zghal **1994**).

a.2. Eocene

The Lower Eocene is formed by limestone with nummulites or white-yellow dolomite with mollusk mussels. A conglomerate surface marks the Eocene base while its top is formed by marls and yellow clays from the Middle Eocene (El Ghali **1993**). In the anticline of Jebel Baten Damous, the Ypresian is represented by massive glauconious limestone, clear dolomites in the middle part and silicified limestones at the top with an average thickness of around 10 m (El Ghali **1993**).

At Mghilla mountain, the dolomitic limestones of the El Garia formation (Ypresian-lower Lutetian) deposits on its eastern flank and have an average thickness that varies between 10 to 15 m. In Jebel Lassouada, the Ypresian materialized by the Métlaoui formation is made up of black dolomites surmounting by phosphate dolomites and a basal pudding with pebble and phosphate matrix (Creuzot and Ouali **1989**).

The Middle to Late Eocene series shows distinctive facies. They correspond to the Chérahil formation formed by two lithologically different sets where we find alternations of lumachellic limestones with marly clays (Burolet 1956).

a.3. Oligocene

The Oligocene forms the frame of Labaeid mountain and covers the eastern flank of Mghilla mountain. On the east part of Labaeid mountain, the Oligocene is formed by alternating white sandstone beds with oblique stratifications, green marls, clay levels and containing in their top part quartz dragees sometimes conglomeratic levels (Boukadi 1994).

At Lassouada mountain, the Fortuna formation base is marked by a series of clays and sands covered by alternating fossiliferous limestone sandstones with sandy clays. The top of this series is presented by continental red clays dated Aquitanian-Burdigalian (Creuzot and Ouali 1989).

b. Neogene

Red silts and laterites compose the Messioua formation (Aquitanian) of continental origin. At the eastern periclinal end of Labaeid mountain, we find a thick gypsum series alternating with variegated clays and sandstone banks (120 to 150 m). Above these red silts are deposited fossiliferous sandstone limestones with marly intercalations and thicknesses varying between 20 to 80 m. At the base of these limestones, we find a significantly reduced thickness (Ben Jemiaa 1986; Blondel 1991; El Ghali 1993). According to Bismuth (1984), these limestones are of the Langhien age, resting in discordance with the previous levels.

The Langhian-Serravallian-Tortonian encompasses three different stratigraphic series:

- The “**Mahmoud**” formation materializes the Langhien-Serravallian, it is formed by green clays at the base and sandy at the top and presenting a greater thickness (65 m) at the level of the southern flank of Labaeid mountain constituting at the regional scale a continuous level (Biely et al. 1972).
- The second series, which is the “**Beglia**” formation, shows significant thickness across the region (500 m at the Labaeid mountain). It is formed by whitish sandstones (Figure 28b), sands with oblique stratifications sometimes showing quartz dragees' beds and containing rare sand lenses (Burolet 1956; Biely et al. 1972; Fournie 1978; Bismuth 1984).
- The third Serravallian-Tortonian series is represented by the “**Saouaf**” formation. These are clays containing gypsum with fine sandstone intercalations (Figure 28a), about ten

meters thick and organized in small perched layers (Zouari 1998). The thickness of this series is variable, with a maximum of 600 m.

The Messinian-Pliocene series is discordant with the underlying series. It is formed at the base by sands and red silts and the top by conglomerate levels in the western region of Labaïd mountain (El Ghali 1993).

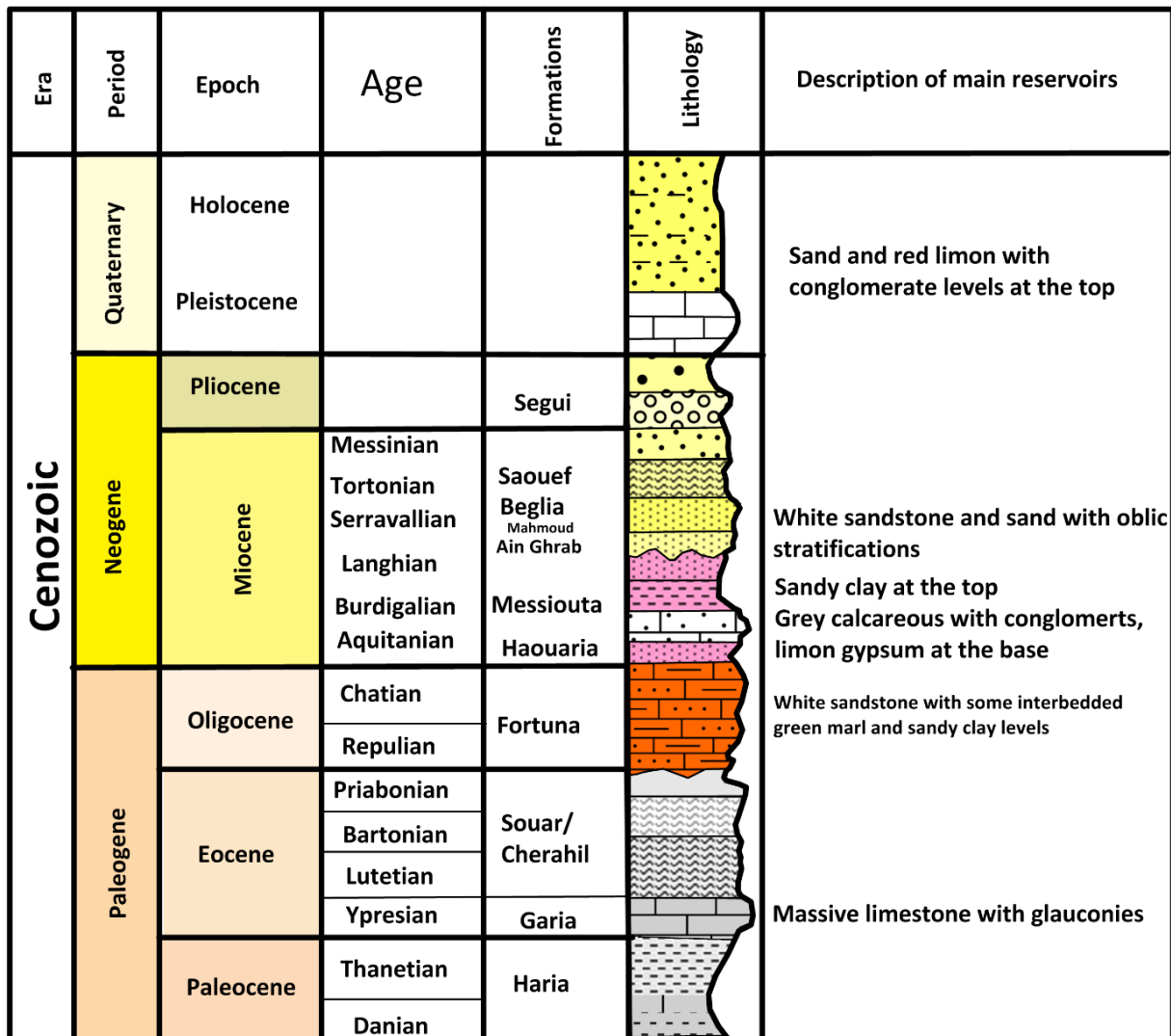


Figure 27. Synthetic log of the Cenozoic series

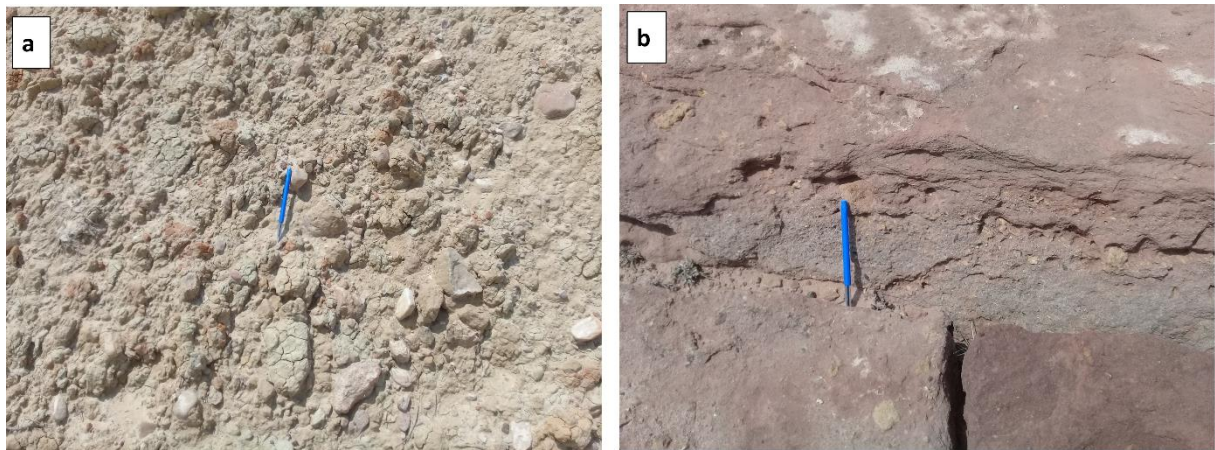


Figure 28. (a) The Saouef formation exposed at the surface near the Mghilla mountain (b) The Beglia formation exposed at the surface (pictures were taken in Jun 2019)

c. Quaternary

The Quaternary deposits are of negligible thickness (Koschel [1980](#); Zouari [1998](#)). In the Hajeb Layoun-Jelma basin, the Quaternary deposits are from 10 to 60 m thick, mainly composed of coarse sand. They constitute an aquifer containing a free water table fed by the floods of server rivers.

III. Structural setting

Tunisia's intricate structural pattern is attributed to major Mesozoic-Cenozoic orogenies recognized at the North African plate margin scale (Dhahri et al., [2015](#)). The study area is located in the Atlassic domain, west of the N-S axis, which occupied most part of Tunisia ([Figure 22](#)). The study region is affected by major accidents with a WNW-ESE, SW-NE, NS and NNE-SSW orientation (Zouaghi [2008](#); Khazri and Gabtni [2015](#); Jellalia et al. [2015](#)) ([figure 29](#)).

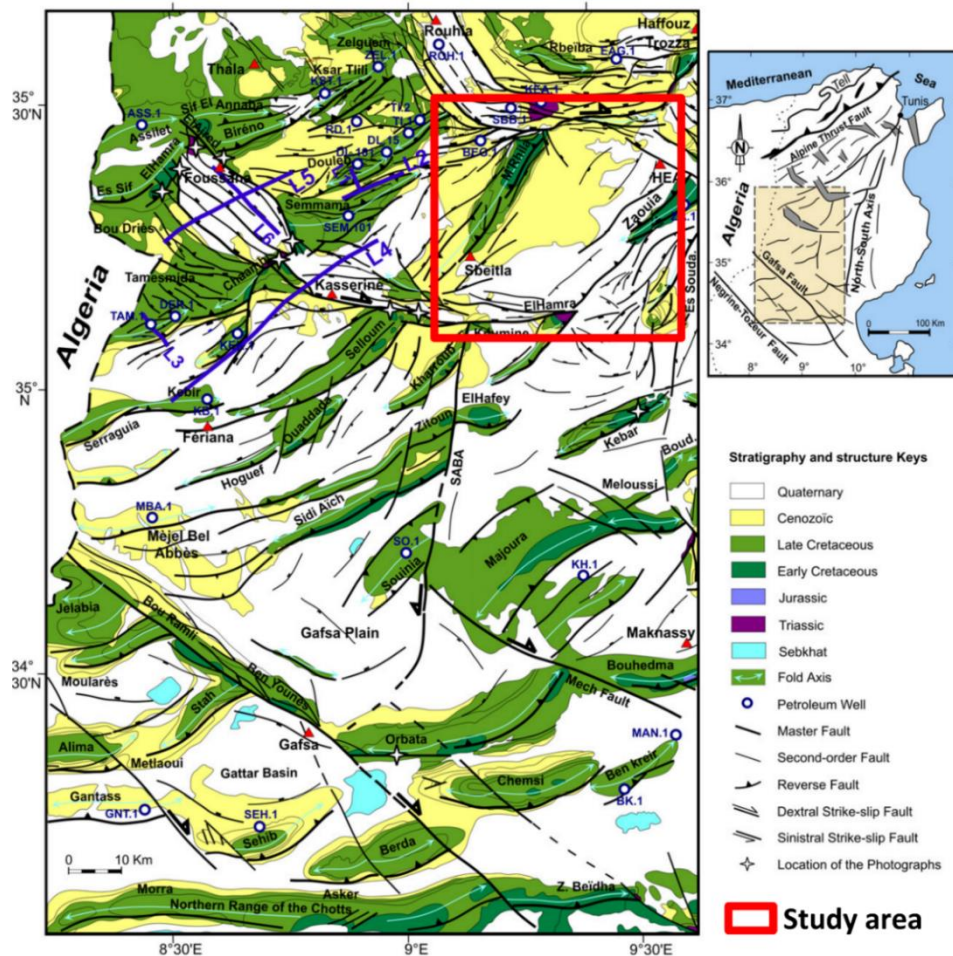


Figure 29. Structural map of the main deformations in central Tunisia (Zouaghi 2008)

1. Anticlines

The study region is formed by a set of anticlinal structures with a Cretaceous core. The folds in this region are often in a NE-SW, E-W atlas direction (Figure 29). They correspond to multi-kilometer anticlinal structures built during the compressive phases of the Miocene and post-Lower Pleistocene ages (Chihi 1984; Zargouni 1985; Soyer and Tricart 1989; Boukadi 1994). The anticlinal structures (Mghilla mountain, Labaeth mountain, Zaouia-Roua mountain, Lassouada mountain, Hamra, and koumine mountain) constitute the geomorphological boundaries for the Hajeb Layoun Jelma syncline basin.

1.1 Mghila mountain

The Mghila mountain is part of the central atlas and forms a NE-SW trending anticline characterized by a single periclinal southern termination (Figure 29).

The Mghila mountain exposes the Upper Cretaceous deposits in the periphery and Lower Cretaceous sediments in anticline's core (Figure 30). The Abiod Formation in Mghila

mountain consists of a limestone bar capped by a dolomitic bed. The Abiod Formation (Campanian) is underlain by the upper marls of the Santonian Aleg Formation and overlain by the continental paleosol of the Aquitanian (Messiouta Formation).

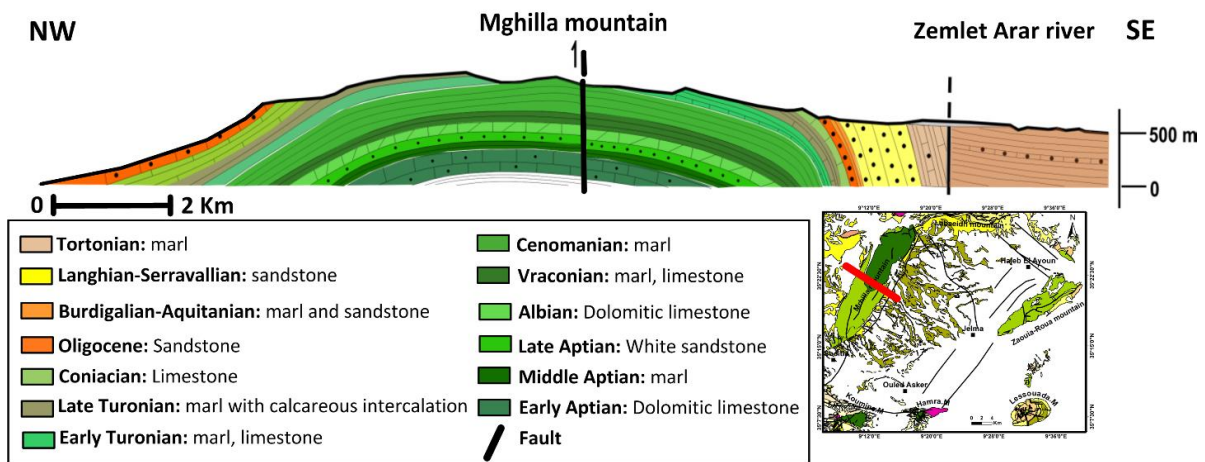


Figure 30. NW-SE cross-section through Mghilla mountain

1.2 Lassouda mountain

The Lassouda mountain is located in the south-Est part of the study area (Figure 23). Creuzot and Ouali (1989) assert that the Lassouda mountain is the most remarkable compared to the neighboring massifs because of its particular shape similar to a faulty dome (Figure 31).

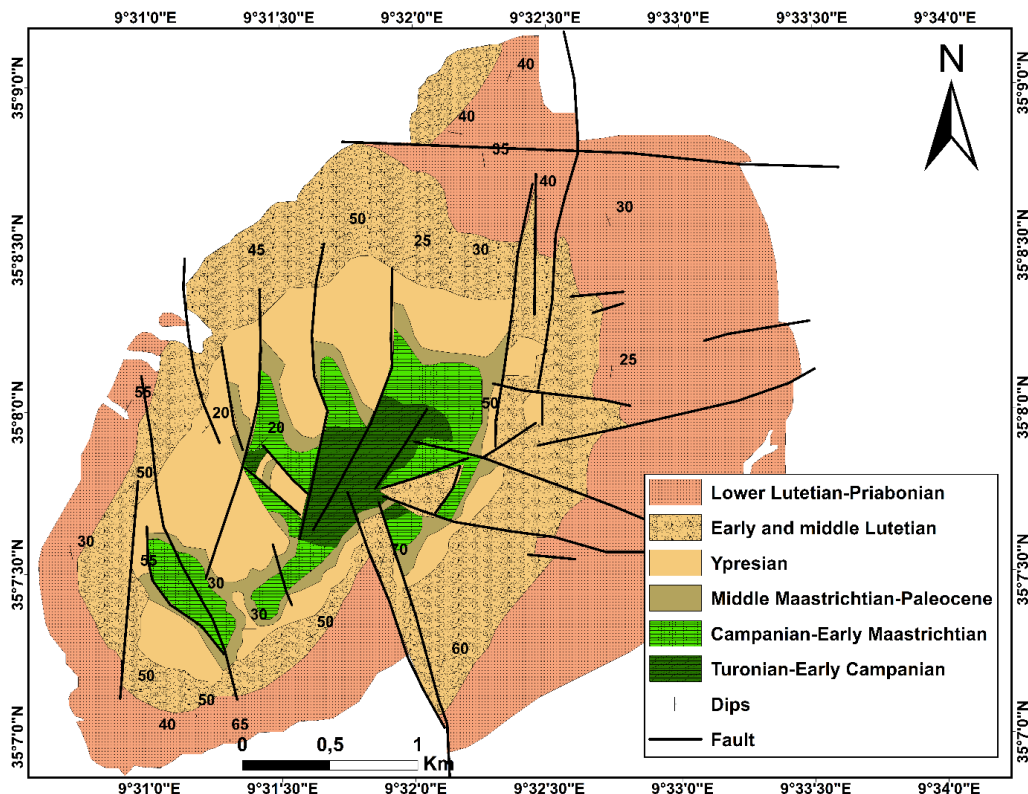


Figure 31. Geological map of Lessouda mountain (Matmati et al., 1992)

1.3 Hamra mountain

The Hamra anticline presents 3 km long and 1.5 km wide. The Atlas fold of Hamra-Zaouia is a vast dome of NE-SW orientation, asymmetrical. It consists mainly of Cenomanian land. The extension of the Roua and the Hamra fold could present a veritable hydrogeological barrier separating the syncline basin of Hajeb Layoun from that of Oued El Hjal.

1.4 Labeidh mountain

The structure of Labeidh mountain constitutes a “fold-fault” whose sedimentary series bear a significant stratigraphic gap. Within this structure, the Eocene rests directly on Aptian dolomites. Halokinetic pulses also marked the evolution of the Jebel Labaeid and that of the Jebel Mghilla. The structure of Jebel Labaeid is essentially affected by two networks of faults, namely the E-W network and the N140 network. The E-W accident, which delimits the southern edge of the Sbiba ditch, could be the most representative accident of this network. Towards the east, this E-W fault curves towards direction N ° 60 to join the Trozza massif. Network N140 is marked regionally. This network of faults is expressed both within the Sbiba ditch and throughout the structure of Labaeid. The western sector of Labaeid is torn by an important dextral indentation oriented N140. It is marked by abnormal contact between the Aquitanian bars, verticalized with the Miocene series. Towards the eastern end, another fault N140, which plays in dextral step, affects the carbonate bar of Ain Ghrab. The Hajeb Layoun ditch is made up of this network of major N140 faults (Ayadi 2002).

1.5 Zaouia mountain

The Zaouia mountain is located in the Eastern part of the Basin (Figure 23). The Zaouia is formed by sandy and dolomitic marls with rare calcareous intercalations, as shown by the geological section made at Jebel Zaouia (Figure 32). The anticlines of Jebels Zaouia-Roua and Jebel Hamra, discontinuous on the surface, are linked in the subsurface through the underground bulge of Ouled Asker (Koschel 1980). The Zaouia-Roua and Hamra chain is shuttered and dumped towards the South-East

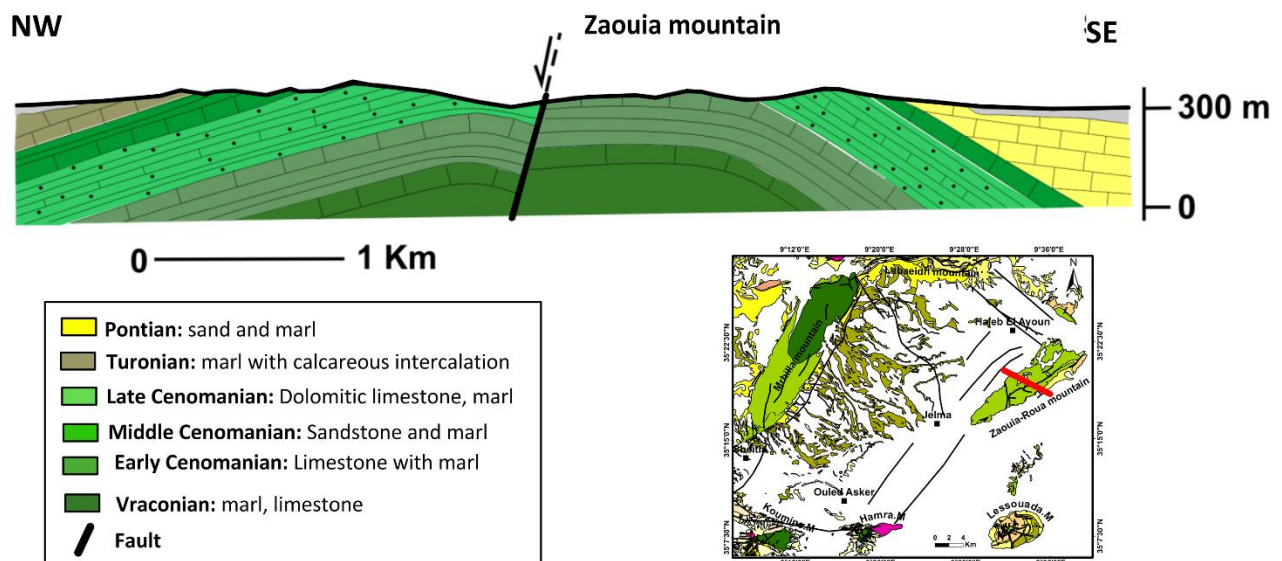


Figure 32. NW-SE cross-section through Zaouia mountain

2. Syncline of Hajeb Layoun-Jelma

The anticlines mentioned above take place on the plain of Hajeb Layoun-Jelma. The anticline of Jebel Mrhilla bound the syncline of Hajeb Layoun-Jelma in the North-West, Jebel Labaeid in the North, Jebel Zaouia in the North-East, and Jebel Hamra in the South. It constitutes a sizeable synclinal basin filled mainly with "Tortonian-Aquitainian" deposits with extensive Quaternary overlaps. The Hajeb Layoun-Jelma syncline is affected by the Hajeb Layoun fault in the northeast part (Jellalia et al., 2015).

3. Faults

The sedimentary cover shows an asymmetric arrangement of the blocks which have been controlled by deep faults associated with the tectonic movements of the Triassic salt (Bédir 1995; Zitouni 1997; Hlaim 1999; Zouaghi et al., 2002, 2005, 2007). These faults have been interpreted as pre-Triassic anomalies (Bédir 1995).

3.1 Hajeb Layoun Fault

The Hajeb Layoun fault, with a discharge of 150 to 250 m and which dampens towards the NW (Koschel 1980), brings a predominantly sandy uplifted compartment into contact with a predominantly clayey collapsed compartment, thus interrupting the hydraulic continuity of the water tables and playing the role of a hydraulic threshold which is characterized by the sources of Hajeb Layoun.

3.2 Mrhilla Fault

This is a directional fault that limits the eastern flank of Jebel Mrhilla. It brings the steeply dipping Oligocene sandstones into contact with the upper Miocene subhorizontal clays of the Hajeb el Ayoun syncline (Koschel 1980; Jellalia 2015). This structure develops from a flexure in the Sbeitla region to a normal fault at Fom el Guelta and finally overlaps at Ain Ghename.

3.3 Sidi Maâmar fault (Hammam sahline)

The region of Sidi Maâmar is affected by a fracturing network made up of two major directions:

- N110 to N130, characterizing the transverse faults, which are at the origin of the ditch of Hammam Sidi Maâmar. These faults affect the entire sedimentary series;

- N05 to N015, essentially characterizing the directional fault of Jebel Baten-Damous, the fine mapping surveyed in the vicinity of the source clearly shows the compartmentalization of the zone by brittle tectonics and the vital role that the network of vertical faults can play in the flow of water from the deep aquifer to the ground surface. These are secondary faults of a branch of the main fault trending WNW-ESE.

Besides, the Hammam Sahline (or H. Sidi Maâmar) fault crosses the graben of Oued Zeroud and continues at Jebel Zaouia to Oued Arar. Its route is indicated by numerous thermal and sulfurous springs, particularly that of Sidi Maâmar and Ain Chenama which emerge at the intersection of this transverse fault with faults on the edge of the graben Wadi Zéroud.

Chapter III: Hydrogeology of the study area

I. Introduction

A hydrogeological investigation is an essential tool for groundwater characterization. The identification of the formations and their sub-surface extensions, as well as the identification of the geological structures, are excellent tools for the hydrogeological characterization of basins (Smida 2008; Jallalia et al., 2015; khazri et Gabtni 2018; Thebti et al., 2018).

The Hajeb Layoun Jelma basin's water resource is considered the most important resource in central Tunisia. Most than 80% of its resources are used by the National Water Supply and Distribution Company (S.O.N.E.D.E) to alimented many around regions by the drinking water. This basin is characterized by the Hayet mineral water, which is being in exploitation since the year 1988. The resources of this groundwater are used in different sectors: irrigation, drinking, and industry.

Faced with the over-exploitation, the population growth, and the agricultural development in HJB, the search for new underground water becomes necessary in this basin. The identification of Hajeb layoun jelma's aquifers and geometry is based on various studies (Gassara, 1980; Koschel 1980; Mansouri, 1980; Mamou, 1981; Amouri, 1994; Hajjem, 1999; Ouda, 2000; Dassi, 2004; Smida 2008; Jallalia et al., 2015; Thebti et al., 2018). This research is based on various published data by the water management authorities (CRDA Sidi Bouzid) (well log, transmissivity data, abstraction, piezometry, and springs.....).

This work is focused on the delimitation of the shallow and the deep aquifer, the determination of the groundwater recharge and discharge zones, the analysis of the water table's historical data for both aquifers (shallow and deep), the establishment of the piezometric maps for both aquifers in order to know the direction of the groundwater flow, the hydraulic gradient and finally the determination of HJB aquifers' characterization.

II. Aquifers structuration

The previous geological and stratigraphic studies (Koschel 1980; Smida 2008; Jallalia et al., 2015; Thebti et al., 2018) and the interpretation of the wells' logs revealed that HJB is a multilayer aquifer system, consisted of five main aquifer layers (Table 2) coincide with the following Formations (from the bottom to the top): (i) Abiod, (ii) Ain Grab, (iii) Beglia

(maximum thickness equal to 500 m), (iv) Plio-Quaternary deposits; which increase from 0 m to the West limit to over 150 m to the Eastern limit.

The Hajeb Layoun-Jelma basin comprises two main aquifers (the most exploited aquifers); the shallow aquifers (Plio-Quaternary) and the first deep aquifer coincide with the Beglia formation. Therefore, in the present study, only these two aquifer layers have been taken into account:

- √ The shallow aquifer is logged in the sand and sandy clays layers of the Plio-Quaternary deposits, and it is unconformably set on the Saouef formation. The shallow aquifer limits published by the DGRE have not been considered since they cover all the basin. The shallow aquifer's new delimitation is related to the thick and continuous of the Plio-Quaternary deposits. We have eliminated the perched and the discontinuous aquifers logged in the clay of the Saoued formation (West part of the basin). In 2018, more than 2328 wells captured this aquifer with an abstraction rate equal to $20.94 \times 10^6 \text{ m}^3/\text{year}$, which indicates an abstraction of 140% (DGRE 2018). The shallow aquifer recharge originated from the direct recharge from rainfall and the direct infiltration through floods descending from the mountains.
- √ The Beglia aquifer is usually confined due to the superimposition of the clayey Saouaf formation. However, in HJB's southern part, this aquiclude has been eroded, allowing the Beglia formation to be closer to Plio- Quaternary aquifers, with an interposition of a lateritic layer (Koschel 1980). Due to the lateritic layer's lateral discontinuity, somewhere, the Plio-Quaternary and the Beglia aquifers can interact from the hydraulic point of view (Koschel 1980). The deep aquifer delimitation was made based on the previous geological and stratigraphic studies. The aquifer limit was based on the DGRE boundary, but we have eliminated the zones without hydrogeologic information (borholes and piezometers). The Beglia aquifer presents a good quality in many Hajeb Layoun-Jelma basin regions which is transported by the National Water Supply and Distribution Company (S.O.N.E.D.E) to supply by drinking water the Sidi Bouzid and Sfax government. The S.O.N.E.D.E exploitation of the Beglia aquifer exceeded $20 \times 10^6 \text{ m}^3/\text{year}$ (DGRE 2018). This aquifer's total abstraction is equal to $33.4 \times 10^6 \text{ m}^3$ in 2018, indicating an abstraction of 120% (resources equal to $27.8 \times 10^6 \text{ m}^3$). The Beglia aquifer's recharge is originated from the direct infiltration through floods descending from the mountains occurring in the exposed aquifer at the surface (West part).

Table 2 Diagram showing the different aquifers of HJB

Age	Formation name	Lithology	Layer type	
Quaternary		Gravel and sand	Shallow aquifer	
N e o g e n e	Pliocene		Segui	
	Tortonian	Souaf	Aquiclude	
	Serravallian	Beglia	Sandstone	Deep aquifer
	Langhian	Mahmoud	Green clays	Aquiclude
		Ain Grab	Sandstone	Deep aquifer
	Aquitanian	Messiouta	Sandstone and sandy clays	Aquitard
	P a l e o g e n e	Oligocene	Fortuna	Sequence of sandstone and clay
Eocene			Sandy marl	Aquitard
Paleocene		El Haria	Clay	Aquiclude
Cretaceous		Abiod	Limestone, dolomite and marl	Deep aquifer

Captured aquifer 

III. Geometric characterization of the reservoir layers

1. Geometry of aquifers

The Hajeb Layoun-Jelma basin is a wide NE-SW directed syncline filled with Tertiary and Quaternary deposits and limited by anticlines cored by Lower Cretaceous units (Koschel 1980; Castany 1982; El Ghali 1993; Boukadi 1994; Abbas 2004). This basin is drilled by more than 137 deep boreholes and 2328 shallow wells, capturing several aquifer levels with different characteristics. Several correlations (Figure 33) from different directions were made to identify the main aquifers' extension

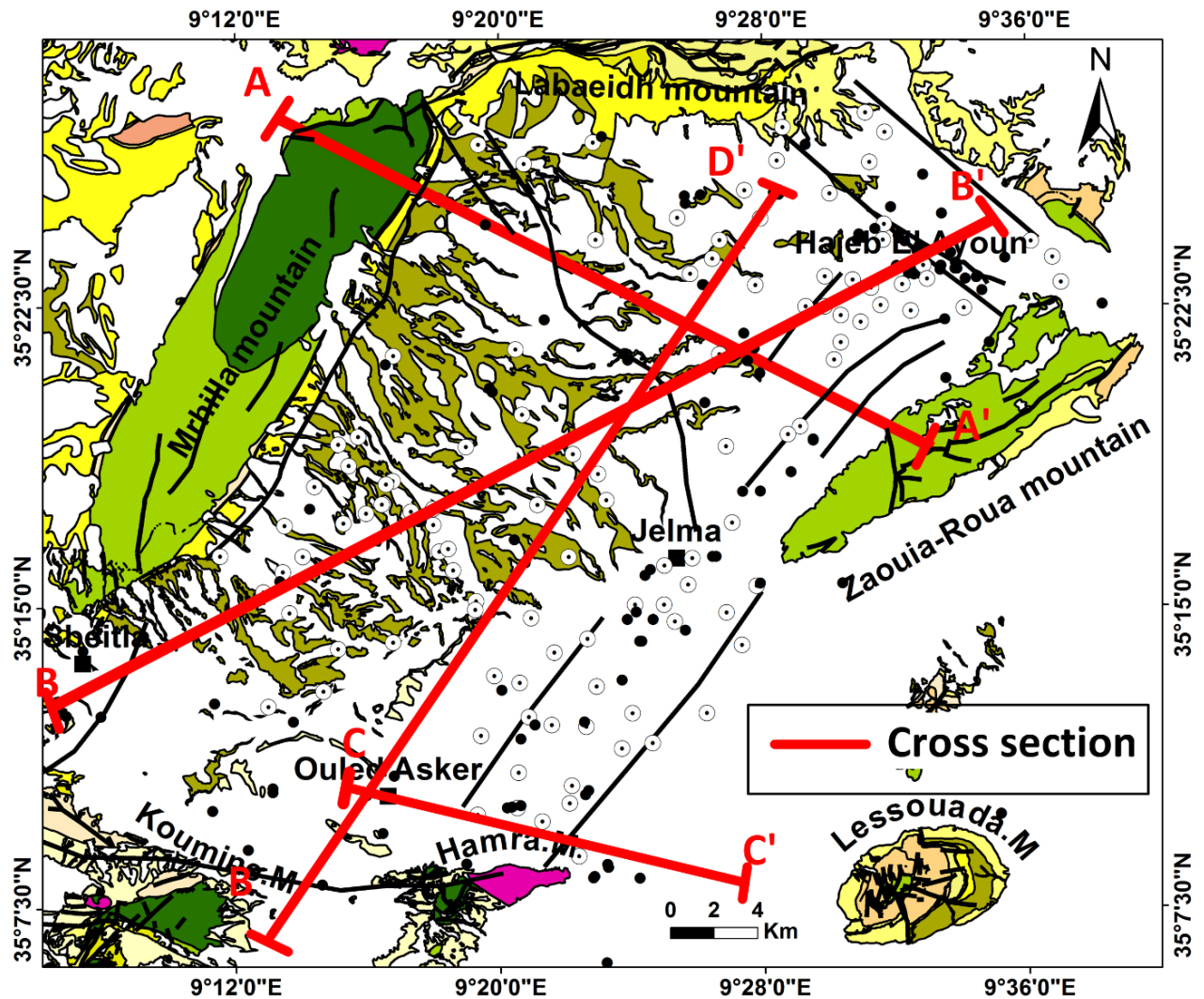


Figure 33. Localisation of deep and shallow wells and the various cross section in Hajeb Layoun-Jelma basin (for the legend, see figure 24)

1.1. Cross-section NW-SE

The cross-section A-A' (**Figure 34**), in a NW-SE direction, connects the following boreholes: Zaghmar (N°IRH: 17442/4), Djilma (N°IRH: 17598/4), Chastel II (N°IRH: 17212/4), Djilma 13 (N°IRH: 17706/4), Djilma 14 (N°IRH: 17737/4), Bled Mejri bis (N°IRH: 18306/4) and El Khedairia (N°IRH: 19105/4).

This cross-section shows that the Miocene series is continuous over the entire Hajeb Layoun-Jelma syncline and extends along with the E-W limit with thickness variation; the maximum thickness is located in its central part. We can conclude that the Hajeb Layoun-Jelma basin presents a multi-layer aquifer system with alternating sandy, sand-clay, sandstone series separated by clay layers. The results show the existence of three main reservoirs. These levels are from bottom to top:

The Langhian aquifer

The Langhian aquifer layer is formed by a sandstone layer intercalated, sometimes by marly and clay levels. This aquifer is lodged in the coarse sandstones of the Aïn Ghrab formation. The green clays of the Mahmoud formation play as an aquiclude set on the Langhian aquifer.

This aquifer keeps the same thickness in the center of the basin with an average thickness of approximately equal to 120 m (**Figure 34**). The Langhian aquifer is captured by three wells in this cross-section (Djilma (N°IRH: 17598/4), Chastel II (N°IRH: 17212/4), and Djilma 13 (N°IRH: 17706/4)).

The serravallian aquifer

The sands and sandstones of the Serravallien (Beglia formation) represent the Hajeb Layoun-Jelma basin's main aquifer. It is captured by most of the deep boreholes in this region. In the NW-SE direction, over the entire extent of the Hajeb Layoun-Jelma syncline, the Serravallian is covered by the aquiclude of the Tortonian clays (Saouef formation).

From NW to SE, the beglia aquifer shows moderate thickness variation. The reservoir thickness starts low at the Zaghmar well (N°IRH: 17442/4) with thickness equal to 97 m. It attains the maximum thickness at the Djilma 14 well (N°IRH: 17737/4) with a thickness equal to 556 m and the thickness reduced to zero in El Khedair well (N°IRH: 19105/4) (**Figure 34**). The Beglia aquifer presents almost heterogeneous lithology, between the different wells, with some intercalation of marl.

The Serravallian aquifer is captured by two wells in this cross-section: Zaghmar (N°IRH: 17442/4) and Bled Mejri bis (N°IRH: 18306/4), with different position of the screen.

The Plio-Quaternary aquifer

This reservoir is characterized by mince thickness (from 0 to 39 m). In the west part, around the exposed Saouef formation, it is perched, discontinuous layers lodged in sandy to sandy-clay deposits (**Figure 34**), which present under-flow aquifer related to the runoff of rivers coming from Mghila mountain.

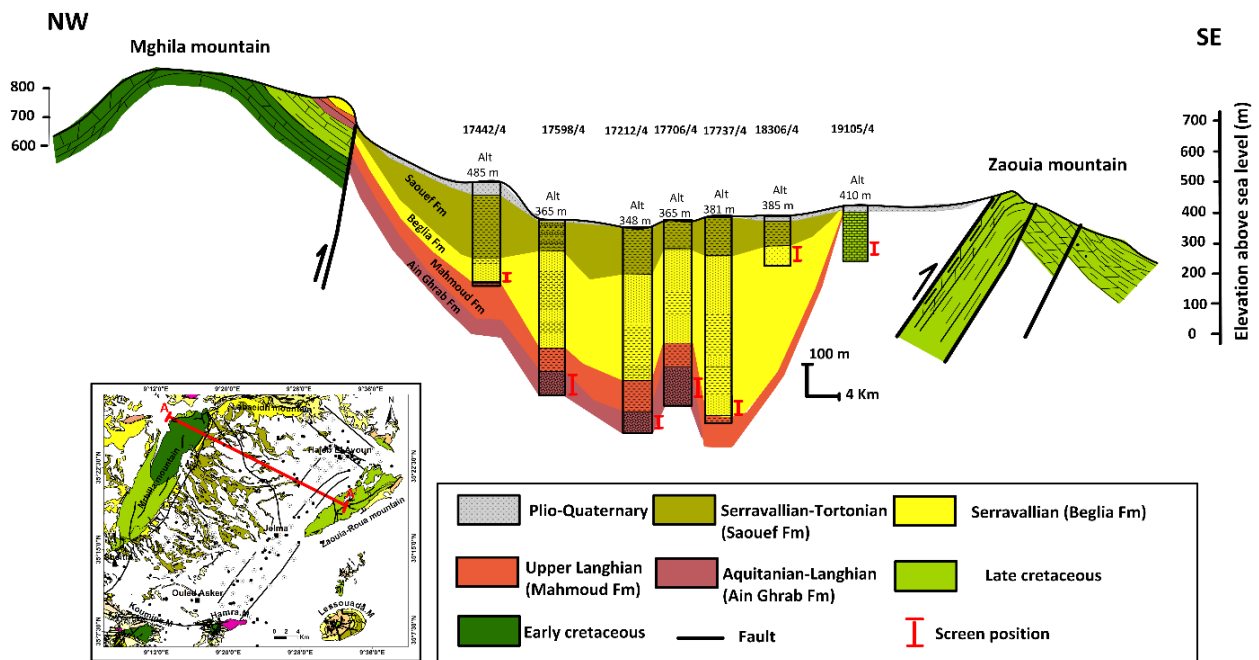


Figure 34. Cross-section A-A' (NW-SE) showing the principal aquifers in HJB

1.2. Cross-section NE-SW

The cross-section B-B' (Figure 35), in a SW-NE direction, connects the following boreholes: 6750/4, 7078/4, 7184/4, Mghilla II (N°IRH: 18823/4), Mghilla I bis (N°IRH: 17847/4), Djilma 14 (N°IRH: 17737/4), Djilma 13 (N°IRH: 17706/4), Hadjeb 9 (N°IRH: 19049/4), Hadjeb Cuir (N°IRH: 14008/4), Hadjeb Textile (N°IRH: 10928/4), Hadjeb 1 bis (N°IRH: 16247/4) and Hadjeb 10 (N°IRH: 11767/4). It shows the lateral and vertical continuity of the aquifer system from the NE to the SW. Four main levels are present, separated by impermeable and semi-permeable levels. From bottom to top, we found:

✚ The Langhian aquifer

It is formed by coarse sandstone, materialized by the Aïn Ghrab formation with an average thickness of around 120 m in the plain's center. It is trapped by a clay level (Mahmoud Fm) of an average thickness of 100 m.

✚ The serravallian aquifer

It is located in sandstone and sandy-clay formations with an average vertical extension of around 700 m in the basin's center. The average thickness of the Béglia formation goes from 60 m at hole 14008/4 to 600 m at hole 17737/4. Beyond this well, the thickness of the reservoir decreases further to the SW to reach 100 m at the level of borehole 18823/4. The third level is clayey, materialized by the Saouaf formation. It has variable thicknesses with a maximum of 160 m in the center of the basin while it narrows towards the NE to reach 40 m.

✚ The Plio-Quaternary aquifer

The Plio-Quaternary, which represents the fourth level, is thin, it is a discontinuous sheet and only exists in a few regions. It is housed in the first 50 m, it is formed by quaternary detrital deposits consisting essentially of alternations of sands, clays, clay sands and sandy clays. Basically, this section illustrates a thickening of the reservoir series in the middle of the plain, it shows an important deepening in the center of the basin.

We can distinguish two distinct zones from this cross-section: a platform zone with a shallow dip on the NE side, the shallow boreholes. This zone is limited on the NE side by the Hajeb Layoun graben's normal fault characterized by the emergence of several sources. A second zone is characterized by a strong dip followed by a subsidiary zone, which represents the Ouled Asker basin, limited on the SW side by the reverse and directional fault of Mghilla. The latter represents the western limit of the aquifer system bringing the Saouaf formation's marls into contact with the Miocene sandstones.

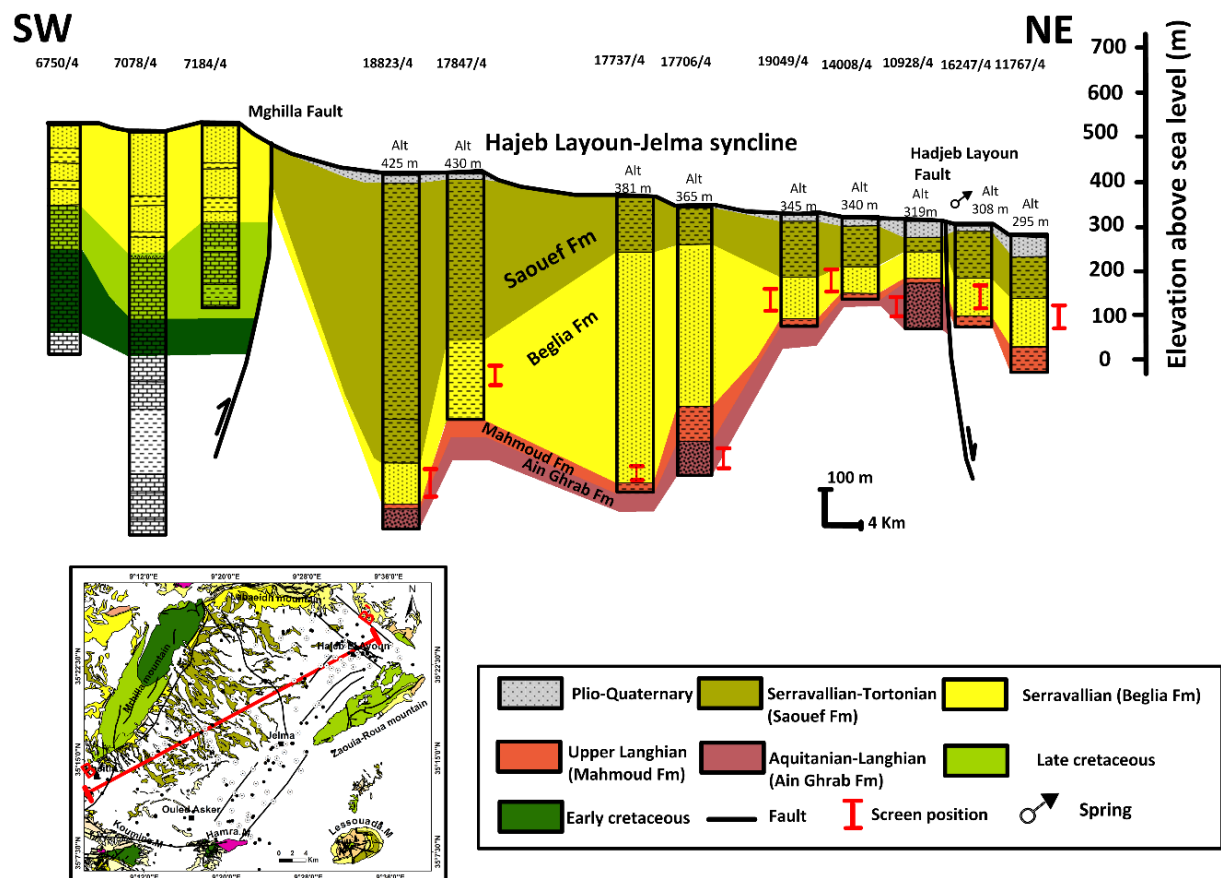


Figure 35. Cross-section B-B' showing the principal aquifers, in HJB, in a NE-SW direction

1.3. Cross-section W-E

The cross-section C-C' (Figure 36), in a W-E direction, connects the following boreholes: Cebbala (N°IRH: 18848/4), Ouled Asker II (N°IRH:18850/4), Ouled Achour (N°IRH: 19798/4) and N°IRH: 19021/5. It shows the closing of the continuity of the Beglia aquifer system from the N-NW to the S-SE.

Two main aquifer levels are present, separated by impermeable and semi-permeable levels. A normal fault (N-NE, S-SW) in the south-eastern part of Hajeb Layoun Jelma basin play as a hydraulic barrier between the Hajeb Layoun-Jilma basin and the Oued El Hjal basin. The Oued El Hjal basin is crossed by some deep boreholes, which indicate high salinity (borehole reports, CRDA Sidi Bouzid).

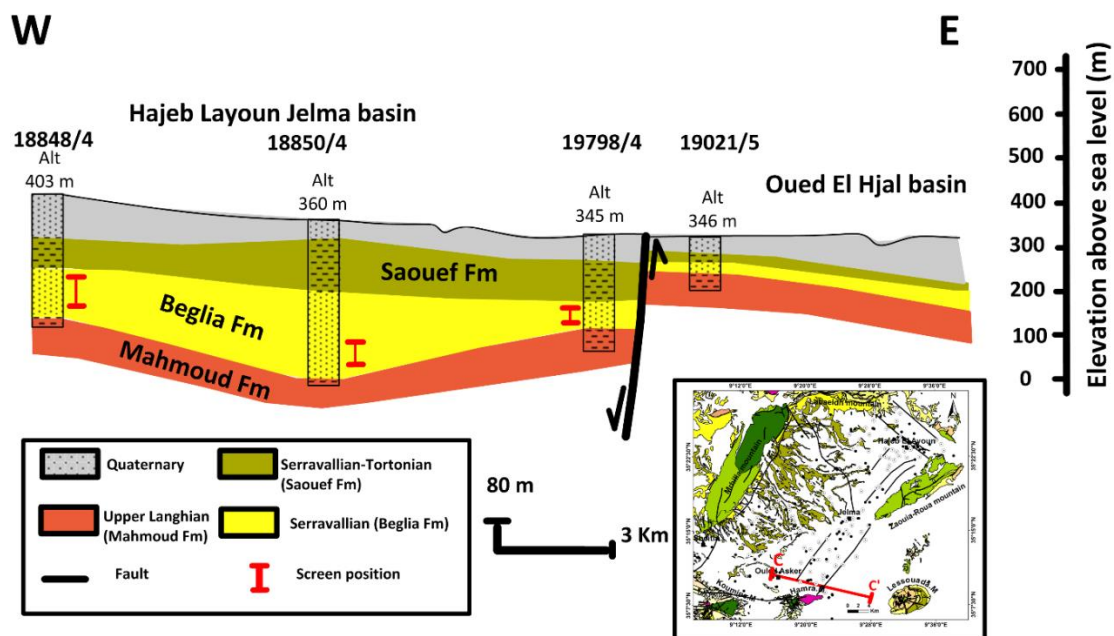


Figure 36. Cross-section C-C' showing the closing of the HJB in the southern-east part

1.4. Cross-section S-N

The cross-section D-D' (Figure 37), in a NW-SE direction, connects the following boreholes: Menaker (N°IRH: 7603/4), Ouled Asker II (N°IRH:11578/4), Ouled Asker I (N°IRH: 10426/4), Djelma V (N°IRH: 13539/4), Mghilla 10 (N°IRH:18795/4), Djilma VII (N°IRH: 13994/4), Djilma 8 (N°IRH: 15980/4), Chastel II (N°IRH: 17212/4), Hajeb 8 bis (N°IRH: 17598/4).

It shows the lateral and vertical continuity of the aquifer system from the south to the north side. The Hajeb-Jelma basin is limited to the south by the Kasserine fault (**Figure 37**).

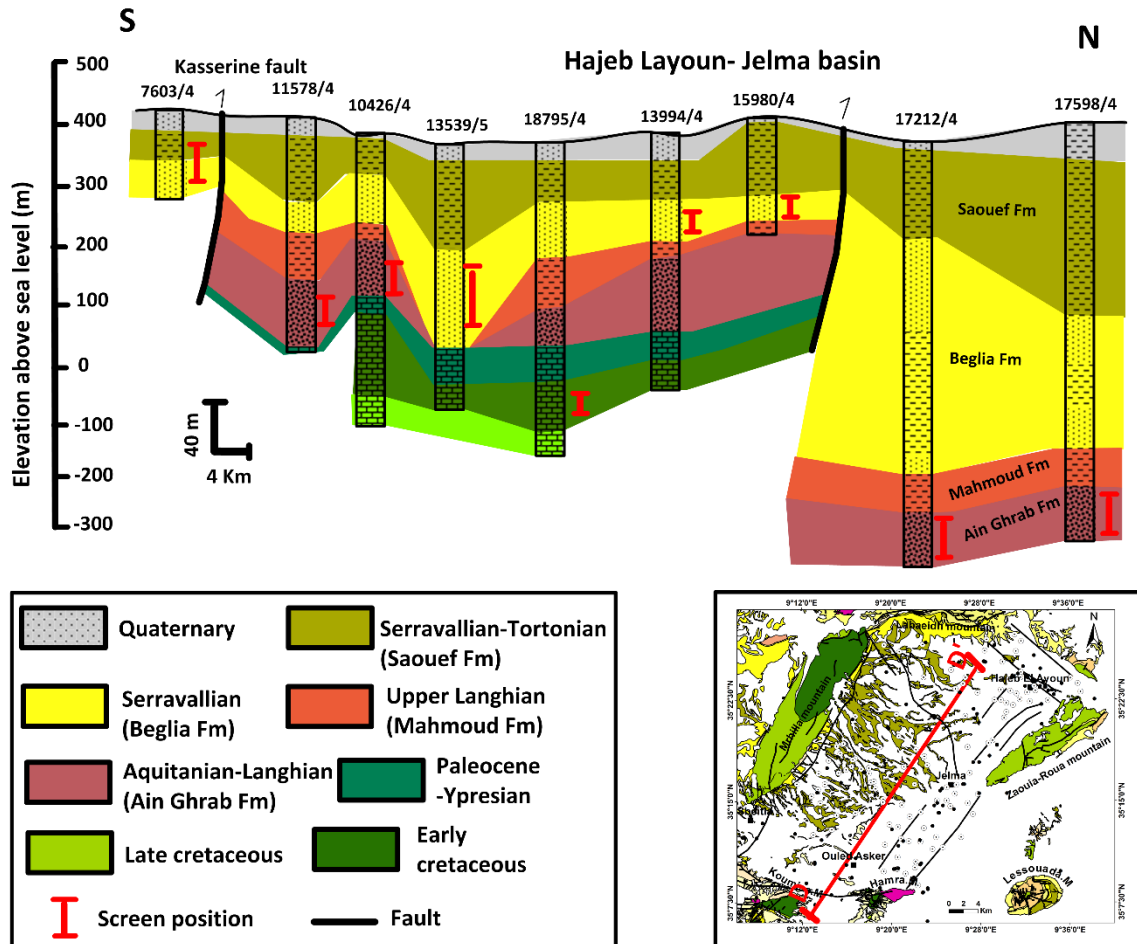


Figure 37. Cross-section D-D' showing the closing of the HJB in the south part

2. Top/ Bottom of aquifers

The bottom/top of each aquifer was extracted from the wells logs based on the formations' identification defined by Thebti (2018), Jallalia (2015) and Koschel (1980).

The top of the Shallow aquifer coincides with the elevation model. It ranged between a maximum of 485 and a minimum of 308 m (**Figure 38**), except for the under-flow aquifers, which no have been taking into consideration in this work. The bottom of the shallow aquifer is ranged between 20 m and 70 m. The maximum thickness is located in Jelma region.

The top of the Beglia deep aquifer coincides with the bottom of the aquiclude, which is compressed between 200 m and 160 m.

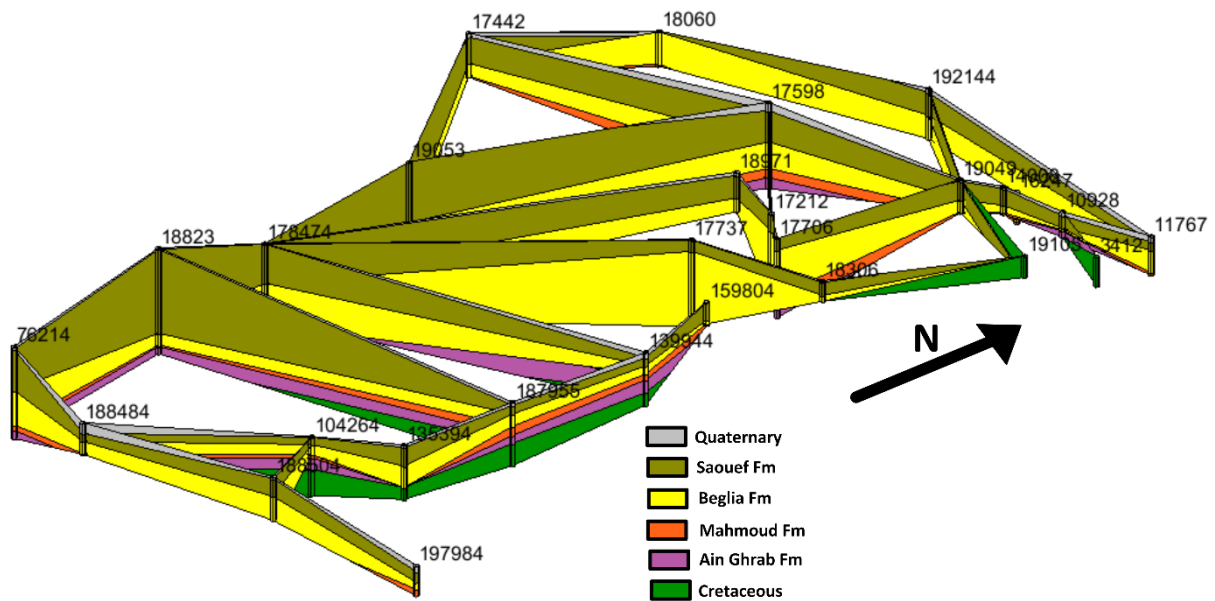


Figure 38. Multi-cross sections showing the lateral variation of the thickness of the different layers

IV. HJB aquifers characterization

The data available is presented in various formats: paper, digital files, thematic maps and it is collected from reports from DGRE and CRDA Sidi Bouzid.

The analysis of the spatial distribution of the hydrogeological parameters, namely the permeability of the aquifer, the transmissivity, and the storage coefficient, are very useful for calculating the exploitable geological reserves as the flow rate and velocity of groundwater. These are average values calculated from pumping tests from shallow and deep boreholes.

1. Transmissivity (T)

The parameter governs the rate of water flowing per unit in a saturated zone of a continuous aquifer, measured in a direction orthogonal to that of the flow (Castany 1967). For the deep aquifer, the results of the pumping tests given by DGRE indicate values varying from 5.10^{-4} to $6.10^{-2} \text{ m}^2 / \text{s}$ (Appendix 2). The shallow aquifer's transmissivity value is given only for two wells ($6.10^{-2} \text{ m}^2 / \text{s}$ and $6.10^{-2} \text{ m}^2 / \text{s}$). A pumping test campaign was made to measure the transmissivity for several shallow wells.

2. Permeability (K)

Permeability is the ability of a reservoir to allow water to pass through under a hydraulic gradient. Indeed, it expresses the aquifer environment's resistance to the flow of water passing through it (Castany 1982). The permeability data are obtained from pumping tests (CRDA, Sidi

Bouzid). The Hajeb Layoun-Jelma aquifer is characterized, in the south, by low permeability. The horizontal permeability can reach 10^{-4} m / s. The vertical permeability, recorded at the level of the Ouled Achour piezometer, is $1.6 \cdot 10^{-9}$ m / s.

3. Storage coefficient

The storage coefficient corresponds to the volume of water extracted from a slice of 1 m² of a horizontal surface for a piezometric drop of 1m. This parameter is linked to the compressibility and expandability of the water, the reservoir environment, the thickness of the aquifer and the screen's thickness. In the deep aquifer, the coefficient varies between 7×10^{-4} to 22×10^{-4} .

V. Groundwater abstraction evolution

Four aquifers from the Hajeb Layoun-Jelma basin are exploited: the shallow aquifers (Mio-plio-Quaternary), the first deep aquifer which coincides with the Beglia formation and the two Cretaceous deep aquifers (DGRE designation: Jelma 3 and Jelma 4).

The abstraction's assessment, its evolution over the years, and the number of wells is based on the data published by DGRE and CRDA during the period 1973-2019. These data are updated every five years for the shallow aquifer and each year for the deep aquifer. The total abstraction of HJB in 2019 is equal to 58.45×10^6 m³. However, the total resource is equal to 42.8×10^6 m³ which indicates a deficit of 15.65×10^6 m³ (Figure 39) (DGRE 2018).

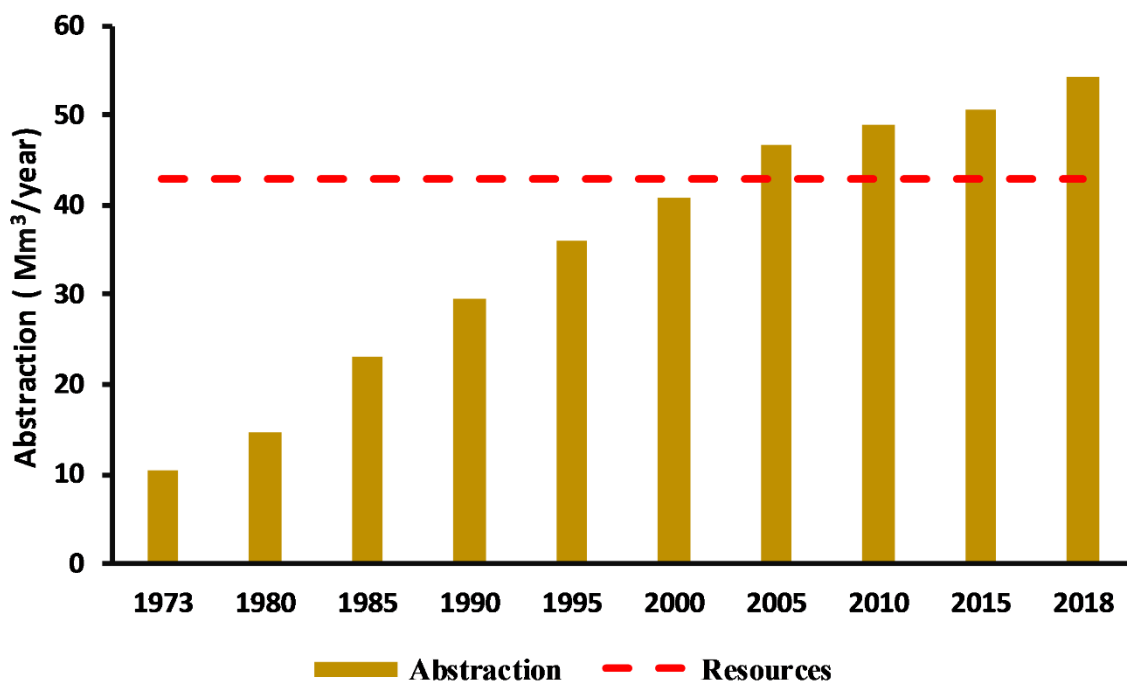


Figure 39. Abstraction and resources of HJB during the period 1973-2018

1. Shallow aquifer

The shallow aquifer wells tapped the majority of HJB's area. In 2018, the resource calculated by DGRE equal to $15 \times 10^6 \text{ m}^3$ and the abstraction equal to $20.94 \times 10^6 \text{ m}^3$ indicated an abstraction of 140% with a deficit equal to $5.94 \times 10^6 \text{ m}^3$. This over-abstraction engendered a decrease in the water quality. In fact, in the last decades, water salinity was increased from 0.5 g/l to 1 g/l (DGRE 2018). This over-exploitation is manifested by the increase of the number of wells (Figure 40): in 1974, 226 shallow wells tapped the shallow aquifer with an abstraction rate equal to $7.94 \times 10^6 \text{ m}^3/\text{year}$. In 2018, the number of wells increased to attend 2328 wells extracting a volume equal to $20.94 \times 10^6 \text{ m}^3/\text{year}$ (Figure 40). In 2019, the shallow aquifer was captured by 4446 wells with a rate equal to $20.96 \times 10^6 \text{ m}^3/\text{year}$ (DGRE 1973-2019).

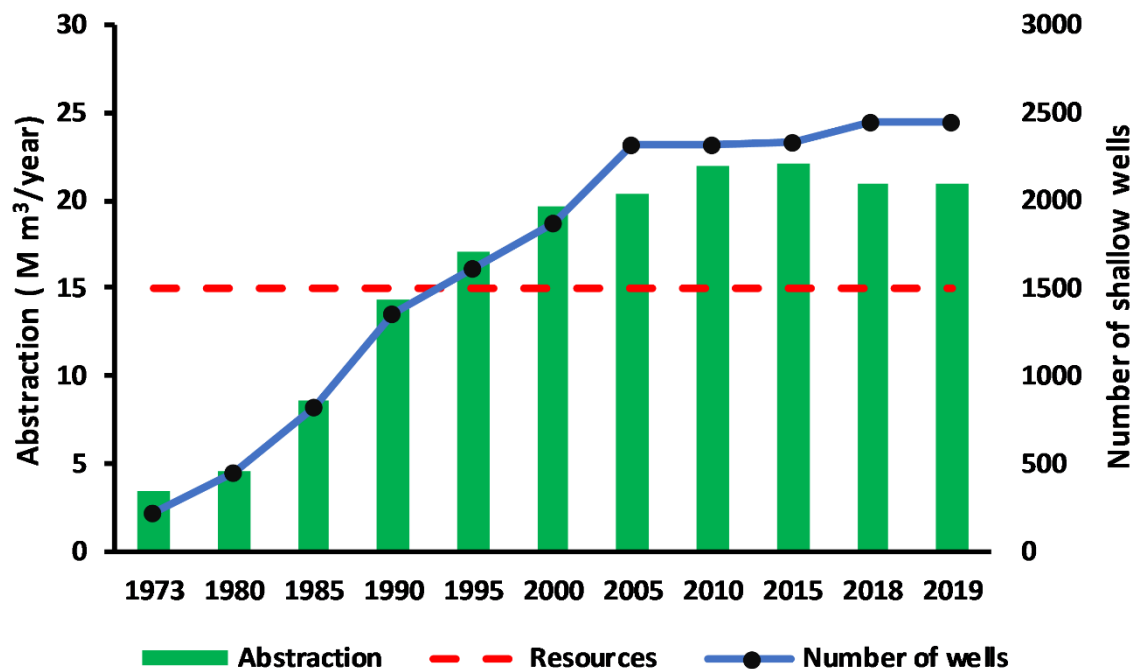


Figure 40. Evolution of the shallow aquifer abstraction and its number of wells

2. Beglia aquifer (Serrevallian)

Most of the wells capturing this aquifer are located in the labaidh region, Ben Mrad region, Felta and El Soud region. The Beglia aquifer is captured by 137 wells (DGRE 2018).

The Beglia aquifer presents a good quality in many regions of HJB, which is transported, by S.O.N.E.D.E, to alimente by drinking water in the Sidi Bouzid and Sfax regions.

The S.O.N.E.D.E exploitation of the Beglia aquifer exceeded $20 \times 10^6 \text{ m}^3/\text{year}$ (DGRE 2018). This aquifer's total abstraction is equal to $33.4 \times 10^6 \text{ m}^3$ in 2018 (Figure 41), which indicates an abstraction of 120% (resource equal to $27.8 \times 10^6 \text{ m}^3$).

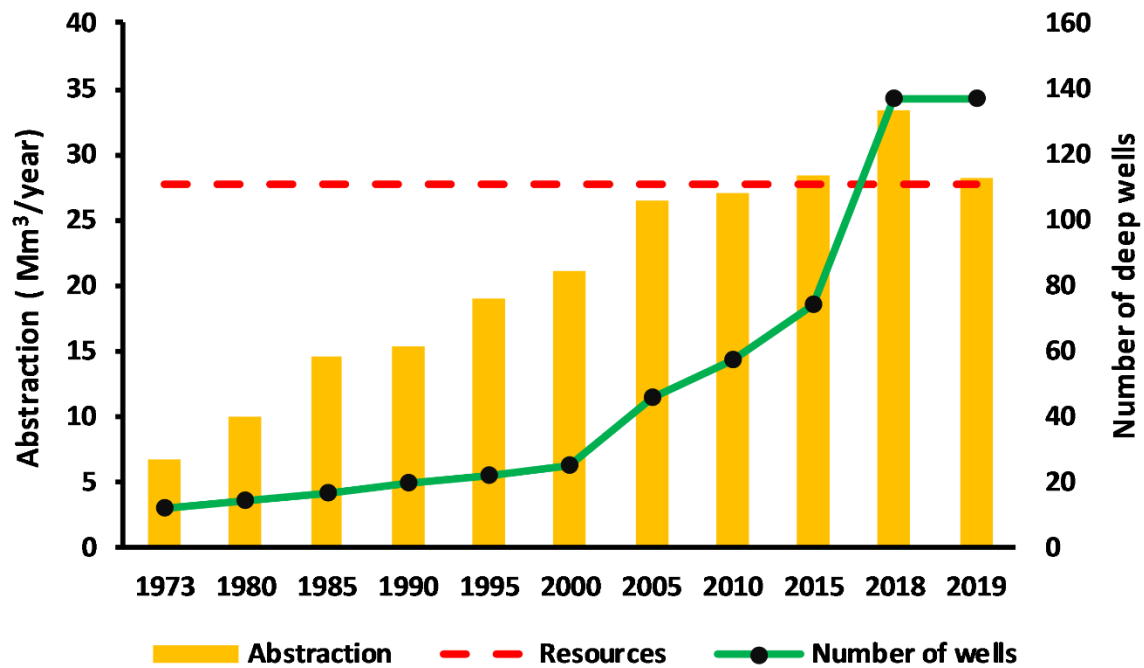


Figure 41. Evolution of the deep aquifer abstraction and the number of wells

The water pumped from the Beglia aquifer is used in different water needed sectors. In 2017, the total abstraction from this aquifer was equal to $26.44 \times 10^6 \text{ m}^3$, which is divided into three uses sectors (DGRE 2017) (Figure 42):

- The S.O.N.E.D.E uses a rate of $14 \times 10^6 \text{ m}^3$ ($\approx 53.02\%$) for the drinking water alimentation of various regions.
- An abstraction equal to $12.37 \times 10^6 \text{ m}^3$ ($\approx 46.82\%$) is used for the irrigation practices
- A very low rate equal to $0.041 \times 10^6 \text{ m}^3$ ($\approx 0.16\%$) is used for the industry sectors

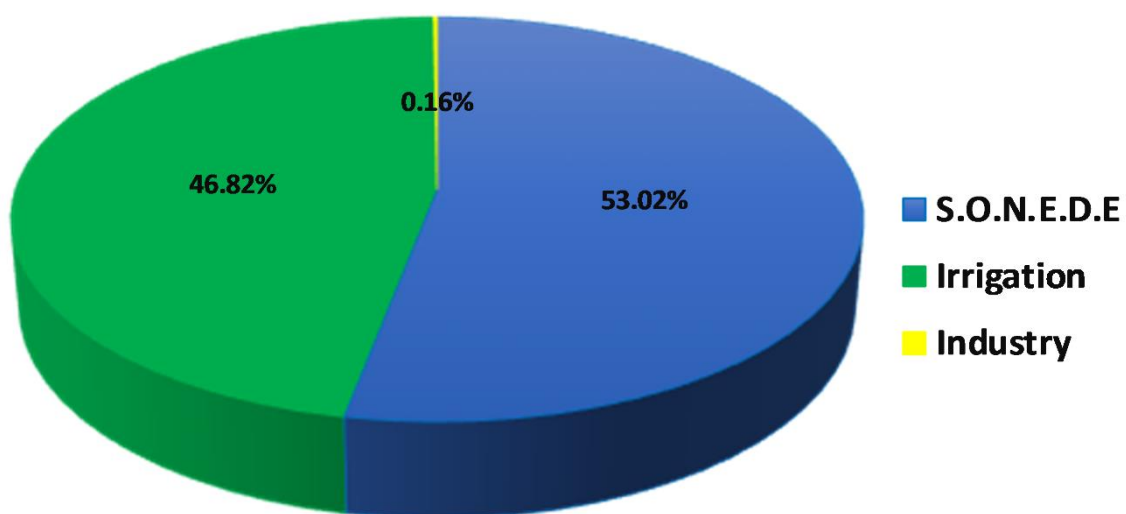


Figure 42. The different uses sectors of the Beglia deep aquifer (DGRE 2017)

3. Hayet Mineral water

The Hayet mineral water is pumped from the “*Baten El Ghazel*” deep well, located in the north of the study area, which extract the water from the Beglia aquifer from a depth of 184 meters. This well is drilled at the end of the year 1987 and is in exploitation in 1988. This mineral water is distributed in a bottle of 1.5 liter. **Figure 43** shows this well's abstraction: has been equal to $0.014 \times 10^6 \text{ m}^3$ in 1988. It has attended a maximum of exploitation in 2009 with a rate equal to $0.12 \times 10^6 \text{ m}^3$ and the abstraction in 2017 equal to $0.041 \times 10^6 \text{ m}^3$ (DGRE 1973-2019). The water quality assessment of this well, in this work, showed an ‘excellent’ water quality (See Part 3/Chapter 1).

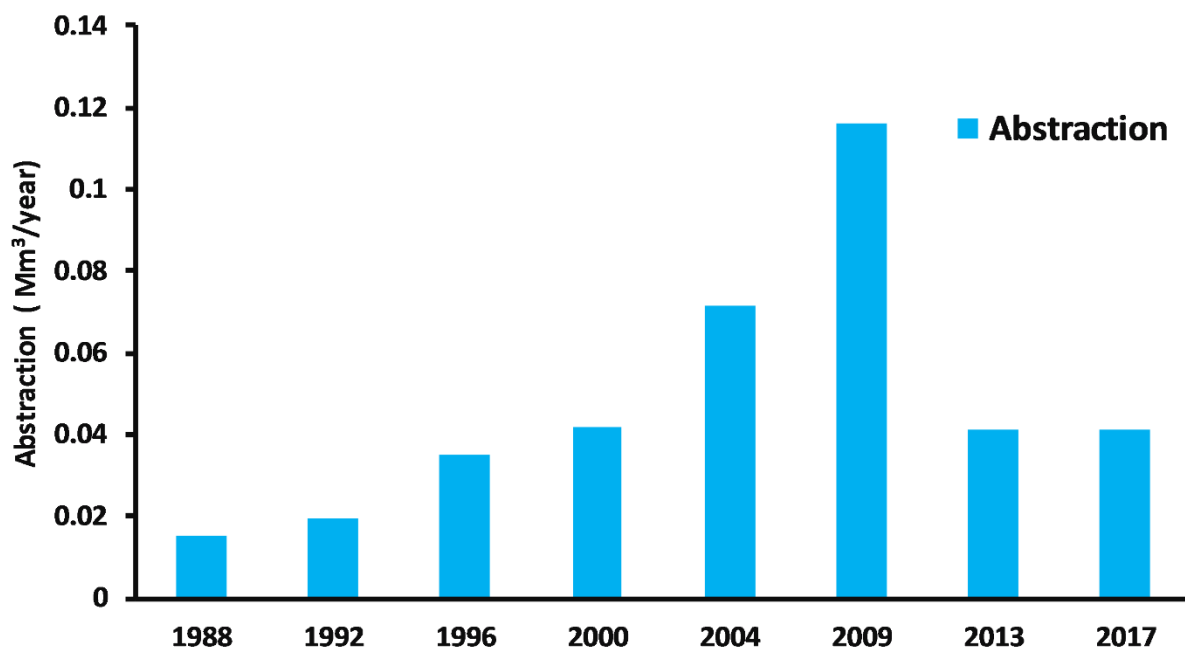


Figure 43. Evolution of the Hayet mineral water abstraction

4. Ain Ghrab aquifer (Aquitainian)

Since the year 1980, this water reservoir is being in exploitation. It is designed “Jelma 3” by the DGRE. The water direction authorities do not control this aquifer's piezometry level since this spatial distribution is not identified. For that, this aquifer is not taken into consideration in this work.

This deep aquifer is exploited by only 7 wells (DGRE 1973-2019). The S.O.N.E.D.E exploited this aquifer for drinking uses, for the Sfax region, using 4 wells, with an abstraction rate equal to $6.45 \times 10^6 \text{ m}^3$ (DGRE 1973-2019) (**Figure 44**). The other three wells are used for drinking water alimentation for Sidi Bouzid governmental institution (Agriculture administration, School...) and its total abstraction is equal to $0.14 \times 10^6 \text{ m}^3$ (DGRE 1973-2019).

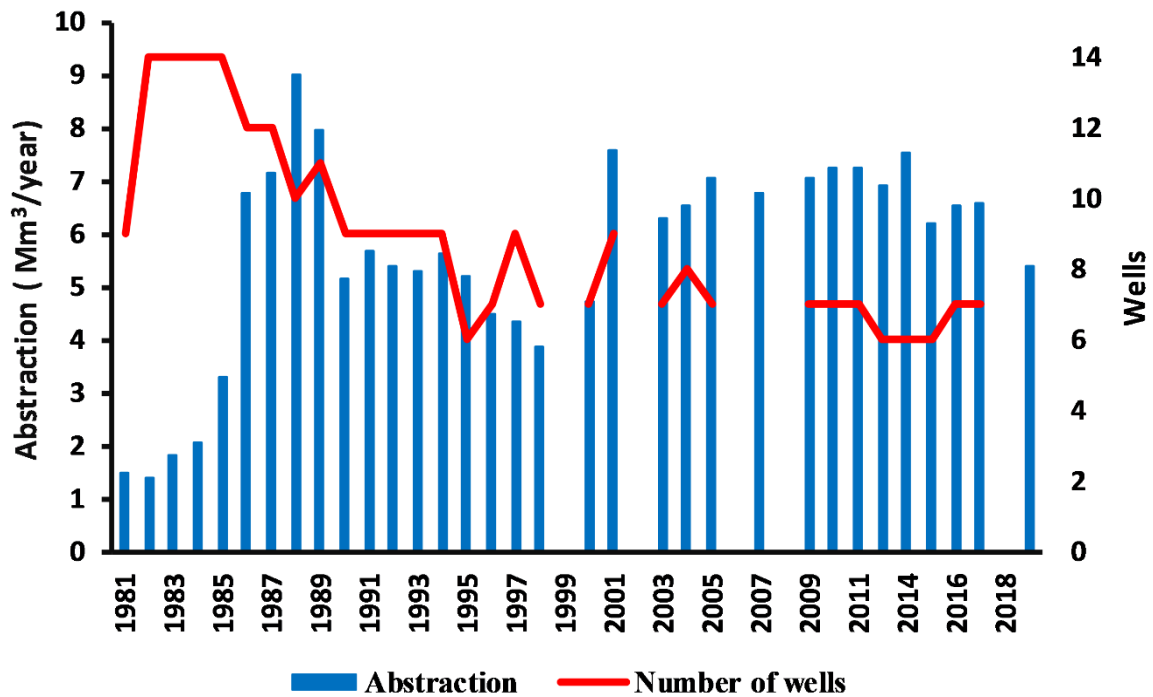


Figure 44. Evolution of the Ain Ghrab aquifer abstraction and the number of wells

5. Cretaceous aquifer (Aptian)

This aquifer is exploited by the S.O.N.E.D.E using only one well (Hajeb Gare: n°IRH: 3412/4) located in the Zaouia mountain and captured the Aptian marly limestone. S.O.N.E.D.E pumped this well for drinking uses for 24 years (1974-1997) (Figure 45) (DGRE 1973-2019).

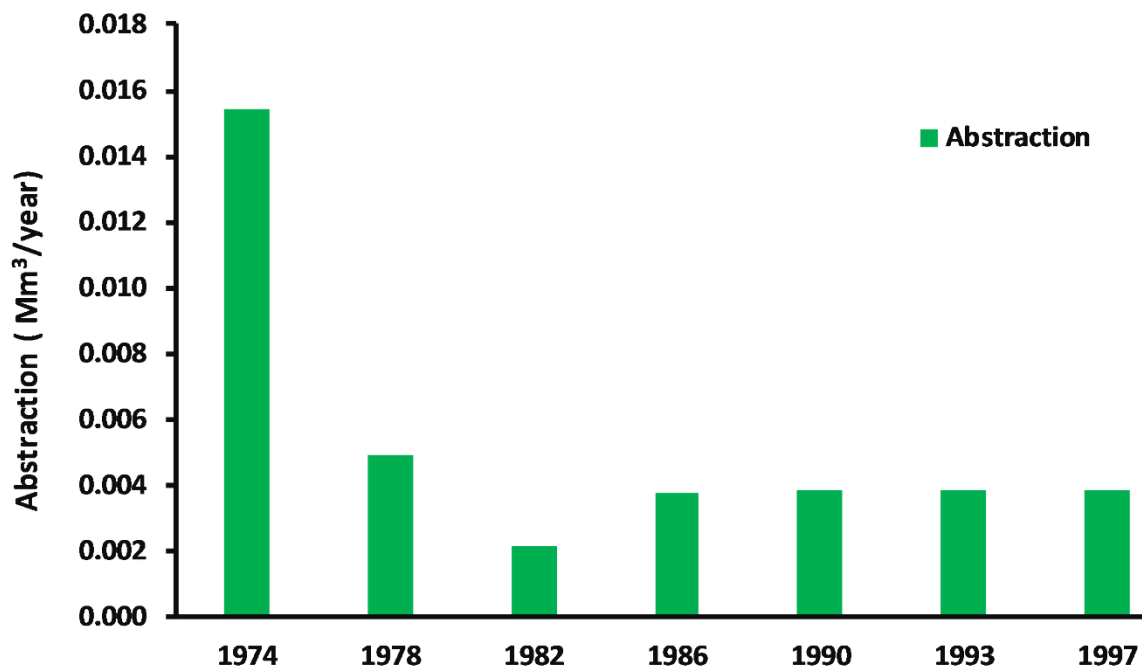


Figure 45. Evolution of the Aptian aquifer abstraction

VI. Groundwater regime and piezometric contour lines

1. Historic data

The surveillance of the piezometric level of the aquifers of HJB has started in 1973 (Appendix 3). Six piezometers control the Beglia deep aquifer (Figure 46) and the shallow aquifer is controlled by two piezometers and several shallow wells (Figure 48). The over-exploitation of both aquifers resulted in a decrease in the water table.

1.1. Shallow aquifer

The average yearly decline for the shallow aquifer, over the period 1973-2018, is equal to 0.4 m/year (DGRE, 1973-2018) (Figure 47).

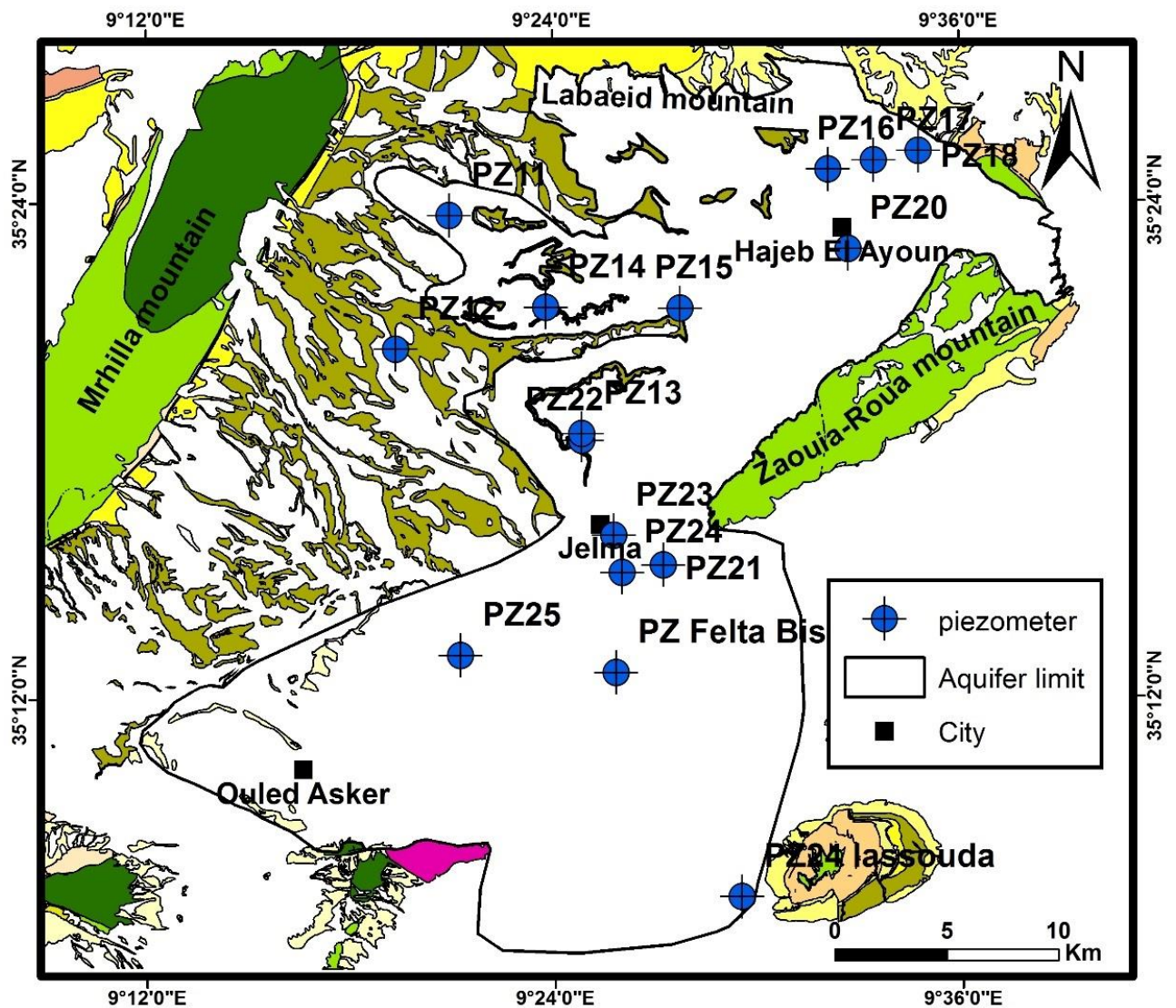


Figure 46. Location of the piezometers controlling the shallow aquifer

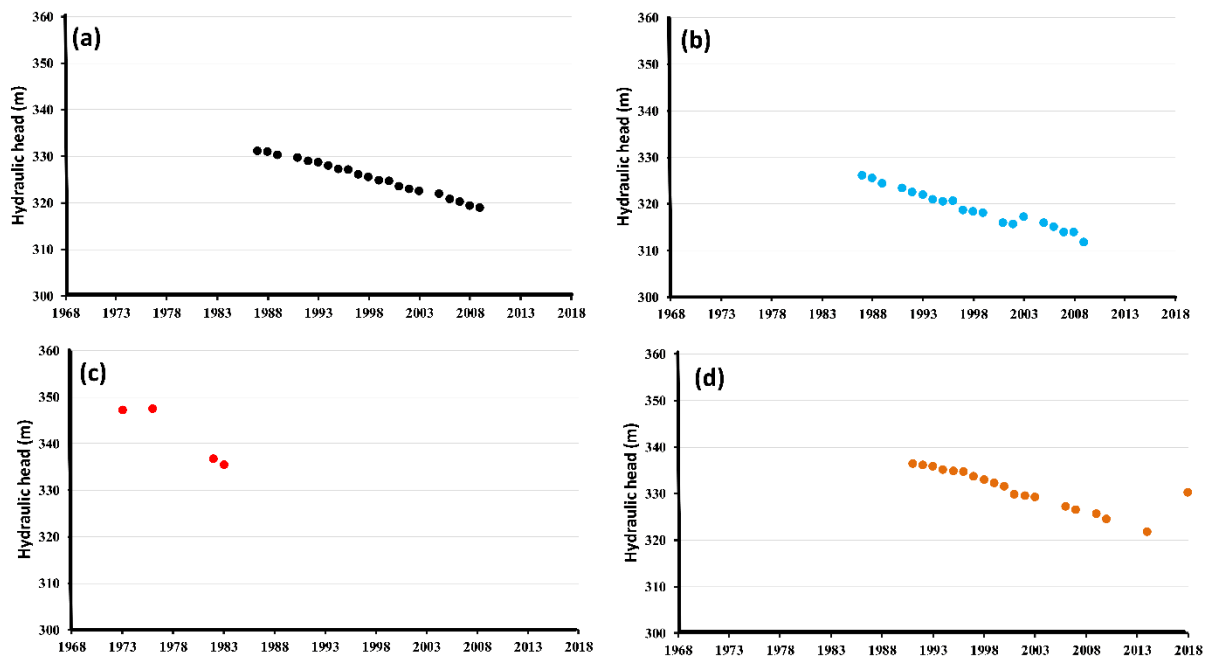


Figure 47. The shallow water table decline in four selected piezometers: (a) well n°27, (b) Pz 21, (c) Pz 20 and (d) Pz 24

1.2. Beglia deep aquifer

This aquifer is the only deep aquifer controlled in the Sidi Bouzid region since 80% of its resource is exploited by the S.O.N.E.D.E. It is surveyed by 6 piezometers (Pz₁, Pz₂, Pz₃, Pz₄, Pz₅, Pz₁₀) for 47 years (1973-2019) (Figure 48). The six piezometers are located in the northern part of the study area, which presents a problem in drawing the piezometric map.

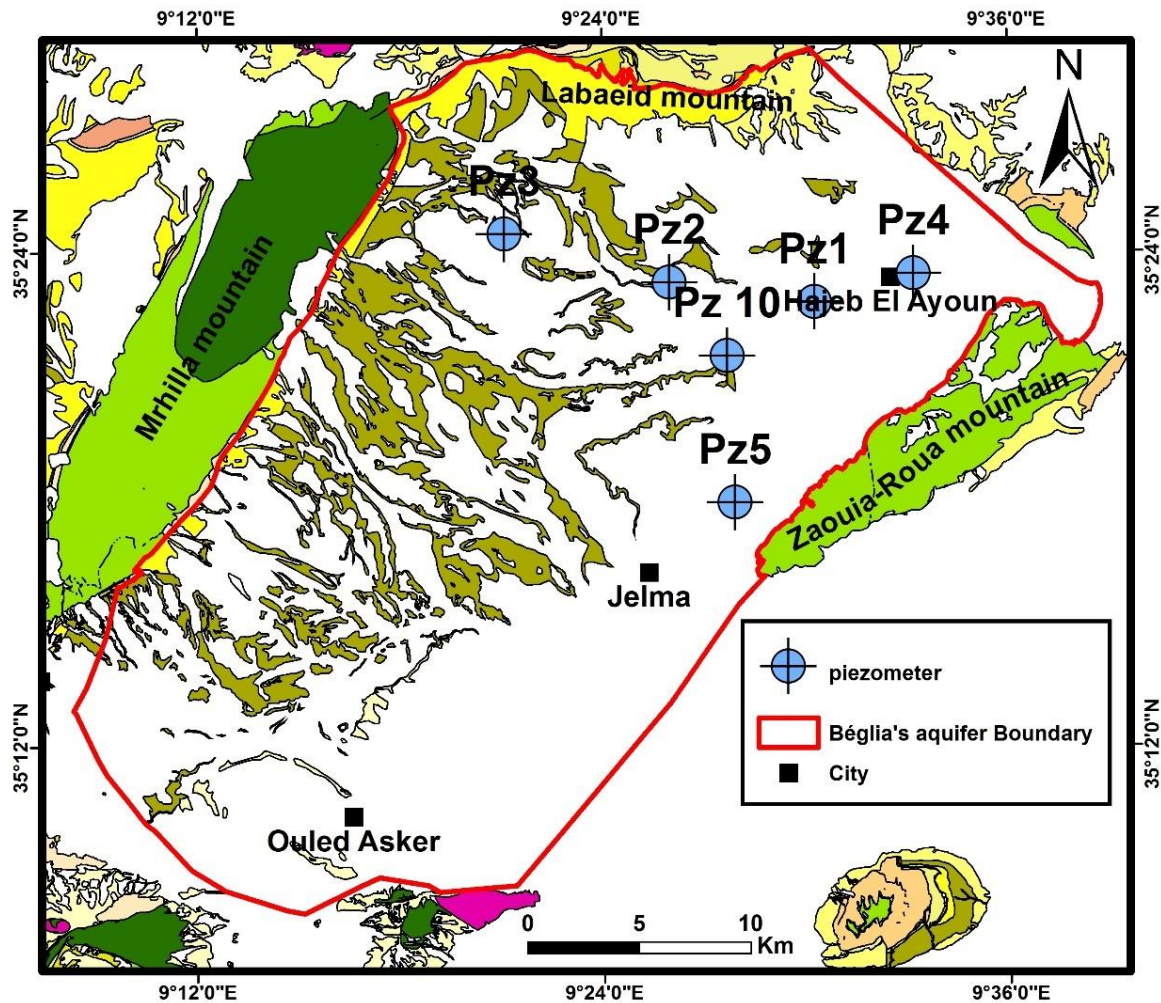


Figure 48. Location of the six piezometers controlling the Béglia aquifer

The over-exploitation resulted in a high decline of piezometric levels (**Figure 48**). As shown in **Table 3** the total decline varied from 27.79 m to 10.57 m (DGRE **1973-2018**), which signifies that this aquifer has a yearly piezometric decline varying from 0.2 to 0.7 m/ year (**Figure 49**).

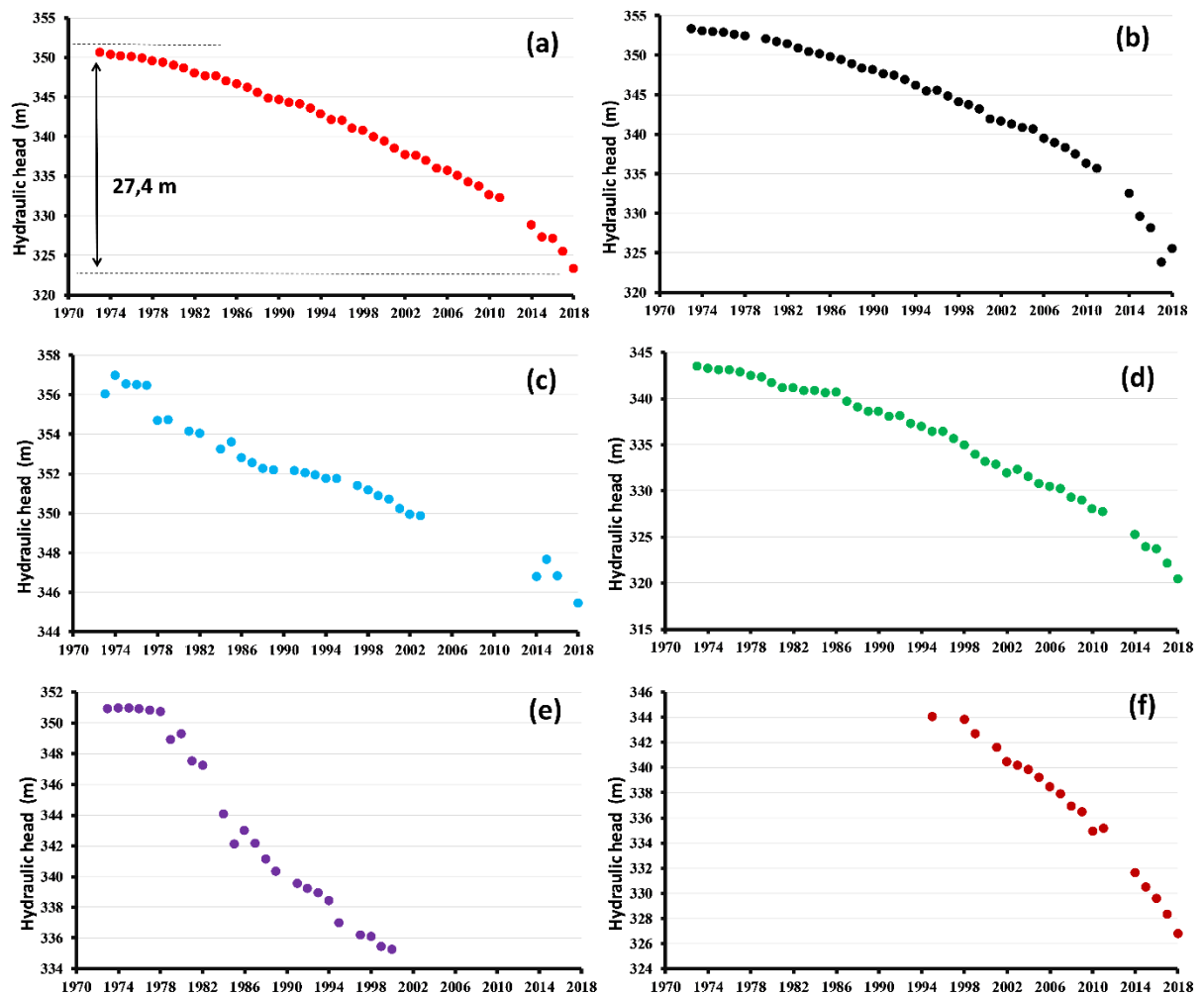


Figure 49. The evolution of the piezometric level of the deep aquifer at six selected piezometers: (a) Pz1 (Hadjeb), (b) Pz2 (Ben Mrad), (c) Pz3 (Zoghmar), (d) Pz4 (Hadjeb ville), (e) Pz5 (Ghedir Gaied) and (f) Pz10 (Chastel bis)

Table 3 Total decline of water table in deep aquifer during the period 1973-2018

Piezometer	N°IRH	Period	Duration (years)	Total decline (m)	Average decline (m)/year
Pz1	13590/4	1973-2018	46	27.38	0.6
Pz2	13598/4	1973-2018	46	27.79	0.6
Pz3	13947/4	1973-2018	46	10.57	0.2
Pz4	13973/4	1973-2018	46	23.02	0.5
Pz5	13949/4	1973-2000	28	15.62	0.6
Pz10	19205/4	1995-2018	24	17.25	0.7

2. Flow direction

For the deep aquifer, the main groundwater flow direction is from the west coming from Mrhilla Mountain (Recharge zone), toward the central part of Hajeb Layoun, where groundwater is divided into two parts: the first discharges at Hajeb Layoun fault and the second at the level of some faults in the north part of Zaouia-Roua Mountain (Figure 50). The discharge areas are manifested by springs. For the shallow aquifer, the main flow-direction is from the east to the west in the southern part, and two direction flows in the northern part: East to the West and south to the north (Figure 51).

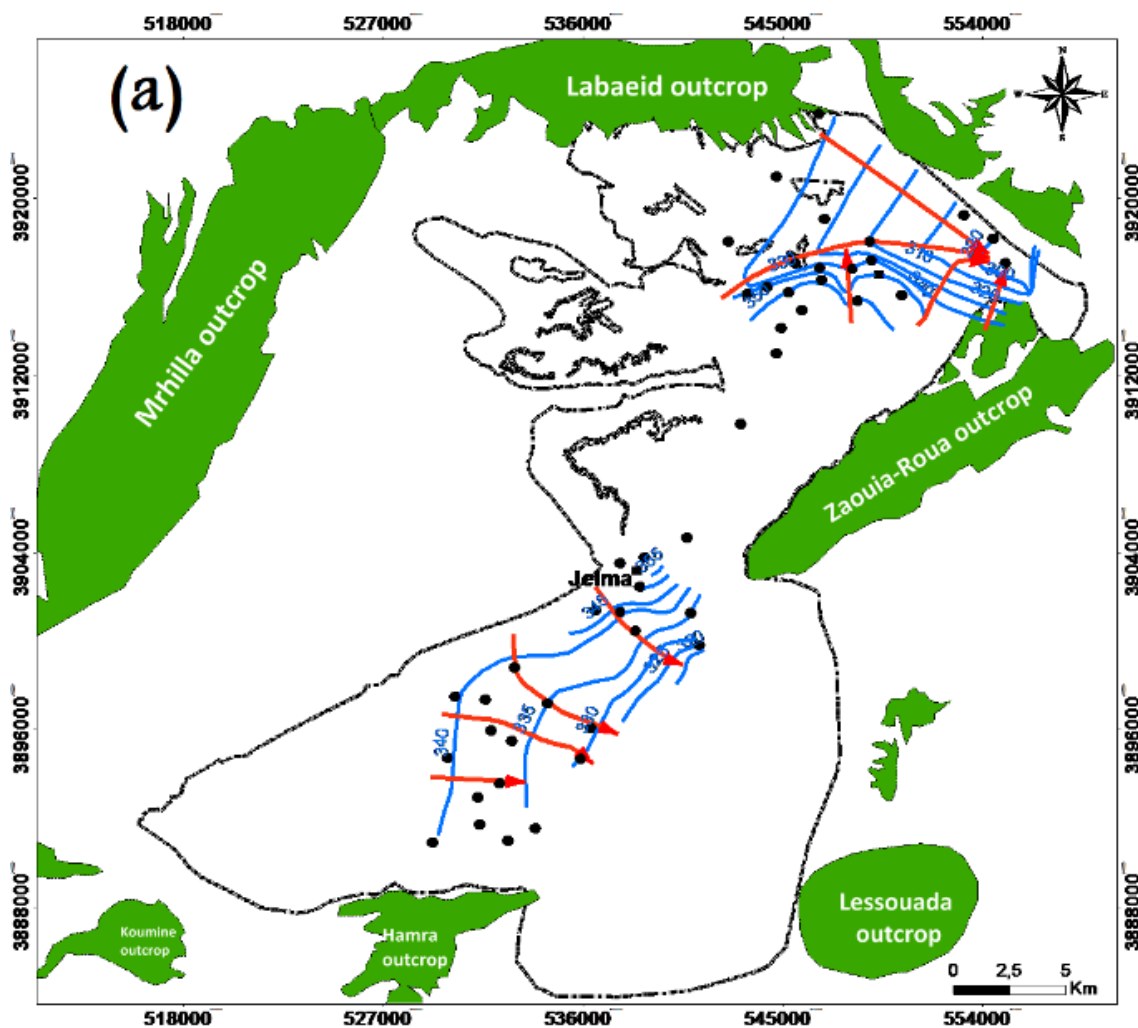


Figure 50. Piezometer map of the shallow aquifer in 1973

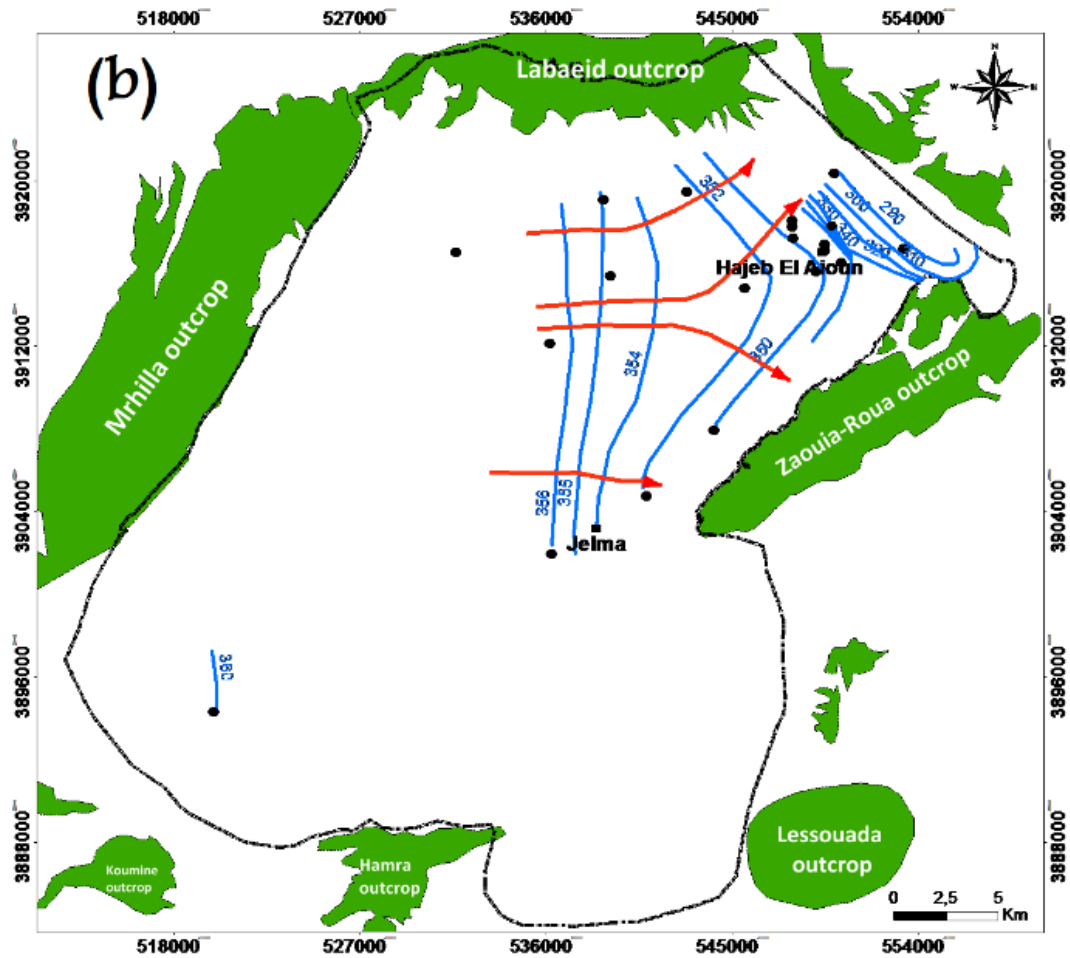


Figure 51. Piezometer map of the deep aquifer in 1973

VII. HJB's water distribution for the Sfax region

Sfax's groundwater has a high salinity content (DGRE 2018). The water of the deep aquifer of Sfax presents a mean salinity of about 3.5g.l^{-1} mixed with another water to be appropriate for drinking uses (DGRE 2018).

The Sfax region was alimented mainly by the Sbeitla 's water, which gushes at the height of the remains of the ancient Suffetula. The water pipe was carried out between 1907 and 1914 with a flow rate equal to 100 l.s^{-1} . With the population growth and the socio-economic development, the consumption has exceeded the old installation's capacity. For these reasons, during the years 1945 and 1953, extension works were undertaken to capture some wells from the Sbeitla region.

To meet the water needs of the region of Sfax, S.O.N.E.D.E decided to exploit the reserves of the deep aquifer of Hajeb-Djelma basin; for this, it built the second adduction to the one already existing with a maximum flow of 400 l.s^{-1} .

The wells intended by the S.O.N.E.D.E are nine: Hajeb7bis (19038/4), Hajeb8 (18561/4), Djelma7 (13994/4), Djelma8 (15980/4), Djelma9 (15984/4), Chastel2 (7809/4), Djelma13bis (17706/4), Djelma14 (17737/4), Bled Mejrj bis (18306/4) (**Figure 52**). In 2018, the S.O.N.E.D.E exploitation of the Beglia aquifer exceeded $20 \times 10^6 \text{ m}^3/\text{year}$ (DGRE **2018**).

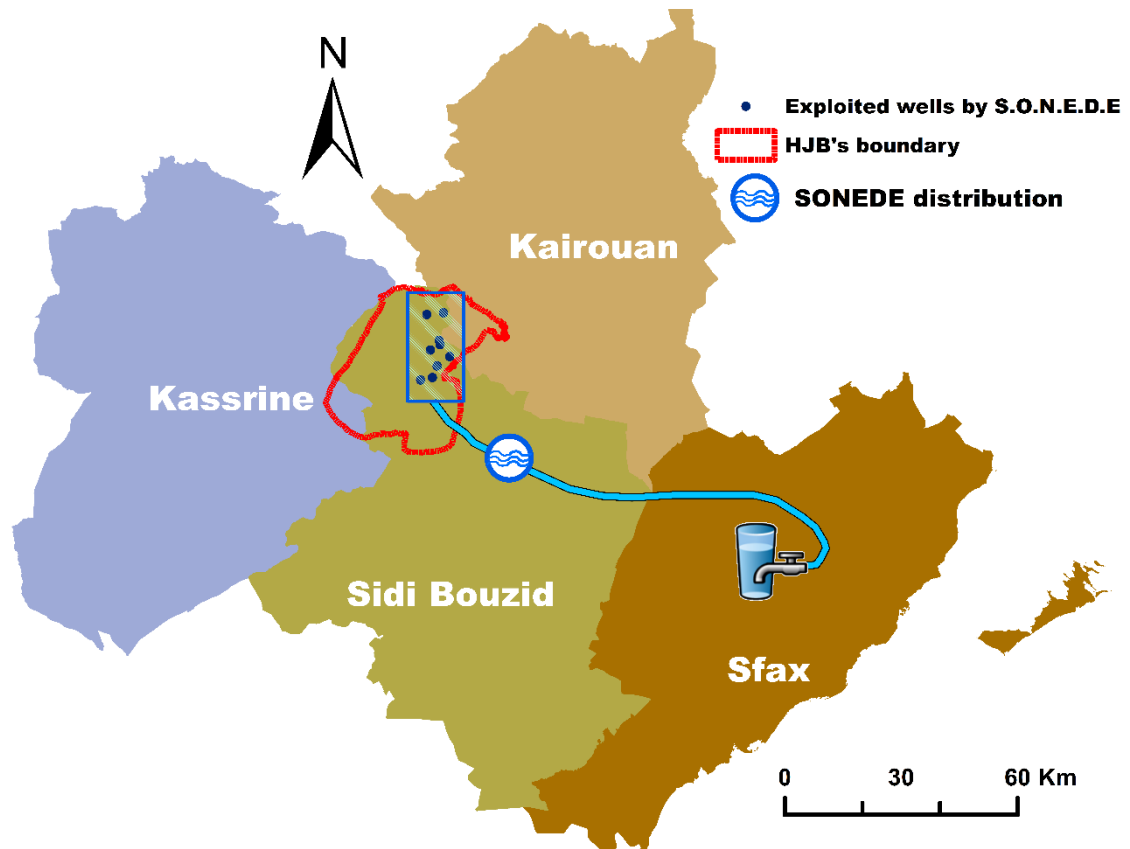


Figure 52. Distribution of HJB's water to Sfax

VIII. Groundwater Recharge

The groundwater recharge in the HJB is originated from the direct infiltration through floods descending from the mountains, occurring in the shallow aquifer (Quaternary deposits) and the deep aquifer where the Beglia aquifer is exposed at the surface (West part). Five years of the monthly measured water table, between January 2005 and December 2009, for four selected piezometers are shown in **Figures 53** and **54**. The water table's deep and shallow aquifers' fluctuation presents falls and rises caused by the outflow (exploitation) and inflow (the recharge process) of water.

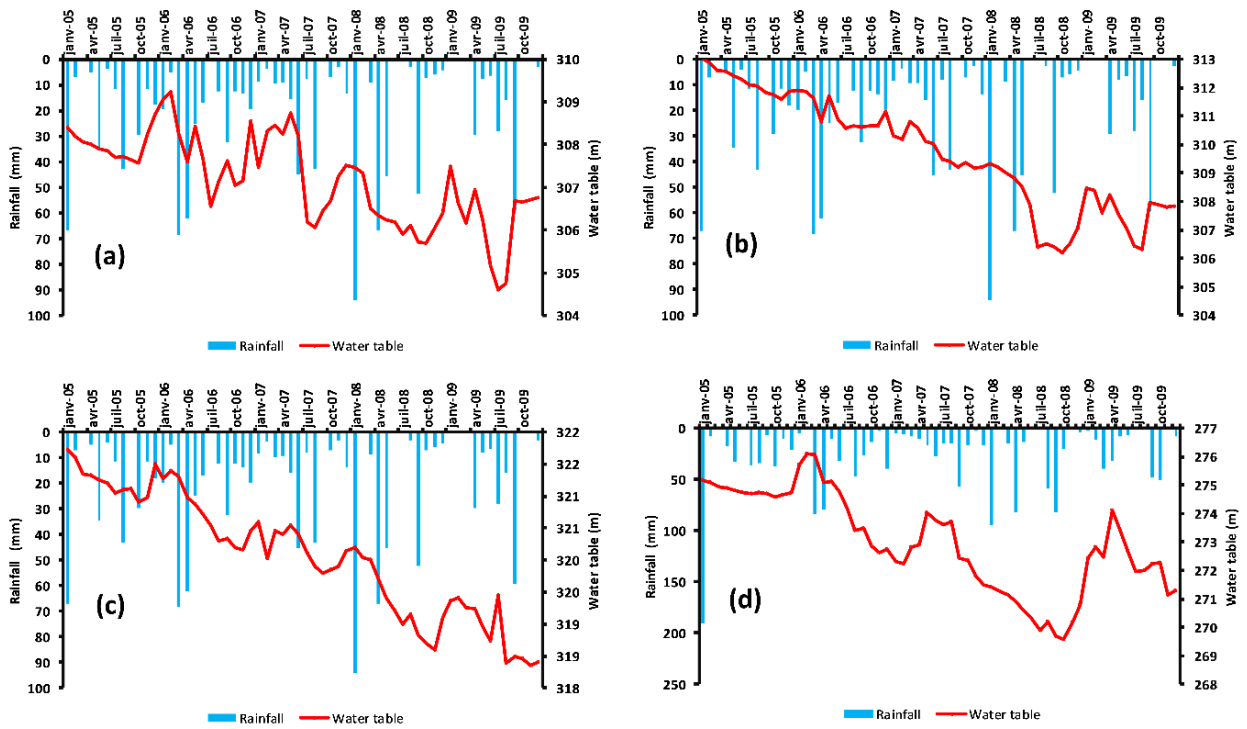


Figure 53. Fluctuation of the shallow piezometric level in response to the rainfall (at piezometers: (a) Pz Felta, (b) Pz 21, (c) Pz 20 and (d) Pz18) in the period January 2005 - December 2009

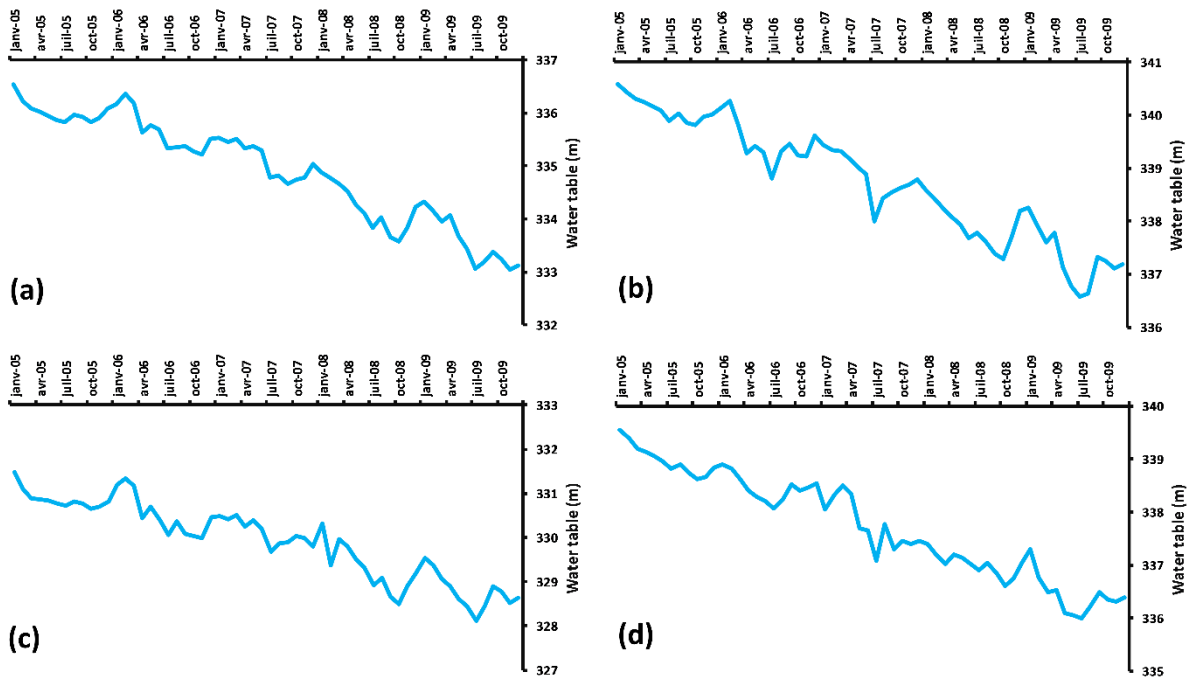


Figure 54. Fluctuation of the deep piezometric level (at piezometers: (a) Pz 1, (b) Pz 2, (c) Pz 4 and (d) Pz10) in the period January 2005 - December 2009

IX. Springs discharge

The HJB contains various springs. In the Eastern part, in labaeidh mountain, five springs are manifested in the Albién calcaires. The sources' rate was decreased from 139 l/s in 1972 to 8 l/s in 2010 and it attains 0.5 l/s in 2019 (Figure 55).

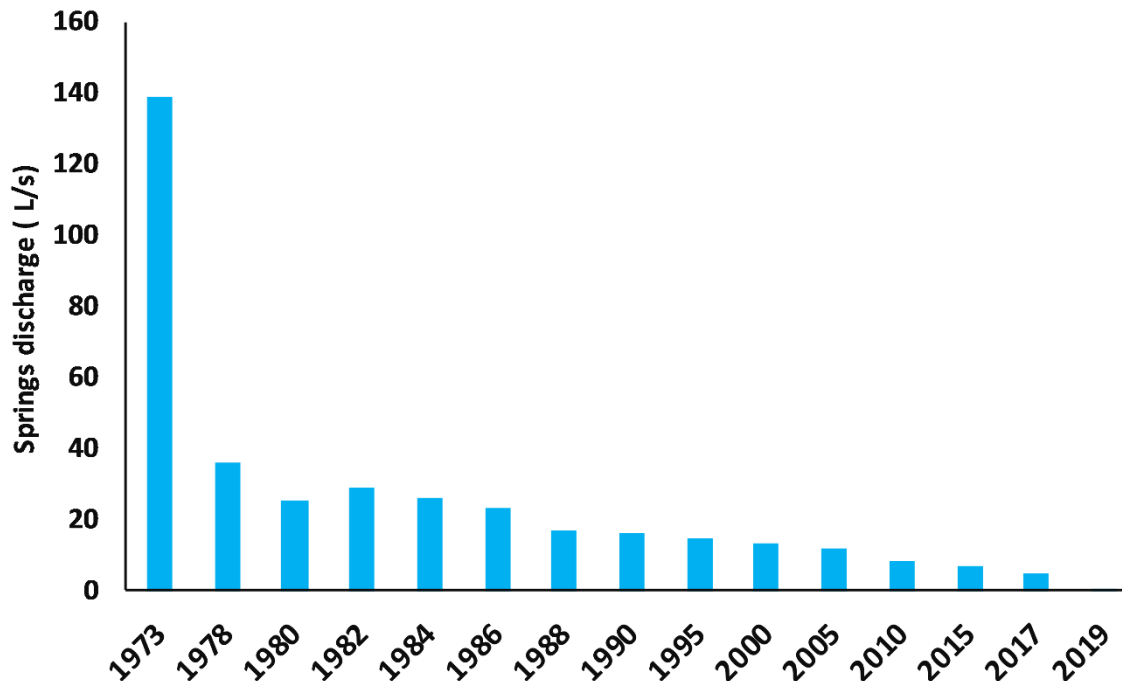


Figure 55. Evolution of the springs discharge in HJB

X. Hydrochemical characterization of HJB

In the Hajeb Layoun Jelma basin, agricultural practices are based on the use of huge quantities of fertilizers, influencing groundwater quality. Urban areas are also a potential source of pollution: the non-treated sewage rejected by the ONAS (National Sanitation Office) in the natural environment of Hajeb Layoun-Jelma basin, which is estimated to an average of 400 m³ by day (DGRE 2017), can have a long-term influence on groundwater resources.

The over-abstraction from this basin can also engender a decrease in the water quality. In fact, in 2018, the total abstraction from HJB, is equal to 58.45×10^6 m³, with a renewable resource equal to 42.8×10^6 m³, indicating a deficit of 15.65×10^6 m³ (DGRE 2018).

To show the irrigation effect on the water quality of HJB we have selected some wells with different locations (irrigated area and non irrigated area) and follow its nitrate and salinity concentration 's evolution over time.

1. Salinity evolution

According to the world health organization, the limit of salinity for water uses is equal to 1 g.l⁻¹ (WHO 2011). In Tunisia, the salinity limit was set as equal to 2 g.l⁻¹ (NT 2013). This difference between both standards reflects the required management of Tunisia's water.

In the Hajeb Jelma basin, the shallow and deep aquifer's water salinity was increased in the last decades. In the agriculture area, in 1996, the well Hajeb 8 ter indicated a salinity equal to 0.41 g.l⁻¹ and it increased in 2006 to attend 0.93 g.l⁻¹. In 2015 it exceeded the WHO limit with a value equal to 1.3 g.l⁻¹. In 2006, both shallow well Leizirig and Hseinia indicated values exceeding both standards (Table 4) (DGRE 2015). The salinity shows a maximum increasing with 0.89 g.l⁻¹ between 1996 and 2015.

In the non irrigated area, in 1996, the salinity distribution indicates a maximum equal to 1.6 g.l⁻¹ in Djilma7 ter well, which does not exceed the national limit. In 2006 the salinity in this well increased to attend 2.1 g.l⁻¹. In this area, the salinity increasing rate in the different wells attend a maximum of 0.45 g.l⁻¹. This increase can be justified by the flow transport of water and contaminant from irrigated to non irrigated areas.

Table 4 Evolution of salinity (g/l) between 1996 and 2006, in selected wells, for different uses (Irrigation and drinking) (DGRE 1996-2006)

Irrigated area	1996	2006	Difference	Non irrigated area	1996	2006	Difference
Hajeb8 ter	0.41	0.93	0.89	Bled mejer	1.30	1.67	0.37
Hajeb8bis	0.4	0.91	0.52	Zoghmar	0.67	0.95	0.27
Hajeb7	0.5	1.2	0.7	Djilma13	1.3	1.47	0.17
Chastel	0.8	1.4	0.6	Djilma6	1.20	1.26	0.06
Ben mrad	0.6	1.3	0.7	Baten ghzel	0.2	0.21	0.01
Celta	0.8	1.45	0.65	Zoghmar2	0.6	0.96	0.36
Chouaihia	0.48	0.97	0.54	Djilma7 ter	1.6	2.1	0.3
Zeller	0.96	1.65	0.69	Djilma9	1.2	1.55	0.35
Leizirig	1.4	2.45	1.05	Hajeb9	0.9	1.3	0.4
Hseinia	2.6	2.85	0.66	Hajeb10	1.2	1.65	0.45
F.C.lainier	0.96	1.37	0.81	Djilma14	2.3	2.55	0.25
Hajeb gare	0.6	1.2	0.6				

2. Nitrate evolution

As with all water elements, the nitrate has a limit not to be exceeded. In Tunisia, the standard limit of nitrate is equal to 45 mg.l⁻¹ (NT 2013). The international standard is equal to 50 mg.l⁻¹ (WHO 2011).

The recorded analysis results from DGRE show an increase of nitrate concentration from one year to another (DGRE 1996-2006). For the shallow wells located in irrigated area, in 1996, all wells present nitrate content less than both the standard limits (Table 5). The standard limits are exceeded by some well in 2006, with a maximum value equal to 98 mg.l⁻¹. The non irrigated area shows that all water respects the standard limit. Based on the data published by DGRE, the high level of nitrate content is related to shallow wells located in irrigated areas.

Table 5 Evolution of nitrates concentration (mg/l) in selected shallow and deep wells between 1996 and 2015

Irrigated area	1996	2006	Difference	Non irrigated area	1996	2006	Difference
Hajeb8 ter	02	28	26	Bled mejer	0.10	0.22	12
Hajeb8bis	01	29	28	Zoghmar	0	0.18	0.18
Hajeb7	00	25	25	Djilma13	13	32	19
Chastel	04	34	39	Djilma6	12	23	11
Ben mrad	02	28	26	Baten ghzel	0	0.6	0.6
Celta	20	58	38	Zoghmar2	0	19	19
Chouaihia	03	29	26	Djilma7ter	08	14	16
Zeller	02	32	30	Djilma9	11	24	13
Leizirig	20	63	41	Hajeb9	15	34	19
Hseinia	24	69	25	Hajeb10	22	42	20
F.C.lainier	81	98	17	Djilma14	10	28	18
Hajeb gare	29	44	15				

XI. Conclusion

The Hajeb Layoun-Jelma basin is filled with detrital deposits separated by impermeable (clays) and semi-permeable (sandy clays) levels. The Miocene series are continuous over the entire basin and extend across the region from the western edge reliefs to the eastern limit of the basin. The stratigraphic levels identified are:

- The Langhien: It is formed by marly and clay levels and sometimes sandstone. They contain very porous horizons,
- The Serravallian: The sands and sandstones of the Serravallian (Beglia formation) represent the Hajeb Layoun Jelma basin's main aquifer. The Serravallian aquifer is covered by the clay of the Tortonian clay (Saouef formation), which separates it from the overlying aquifer levels.
- The Tortonian: The lithological description of the boreholes shows sandy levels with variable thicknesses lodged in clay and marly formations;

- The Plio-Quaternary water table is discontinuous and lodged in sandy to sandy-clay formations and sometimes in clay formations.

The Hajeb Layoun Jelma basin receives an alimentation by rainfall infiltration. The groundwater of HJB is over-exploited by more than 3000 wells, and this over-abstraction engendered the decrease in water quality and quantity. The agriculture practices also have a high effect on the decreasing water quality of HJB.

Part 2 Materials and Methods

Chapter I Geo-database elaboration

Chapter II Geochemical characterization

Chapter III Groundwater flow Modeling

Chapter IV Vulnerability mapping and Contaminant transport modeling

« Do not waste water even if you were at a running stream »

Mahomet (salla allah)

Chapter I: Geo-database elaboration

I. Data gathering and analysis

Data collection is the first step in this research. The data collected can be mainly classified into two types: data present in maps such as topographic, geological maps, and point information collected from Tunisian water agency at the national and local levels (DGRE and CRDA of Sidi Bouzid) and previous studies. The database (BD) and the Geographic Information System (GIS) developed to include the inventory of all water points located in the various aquifers studied (boreholes, surface wells, springs, and piezometers) and their main characteristics (location, year of creation, altitude, etc.), historical data for rainfall, operation, and piezometry. The database and the GIS then provide the elements necessary for constructing the hydrogeological and the geochemical models.

1. Maps data

1.1 Topographic data

These data are available at the National Office of Topography and Cartography (OTC) and the Regional Commissariat for Agricultural Development (CRDA) of Sidi Bouzid in the form of digital topographic maps. The topographic map of Hajeb Layoun Jelma basin was created with the assembling, under the ArcGIS software, of nine maps at 1 / 50.000 scale: Hajeb El Ayoun, Jelma, Fayedh, Sidi bouzid, Sbeitla, Ghabet Kisra, Haffouz, Ar-Rouhyya, and jbal Mghila.

1.2 Geological map

The surface geological data are taken from the National Office of Mines (ONM) and the CRDA of Sidi Bouzid in the numeric form of six maps (scale 1 / 50.000) (Sbiba map, Trozza map, Mghilla map, Hajeb Layoun map, Sbeitla map, and Lassouada map).

2. Punctual data

2.1 Climatic data

The climatic data is crucial for the water balance calculation for the aquifer system and the determination of the study region's bioclimatic stages. The rainfall, evaporation, wind speed, and temperature data are taken from the National Meteorological Institute (I.N.M.) and the

CRDA of Sidi Bouzid. These data are grouped in tables were monthly and annual averages are calculated and represented in diagrams (see pages 32 to 41).

2.2 Piezometric data

Piezometric data is acquired from the CRDA of Sidi Bouzid in the form of piezometric observations of monitoring points (period 1973-2018). Part of the data is provided in a database containing a systematic inventory of all the Sidi Bouzid region's water points.

2.3 Wells data

These data are available from the CRDA of Sidi Bouzid in the form of drilling reports. Each borehole is described by a set of geological and hydrogeological, hydrodynamic data (coordinates (X, Y, Z), depth, screen position, nature of the aquifer, and static level, transmissivity, stratigraphic log, etc.).

2.4 Hydrochemical data

This component is formed by historical data (salinity and nitrates) and available from the CRDA of Sidi Bouzid.

II. *Geographical information system*

Geographic Information System (GIS) is an acquisition system for management, editing, visualization, analysis, and representation of spatial data (Longley et al. 2015).

GIS has a significant impact in all the domains concerned with management and spatial information analysis, such as the water domain. GIS is often presented as only one software to many tools (Saidi et al., 2006).

A GIS database was developed to make useful tools from available data to understand the functioning of HJB better. Under ArcGis 10.3, a database has been established, including the inventory of all deep and shallow wells implemented in different aquifers and their main characteristics (Localization, year of creation, borehole depth) and historical data (rainfall, piezometry and withdrawals). The thematic maps, such as piezometric maps, geological maps, land use and distribution maps of some parameters such as salinity and quality indices of the study area were obtained from 1:50000 scale. They were georeferenced under the UTM coordinate system. The coordinates of each well were measured by using, in the field, a global positioning system (GPS).

The extraction of the study area topographic map was made using the clip function. This map was digitized by GIS software. Several layers of information are digitized from the topographic map: the contour lines, the hydrographic network, the road network, the water points, the side points, the wetlands (sebkhas), the plant cover ... The maps used in this work were published in 1992 (UTM division).

The geological map of the Hajeb Layoun Jelma basin (**Figure 24**) was created, using ArcGis, by assembling six geologic maps with a scale of 1/50.000 and the numerisation of the different deposits. Six geological maps are digitized and assembled. Several layers of information are extracted from geological maps such as lithology, facies and age of geological layers, the permeability of outcropping facies, faults, and dip layers ...

In the geochemical study, the spatial distribution of different quality indices such as salinity, WQI, EWQI, and ImpWQI was obtained by the IDW method.

Chapter II: Geochemical characterization

I. Introduction

Water is the principal component in the earth that supports the life of all living. Groundwater is a very important source of water, specifically in the semi-arid and arid regions. It supports all types of uses (drinking, irrigation, and industrial....) (Hamzaoui Azaza et al., 2020). However, groundwater is threatened by severe problems caused by natural/anthropogenic factors, such as extensive agricultural activities, marine intrusion, population growth, industrial development...etc. (Zammouri et al., 2013). This factor engendered a degradation in the quality and the quantity of groundwater in many countries. For example, Ameer et al., (2016) finding that the water quality in northeast Tunisia is at a poor level due to the nitrate pollution originate from the excessive use of nitrate-rich fertilizers. Adimalla (2019) conducted a study on the effect of the rapid urban activities (South India) on water quality and the human health risk related to nitrate and fluoride pollution. Mnassri et al., (2018) demonstrate that the sources of the groundwater salinization (Central-eastern Tunisia), which the salinity exceeding 6 g.L^{-1} , originate from anthropogenic/natural factors (dissolution of halite, precipitation of carbonate coupled with the dissolution of gypsum, evaporation and intensive irrigation practices). Ligavha-mbelengwa et al. (2020) conducted a work investigating factors influencing the water quality (South Africa). They indicated that both anthropogenic and natural factors are controlling the groundwater quality of this site.

Water quality has a strong relationship with health risk (Ricolfi et al., 2020); for this, the water quality evaluation is critical and widely studied in many regions worldwide (Barbieri et al., 2019; Su et al., 2019; Asadi et al., 2020).

Various methods are used for the water quality evaluation; for drinking uses, we cited: the "Water quality index" "WQI" (Ghouli et al., 2018), "the Entropy water quality index" (Islam et al., 2017), "the improved water quality index" (Wang et al.2018; Zhang et al., 2020), the fuzzy logic method coupled with WQI (Moghari et al., 2015) etc.... For the irrigation uses, the evaluation of water quality is based on classic indices such as the electrical conductivity 'EC', the percent sodium 'Na%', alkalinity hazard 'SAR' and Kelly ratio 'Kr'.

In Africa and specifically in Tunisia, which groundwater is practically the main water's source in many regions, the evaluation of water quality was taking, recently, many attentions by the hydrogeologists which show that various regions are facing a decline in

groundwater quality (Ghouili et al., 2018; Mnassri et al., 2018; Hamzaoui-Azaza et al., 2020 etc..).

The Hajeb Layoun Jelma basin (HJB), the subject of this study, is located in central Tunisia. It is extending for over 1380 km² which represents 0.8% of the national territory and has about 172.003 inhabitants (INS 2014), corresponding to approximately 1.54% of the Tunisian population and which was 50,306 inhabitants in 1972 (Koschel 1980). The population growth (more than three times) plays a strong effect on the water request and has a significant effect on water resources. The HJB aquifer system is essential to both the southern and the central part of Tunisia. The deep aquifer water is transported to the Sfax city located at 180 km away from the HJB. During the last decades, the HJB presented a development of agriculture activities based on fertilizers and pesticides to improve agricultural production. This development has significantly affected pressure on groundwater resources: the water extraction increases for both aquifers (shallow and deep aquifer) from $14.8 \times 10^6 \text{ m}^3$ in 1973 to $58.45 \times 10^6 \text{ m}^3$ in 2018, with almost 2328 shallow wells and 137 deep wells (DGRE 1973-2018). These human activities have put increasing pressure on the groundwater quality of these aquifers.

To check HJB's water safety, 28 water samples collected from shallow and deep aquifers tapping the HJB have been interpreted using statistical and geochemical methodologies to wholly understand groundwater quality distribution patterns. This research aims to study groundwater hydrochemistry and identify the purposes of using the HJB for human consumption, irrigation using combined GIS and geochemical methods.

The steps followed, in this research, was resumed in **Figure 56**.

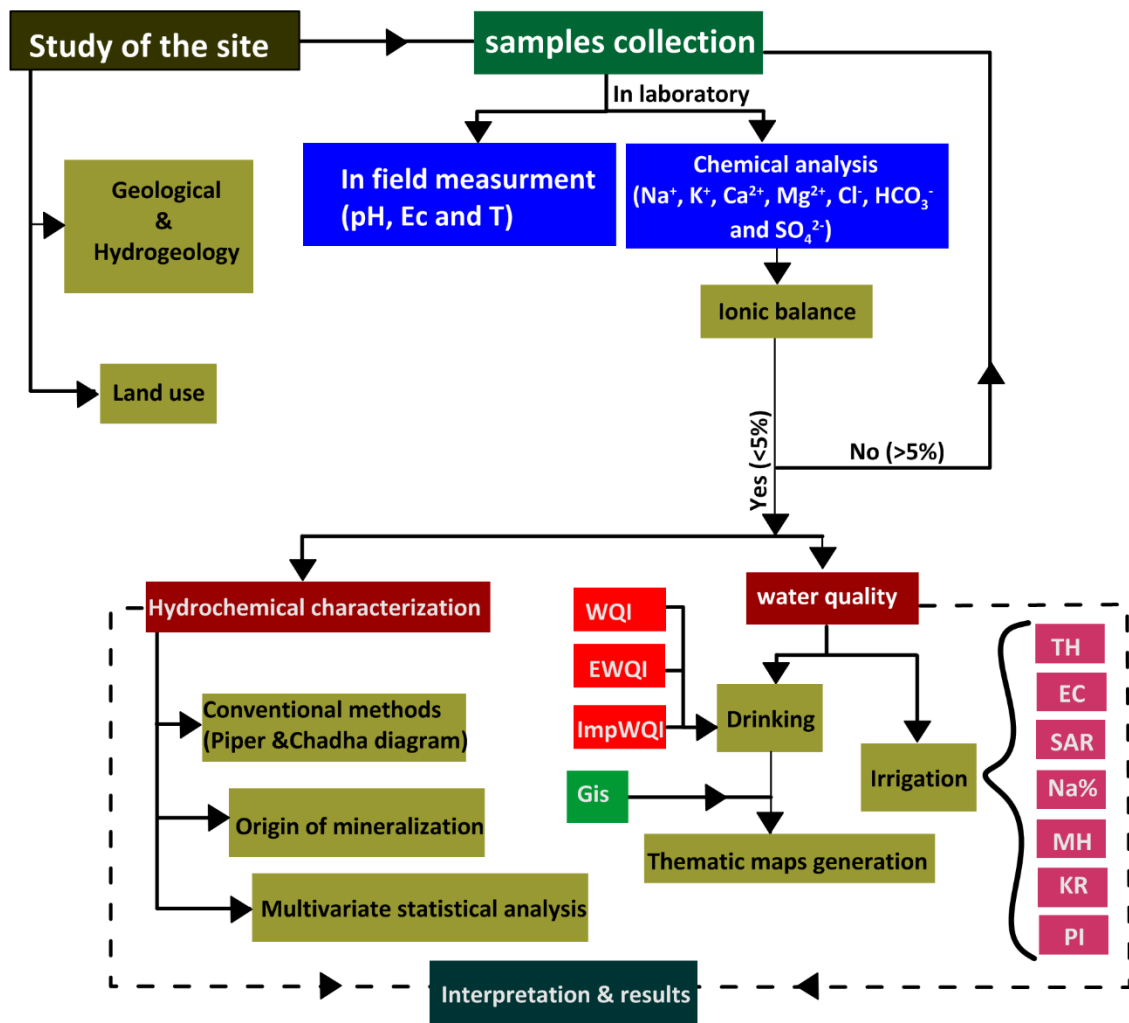


Figure 56. Flow chart showing the methodology applied in the HJB's water evaluation

II. Samples collection and analysis

In February 2017, a total of 28 samples were taken from wells in Hajeb Layoun-Jelma basin (humid period): 14 samples from the Beglia aquifer, 10 from the shallow aquifer (from depth of approximately 10-50 m) and 4 from springs (Figure 57).

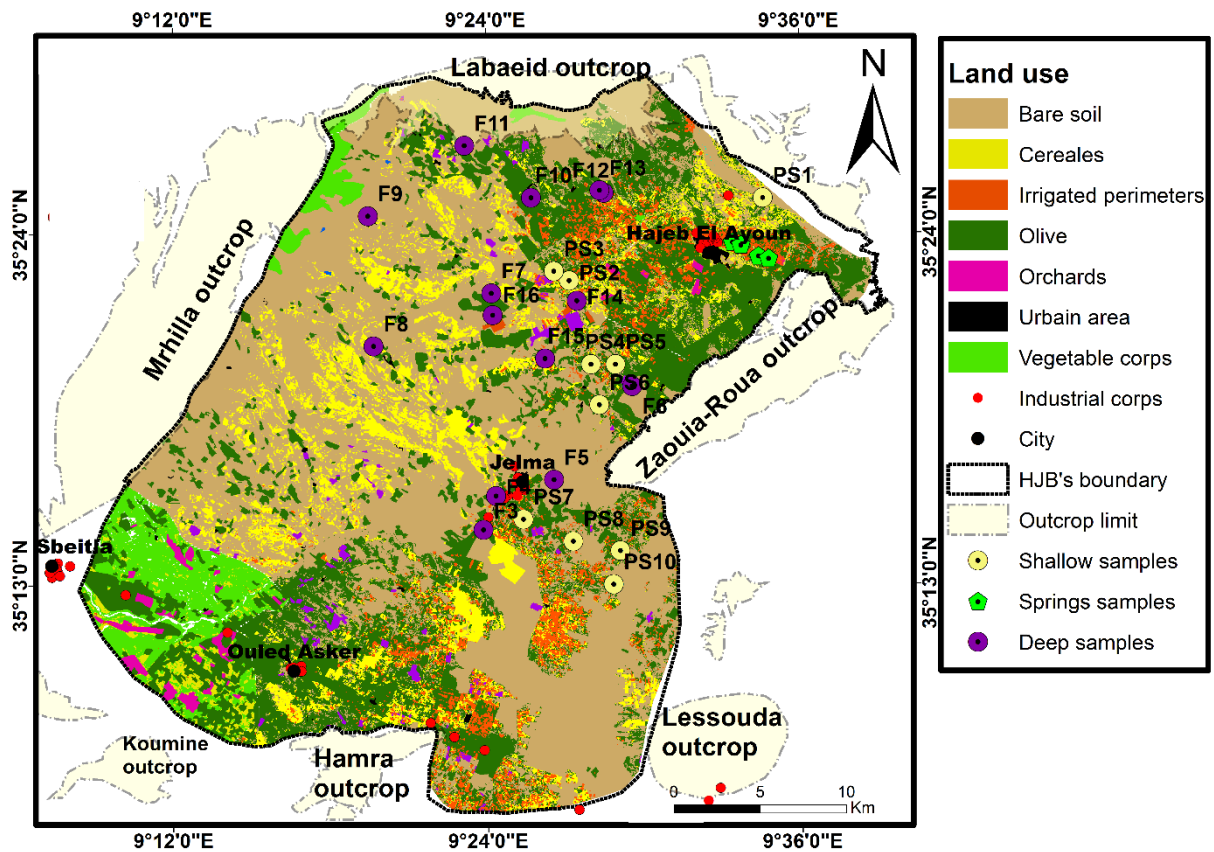


Figure 57. water samples location

In the field, to avoid residual water's influence, each well was pumped, for at least 30 min, until steady-state chemical conditions were obtained. According to the standard procedures given by Eaton et al., (1950), the samples of HJB were collected using pre-cleaned and rinsed (distilled water and water sample) polyethylene bottles (1L).

The physical parameters (including temperature (T), pH, and electrical conductivity (EC)) were measured in the field (under minimal atmospheric contact) using handheld analyzing kits, which were calibrated in the first in the laboratory using standard solutions before use.

After sampling, samples were labeled, taken to the laboratory and stored below 4 °C. The chemical analyzed parameters include major anions and cations (Sodium (Na⁺), Potassium (K⁺), Calcium (Ca²⁺), Magnesium (Mg²⁺), Chloride (Cl⁻), bicarbonates (HCO₃⁻), Sulfate (SO₄²⁻)). In order to validate the analysis results, the charge balance errors (%E) was calculated, for all samples, using the following formula:

$$\%E = \frac{|\sum C - \sum A|}{\sum C + \sum A} \quad (\text{Eq 4})$$

Where C: cations in meq/l and A: Anions in meq/l

The charge balance error checking of HJB's samples showed that the analysis results are judged perfect (average %E \approx 1.59% < 5%).

III. Hydrochemical characterization

1. Conventional methods

The identification of hydrochemical processes for both aquifers of HJB (shallow and deep), was obtained by constructing several diagrams such as the Piper diagram (Piper 1944) and Chadha diagram (Chadha 1999).

2. Origin of mineralization

Different reactions can be derived from the interaction water-rock, then defining the chemical water type. To understand the chemical processes, we have elaborated the correlation matrix and also, we have established some correlations between selected major ions.

These correlations can help analyze the primary reactions that have formed current water chemistry and identify groundwater mineralization origin.

The Gibbs' diagram (Gibbs 1970) was also used to understand groundwater chemistry's main mechanisms.

3. Multivariate statistical analysis

In the geochemical study, each variable's separate study is an essential phase in analyzing chemical behavior, but it is often insufficient. Therefore, the data should be analyzed considering their multidimensional nature (Hamzaoui Azaza et al., 2011).

Multivariate statistical analysis (MSA) is a multidimensional analysis widely used to identify the sources of solutes in a groundwater system and understand the water quality well. It allows the comparison of all water samples and identifies their different solutes' origin (Hamzaoui Azaza et al., 2011).

MSA was chosen to determine the inter-data relationships of the HJB's samples. 12 Physico-chemical parameters were analyzed in 28 samples collected in 2017; these variables (pH, EC, Salinity, O₂, Na⁺, Ca²⁺, Mg²⁺, K⁺, Cl⁻, HCO₃⁻, and SO₄²⁻) were successfully used in the principal component analysis. The parameters used in MSA referred to different units of measurement (meq/l, us/cm.....), so their values should be standardized; we have used the following transformation function (Medina-Gomez and Herrera- Silveira 2003):

$$Z = (X - \mu) / \sigma \quad (\text{Eq 5})$$

Where Z : the standardized value, X : the original value of the measured parameter, μ : the mean of the variable and σ : the standard deviation.

4. Geochemical modeling

To identify the water interaction with rocks, a saturation index was computed. SI quantifies water deviation from equilibrium based on the dissolved minerals (Hamzaoui-Azaza et al., 2013).

The SI presents a coefficient reflecting the degree of saturation of water about a given mineral. It is computed using the following formula:

$$SI = \log(IAP/Kps) \quad (\text{Eq 6})$$

Where IAP: Ion activity product and KSP: Solubility product.

If SI is equal to zero, it presents a solubility equilibrium in relation to the selected mineral phase of the water. If $SI < 0$ (negative value) it designates undersaturation (mineral dissolution) and if $SI > 0$ (positive value), it indicates supersaturation (mineral precipitation).

The saturation index was computed using PHREEQC Interactive software (Parkhurst et Appelo 1999).

IV. *Water quality assessment*

1. Drinking use

1.1 Standards of drinking

To maintain human health, the World Health Organization “WHO” has set limit values not to be exceeded if we want to respect international standards of consumption. Also, all countries of the world do not follow the same standards; each country has defined their propriety standards of drinking water quality. Some adopt their standards and others choose those recommended by WHO (WHO 2011).

Tunisia has fixed national standards (NT.09.14) for the potability of the water. The difference between the Tunisian standards and WHO limits reflect the required management of water in Tunisia.

1.2 Drinking index

The assessment of suitability for drinking purpose in HJB, was evaluated using three indices: water quality index “WQI”, entropy water quality index “EWQI” and improved water quality index “ImpWQI”.

a. Water quality index (WQI)

The WQI method is frequently used to assess drinking water quality (Ghouili et al., 2018; Asadi et al., 2020). The calculation of WQI is based on the standards suggested for uses, where 9 groundwater quality parameters are considered: pH, EC, HCO_3^- , Cl^- , SO_4^{2-} , Ca^{2+} , Mg^{2+} , Na^+ and K^+ .

For computing the WQI, weights (w_i) are assigned for each parameter: the weight of “5” has been attributed to five parameters: EC, Mg^{2+} , Na^+ , Cl^- and SO_4^{2-} their major role in quality assessment. A minimum weight equal to “1” has been given to HCO_3^- and K^+ since their less significant role in quality evaluation and medium weights of 2 and 3 has been assigned to Ca^{2+} and pH. The WQI is computed on following up the formulas (7), (8) and (9):

$$RWi = \frac{wi}{\sum_{i=1}^n wi} \quad (\text{Eq 7})$$

$$Qi = \frac{Ci}{Si} \times 100 \quad (\text{Eq 8})$$

$$WQI = \sum RWi \times Qi \quad (\text{Eq 9})$$

Where w_i : weight for each parameter, RWi : relative weight for each parameter, n : number of parameters, C_i : concentration of parameter i (Each water sample, (mg/L)) and S_i : Drinking use’s standard (WHO 2011).

The ranges of water quality were determined according to the WQI; we have classified the water samples according to the ranges of WQI values (Table 6). The spatial distribution of WQI values was prepared using a weighted inverse-distance interpolation (IDW) technique.

b. Entropy water quality index (EWQI)

The EWQI is widely applied to assess the quality of drinking water (Wu et al., 2011; Islam et al., 2017). For computing the EWQI, according to Islam et al., 2017, when m water samples ($i = 1, 2, \dots, m$) are taken to evaluate the quality and each sample is analyzed for “ n ” parameters ($j = 1, 2, \dots, n$), the following steps have been followed:

- In the first step, eigenvalue matrix, A , was constructed as follow:

$$A = \begin{pmatrix} A_{11} & A_{12} & \dots & \dots & A_{1n} \\ A_{21} & A_{22} & \dots & \dots & A_{2n} \\ A_{31} & A_{32} & \dots & \dots & A_{3n} \\ \vdots & \vdots & \vdots & \vdots & \vdots \\ A_{m1} & A_{m2} & \dots & \dots & A_{mn} \end{pmatrix} \quad (\text{Eq 10})$$

- After, the matrix A is converted into a standard-grade matrix B (Eq.11) using the Eq.10.

$$\begin{cases} B_{ij} = \frac{A_{ij} - A_{ij \min}}{A_{ij \max} - A_{ij \min}} & \text{for efficiency type parameters} \\ B_{ij} = \frac{A_{ij \max} - A_{ij}}{A_{ij \max} - A_{ij \min}} & \text{for cost type parameters} \end{cases} \quad (\text{Eq 11})$$

$$B = \begin{pmatrix} B_{11} & B_{12} & \dots & \dots & B_{1n} \\ B_{21} & B_{22} & \dots & \dots & B_{2n} \\ B_{31} & B_{32} & \dots & \dots & B_{3n} \\ \vdots & \vdots & \vdots & \vdots & \vdots \\ B_{m1} & B_{m2} & \dots & \dots & B_{mn} \end{pmatrix} \quad (\text{Eq 12})$$

- Then, the entropy weight (W_j), for each parameter is calculated as follow:

$$W_j = \frac{1 - e_j}{\sum_{i=1}^m (1 - e_j)} \quad (\text{Eq 13})$$

$$\text{Where } e_j = \frac{1}{\ln m} \sum_{i=1}^m P_{ij} \ln(P_{ij}) \quad (\text{Eq 14})$$

$$\text{and } P_{ij} = \frac{1 + B_{ij}}{\sum_{i=1}^m (1 + B_{ij})} \quad (\text{Eq 15})$$

- The rating quality is calculated for the n parameters ($j=1,2,\dots,n$) for all the samples, using the concentration of parameter j (C_j) and the standard limit (S_j), using the following formula:

$$q_j = \frac{C_j}{S_j} \times 100 \quad (\text{Eq 16})$$

- In this study, the rating quality is calculated based on the WHO standard (2011).

Finally, the EWQI is calculated as follow:

$$EWQI = \sum_{j=1}^m W_j \times q_j \quad (\text{Eq 17})$$

c. Improved water quality index (ImpWQI)

The ImpWQI is widely used for assessing the drinking water quality (Zhang et al., 2020).

For computing the ImpWQI, the first step is to determine the weights of the different used parameters. Firstly, the data was normalized to eliminate the influence of the unit. To

calculate the parameters' weight, the CRITIC weighting (Zhang et al., 2020) was used (Eq18-22). The ImpWQI, for each sample, are calculated on following up these equations:

$$C_{ij} = \frac{\sum(a_{ij}-\bar{a}_{ij})(b_{ij}-\bar{b}_{ij})}{\sqrt{\sum(a_{ij}-\bar{a}_{ij})^2 \times \sum(b_{ij}-\bar{b}_{ij})^2}} \quad (\text{Eq 18})$$

$$F_j = \varepsilon_j \sum_{j=1}^m (1 - c_{ij}) \quad (\text{Eq 19})$$

$$W_j = F_j / \sum_{j=1}^m F_j \quad (\text{Eq 20})$$

$$q_j = \frac{a_{ij}}{s_j} \times 100 \quad (\text{Eq 21})$$

$$\text{ImpWQI} = \sum_{j=1}^m W_j \times q_j \quad (\text{Eq 22})$$

Where: a_{ij} and b_{ij} : The original and the normalized data value, respectively,

\bar{a}_{ij} and \bar{b}_{ij} : the average of a_{ij} and b_{ij} , respectively,

F_j : the information amount of the j th parameter,

ε_j : standard deviation of the j th parameter,

c : correlation coefficient,

m : total number of parameter

W_j : the weight of j th parameter,

q_j the rating of the j th parameter

and S_j : the standard limit of the j th parameter (WHO 2011).

The obtained results from the three drinking indices were classified into five classes (Table.6).

Table 6 Classification of groundwater quality based on WQI, EWQI and ImpWQI

Index	<50	50-100	100-150	150-200	>200
Rank	1	2	3	4	5
Water quality	Excellent	Good	Medium	Poor	Extremely poor

2. Irrigation suitability assessment

2.1 Standard indices

Different ionic parameters (in meq/l) were used to assess the irrigation water quality in HJB basing on various indices such as: TH (Total Hardness) (Todd 1980), EC (Electrical conductivity(μs/cm)), SAR(Alkalinity hazard) (Richards 1954), Na%(Percent sodium) (Wilcox 1955), MH (Magnesium hazard) (Raghunath 1987), KR (Kelley ratio) (Kelly 1951), PI (Permeability index) (Doneen 1964) (Eq19-24):

$$TH = 2.5 \times Ca + 4.1 \times Mg \quad (\text{Eq 23})$$

$$\%Na = 100 \times \frac{Na+K}{Ca+Mg+Na+K} \quad (\text{Eq 24})$$

$$SAR = \frac{Na}{\sqrt{(Ca+Mg)/2}} \quad (\text{Eq 25})$$

$$PI = 100 \times \frac{Na+\sqrt{HCO_3}}{Na+Mg+Ca} \quad (\text{Eq 26})$$

$$Kr = \frac{Na}{Ca+Mg} \quad (\text{Eq 27})$$

$$Mh = \frac{Mg}{Ca+Mg} \quad (\text{Eq 28})$$

2.2 Irrigation Water Quality Index (IWQI)

The computing of IWQI is composed by two steps (Meireles et al., 2010). The first step consisted of the parameters selection, taking into account the preponderant water 's use, in this case, irrigation. In the second step, the individual quality measures (q_i) of each variable were calculated (Table 7). IWQI is calculated using the following equation:

$$IWQI = \sum q_i \times W_i \quad (\text{Eq 29})$$

$$\text{With } q_i = Q_{imax} - ((X_{ij} - X_{inf}) \times Q_{iamp}/X_{amp}) \quad (\text{Eq 30})$$

where q_{imax} : maximum value of q_i for the class;

x_{ij} : observed value for the parameter n ;

x_{inf} : parameter value corresponding to the lower limit of the class;

q_{imax} : the maximum value of q_i for the class;

x_{amp} : the class amplitude to which the parameter belongs;

In order to evaluate x_{amp} , of the last class of each parameter, the upper limit was the highest value determined in the physical chemical of the water samples (Meireles et al., 2010).

Table 7 Parameter limiting values for q_i computing (Ayers and Westcot 1985)

q_i	EC	SAR	Na	Cl	HCO ₃
85-100	200<EC<750	2<SAR<3	2<Na<3	1<Cl<4	1<HCO ₃ <1.5
60-85	750<EC<1500	3<SAR<6	3<Na<6	4<Cl<7	1.5<HCO ₃ <4.5
35-60	1500<EC<3000	6<SAR<12	6<Na<9	7<Cl<10	4.5<HCO ₃ <8.5
0-35	EC<200	SAR<2	Na<2	Cl<1	HCO ₃ <1
	Or EC>3000	Or SAR>12	Or Na>9	Or Cl>10	Or HCO ₃ >8.5
Wi	0.211	0.189	0.204	0.194	0.202

Chapter III: Recharge estimation and groundwater flow modeling of HJB

I. Introduction

Groundwater is one of the most valuable natural resources, supporting human health, economic development and ecological diversity (e.g., Celico et al., 2000; Jha et al., 2006; Hamzaoui-Azaza et al., 2013). In the modern world, many problems of water deficiency are related to environmental conditions.

In the semi-arid regions, the groundwater quality and quantity are threatened by several factors; most importantly, the aquifer over-exploitation (e.g., Gaaloul and Cheng 2003; Celico et al., 2002). The negative signs of aquifer mining are further exacerbated by climate-related hazards, mainly dry periods in semi-arid regions. Recently, all the model climate results indicate the accentuation of weather hazards' effects in the next decades (e.g., Kumar 2012), particularly in Mediterranean basins (e.g., Iglesias et al. 2007).

The rainfall has a strong impact on the hydrological cycle. Indeed, annual precipitation variability has direct consequences on aquifers' recharge and groundwater resources (e.g., Kumar 2012). Much attention has been paid to analyzing the climate change impact (e.g., Touhami et al., 2015). In the last decade, many case studies were generated to quantify the likely direct impacts of climate change on groundwater. Many issues are studied, such as the fluctuation of groundwater level; the potential effects on the quantity and quality of groundwater resources and the impacts of climate change on groundwater recharge.

The water resources in the Hajeb El Ayoun-Jelma basin are affected by the over-exploitation. The HJB is the largest one in central Tunisia, containing significant groundwater resources of good quality and mainly used for agricultural needs and drinking water supply for the central Tunisia regions and Sfax region located on the southern coast of Tunisia. The HJB includes several aquifers. The shallow and the first deep aquifer are the most exploited. These aquifers' intense exploitation generated excessive drawdowns varying between 0.6 and 0.9 m/year, which may involve groundwater contamination and high pumping cost. This work aimed to estimate the recharge rate and input it in a hydrodynamic model to assess the impact of withdrawals increase on HJB groundwater resources in the long term to control the groundwater. To conserve the resources and water quality of the Hajeb Layoun-Jelma basin, it

is necessary to stop the increase in exploitation. It could be by reviewing the economic approach to irrigation water to help reduce the exploitation of groundwater.

In this work, the first step was estimating the recharge rate and, after that, the development of the flow model and inputting the recharge and the other parameters. After calibration of the model, it will be used for predictive simulations.

II. Groundwater recharge estimation

1. Introduction

Water is the source of life on our earth. Groundwater is an essential component in the semi-arid region, especially in the arid region, the only water source. According to the World Water Assessment Program (2003), the groundwater provides the water for domestic uses, industrial activity, and agricultural uses with 50%, 30%, and 20%, respectively. Year-by-year, the over-abstraction from the groundwater resource caused a rapid decline in the water table. So, groundwater management is very needed. Artificial groundwater recharge is the most effective method for managing groundwater (Daher et al., 2011; Horriche et Benabdallah, 2020). Knowing the potential zones for groundwater is essential for managing water resources, especially when groundwater forms the main source for water supply.

Mapping of groundwater potentiality has taken attention from many researchers. It has generated using various methods such as: Analytical Hierarchy Process, multi-criteria decision analysis (Hussein et al., 2018), fuzzy logic analysis.

The current study has tried to generate different thematic layers (topography, drainage density, slope, land use/land cover, lithology) in the Hajeb Layoun-Jelma Basin to delineate potential zones. Each thematic layer has been analyzed, integrated, overlaid and proper weights have been assigned to generate a groundwater potential map of the three studied aquifers forming the multilayer aquifer of HJB.

2. Mapping of the groundwater potential recharge

In order to determine the recharge zones, we have adopted the methodology showed in Figure 58. The main focus is to calculate each aquifer's recharge values and mapping the potential recharge zones using GIS. To determine the potential recharge zones of HJB a multi-parametric dataset including Digital Elevation Model (DEM), soil map, land use map, geological map, watershed framework and groundwater boundary was used. The maps were prepared from the digitization of geological and topographic maps on a 1/50.000 scale.

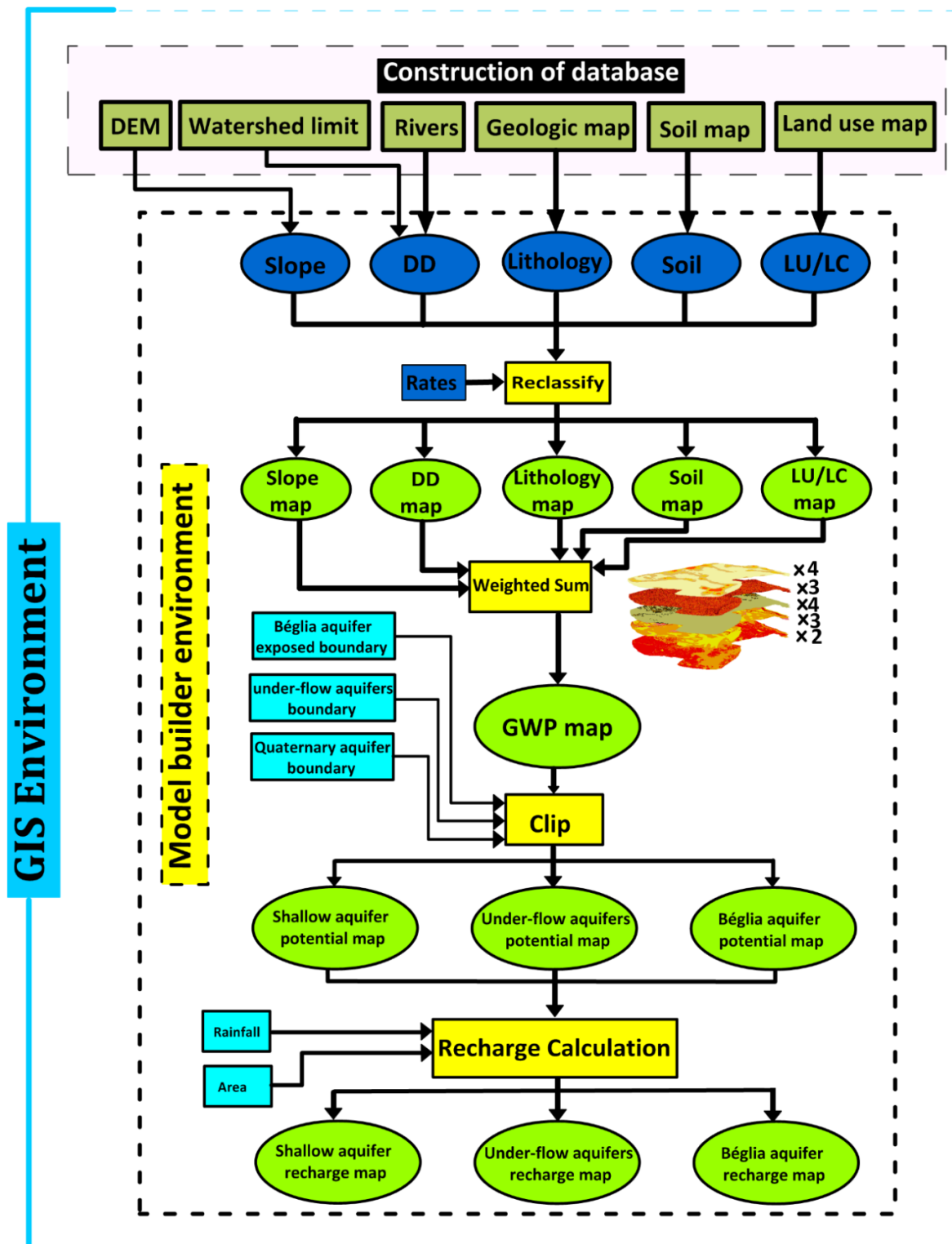


Figure 58. Flow chart showing the methodology adopted in this study

Five thematic maps, with a pixel size equal to 30 m (slope map, drainage density map, lithology map, soil map and land use map) were used to create of the groundwater potential map. The lithological map was prepared by assembling, georectifying, clipping and digitizing six geological maps (Sbiba, J. Essouda, J. Trozza, J. Mrhilla, Hajeb El Aioun, Sbeitla) on a

1/50000 scale. The DEM was used to generate the slope map using ArcGIS tools. Both the soil map and the land use map were produced by the DGRE and was clipped by the groundwater boundary using Arcgis tools. The drainage density was generated using the “line density” tool in Arcgis and was calculated using the following formula (Murthy 2000):

$$DD = \sum L_r / S \quad (\text{Eq 31})$$

where L_r : total length of the river

and S : unit of area

The potential index was determined by weighted-sum all the classified thematic maps, with pixel size equal to 30 m using ArcGIS tools.

Five factors influence the potential index. We have calculated a weight corresponding to their relative importance for the recharge potential based on the inter-relationship between the five factors for each five factors (Figure 59). We have affected an index equal to “1” for the significant effect and “0.5” for the minor effect. After calculating each factor's weight, we have summed the minor multiplied by its index (0.5) and the number of major effects (Table 8).

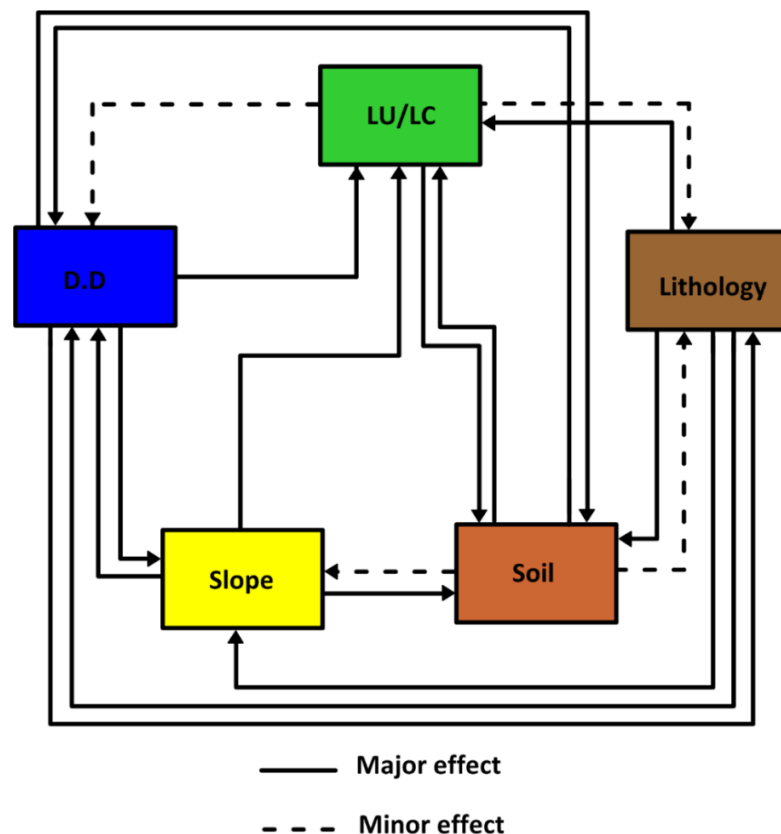


Figure 59. Inter-relationship between the multiple influencing factors of the recharge process

Table 8 Effect of factor influencing relative rates and score for each five-potential factor

Factors	Major effect (A)	Minor effect (A')	Weight (A+A')
Land use	1 x 1	2 x 0.5	2
Lithology	4 x 1	0 x 0.5	4
D.D	4 x 1	0 x 0.5	4
Slope	3 x 1	0 x 0.5	3
Soil	2 x 1	2 x 0.5	3

For each factor, we have classified the features on rates from 1 to 10 (Haouchine et al., 2011) (Table 9) corresponding to their relative importance for recharge intensity. Qualitative evaluation of the different features was affected for each factor based on the recharge class, a rate was assigned as follows: very low rate (1), low (2), low to moderate (3.5), moderate (5), moderate to high (6.5), high (8) and very high (10).

Table 9 Rates classification based on recharge intensity (Haouchine et al., 2011)

Class	Very high	High	Moderate to high	Moderate	Low to moderate	Low	Very low
Rate	10	8	6.5	5	3.5	2	1

The groundwater potential index of each pixel was calculated in the HJB by the following formula:

$$\text{GPI} = L_r \times L_w + Lu_r \times Lu_w + DD_r \times DD_w + S_r \times S_w + Sl_r \times Sl_w \quad (\text{Eq 32})$$

Where GPI is the groundwater recharge potential index, L is the lithology index, S is the slope index, D is the drainage density index, Lu is the land-use/land-cover index, and Sl is the soil index. The subscripts w and r refer, respectively, to the weight of each factor and the rate of sub-features of each factor.

3. Recharge estimation

To calculate the quantity of water recharging the three types of aquifers in the HJB, a simplified calculation for the proposed recharge rates is used (UN 1967). The estimation of the total infiltration water volume (V_{inf}) is calculated as:

$$V_{inf} = P_{moy} \times A \times R_r \quad (\text{Eq 33})$$

Where P_{moy} is the average annual precipitation volume,

A: the area

And R_r is the recharge ratio

The R_r is calculated based on the recharge percentages (Table 10) indicated by FAO (1967).

The R_r is calculated as follows:

$$R_r = (\% \text{ area-low} \times 0.075 + \% \text{ area-moderate} \times 0.15 + \% \text{ area-moderate to high} \times 0.25)$$

Table 10 Groundwater recharge potential zones and infiltration percentages (FAO 1967)

Class	low	moderate	Moderate to high
%	5-10	10-20	20-30
Average	7.5	15	25

4. Geographic information system and model builder

Under ArcGis 10.3, a database has been established, including the inventory of data used in elaborating the thematic maps such as geological maps, land use/ land cover map, river networks, DEM and soil map. The five thematic maps were obtained from 1:50000 scale under the UTM coordinate system and WGS 84 (32N) datum projection. The groundwater potential recharge (Figure 60) was developed, under ArcGis 10.3, using the ‘model builder’ tool. This tool has automated the model workflows. The five thematic maps were analyzed with a pixel size equal to 30 m. Various tools were integrated into the model builder to establish the thematic maps and generate the groundwater potential map. The slope map was derived from the DEM using the ‘slope tool’ (3D Analyst), the drainage density was established basing on the rivers network using the ‘line density tool’ (Spatial analyst), the lithology map was derived from the geological map using the digitalization. The resulting map was obtained by merging the five weighted maps using the ‘weighted sum tool’ (Spatial analyst).

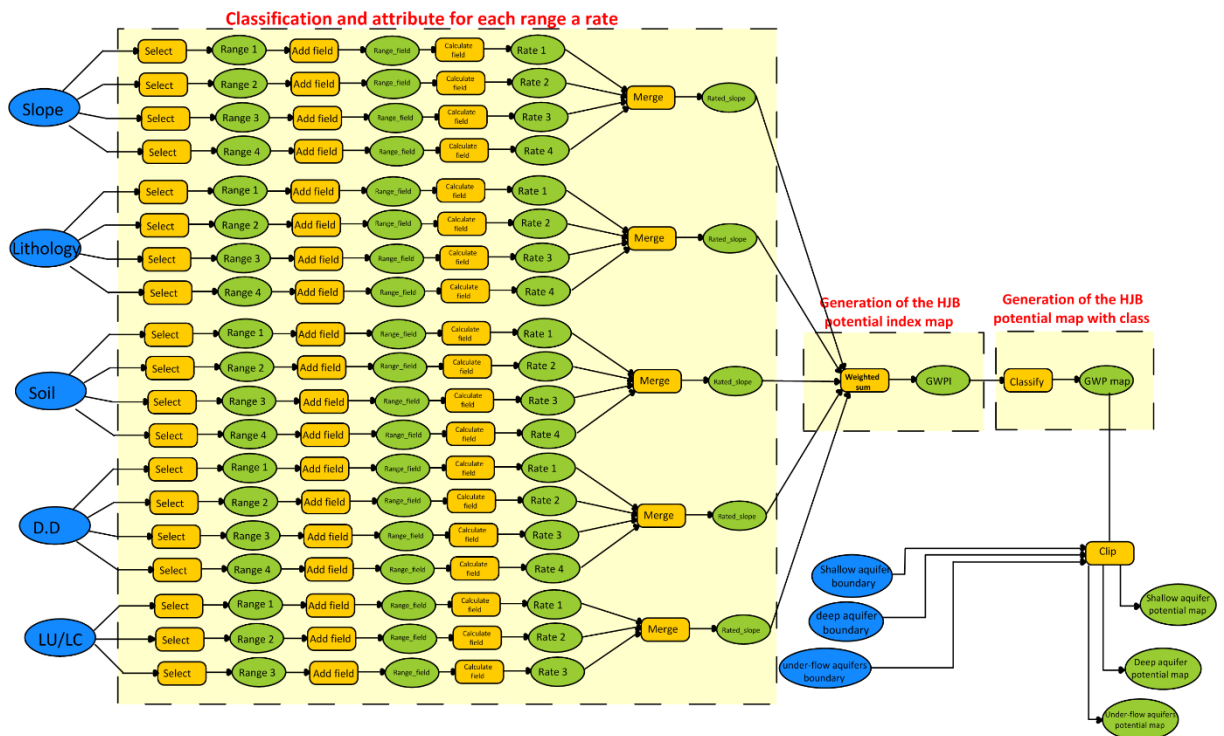


Figure 60. Structure of model builder used to generate the potential groundwater maps of Hajeb Layoun Jelma aquifers

5. Conclusion

For estimating the recharge rate of the two main aquifers, we have used the multi criteria method. Several thematic layers were used to generate the groundwater potential map (topographic, drainage density, slope, land use land cover, lithology). The computed rates will be used as input in the numerical model.

III. Groundwater modeling of HJB

1. Design steps of a hydrogeological model

The bad use of groundwater generates decreasing water table and water quality such as salinity increasing and water contamination. To avoid these situations, harmful to resource sustainability, hydrogeologists are asked to predict aquifer systems' behavior and propose exploitation programs in the next years. This is possible by developing a mathematical model of the aquifer system (Anderson *et al.*, 1992; Zammouri 2007). In the majority of cases, models are developed for predictive purposes. However, developing a model is also to understand the aquifer system or the hydrogeologist's orientation in the future collection of information on the aquifer (Anderson *et al.*, 1992). There are many methodologies for the design of a hydrogeological model (Anderson and Woessner, 1992; Bear *et al.*, 1992; Kumar, 2002), but all follow the same general diagram (Figure 61).

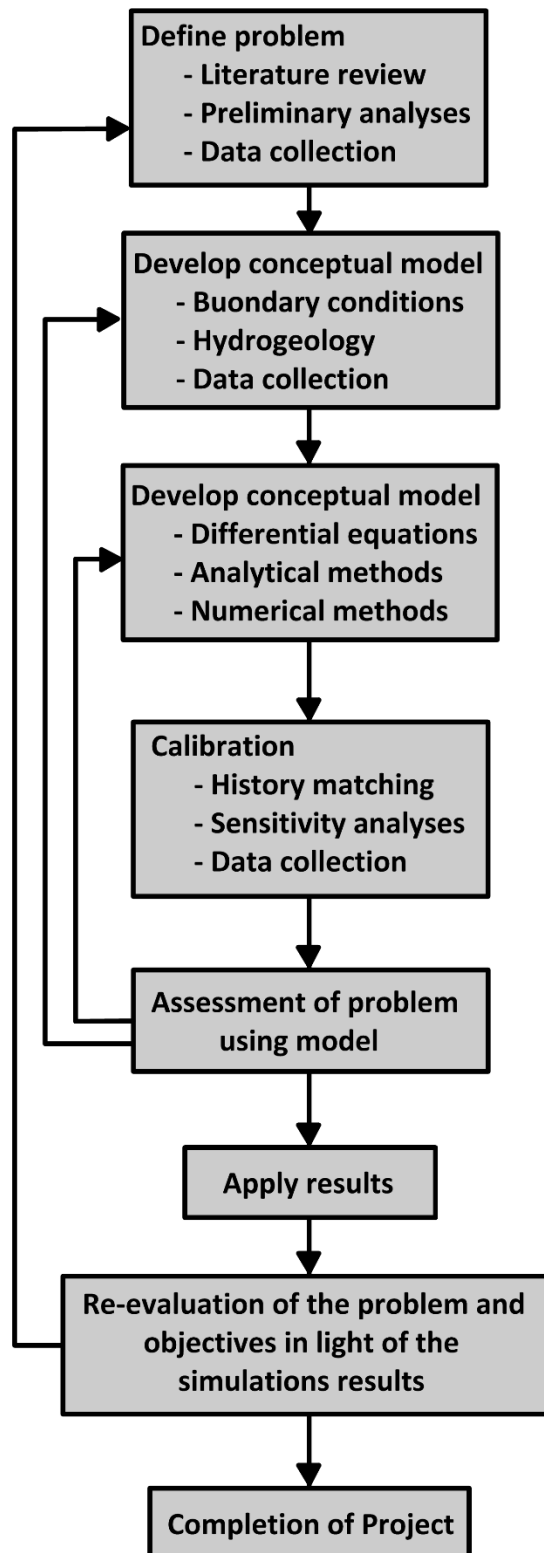


Figure 61. Flow chart of the groundwater flow modeling process (Reilly 2001)

1.1 Model Objectives

Model objectives should be defined to explain the purpose of using groundwater modeling. The usual objectives of modeling, according to Bear (1993) are :

- To make predictions about the behavior of the aquifer system in response to stress.
- To obtain necessary information for certain recommendations.
- To get a better understanding of the hydrogeological, chemical or geological system.
- To provide the necessary information to define the system.
- To provide information to assist in the organization of new tests in situ (eg pumping, tracing).

1.2 Hydrogeological Characterization

To understand the importance of flow or solute transport processes, it is necessary to know the study site's hydrogeological conditions. This information is derived from the integration and analysis of hydrogeological data (rock permeability, hydraulic head, etc...) and geological data (stratigraphy, mineralogy, etc.) acquired using various techniques (mapping, drilling, seismology, piezometry, etc...) (Ross *et al.*, 2004). Without site characterization, it is impossible to select a suitable model or develop a reliably calibrated model.

1.3 Model Conceptualization

In reality, the modeled system is very complicated. Therefore, it is necessary to simplify the description of this system. Model conceptualization is the process in which data describing field conditions are assembled in a systematic way to describe modeling objectives and specific questions to be answered (groundwater flow, contaminant transport processes in study site...). The model conceptualization helps in determining the modeling approach and which model software to use.

1.4 Modeling Software Selection

This step consists of assumptions and choices made in a mathematical model that aims to solve the water flow equations. The selected model should be able to simulate conditions encountered in the study site. Following the numerical model's construction, the hydrogeologist integrates the geological model, the mathematical model, field data, and properties of the basement (porosity, permeability, piezometry, etc...) (Kumar 2001).

1.5 Model Design (Input Parameters)

The model design includes all parameters that are used to develop a calibrated model. The input parameters include model grid size and spacing, layer elevations, boundary

conditions, hydraulic conductivity/transmissivity, recharge, any additional model input, transient or steady state modeling, dispersion coefficients, degradation rate coefficients etc.

1.6 Model Calibration

Model calibration consists of modifying values of model input parameters to match field conditions within acceptable criteria. Model calibration requires that field conditions at a site should be adequately characterized. Lack of site characterization may result in a model calibrated to a set of conditions that are not representative of actual field conditions.

1.7 Model Verification

A calibrated model uses selected values of hydrogeological parameters, sources and sinks and boundary conditions to match historical field conditions. The process of model verification may result in further calibration or refinement of the model. After the model has successfully reproduced measured changes in field conditions, it is ready for predictive simulations.

1.8 Predictive Simulations

A model may be used to predict some future groundwater flow or contaminant transport conditions. The model may also be used to evaluate different remediation alternatives. However, errors and uncertainties in groundwater flow analysis and solute transport analysis make any model prediction no better than an approximation. For this reason, all model predictions should be expressed as a range of possible outcomes that reflect the assumptions involved and uncertainty in model input data and parameter values.

1.9 Post-audit and model updating

Groundwater models are used to predict the migration pathway and concentrations of contaminants in groundwater. Errors in the predictive model, even though small, can result in significant errors in solutions projected forward in time. Performance monitoring is required to compare future field conditions with model predictions.

A sensitivity analysis is the process of varying model input parameters over a reasonable range (range of uncertainty in the value of the model parameter) and observing the relative change in model response. Typically, the observed change in hydraulic head, flow rate or contaminant transport are noted. Data for which the model is relatively sensitive would require future characterization instead of data for which the model is relatively insensitive.

2. GMS software

There is several software used in groundwater modeling. The most widely used numerical groundwater flow model is Modflow for its reliability (El-Bihery 2009). It is developed by the United States Geological Survey (USGS) in 1984 (McDonald and Harbaugh, 1988, Chiang and Kinzelbach, 1998).

In this study, for model pre- and post-processing, Processing MODFLOW (PMWIN) was utilized (Chiang and Kinzelbach, 2001). The modular three-dimensional multi-species transport model MT3DMS (Zheng and Wang, 1999) included in PMWIN can be used to build a transport model.

In this work, GMS software was selected to modeling the HJB resources. Two approaches can be used to construct a MODFLOW simulation in GMS: grid or conceptual model. The grid approach works directly with the 3D grid and applies sources/sinks, and other model parameters on a cell-by-cell basis. In the conceptual approach, all data are introduced as coverages, the model will be converted to a grid-based model, the starting head will be assigned, and the simulation will then be run.

3. Flow modeling approach of HJB

Three main steps are used to develop a management tool, which helps forecast the behavior of the multilayer aquifer system of the HJB in the next decades. The first stage is the data gathering from the Tunisian water agencies completed by data published in previous studies. The collected data are analyzed and synthesized in a database and a geographic information system (GIS). The second step consisted of elaborating the conceptual model, developing and calibrating the groundwater flow model. The last step is exploiting the calibrated model to simulate various management alternatives and assess the climate change effect.

3.1 Model conceptualization


Conceptual modeling is the first stage in modeling (Anderson and Woessner; 1992). The model conceptualization of an aquifer system to be modeled influences the numerical model's reliability and capacity to reproduce the aquifer's flow and conditions (Hamzaoui-Azaza et al., 2020). It consists of defining the modeling objective, gathering and analyzing data, formulating the boundary conditions, identifying variables and unknowns of the system, defining the modeling approach and choosing the modeling software.

Data collected from the Tunisian water agency (DGRE) and previous modeling studies (Zammouri; 1988) are analyzed to develop the conceptual model. In the second modeling stage, the conceptual model is converted to a numerical model using MODFLOW-2000, under GMS software, a modular finite difference groundwater model code which is largely used (Zammouri et al., 2013). For model pre- and post-processing, Processing MODFLOW (PMWIN) was utilized (Chiang and Kinzelbach 1998).

The domain of the HJB model corresponds to the geographical boundaries of the study area. The model includes two layers (Table 11). The first layer represents the shallow aquifer, and the second one represents the deep aquifer. The boundary conditions correspond to the recharge areas and the natural outlets (Figure 62). The wadis' springs and leakage are represented as drains whose measured outflow discharge should be reproduced in the aquifer system's water balance after model calibration. Imposed flux conditions are used to represent pumping and recharge. The evapotranspiration condition is applied in the southeastern HJB where shallow aquifer waters are subject to evaporation.

Table 11 Diagram showing the conceptual model of HJB

Age		Formation name	Lithology	Layer type
Quaternary			Gravel and sand	Shallow aquifer
Neogene	Pliocene	Segui		
	Tortonian	Souaf	Gypsum clay and clays	Aquiclude
	Serravallian	Beglia	Sandstone	Deep aquifer

 Captured aquifer

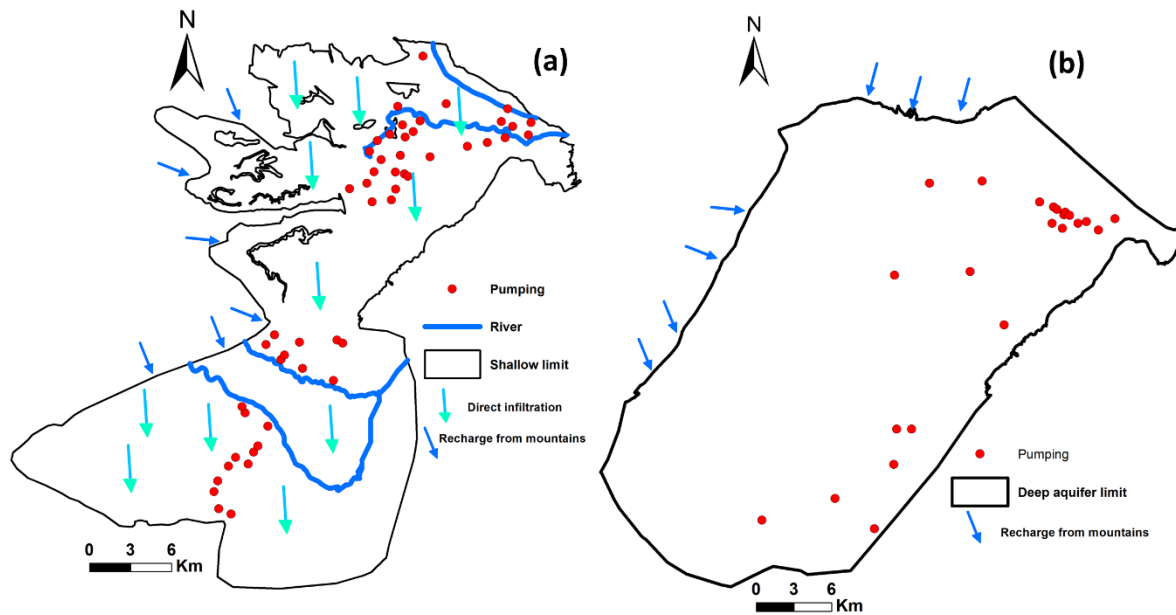


Figure 62. Plan view of the site to be modeled (a) shallow aquifer and (b) deep aquifer

3.2 Steady state

The period taken as a reference for the steady-state calibration of the model is 1973, in which the aquifers are considered to be in a steady state of equilibrium on a basin-wide level. The reproduction of piezometry and the discharge of springs and drainage by wadis are taken as calibration criteria. The universal kriging technique was chosen to elaborate the piezometric reference maps. Experimental variograms of observed piezometry of shallow and deep aquifers are computed and adjusted. Cross-validation is applied to judge the reliability of the chosen variogram model. The difference between the observed and kriged piezometry at piezometric measurements points must be minimum.

In order to calibrate the groundwater flow model in the steady state, we proceed to the modification and the gradual adjustment of parameters that govern the groundwater flow, which the most important is horizontal transmissivities. In fact, the transmissivity distribution of aquifers is not available. Few values obtained by pumping test are available. The measured transmissivities provide values ranging from 1.4×10^{-3} to 5.8×10^{-2} (Table 12). The high transmissivities are located along the zone of Hajeb El Ayoun. The bulk of the permeability values obtained from pumping tests between 10^{-3} and 8.8×10^{-2} m/s. Different transmissivity fields are tested to obtain calculated piezometric distributions as similar as possible to those of reference. The model calibration is considered satisfactory when the difference between the measured and the simulated values of piezometry and natural outlet discharge is minimal.

Table 12 Hydrodynamic characteristics of HJB aquifer (deduced from pumping tests) (Kochel 1980)

Well number	Well name	Total depth	Captured aquifer	Screen length (m)	Transmissivity ($10^{-2} \text{ m}^2 \text{ s}^{-1}$)	Hydraulic conductivity (10^{-2} m s^{-1})	Storage coefficient (10^{-4})
1	3396/4	110	Sr	24	3.8	3	13
2	5336 bis/4	125	Sr	35	4	3.6	12
3	5336 /4	323	Sr	53	4	3.6	12
7	7024/4	798	Sr	78	7	4	-
9	7809/4	160	Sr	61	5.5	4	-
10	8804/5	189	MP	41	1.4×10^{-1}	2.3×10^{-6}	-
11	8804bis/5	150	MP-Sr	44	7×10^{-1}	4.6×10^{-5}	-
12	9156/4	520	Sr	72	4.2	2.3	-
13	10009bis/4	396	Sr	53	4.2	2	-
14	10417/4	182	Sr	70	4.7	3.2	9
15	13590/4	206	Sr	25	5.8	3.6	14.8
16	10418/4	120	Sr	52	4.6	8.8	-
17	6648/4	91	Sr	26	5	3.8	10
20	10923/4	169	Sr	51	4.6	3.8	-
22	11767/4	283	Sr	97	1	1	-
23	11758/4	170	Sr	70	0.6	1	-
25	13272/4	170	Sr	40	2.2	5	-
30	13994/4	300	Sr	52	1.9	3.7	-
31	14008/4	199	Sr	48	4	3.6	-

Sr: Serravallian (Begliia formation)

3.3 Transient state

The model calibration in the transient state is necessary to verify proper model operation in a historical period. The aquifers system underwent constraints different from those used for the model calibration in steady state.

For the transient simulations, the aquifer's geometric and hydraulic conductivities are the same as those used for the steady-state simulations. The steady-state model's resulting flow field is used as the initial condition for the flow system's subsequent transient simulations. The calculated piezometry by the model is compared to observed piezometry. When the coincidence between the calculation results and measurements is satisfactory, we may conclude the model reliability. For the HJB, the period from 1974 to 2019 is taken as the reference period for transient calibration. The initial conditions correspond to the aquifer system state calculated in 1973, representing the steady state.

3.4 Predictive simulations to the year 2050

When the calibration target was almost reached for all the observation points, the model was used to assess the impact of the over-exploitation of HJB. For this purpose, a groundwater simulation model was extended to the year 2050 with various management alternatives. In the first scenario (S1), the groundwater withdrawals in 2019 were maintained over the whole basin until 2050. In the second scenario (S2), an increase ($\times 1.5$) in groundwater pumping is assumed for the shallow and the deep aquifer.

The third scenario (S3) present the same conditions of pumping that the first scenario but with the climatic change effect using climate model results. Several climate simulation models cited in the literature were used to study the climate change effect on hydrological cycle components and water resources in Mediterranean basins (Le Treut [2010](#), MARH [2009](#)). The HadCM3 model was selected to study the effect of climate change on HJB groundwater resources since it is more appropriate for Tunisia according to previous works (MARH [2009](#), Hajri [2013](#)). It is a coupled atmospheric-ocean general circulation model developed by the Hadley Centre (Gordon et al. [2000](#)).

4. Conclusion

In the first step, MODFLOW code (GMS software) was used to reconstruct the hydrodynamic model of the studied aquifers in both steady (1973) and transient (1974-2019) states. Various management scenarios were applicated using the calibrated model to predict the future HJB resources.

Chapter IV: Vulnerability mapping and Contaminant transport modeling

I. Introduction

In semi-arid regions, groundwater is a significant, valuable natural resource since it is used to satisfy most water needs (Asadi et al., 2017). In the modern world, many problems of water are related to environmental conditions. Around the world, the groundwater quality and quantity are threatened by several factors (salinization, over-exploitation, pollution, and contamination...), which most importantly is the contamination. Several studies pay attention to the evaluation of groundwater quality (Gouilli et al., 2018). The groundwater pollution in many regions is becoming more and more severe because of the over-exploitation (Celico et al. 2002), the increase of urbanization, and the continuous development of agricultural activity (Rouabhia et al. 2008). In many regions, groundwater quality has been degraded due to farming activities and other land uses using fertilizers and pesticides in huge quantities (Focazio et al., 2008; Hamzaoui-Azaza et al., 2013). The protection and preservation of this resource are significant.

To deal with this danger, a prediction of aquifer systems' behavior following contamination is recommended to ensure the development and management of the territories that allow the preservation of the quality of the resource.

The groundwater vulnerability reflected the facility of pollution's access from the ground surface to groundwater (Margat 1968; Civita 1994). The vulnerability consists of the study of groundwater pollution, which allows better groundwater management and suitable interventions in the case of contamination. It also makes it possible to specify the areas affected by anthropogenic activities. Assessment of aquifer's vulnerability is the standard tool for protecting groundwater from potential sources of pollution. They are valuable for any future decision. Much attention has been paid to groundwater vulnerability analysis (Neshat et al. 2014; Jarray et al. 2017; Shrestha et al. 2016; Abdeslam et al. 2017).

According to Schnebelen et al. (2002), we distinguish two vulnerability types: intrinsic vulnerability and specific vulnerability. Intrinsic vulnerability refers only to the aquifer's hydrogeological properties and, therefore, to the natural environment's characteristics, determining groundwater sensitivity to pollution by human activities. The specific vulnerability relates to both hydrogeological properties and the nature of potential contaminants that may

modify groundwater quality. It takes into account the properties of pollutants and their relationships with various components of intrinsic vulnerability.

Various models for assessing groundwater vulnerability are generated. We can classify it into three classes: the indexed models (or cartographic approach), the statistical models, and the simulation models. The indexed models are used to assess the intrinsic vulnerability-based only on aquifer properties (Ghouili et al. 2020). The simulation models are a simplification of reality and are also used to calculate the specific vulnerability. These models consist of finding a numerical solution to mathematical equations representing the process of contamination's transfer (Hamzaoui-Azaza et al. 2020). The statistical models are used to calculate the specific vulnerability based on a variable that depends on contaminants' concentration or a probability of contamination. These statistical models integrate the distribution of an element in the study area and estimate the probabilities of the aquifer contamination.

Many intrinsic methods are used to assess groundwater vulnerability; DRASTIC (Barzegar et al. 2019), GOD, COP (Bagherzadeh et al. 2018), SINTACS, CRIPTAS (Mfonka et al. 2018) and SI (Ghouili et al. 2020). The Drastic, SINTACS approaches are the most widely used methods in this field of research. The choice of a method depends on the availability and reliability of vulnerability factors and the applied techniques' objectives.

During the last decades, the Hajeb Layoun Jelma basin has been marked by an economic development based on intensive agriculture under irrigation. This is characterized by the intense use of chemical fertilizers, parallel with pesticides, which presents a significant risk for groundwater resources sustainability.

To determine the vulnerability of groundwater in the Hajeb Layoun Jelma basin (HJB), we have used both intrinsic (DRASTIC model) and specific models (simulation model).

The DRASTIC method (Aller et al. 1987) was chosen based on data availability, coupled with a Geographic Information System (GIS). It is a parametric method based on seven parameters: the water depth, the net recharge, the aquifer lithology, the soil pedology, the topography, the hydraulic conductivity of the aquifer and the impact of the vadose zone through the unsaturated zone lithology.

This research aims to implement an assessment tool controlling the groundwater vulnerability of the Quaternary aquifer of HJB using the DRASTIC model combined with a geographic information system (GIS) also using simulation models of salinity transport. This

study also aims at evaluating the most parameter influencing the vulnerability using sensitivity analysis.

II. Groundwater vulnerability assessment using the indexed method

1. Description of the DRASTIC model

The concept of groundwater vulnerability to contamination was initially familiarized by Margat (1968). The concept of the Drastic model was defined by Aller et al. (1987). It is based on the concept of hydrogeological setting, defined as a composite description of all significant geologic and hydrologic factors that affect and control the groundwater movement throughout an area. The Drastic model is one of the overlay/index methods and is a powerful tool for assessing groundwater vulnerability, and it is widely used (Secunda et al., 1998; Celico et al., 2005; Celico et al., 2008; Jarray et al., 2017; Abdeslam et al., 2017).

This work aimed to assess the vulnerability for the shallow aquifer of Hajeb Layoun Jelma aquifer using the DRASTIC model coupled with geographic information system GIS (ArcGIS 10.3). Different ratings are consequently assigned to each parameter based on a range of information within the parameter and subsequently, summed-up with their respective weights to produce a vulnerability rating or DRASTIC index (DI) determined by this formula:

$$DI = \sum Ri \times Wi \quad (\text{Eq 34})$$

Where R: is the rating value,

W: is the weight assigned to i:

i: D, R, A, S, T, I, and C represent the seven parameters.

2. Determination of DRASTIC parameters

To create the vulnerability map of the shallow aquifer, seven parameters were determinate: Depth to water table (D), net aquifer Recharge rates (R), Aquifer media (A), Soil media (S), Topographic (T), Impact of vadose zone media (I) and hydraulic Conductivity (C) (Figure 63).

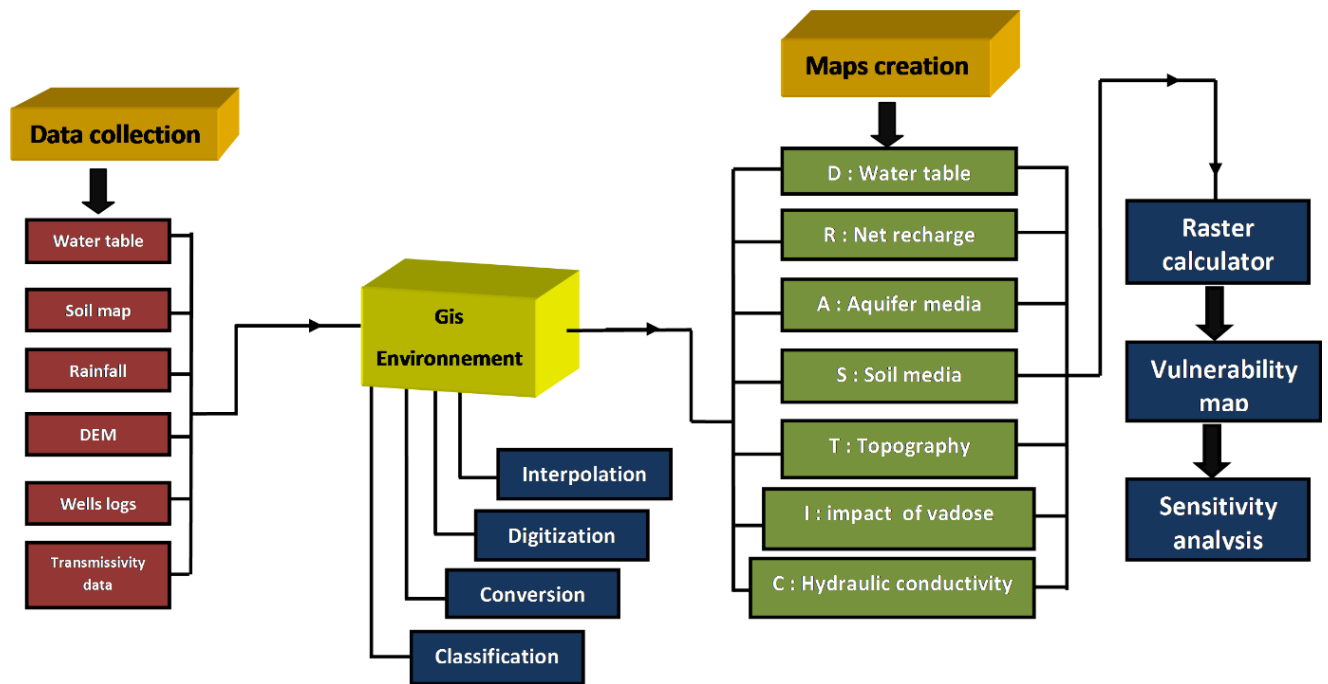


Figure 63. Flow chart of the methodology used for the shallow aquifer vulnerability evaluation

The different hydrogeological parameters used to create the DRASTIC model were collected from several sources (**Table 13**) and converted into thematic maps using ArcGIS 10.3. All parameters were assigned a weight and rating based on a range of information within the parameter, the weight of each parameter depends on the impact of potential pollution.

Table 13 Sources of data used for the production of the DRASTIC model

Parameters	Types of data	Acquisition mode
D Depth to water	Piezometric Yearbook 2017 (DGRE)	Interpolation
R Net Recharge	Rainfall Data (1968-2015) (DGRE)	Interpolation
A Aquifer media	wells and piezometers reports (CRDA of Sidi Bouzid)	Interpolation
S Soil media	Soil Map (CRDA of Sidi Bouzid)	Numerisation
T Topography	Mosaicking of 9 Topographic map (1 / 50.000)	Numerisation
I Impact of vadose zone	wells and piezometers reports (CRDA of Sidi Bouzid)	Interpolation
C Hydraulic Conductivity	wells and piezometers reports (CRDA of Sidi Bouzid)	Interpolation

For the standard Drastic, the most significant weight is allocated five; the least significant is allocated. For the pesticide Drastic the high weight (equal to 5) was assigned to “the water table depth” and “soil media” and the lowest was assigned to the aquifer’s hydraulic conductivity (**Table 14**).

Table 14 Drastic parameters: range, rating and weight value for the study area (Standard and Pesticide Drastic) (Aller et al., 1987)

Drastic items	Range	Rating	weight	
			Standard	Pesticide
Groundwater level (m)	>31	1		
	23-31	2		
	15-23	3		
	9-15	5	5	5
	4.5-9	7		
	1.5-4.5	9		
Recharge Piscopo (2011)	3-5	1		
	5-7	3		
	7-9	5	4	4
	9-11	8		
Aquifer media (m/s)	1.5×10^{-5} - 5×10^{-5}	1		
	5×10^{-5} - 15×10^{-5}	2		
	15×10^{-5} - 45×10^{-5}	4	3	3
	45×10^{-5} - 450×10^{-5}	8		
Soil media	Clay Loam	3		
	Sandy clay	4		
	Sandy loam	6	2	5
	Loamy sand	7		
	sand	9		
Topography	0-2	10		
	2-6	9		3
	6-12	5	1	
	12-18	3		
	>18	1		
Impact of vadose zone (m/s)	10^{-5} - 10^{-3}	5	5	4
	10^{-3} - 10^{-2}	6		
Hydraulic conductivity	5×10^{-5} - 2×10^{-4}	2		
	2×10^{-4} - 4×10^{-4}	4		
	4×10^{-4} - 5×10^{-4}	6	3	2

The seven parameters of the Drastic model can be classified into two classes:

- The static parameters (time-independent parameters: Topography "T" and soil type "S")
- The dynamic parameters which change in time (the depth of the aquifer "D", the net recharge "R", the formation of the Aquifer "A", the impact of the unsaturated zone "I" and the hydraulic conductivity of the aquifer "C"). In fact, the spatio-temporal variation of the rainfall causes a variation of the aquifer recharge which affects the water table. The increase of the recharge results in the decrease of the depth to the aquifer and the decrease of the thickness of the unsaturated zone, therefore its causes the variation of the horizons which compose it (the variation of the lithology of the horizons constituting the saturated and

unsaturated zone, because the study area has a significant heterogeneity of facies). So, the infiltrated water variability will consequently generate variations in the time of these four parameters.

2.1.Static parameters

a. The Soil media (S)

It is the controlling parameter of infiltration and movement of contaminants. Fine materials (clays and silts) and organic matter in the soil reduce intrinsic permeability. For the Hajeb Jelma basin, the soil map published by CRDA of Sidi Bouzid is classified in five soil classes (**Table 14**) and to each one, a rating value is attributed (**Table 14**). The index soil is calculated by multiplied all attributed rating by the weighting factor.

b. The Topography (T)

It represents the slope of land surface. For HJB, this parameter is obtained by digitizing and assembling nine topographic maps (scale 1: 50.000) using ArcGIS software. Using the extensions "Spatial Analyst" and "3D Analyst" the topographic map is transformed into Digital Elevation Model (DEM). ArcGIS software is used to automatically generate a slope map from the DEM (pixel size = 30 m). Then, to generate the slop index, the slope map is reclassified with the drastic rating (**Table 14**) and converted into grid coverage (pixel size = 30 m) and finally multiplied by the topographic weight.

2.2.Dynamic parameters

a. The depth of the water table (D)

It represents the vertical distance that the contaminant percolates from the ground surface to the aquifer. This parameter is obtained by interpolation of the data relating to the shallow wells and piezometers inventoried. After we have classified according to the ranges for the water table given by Aller (**1987**), the depth index is obtained due to multiplying $D_r * D_w$ (r : ratings and w : weight).

b. The net recharge (R)

The net recharge is an amount of water that recharges the aquifer; recharge water is available to transport a contaminant vertically to the water table and horizontally within the aquifer. Rainfall data were collected from the CRDA of Sidi bouzid. The recharge map was generated using the following formula:

$$\text{Recharge index} = \text{Slope (\%)} + \text{Rainfall} + \text{Soil permeability} \quad (\text{Eq 35})$$

Several studies have used this method given by Piscopo (2001) to calculate the recharge index (Muheeb et al. 2009; Rezaei Moghaddam et al. 2018), in which net recharge was calculated by a combination of ratings for slope, soil permeability, and rainfall (Table 15).

Table 15 Intervals and ratings of the recharge and the three parameters that control it based on the Piscopo method (2001)

Parameter	Range	Rating
Slope %	<2	4
	2-10	3
	10-33	2
	>33	1
Rainfall (mm)	<500	1
	500-700	2
	700-850	3
	>850	4
Soil Permeability	Very slow	1
	Slow	2
	Moderate	3
	Moderate-High	4
	High	5

The Formula is based on two static parameters (slope and Soil) and one dynamic parameter (Rainfall); the slope in the study area was derived from the DEM and classified according to the criteria given in Table 14.

The resulting slope map was converted into grid coverage, the soil map was classified based on the criteria given in Table 3 and was then converted into grid coverage (pixel size = 30 m). In the final the three maps resulted was summed-up to generate the indexed recharge map using the “weighted sum” tool in ArcGIS software.

c. Aquifer media (A)

The thickness of the the saturated zone is defined as the difference between the thickness of the entire aquifer and the static level. This parameter was calculated using the equivalent permeability of the saturated zone. The permeability of the shallow aquifer is not available. To calculate this parameter, we have affected

To calculate the equivalent permeability of the aquifer, we have used the following formula:

$$KH eq = \frac{\sum_{i=1}^{i=x} (Hi \times Ki)}{\sum_{i=1}^{i=x} Hi} \quad (\text{Eq 36})$$

Where KHeq: Horizontal equivalent permeability (m/s),
 H: Thickness of the layer i (m),
 K: Permeability of the layer i (m/s).
 i (1 to x): layers that contain the aquifer

The distribution of the saturated zone's equivalent permeability was calculated then classified according to the table given by Aller in 1987 (Table 14).

d. The vadose zone (I)

It is defined as the part between ground surface and top of the shallow aquifer; where the pores are partially saturated with water. The permeability of the vadose zone controls the flow of pollutants and their arrival at the water table; the infiltration of contaminants is guided by the layers' lithological characteristics that control their paths sub-surface trajectories.

This parameter is obtained according to the litho-stratigraphical cross-section realized from the available litho-stratigraphic logs. After limiting the reservoir level and the unsaturated zone, the equivalent vertical permeability is calculated using the formula 4.

$$KVe q = \frac{\sum_{i=1}^{i=x} Hi}{\sum_{i=1}^{i=x} (Hi / ki)} \quad (\text{Eq 37})$$

Where KVe q: Vertical equivalent permeability (m/s),
 H: Thickness of the layer i (m),
 K: Permeability of the layer i (m/s).
 i (1 to x): layers of the vadose zone.

The values obtained are interpolated on the entire area of the shallow aquifer and reclassified according to the Drastic model classes. A rating was assigned to each interval and was multiplied by the vadose zone's weight to obtain the vadose zone map index.

e. The hydraulic conductivity (C)

It refers to the ability of the aquifer to transmit water. The hydraulic conductivity of the shallow aquifer is not available. To calculate this parameter, we have based on estimated values according to the permeability table of Castany (1982).

This factor's spatial distribution is obtained by correlation and inverse distance weighted (IDW) interpolation of estimated values at the level of shallow wells and piezometers.

To generate the vulnerability map, we have summed-up with the weigh (Standard and Pesticide) all seven grid maps ('D', 'R', 'A', 'S', 'T', 'I' and 'C') and range with the degree of vulnerability (Table 16).

Table 16 Drastic range and its vulnerability class (Civita 1994)

Drastic index	Vulnerability class
<80	Very low
80-120	Low
120-160	Moderate
160-200	High
>200	Very High

3. Sensitivity analysis

Aquifer vulnerability assessment requires validation to reduce subjectivity in selecting rating ranges and weight and increasing reliability. Sensitivity analysis provides helpful information on the influence of rating and weighting values assigned to each parameter and helps hydrogeologists judge the significance of subjectivity elements. There are two types of sensitivity analysis: The single parameter sensitivity analysis introduced by Napolitano and Fabbri (1996) and map removal sensitivity analysis introduced by Lodwick et al. (1990).

3.1 The single parameter sensitivity

The weight values assigned to the Drastic parameters are essentially arbitrary (Al-Adamat et al., 2003), and the vulnerability index is susceptible to these values. Single parameter sensitivity can be made to compare the real weight and the “theoretical” weight used in DRASTIC (Napolitano and Fabbri 1996). This formula computes the real or the “effective” weight:

$$E_w = \frac{100 \times R \times W}{V} \quad (\text{Eq 38})$$

Where E_w : the “effective” weight of each parameter

R: the rating value

W: the weight for each parameter,

V: the overall vulnerability index.

3.2 Map removal sensitivity analysis

This analysis describes the vulnerability map's sensitivity when removing one or more maps (Lodwick et al., 1990). It is calculated using the following formula:

$$Vs = 100 \times \left(\frac{V}{N} - \frac{V'}{n} \right) / V \quad (\text{Eq 39})$$

Where V: The unperturbed vulnerability indices

V': The perturbed vulnerability indices

N: Number of layers used to calculate V

n: Number of layers used to calculate V'

4. GIS and model builder

Under *ArcGis 10.3*, a database has been established, including the inventory of all data used for the vulnerability map creation (localization and water table depth for each well, soil type, DEM, Rainfall station location, and their measurement). The Drastic model was developed, under *ArcGis 10.3*, using the ‘model builder’ tool. This tool has automated the model workflows. The thematic maps, such as location map, geological map, land use, distribution maps of the seven drastic parameters (Depth of the water table, recharge, Aquifer media, soil media, topography, the impact of vadose zone and the hydraulic conductivity) and the vulnerability map were obtained from 1:50000 scale under the UTM coordinate system and WGS 84 (32N) datum projections. The coordinate of each well was measured by using, in the field, a global positioning system (GPS). The interpolation technique obtained the water table's spatial distribution, Aquifer media, vadoze zone, and hydraulic conductivity through IDW.

5. Conclusion

This study aims to assess groundwater vulnerability in the Hajeb Layoun Jelma basin using the indexed model. Based on the available data related to the study area, we have chosen to use DRASTIC model to assess the vulnerability of shallow aquifer.

DRASTIC models have seven parameters: Depth to water, net Recharge, Aquifer media, Soil media, Topography, Impact of the vadose zone and Hydraulic Conductivity. Each parameter has a weight ranging from 1 to 5. It was further assigned a rating, typically from 1 to 10, based on a range of information within the parameter. Higher ratings and weights indicated a higher risk of vulnerability.

III. Modeling of pollutant transport

1. Introduction

Demographic growth, climatic conditions, socio-economic development in the HJB engendered an increase in the water abstraction of groundwater to satisfy all these needs. The over-abstraction from this groundwater and the intensive agriculture activities led to the degradation of the water quality. In fact, in the last decades, the shallow water salinity of HJB, was increased from 0.5 to 1 g/l (DGRE 2018). So, it is essential to study the impact of the overexploitation, from this basin, on water quality by employing the solutes transport model. The solute transport was based on the calibrated groundwater flow models.

In this research, the MT3DMS package (three - dimensional multispecies transport model) has been used (Zheng & Wang 1999; Chen et al. 2013). Both MT3DMS and MODFLOW code has a similar modular structure. The MT3DMS code allows for the simulation of advection, dispersion/diffusion, chemical reactions and source/sink mixing (Maliva & Missimer 2012).

It has been used to simulates the Spatio-temporal distribution of the water salinity over the entire shallow aquifer in the Hajeb Layoun Jelma basin. The transport model is developed based on the calibrated steady state hydrodynamic model.

2. Theoretical description of the pollutant transport process

2.1 Equation

The differential formula of 3D transport of pollutant in the aquifer is (Freeze and Cherry 1979; Zheng wnd wang 1999):

$$\frac{\partial(nC)}{\partial t} = \frac{\partial}{\partial x_i} \left(nD_{ij} \frac{\partial C^k}{\partial x_j} \right) - \frac{\partial}{\partial x_i} (nv_{si}C^k) + q_s C_s^k + \sum R_n \quad (\text{Eq 40})$$

Where

C: Solute concentration (M.L⁻³)

n: the porosity of the medium, t was the time (T), x_i represented the distance along the Cartesian coordinate axis,

D_{ij} was the hydrodynamic dispersion coefficient tensor (L²/T), v_{si} was the seepage or linear pore water velocity (L/T);

It was closely related to the darcy flux solved by this equation:

$$v_{si} = \mathbf{qi}/n \quad (\text{Eq 41})$$

With: q_s was defined as the volumetric flow rate per unit of volume of the aquifer; C_s^k was the concentration of the source or sink flux of salinity M/L) and R_n was the chemical reaction.

2.2 Advection

The advection describes the transport of miscible pollutants, a dissolved chemical species, in the entire void space with the same groundwater velocity (Bear and Cheng, 2010).

$$\text{Advective equation} = \frac{\partial}{\partial x_i} \times (\theta c v_i) \quad (\text{Eq 42})$$

With θ : the porosity of the porous medium (1);

v_i : velocity of the phase (LT-1)

c : average concentration of the contaminant (L-3);

2.3 Dispersion and diffusion

The dispersion in porous media is defined as spreading pollutants over a large region (Anderson 1979, 1984). In groundwater, dispersion is usually called hydrodynamic dispersion (Bear, 1972). It is expected from the average velocity. This phenomenon results from mechanical dispersion, defined as the deviations of the velocity from the average of groundwater velocity on a microscale and the molecular diffusion (D_d) determined by concentration gradients. Mechanical dispersion is mixing caused by local variations in velocity around the mean flow velocity, v_x . It is described with the mechanical dispersion coefficient (D'). The molecular diffusion is usually insignificant compared to mechanical dispersion effects (Zheng and Wang 1999).

The hydrodynamic dispersion coefficient (D) is sum of D_d and D' or

$$D = D_d + D' \quad (\text{Eq 43})$$

In three dimensions, the coefficient D' has three components along with three perpendicular coordinates (x, y, z) which are expected to be proportionate to three groundwater velocity components u_x, u_y and u_z :

$$D'_x = \alpha_L u_x; D'_y = \alpha_T u_y; D'_z = \alpha_V u_z \quad (\text{Eq 44})$$

Where α_L, α_T , and α_V are the longitudinal dispersivity, the horizontal transverse dispersivity, and the vertical transverse dispersivity, respectively.

There are numerous methods for approximating the apparent longitudinal dispersivity. The simplest method is a rule of thumb (Gelhar, 1993). This rule is based on the observation that the longitudinal dispersivity increases with an overall scale or the travel distance (L) of a

contaminant from a source, meaning that the apparent longitudinal dispersivity is one-tenth of L (ASTM, 1994) or

$$\alpha_L = 0.1 * L \quad (\text{Eq 45})$$

Where L is the average travel distance of the plume.

Neuman (1990) proposed the better scale-dependent using universal scaling, an empirical method for estimating α_L :

- $\alpha_L = 0.0175 L^{1.46}$ for L less than and equal to 100 m and
- $\alpha_L = 0.32 L^{0.83}$ for L larger than 100 m.

Where L is the average travel distance of the plume.

The dispersion of a contaminant in a heterogeneous aquifer is a problematic process principally caused by groundwater velocity variations at different scales. This variation is affected by the variation of hydraulic conductivity (Lovanh et al., 2000). It is suggested that Neuman's (1990) method should be used when the hydraulic conductivity data is limited, which is the case.

The transverse dispersivity (α_T) is generally equal to 30% of the longitudinal dispersivity, and the vertical dispersivity (α_V) is 5% of the longitudinal dispersivity (ASTM, 1994). The US EPA (1986) specifies that the transverse dispersivity is equal to 33% of the longitudinal dispersivity and the vertical dispersivity varies from 52.5 % to 10 % of the longitudinal dispersivity.

2.4 Sinks and sources

The fluid sink or source term of the equation signifies the solute mass is entering the model domain through sources or parting the model through sinks (Zheng and Wang, 1999). Sinks or sources are classified into point sinks or sources or distributed sinks or sources. The first class includes wells, rivers and drains. Constant-head and general head boundaries in the hydrodynamic flow model are considered as point sinks or sources. The distributed sinks/sources contain recharge and evapotranspiration (Mehl et al., 2006).

It is essential to identify the concentration of the source water. In contrast, the concentration of sink water cannot be identified, and it is usually the same as the concentration of groundwater in the aquifer at the sink site (Zheng and Wang, 1999).

2.5 Chemical reactions

Zheng and Wang (1999) explained the capability of MT3DMS to handle the equilibrium-controlled linear and nonlinear sorption, the no equilibrium sorption and the first-order reaction, which represent the radioactive disintegration provide the biodegradation representation. The sorption is defined as the mass transfer process between the pollutants dissolved in groundwater and the pollutants sorted on the porous media.

To conclude, it is necessary to define and specify initial and boundary conditions to solve the transport equation.

3. Description of MT3DMS model of HJB

3.1 Construction of the steady-state solute transport model

In this stage of the research, only an overall concentration, identified as the total dissolved solids (TDS), will be retained.

The conceptualization of the solute transport model is identical to that of the groundwater flow models. The layer number was limited to one which present the unconfined shallow aquifer. It requires defining the model parameters' initial distribution (effective porosity and dispersivity) and the boundary conditions. The first step is to reconstitute the observed initial state and calibrate the transport model over a historical period.

3.2 Boundary conditions

The upstream boundaries of the model domain, which represents the subsurface groundwater inflow boundary, are assigned as fixed concentrations based on the observed initial concentration distribution in the study area. Transport conditions are closely related to the direction of flow. The piezometric level adopted is that resulting from the calibrated steady-state flow model. In our simulation, we imposed an initial concentration fixed at $t = 0$; $C = C_0 = 1.5$ g/L for the salinity over the irrigated areas. This concentration represents a value lower than all the concentrations measured in well located in the irrigated area.

3.3 Effective porosity

This parameter is decisive for calculating the sufficient velocities at any point and specifying the convection and dispersion flows. It is also particularly crucial for distributing the steady-state and transient levels because it controls all the mixing water processes and the

resulting concentrations. Data about this parameter are rare. The initial porosity distribution is based on available data and previous studies.

3.4 Prediction solute transport model

For groundwater management, it is better to understand the future pollutant movement along with the flow directions. The groundwater quality varies according to the groundwater flow line (Edmunds *et al.* 2001).

This part's main objective is to identify the future chemical changes taking place along the different flow lines with the same direction of shallow aquifer's flow.

4. Conclusion

The transport model simulates the migration of salts in the natural environment within the studied shallow aquifer in HJB. The calibrated steady state model serves as initial conditions for transient transport model. Porosity and dispersivity are used to adjust the model.

Part 3 Results and discussions

Chapter I Geochemical characterization

Chapter II Groundwater flow Modeling

Chapter IV Vulnerability mapping and Contaminant transport modeling

"A l'échelle cosmique, l'eau liquide est plus rare que l'or."

Hubert Reeves

Chapter I: Geochemical characterization

I. Hydrochemical data

A statistical view of hydrochemical parameters (min, max and standard deviation) is given in **Table 17**. The pH data ranged from 7.15 to 8.45 and 7.63 to 8.24 for the shallow aquifer/springs and the deep aquifer samples, respectively. These results show that: the both aquifers have a pH close to neutrality with a slight tendency toward the basic composition. The temperatures are characterized by heterogeneous values varying from 10.3 to 24.8 °C and 13.1 to 30.2 °C for the shallow and the deep samples, respectively. The temperature of water depends on the well depth, with an average value and standard deviation equal to 17.9 °C and 3.97 °C, for the shallow/springs samples, and equal to 22.8 °C and 4.96 °C for the deep aquifer samples. For the shallow and springs samples, the electrical conductivity values vary from 1544 to 9770 $\mu\text{S}/\text{cm}$ with a mean of 2685 $\mu\text{S}/\text{cm}$. For the Deep aquifer samples, the EC varies from 393 to 3960 $\mu\text{S}/\text{cm}$ with a mean of 1729 $\mu\text{S}/\text{cm}$.

For the both type of samples (Shallow aquifer/Springs and deep aquifer), the chemical analysis indicated that the abundance order of the major cations is $\text{Na} > \text{Mg} > \text{Ca} > \text{K}$. For the shallow and springs samples, the concentration of major cations; Na^+ , Ca^{2+} , Mg^{2+} , and K^+ are ranged from 142.6 to 1075, 37.8 to 70.4, 41.8 to 148.23, and 4.68 to 19.89 mg/l with a mean value of 265.54, 47.2, 84.38, and 7.61 mg/l, respectively. For the deep samples the cations; Na^+ , Ca^{2+} , Mg^{2+} , and K^+ are ranged from 17.48 to 459.31, 5.8 to 55.6, 0.47 to 117.67, and 2.34 to 15.6 mg/l with a mean value of 138.35, 37.7, 35.53, and 4.88 mg/l, respectively. The order of abundance of the anion is $\text{Cl} > \text{HCO}_3 > \text{SO}_4$. The abundance of these cations and anion is derived from a mineralization process, which can be natural or anthropogenic.

Table 17 Statistical summary of the physical and chemical parameters of HJB samples (Ionic contents in mg/l)

	T (°C)	PH	EC	Salinity	Na^+	Ca^{2+}	Mg^{2+}	K^+	Cl	HCO_3^-	SO_4^{2-}	
Deep	Min	13,10	7,15	393	0,10	17,48	5,80	0,47	2,34	82,36	32,33	4,80
	Max	30,20	8,45	3960	1,80	459,31	55,60	117,67	15,60	935,43	154,33	105,12
	SD	4,96	0,35	961,82	0,52	117,60	13,09	29,16	3,89	240,49	37,09	32,80
Shallow / springs	Min	10,30	7,63	1544	0,70	142,60	37,80	41,80	4,68	341,16	32,33	1,44
	Max	24,80	8,24	9770	6,50	1075,02	70,40	148,23	19,89	1768,61	305,00	235,20
	SD	3,97	0,20	2014,12	1,41	230,09	8,38	27,55	4,71	368,03	87,15	65,05

The groundwater salinity shows a wide variation from 100 to 1800 mg/L with a mean value equal to 700 mg/L and from 700 to 6500 mg/L with a mean value equal to 1400 mg/L for the deep and the shallow aquifers, respectively. The distribution of the salinity presented in **Figure 64** reveals that in the shallow aquifer has high soluble salts in the totality of samples (one sample: Salinity < 1 and 13 samples: salinity >1 g.L⁻¹ with one sample exceeding 6 g.L⁻¹) (**Figure 64**). The deep aquifer has moderate salinity: 3 samples exceeding 1 g.L⁻¹ and the rest (11 samples) indicate salinity less than 1 g.L⁻¹. The high salinity values would be related to the leaching of salts from soils, the use of fertilizers in agriculture activities or/ and return flow from irrigation water (Mnassri et al., 2018). This hypothesis is confirmed by analyzing the samples that are taken from wells located in the irrigated perimeters (see **Figure 22**).

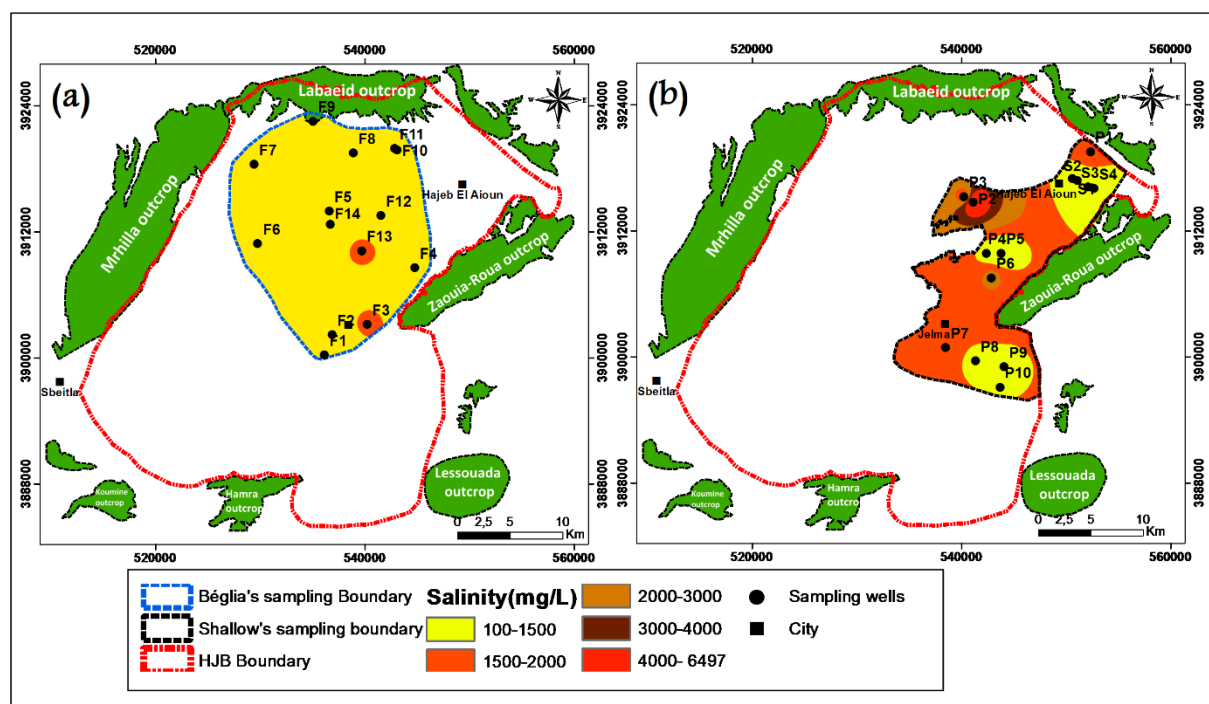


Figure 64. Spatial distribution of salinity: (a): Deep and (b): shallow aquifer. The map was plotted using the IDW method.

II. Groundwater mineralization processes

1. Correlation of parameters

The correlation matrix of the shallow and springs samples indicated that the contents of sodium, magnesium, chloride and calcium are high positively correlated with salinity (**Table 18 a**). These positive correlations indicate the continuous addition of these ions along groundwater flow path. Therefore, these elements contribute to the groundwater mineralization. The concentration of Cl⁻ is correlated with Na⁺ with a correlation index of 0.95, indicating that the halite dissolution may be the important reaction affecting the water chemistry. The electrical

conductivity also shows a perfect positive correlation with Na^+ ($R = 0.98$), Ca^{2+} ($R=0.82$), salinity ($R=0.98$), Cl^- ($R=0.95$) and moderately positive correlation with Mg^{2+} ($R = 0.67$).

Table 18 Pearson correlation matrix of HJB, (a): Shallow wells/Springs, (b): Deep wells, bold indicates significant 50%

(a)	T (°C)	PH	EC	Salinity	Na^+	Ca^{2+}	Mg^{2+}	K^+	Cl^-	HCO_3^-	SO_4^{2-}
T (°C)	1										
PH	-0.53	1									
EC	0.08	-0.26	1								
Salinity	0.03	-0.24	0.98	1							
Na^+	0.12	-0.33	0.98	0.98	1						
Ca^{2+}	-0.34	-0.05	0.82	0.82	0.77	1					
Mg^{2+}	-0.02	-0.11	0.65	0.63	0.63	0.72	1				
K^+	-0.05	-0.28	-0.22	-0.14	-0.16	-0.08	0.09	1			
Cl^-	0.02	-0.26	0.95	0.95	0.95	0.86	0.69	-0.11	1		
HCO_3^-	0.25	0	0.20	0.20	0.21	-0.04	0.34	0.13	0.03	1	
SO_4^{2-}	0.07	-0.10	0.17	0.12	0.16	0.01	0.12	-0.19	-0.05	0.47	1

(b)	T (°C)	PH	EC	Salinity	Na^+	Ca^{2+}	Mg^{2+}	K^+	Cl^-	HCO_3^-	SO_4^{2-}
T (°C)	1										
PH	-0.53	1									
$\text{C}_{25}^{\circ\text{C}}$	0.47	-0.52	1								
Salinity	0.39	-0.55	0.98	1							
Na^+	0.49	-0.49	0.97	0.95	1						
Ca^{2+}	0.26	-0.65	0.77	0.82	0.70	1					
Mg^{2+}	0.14	-0.36	0.75	0.80	0.70	0.69	1				
K^+	0.59	-0.21	0.72	0.65	0.77	0.38	0.40	1			
Cl^-	0.40	-0.40	0.96	0.95	0.97	0.71	0.80	0.75	1		
HCO_3^-	0.42	-0.57	0.61	0.58	0.62	0.61	0.40	0.56	0.58	1	
SO_4^{2-}	0.07	-0.30	0.37	0.46	0.32	0.45	0.60	-0.02	0.34	-0.08	1

The matrix of the deep samples (**Table 18 b**) indicates that EC shows a high correlation (positive) with Salinity ($R = 0.98$), Na^+ ($R = 0.97$), and Cl^- ($R = 0.96$) and moderately positive correlation with Ca^{2+} , Mg^{2+} , K^+ and HCO_3^- with correlation value equal to 0.77, 0.75, 0.72 and 0.61, respectively. Na^+ also shows a high correlation index (positive) with all the major

ions except SO_4^{2-} . The high correlation between some parameters suggests the extent of interdependence and also suggests that these ions may be derived from a common source.

2. Identification of water–rock interaction

To understand the main mechanisms governing groundwater chemistry, Gibbs' diagrams have been used. The weight ratios of ratio I: $[\text{Na}^+ / (\text{Na}^+ + \text{Ca}^{2+})]$ and ratio II: $[\text{Cl}^- / (\text{Cl}^- + \text{HCO}_3^-)]$ are plotting as function of total dissolved solids (TDS), representing Gibbs' diagrams.

This diagram is used to identify dissolved constituents' origin, such as rock weathering dominance, precipitation dominance and evaporation dominance or by combination of these influences (Gibbs 1970). According to Gibbs' diagrams (Figure 65), the data indicates that the chemical composition's HJB samples are governed by evaporation and rock weathering. The importance of evaporation processes and rock weathering are also confirmed by the calculation of the Hounslow ratio $[\text{Cl}^- / \Sigma \text{ anions}]$, which indicates, for both aquifers, two chemical sources: evaporate or brine water sources (ratios > 0.8 and TDS > 500) and rock weathering (ratios < 0.8) (Hounslow 1995).

A plot of Ca^{2+} and SO_4^{2-} shows that for the shallow samples (Figure 66a), one sample below the line 1:1 (PS 3) indicate a deficit in Ca^{2+} , suggesting carbonate precipitation, two samples (PS10 and S1) are close to the bisector line (1:1), indicating that gypsum is the source of calcium. In contrast, most samples are located above the straight dissolution line and indicated an excess in Ca^{2+} , suggesting carbonate dissolution (Figure 66a).

For the deep samples, two samples (F11 and F14) are close to the bisector line (1:1), indicating that gypsum is a source of calcium. In contrast, the majority of the water samples are located above the dissolution straight line and indicated an excess in Ca^{2+} , suggesting carbonate dissolution (Figure 66a).

Evaporation process is also a significant process in controlling the groundwater's chemistry. Both types of samples (shallow/ springs and deep) represented in Figure 66b are very close to the bisector line (1:1) of sodium against chloride's plot, suggesting that salinity is in these wells controlled by halite dissolution.

According to scatter diagrams (Figure 66c), the groundwater mineralization is controlled and minerals dissolution by ion exchange with clay minerals present in the aquifers and reverse ion exchange.

The indicator of carbonate and silicate weathering is confirmed by the $(Ca^{2+}+Mg^{2+})$ against $(HCO_3^-+SO_4^{2-})$ scatter diagrams in **Figure 66d** showing that:

- The shallow and springs samples are distributed at the left and the right part of the 1:1 (line). One sample indicating the abundance of $SO_4^{2-} + HCO_3^-$ by 54 % over $Ca^{2+}+Mg^{2+}$ is a sign of silicate weathering. Most samples located in the left part of the 1:1 (line) indicate that the water samples are related to carbonate rock.
- The deep samples are distributed at the left part of the 1:1 (line) indicating a weathering of carbonates representing the main source of bicarbonate ion.

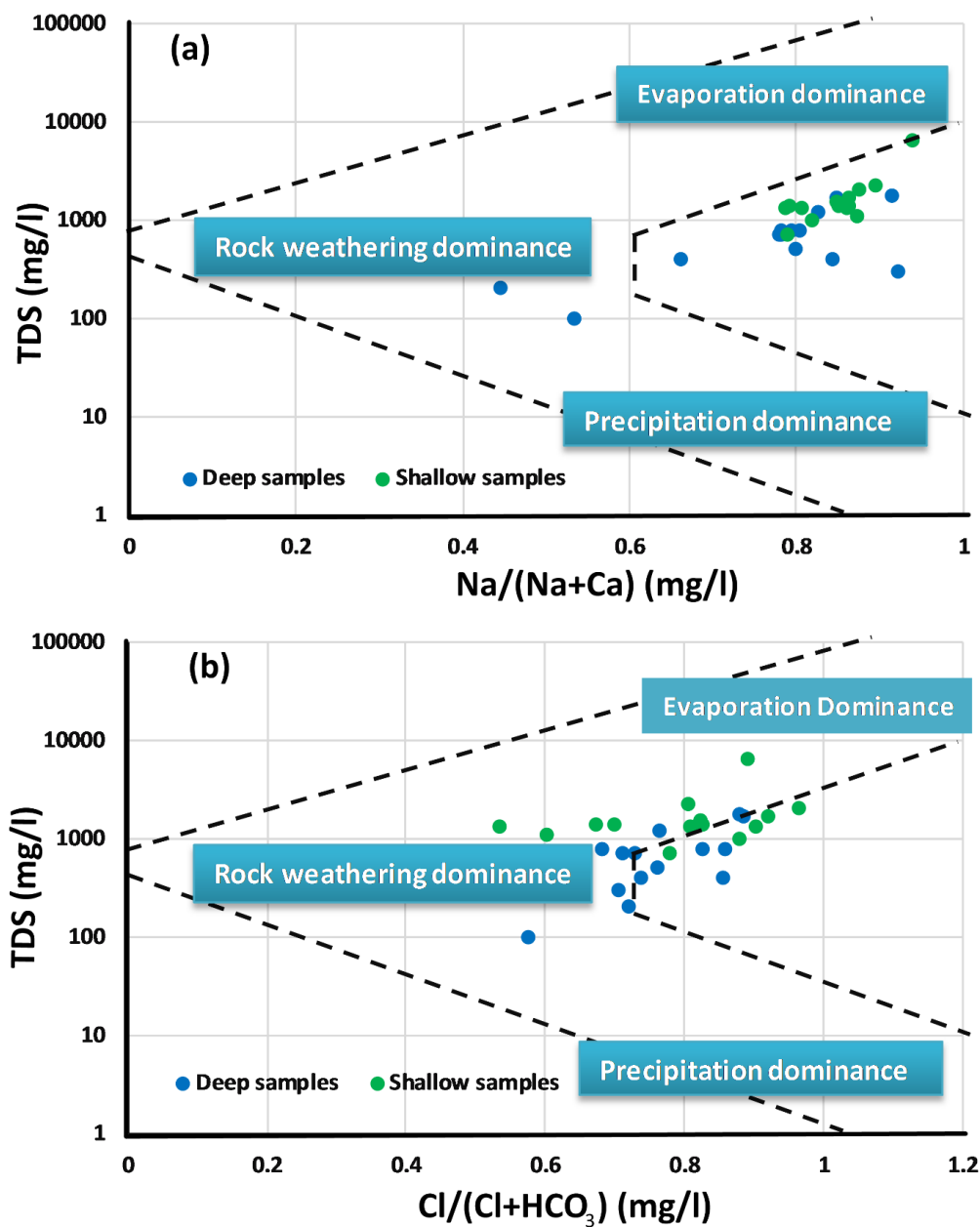


Figure 65. Gibbs' diagrams of the shallow and deep aquifers of HJB: (a) ratio I vs. TDS and (b) ratio II vs. TDS

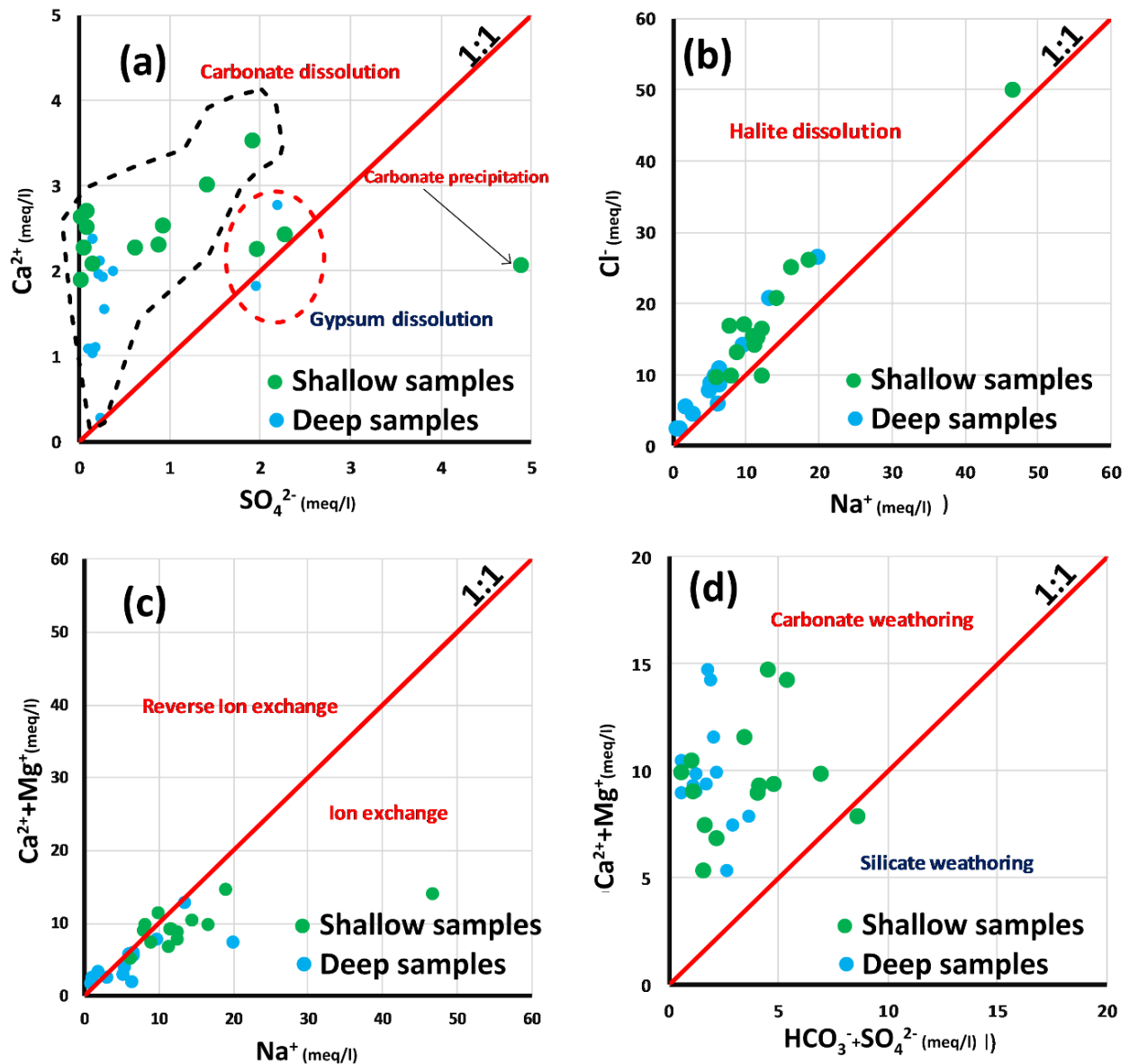


Figure 66. (a) Plot of SO_4^{2-} against Ca^{2+} , (b) Plot of Na^+ against Cl^- , (c) Plot of Na^+ against $(Ca^{2+}+Mg^{2+})$ and (d): Plot of $(HCO_3^-+SO_4^{2-})$ against $(Ca^{2+}+Mg^{2+})$ in meq/l in shallow and deep aquifer water samples

III. Hydrochemical water type

Considering the piper trilinear plot (Figure 67 and Figure 68), we can distinguish three major groundwater groups for the deep aquifer: Na-Cl, Ca-Mg-Cl, and Ca-Cl and two water types for the shallow aquifer: Na-Cl and Ca-Mg-Cl. For the deep aquifer; the first group (Ca-Cl) type waters are highly mineralized. They represent the northwest part of the Beglia aquifer (recharge zone). The high Ca^+ concentration in the northwest part of Beglia aquifer is derived from dissolution of carbonate present in the cretaceous of Dj Mghilla. The second water type is Na-Cl; it presents 78% of the deep aquifer samples and the shallow aquifer. The Na cation is derived from the ion exchange with the adjacent layer's clay (Saouaf formation). In the deep

aquifer, two much closed wells present two different water types (Na-Cl and Ca-Mg-Cl), the Na-Cl water type present 78% of samples while Ca-Mg-Cl is present only in one sample. Based on the wells' screen position, we can detect that the well corresponding to the Ca-Mg-Cl water type presents very different screen position; so, we can conclude that Beglia aquifer present vertical water type stratification.

The chemical data of shallow /springs and deep samples, collected from the studied area, are plotted in the Chadha diagram presented in Figure 10 and Figure 11. All the samples fall in fields 6 and 7. This means that “alkaline earths exceed alkali metals and strong acidic anions exceed weak acidic anion” and “Alkali metals exceed alkaline earths and strong acidic anions exceed weak acidic anions”.

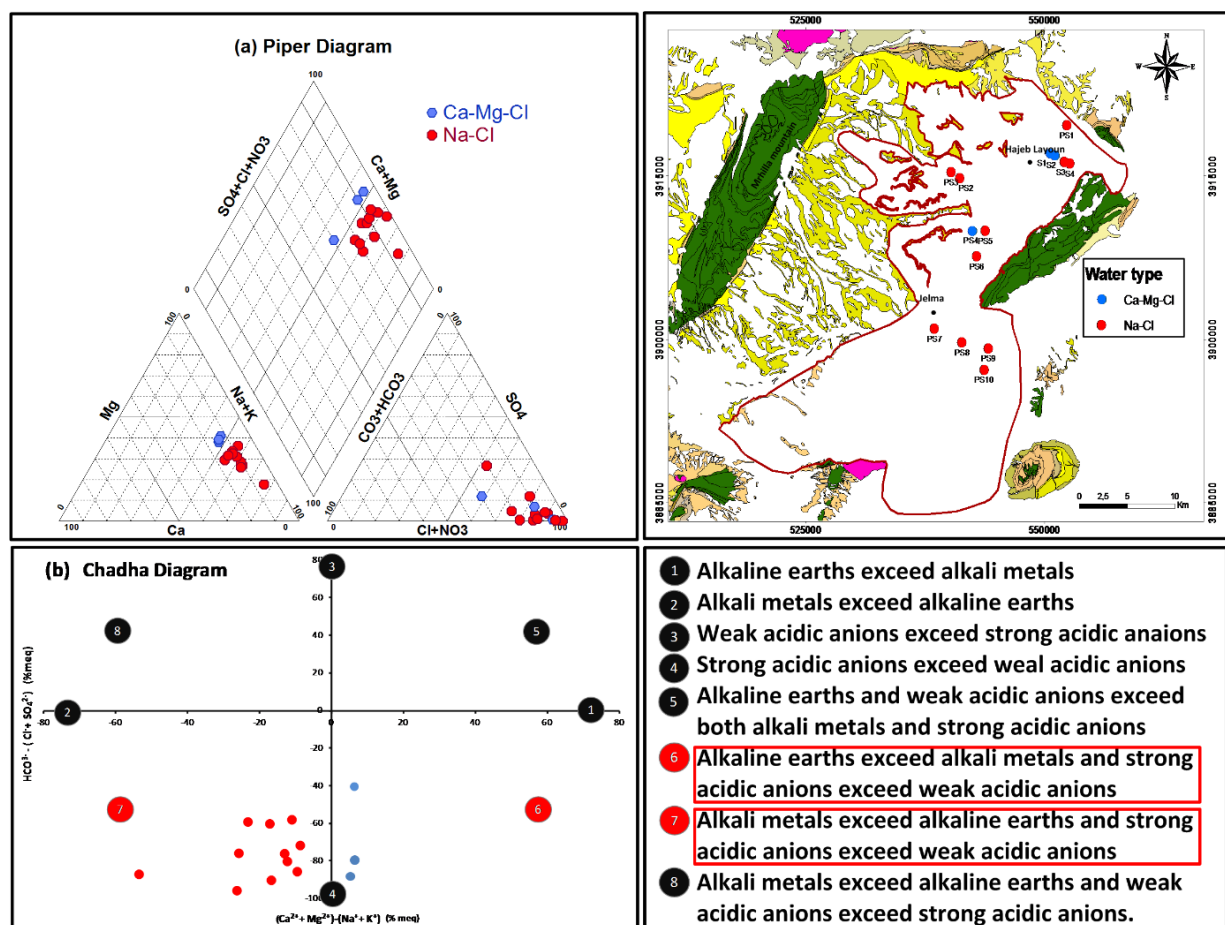


Figure 67. (a) Piper diagram and (b) Chadha diagram of the shallow samples

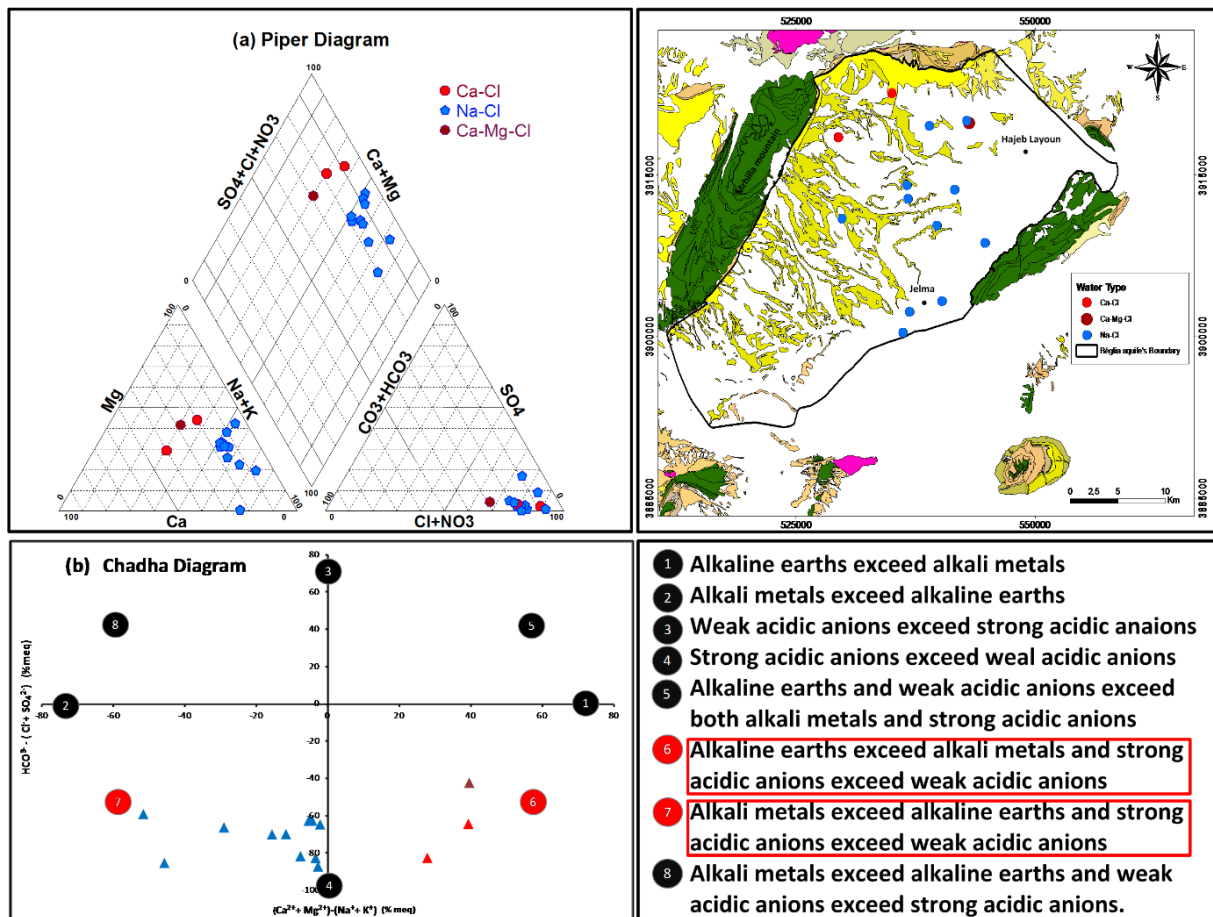


Figure 68. (a) Piper diagram and (b) Chadha diagram of the deep samples

IV. Aqueous geochemical modeling

The water shallow and deep samples relieved from the Hajeb Layoun Jelma basin are equilibrium to saturated by dolomite and calcite and undersaturation by halite, anhydrite, and gypsum (Figure 69).

VII- Saturation of carbonate minerals

Calculated dolomite ((CaMg)(CO₃)₂) and calcite (CaCO₃) saturation indexes (SI) for the shallow and deep samples are presented in Figure 69. SI-Calcite varies from -1.1 to 0.88 for the shallow samples and from -0.06 to 0.41 for the deep samples. SI-Dolomite varies from -0.94 to 1.84 for the shallow samples and -0.22 to 0.82 for the deep samples. The majority of groundwater samples are saturated to under-saturated towards calcite and dolomite (Figure 69), which indicates that the salt content is not influenced by water-carbonated minerals interaction.

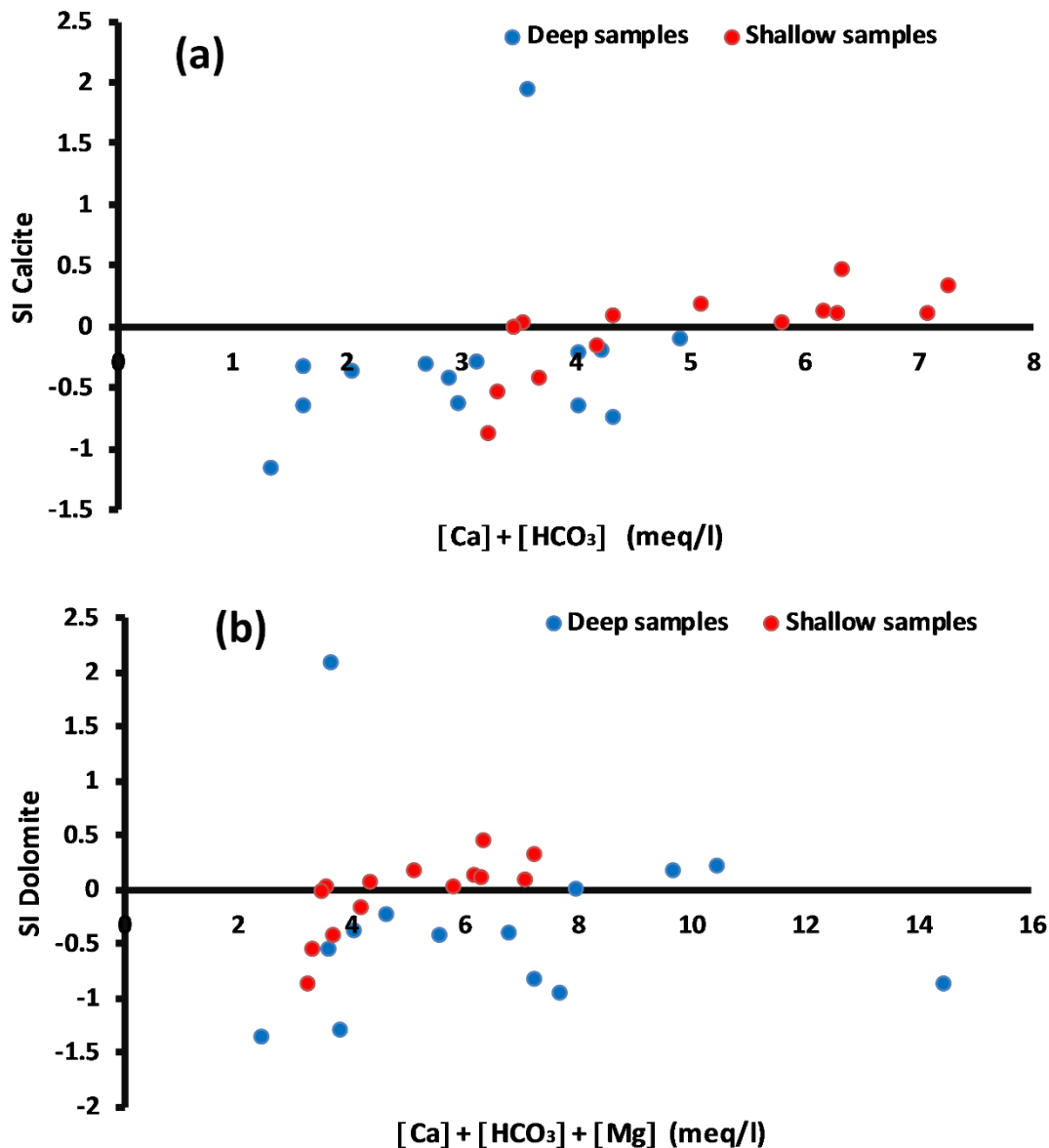


Figure 69. Plot of (a) $[Ca] + HCO_3$ vs SI calcite (b) $[Ca] + [HCO_3] + Mg$ vs SI dolomite

VIII- Saturation of carbonate minerals

SI-Anhydrite varies from -1.05 to -0.03 for humid period and from -1.08 to -0.23 for the dry period. SI-Gypsum varies from -0.81 to 0.2 for the humid period and from -0.86 to 0.01 for the dry period. SI-Halite varies from -5.77 to -4.14 for the humid period and from -5.88 to -4.32 for the dry period. On the other hand, most samples are undersaturated towards sulfate minerals (gypsum and anhydrite) and halite (Figure 70). Therefore, the mineralization of the waters is influenced by the dissolution of gypsum minerals.

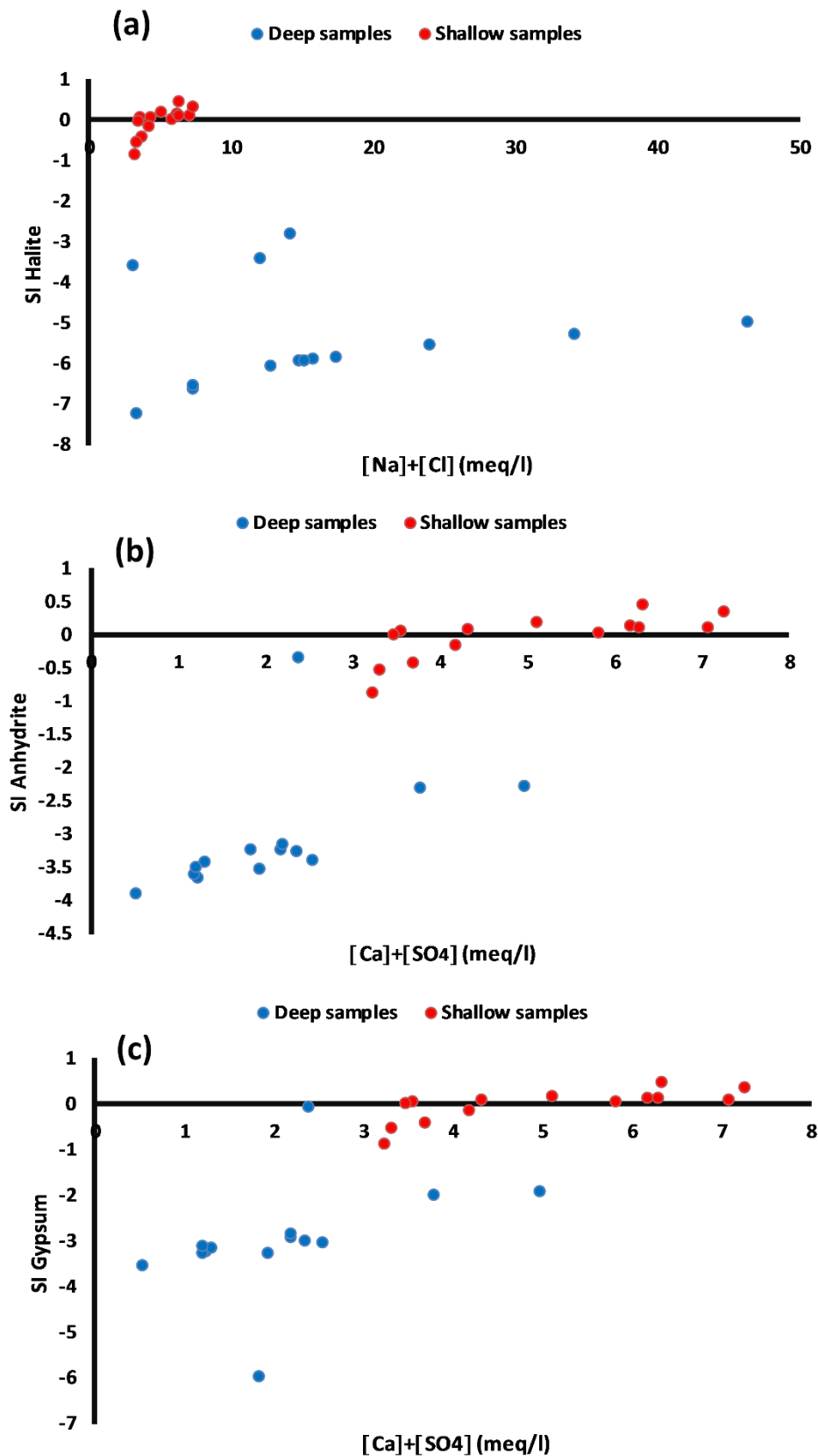


Figure 70. Plot of (a) $[Na] + [Cl]$ vs SI halite (b) $[Ca] + [SO_4]$ vs SI anhydrite (b) $[Ca] + [SO_4]$ vs SI gypsum

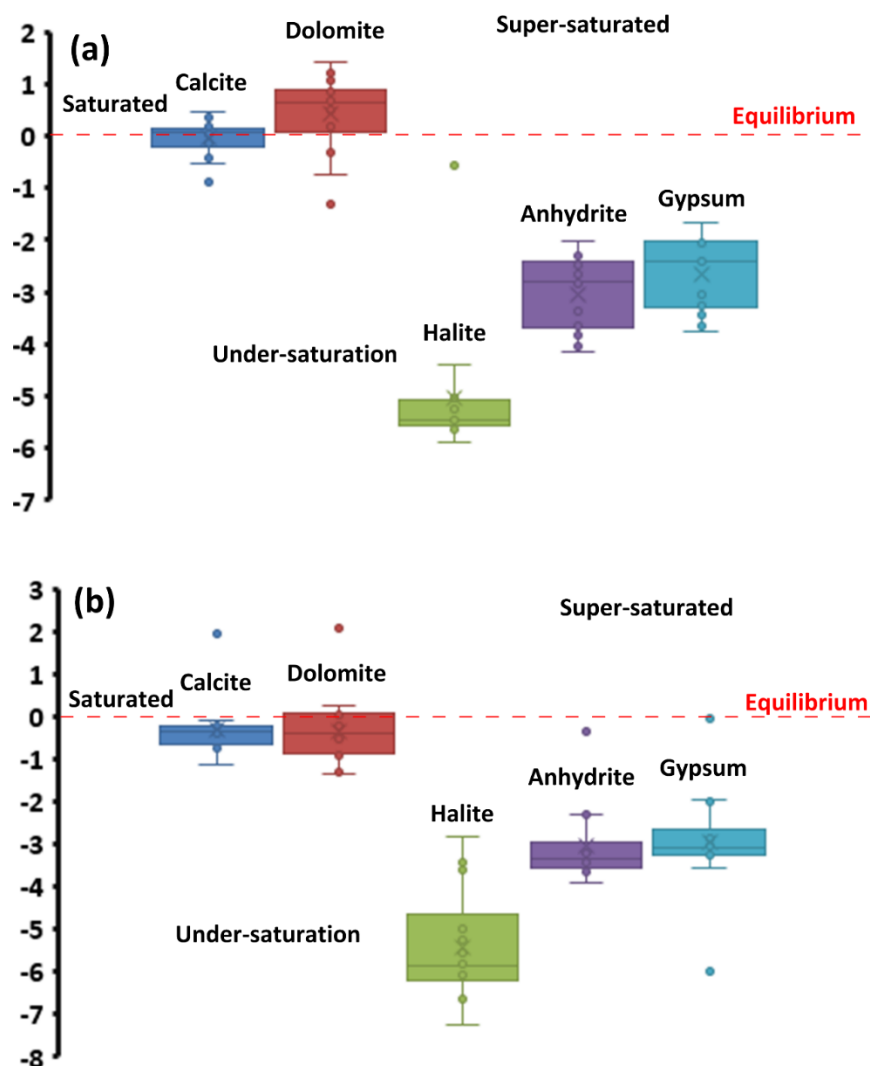


Figure 71. Box plots of saturation index for several mineral (a) shallow (b) deep samples

V. Multivariate Statistical Analyses

The principal component analysis was achieved separately for the two aquifers; a dataset of 28 samples (14 deep samples and 14 shallow and springs samples) and 12 Physico-chemical elements to determine relationships between major elements and physical parameters. **Table 19** shows the eigenvalues, the percentage of variance, each other, and the cumulative percentage.

Table 19 Variance explained by the first three principal components

Component		Eigenvalues	% Total variance	% Cumulative
Shallow Samples	1	5.34	48.55	48.55
	2	1.92	17.45	66
	3	1.34	12.25	78.25
Deep samples	1	6.94	63.11	63.11
	2	1.39	12.64	75.76
	3	1.19	10.85	86.61

The analysis results in **Figure 72** reveal that the first three factors illustrate approximately 78 %, of the total variance, for the shallow and springs samples and 86% for the deep samples. For the shallow and springs samples, the first factor is responsible for about 48 % of the total variance and is well represented by salinity, Na^+ , EC, Mg, Ca^{2+} and Cl^- . These elements ensure the mineralization of the shallow aquifer's water. Consequently, component "1" is defined as the salinity component representing halite weather and evaporate minerals. Component "2" is represented by O_2 , SO_4^{2-} and HCO_3^- . An additional 12.25 % of the total variance was explained in F3 and was represented by K^+ , O_2 , and pH.

For the deep samples, the first factor is responsible for about 63.11 % of the total variance and is well represented by Mg^{2+} , salinity, Na^+ , K^+ , Ca^{2+} , HCO_3^- , Cl^- and EC. This component is defined as the salinity component representing the weathering of halite and evaporates minerals. Component 2 is represented by SO_4^{2-} defined as a factor of sulfates. The third component represents 10.85 % of the total variance, was explained in F3 and was represented by O_2 and pH.

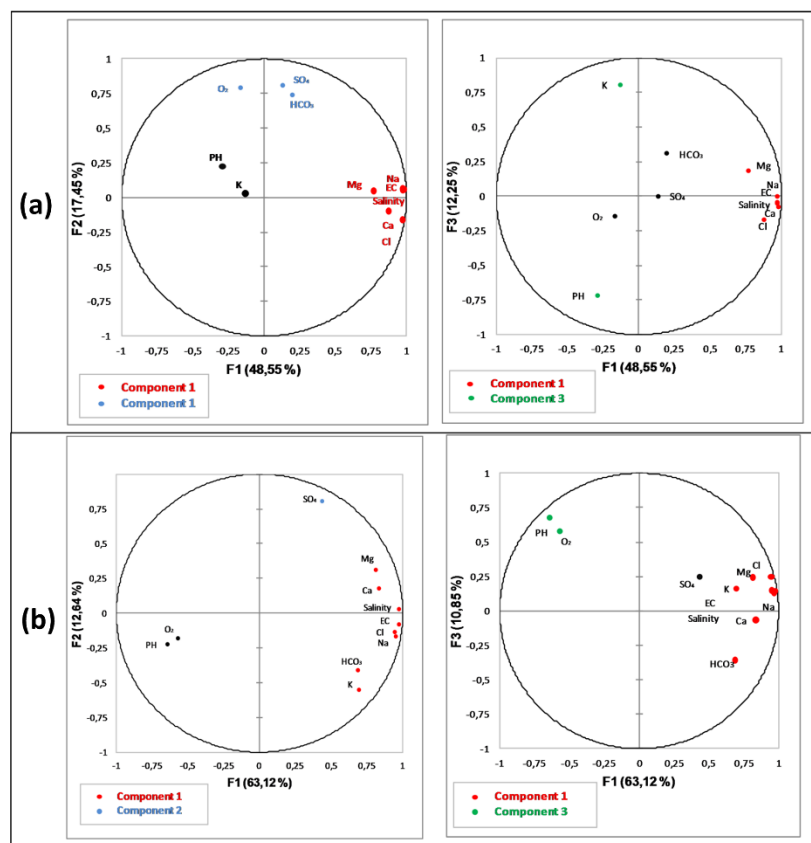


Figure 72. Projection of the variables in the first, second and third factorial plan (Principal component analysis): (a) including all shallow and springs samples in HJB and (b): Deep samples in HJB

VI. *Water quality*

1. Drinking use

- **Standards limits**

The physical (pH and EC ($\mu\text{s}/\text{cm}$)) and chemical parameters (K^+ , Ca^+ , Mg^+ , Cl^- , SO_2^- , Na^+ , HCO_3^- in mg/l) were compared with the world's standard (WHO 2011) and the national standard (NT 2013). As shown in **Figure 73**, all samples ($n=28$) respect the maximum permissible limit, for both WHO and NT standards, for the pH, the potassium (K^+), the calcium (Ca^+), the magnesium (Mg^+), the bicarbonates (HCO_3^-) and the sulfates (SO_2^-).

For the electrical conductivity (EC), the limit given by WHO ($1500\mu\text{s}/\text{cm}$) is not respected by all the shallow samples and most of the deep samples (58%). For the chlorides (Cl^-), all the shallow samples exceeded the WHO limit (250 mg/l) and 29% of the shallow samples exceeded the national limit (600 mg/l). For the deep aquifer, 9 samples (64%) exceeded the WHO limit and two samples (14%) exceeded the national limit (600 mg/l). For the sodium (Na^+) parameter, the permissible value given by WHO (200 mg/l) was respected only by four samples (29%) in the shallow aquifer and exceeded by three samples (21 %) from the deep one. Only one physical parameter and two major ions (one cation and one anion) do not respect the WHO and NT limit in most samples in all collected samples. In total, only 15 % of samples respect the permissible limits of all physico-chemical parameters, given by WHO, which can affect human health.

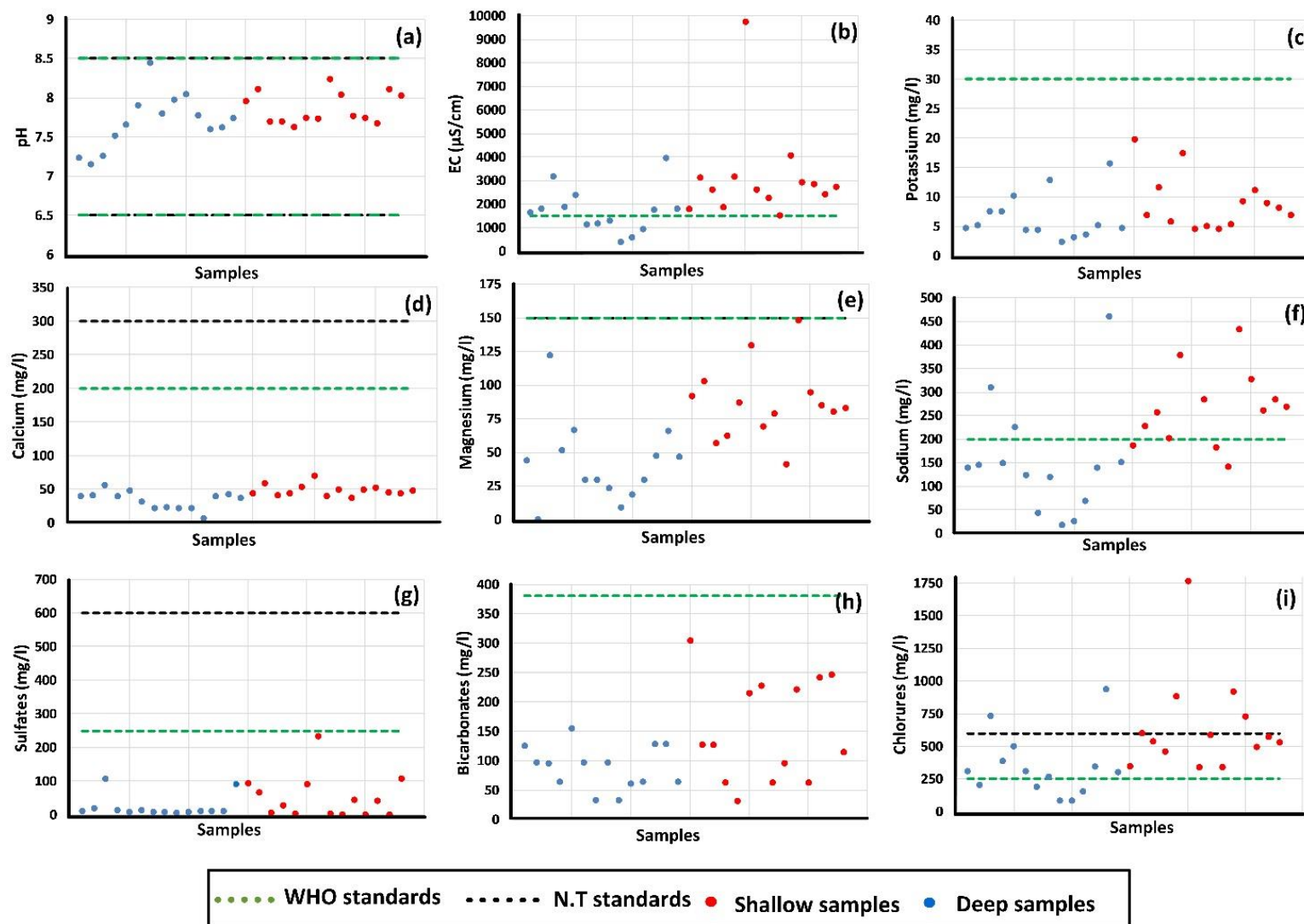


Figure 73. Comparison of major ions concentration (in mg/l) and physical parameters in HJB with WHO standards and Tunisian norms (NT 09-14): (a) pH, (b) EC ($\mu\text{S}/\text{cm}$), (c) K^+ , (d) Ca^{2+} , (e) Mg^{2+} , (f) Na^+ , (g) SO_4^{2-} , (h) HCO_3^- and (i) Cl^-

- **Water quality indices**

The evaluation of water quality, of HJB, for drinking uses, was effectuated using three quality indices; EWQI, WQI and ImpWQI.

The WHO standards were selected to calculate the quality rating scale (Q). The WQI ranged from 64.41 to 328.64 for the shallow aquifer and 22 to 155.61 for the deep aquifer. It shows four classes of both aquifers (**Table 20**), extended from “good” to “extremely poor” for the shallow aquifer and from “excellent” to “poor” for the deep one. For the EWQI, the index value ranged from 55.29 to 248.41 for the shallow aquifer and 22 to 122.8 for the deep aquifer. It shows three classes of both aquifers (**Table 20**), extended from “good” to “extremely poor” for the shallow aquifer and from “excellent” to “Medium” for the deep one. For the ImpWQI, the value ranged from 178.69 to 1011 for the shallow aquifer and from 43.93 to 475.6 for the deep aquifer. It shows various classes of both aquifers (**Table 20**), extended from “poor” to “extremely poor” for the shallow aquifer and from “excellent” to “poor” for the deep one.

Table 20 Classification of shallow and deep samples quality based on the three Indices (EWQI, WQI and ImpWQI)

Index		<50	50-100	100-150	150-200	>200
Water quality		excellent	Good	Medium	Poor	Extremely poor
EWQI	% Shallow aquifer	-	79%	14%	-	7%
	% Deep aquifer	50%	36%	14%	-	-
WQI	% Shallow aquifer	-	36%	50%	7%	7%
	% Deep aquifer	29%	57%	7%	7%	-
ImpWQI	% Shallow aquifer	-	-	-	7%	93%
	% Deep aquifer	7%	14%	22%	-	57%

A correlation was effectuated between the physico-chemical parameters, used in calculating the indices, and the three indices (**Table 21**). For both aquifers, the three indices (ImpWQI, EWQI and WQI) present a low negative correlation with the pH, a low correlation with sulfates (SO_4^-) and a strong correlation with the major physicochemical parameters (EC, Na^+ , Ca^{2+} , Mg^{2+} , Cl^- , HCO_3^-) except, in the shallow aquifer the potassium K^+ and the bicarbonates HCO_3^- present a low correlation value with the three indices (**Table 21**). The correlation values are related to the parameter's weight given in the WQI method and calculated in the two indices (ImpWQI and EWQI). The three indices indicate very similar correlation values for both types of samples (shallow/deep). Still, the EWQI indicate the high values with very negligible differences with the two other indices.

Table 21 Correlation between the various water quality indices (*ImpWQI*, *EWQI* and *WQI*) and physico-chemical parameters for the deep and shallow aquifer

	Index	pH	EC	Na ⁺	Ca ²⁺	Mg ²⁺	K ⁺	Cl ⁻	HCO ³⁻	SO ₄ ²⁻
Deep aquifer	WQI	-0.47	0.99	0.98	0.76	0.82	0.73	0.99	0.59	0.42
	EWQI	-0.47	0.99	0.98	0.76	0.81	0.75	0.99	0.62	0.40
	ImpWQI	-0.46	0.99	0.98	0.76	0.81	0.75	0.99	0.62	0.40
Shallow aquifer	WQI	-0.29	0.99	0.99	0.84	0.7	-0.16	0.97	0.2	0.16
	EWQI	-0.33	0.99	0.99	0.83	0.72	-0.12	0.97	0.24	0.17
	ImpWQI	-0.27	0.99	0.98	0.85	0.69	-0.16	0.99	0.13	0.07

The **figure 74** shows the water quality indices values calculated by the three proposed indices (WQI, ImpWQI and EWQI) in the deep and shallow aquifers. The indices showed similar results regarding EWQI and WQI. The ImpWQI indicates the higher indices values; for the shallow samples, the ImpWQI indices range from 178.69 to 1011, indicating poor to extremely poor water quality. The ImpWQI indicated that the samples with Na-Cl water type indicate the low water quality then the other water types for the deep samples.

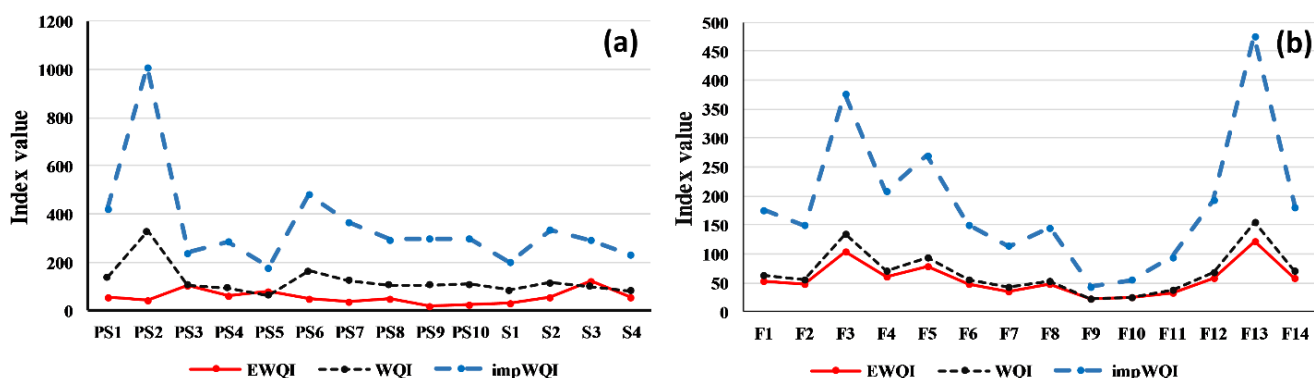


Figure 74. Comparison of the results of the WQI, ImpWQI and EWQI indices using the WHO standard (a) shallow aquifer (b) deep aquifer

The spatial distribution of the water quality based on the three indices (EWQI, WQI and ImpWQI) is shown in **figures 75**. For both aquifers, the ImpWQI method shows the best result. It indicates that the Na-Cl water type coincides with the poor and the extremely poor water quality and the two other indices (WQI and EWQI) indicate good to poor water types. These results reflect the effect of the parameter's weight in the calculation of the water quality index.

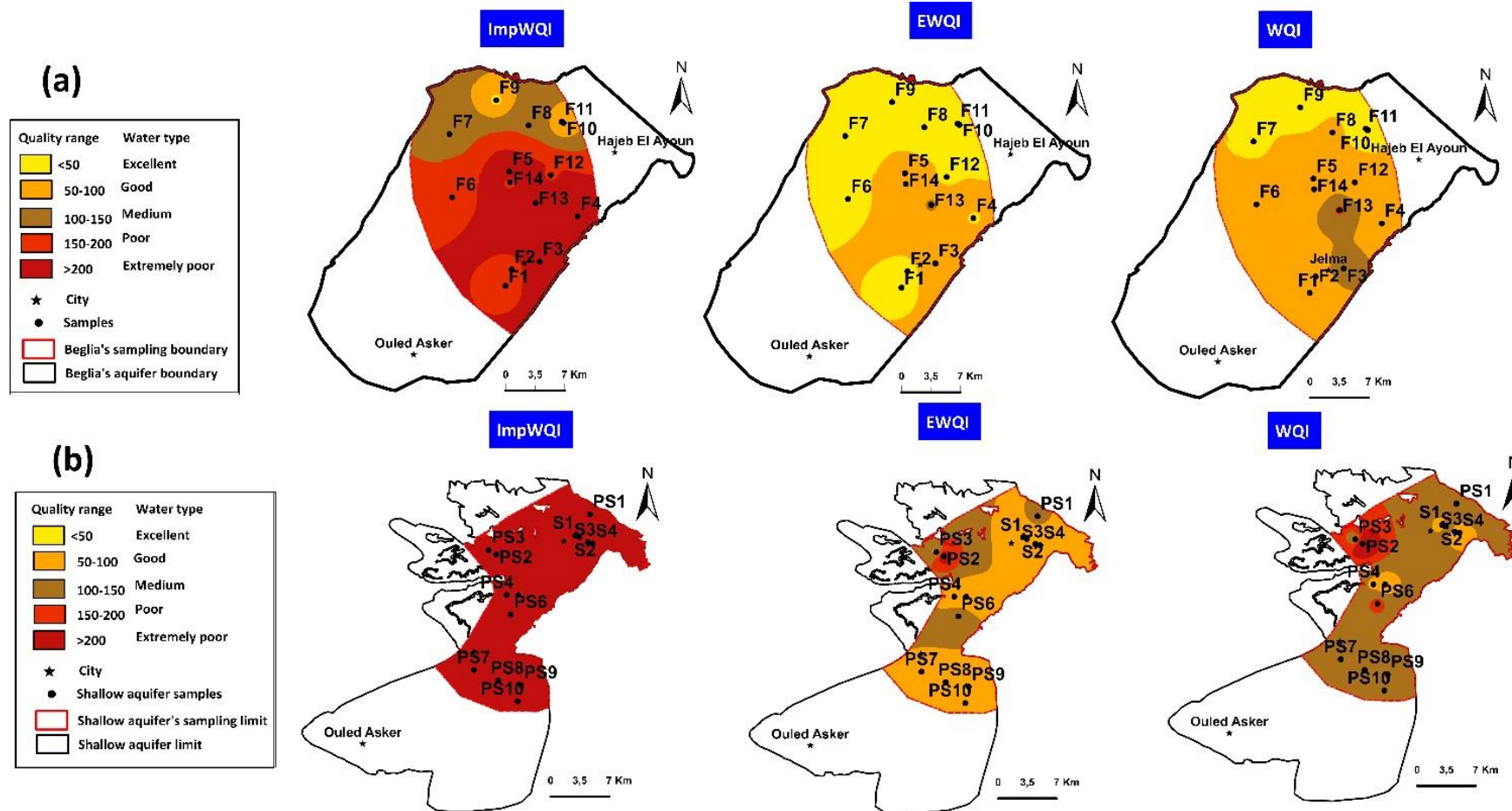


Figure 75. Distribution of the three indices (ImpWQI, EWQI and WQI) based on WHO standard in (a) deep aquifer and (b) shallow aquifer

2. Irrigation purposes

The collected samples were assessed for irrigation uses using different indices. The results are illustrated in [Table 22](#).

- According to the TH (Total hardness) values, all samples of both aquifers present soft water ($TH < 75$).
- The EC values of HJB are ranked into various categories for both aquifers (shallow and deep aquifer). For the deep aquifer; 79% of samples present good to permissible water quality and 21% of samples indicated a doubtful water class (samples with Na-Cl water type). For the shallow aquifer; 21% of samples are permissible, 79% of samples present doubtful to unsuitable water class (including samples with Na-Cl water type).
- The %Na indicated that only 71% shallow samples are permissible for irrigation; the %Na of samples with Na-Cl water type varies from 54.3 to 76.71, indicating permissible to doubtful water quality. For the deep samples, three samples (F7, F9 and F10) present a good water class which coincides with the Ca-Cl and Ca-Mg-Cl water type, 58% (Na-Cl water type) indicate permissible water for irrigation and three samples (Na-Cl water type: F2, F8 and F13) indicate a doubtful water class.
- The SAR values for HJB samples are ranked into two groups; for both aquifers, all samples have a low degree of alkalinity hazards ($2 < SAR < 10$), except three samples with a high alkalinity hazard ($10 < SAR < 18$). Based only on the SAR values, the samples of HJB are distributed on two water classes (“excellent” to “good”) and it can be utilized for most types of soil.
- According to the calculated values of MH (Magnesium hazard) and the PI (Permeability index), all samples of the shallow springs and deep aquifers are unsuitable for irrigation. The calculated values of Kr show that the groundwater samples of HJB, with Na-Cl water type, are more than 1, indicating moderate to unsuitable water quality for irrigation uses.

Based on the seven estimated indices, most of HJB’s samples are unsuitable for irrigation. The shallow samples present an irrigation quality less than the deep samples. It is due the shallow aquifer position; the thickness of the vadose zone, which has a strong effect on the pollutant’s infiltration.

3. WILCOX and USSL classification

The %Na vs. EC values for HJB’s samples were plotted in the Wilcox graphical irrigation water diagram (Wilcox [1955](#)). The diagram shows that 10 samples present a water

quality permissible to doubtful (Na-Cl water type), 3 samples are classed under good to permissible (Ca-Cl and Na-Cl water type), 13 samples are doubtful to unsuitable (Na-Cl water type), and 2 samples are excellent to good (Ca-Cl and Ca-Mg-Cl water type) (figures 76a).

The SAR vs. EC values for groundwater samples of HJB were plotted in the USSL diagram of irrigation water (figures 76b). Based on USSL diagram (US Salinity Laboratory 1954), the water samples shows five categories; “C2-S1” (medium salinity with low sodium), “C3-S1” (high salinity with low sodium), “C4-S2” (very high salinity with medium sodium), “C3-S2” (high salinity with medium sodium) and “C4-S3” (very high salinity with high sodium). Based on the combination between EC and SAR, in USSL diagram, HJB has only two deep samples suitable for irrigation (F9 and F10) (medium salinity with low sodium) which coincide with Ca-Cl and Ca-Mg-Cl water type.

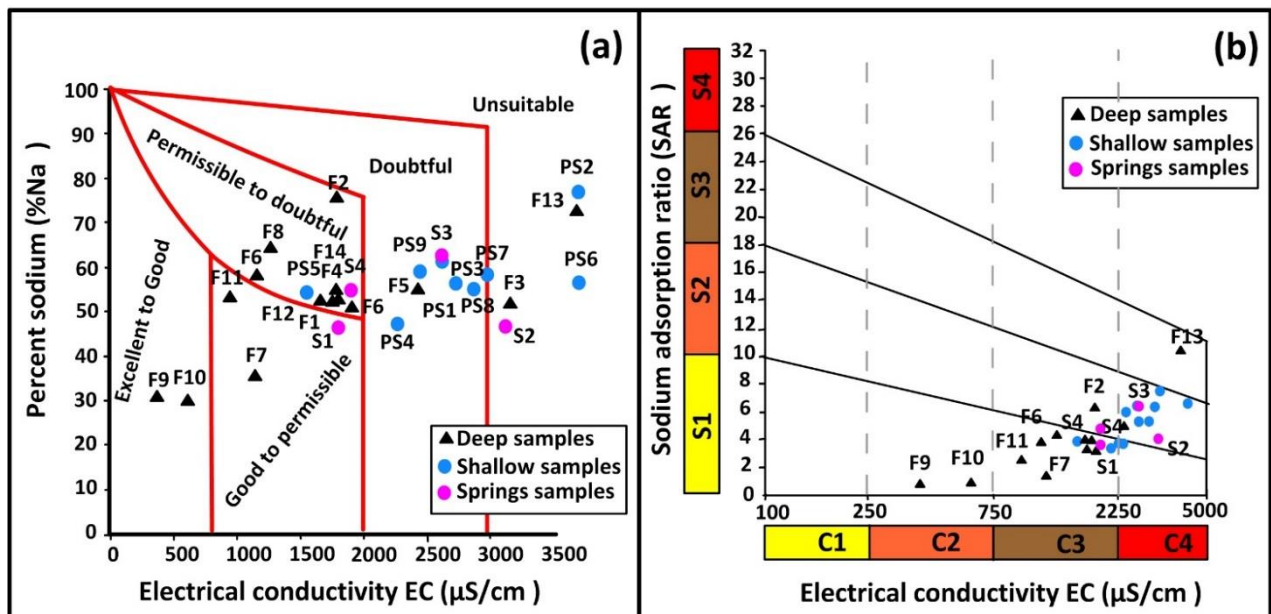


Figure 76. (a) Sodium percentage Vs EC values plot for water quality classification (Wilcox diagram 1955) and (b) USSL classification of HJB samples

Table 22 Irrigation quality indices of Hajeb Layoun-Jelma aquifers

Range	Reference	Classification	Shallow + Springs samples		Deep samples	
			Number of samples	% of samples	Number of samples	% of samples
Total hardness (TH)						
<75	Todd (1980)	Soft	All samples	100%	All samples	100%
75-150		Moderately Hard	-	-	-	-
150-300		Hard	-	-	-	-
>300		Very hard	-	-	-	-
EC ($\mu\text{s}/\text{cm}$)						
<250	Richards (1954)	Excellent	-	-	-	-
250-750		Good	-	-	2	14%
750-2000		Permissible	3	21%	9	65%
2000-3000		Doubtful	7	50%	1	7%
>3000		Unsuitable	4	29%	2	14%
Percent sodium (Na%)						
<20	Wilcox (1955)	Excellent	-	-	-	-
20-40		Good	-	-	3	21%
40-60		Permissible	10	71%	8	58%
60-80		Doubtful	4	29%	3	21%
>80		Unsafe	-	-	-	-
Alkalinity hazard (SAR)						
<10	Richards (1954)	Excellent	All samples except PS2	93%	All samples except F13	93%
10-18		Good	1	7%	1	7%
18-26		Doubtful	-	-	-	-
>26		Unsuitable	-	-	-	-
Magnesium hazard (MH)						
>50	Ragunath (1987)	Unsuitable	All samples	100%	All samples	100%
<50		Suitable	-	-	-	-
Permeability index PI						
<25	Doneen (1964)	Suitable	-	-	-	-
25-75		Moderate	-	-	-	-
>75		Unsuitable	All samples	100%	All samples	100%
Kelley ratio (KR)						
<1	Kelly (1963)	Suitable	3	21%	3	21%
1-2		Moderate	10	72%	10	72%
>2		Unsuitable	1	7%	1	7%

4. Irrigation Water Quality Index (IWQI)

Figure 77 shows results of IWQI in the study area and it is varying from severe restriction (SR) to moderate restriction (MR) according to **Table 23**. The areas with high restriction water quality cover 57.14% of total samples. This category is suitable for irrigation with moderate to high tolerance to salts.

The rest of the study area, which is about 43% fall within the “severe to moderate restriction” categories. These categories of groundwater should be used only with the soil have high permeability and some constrains in type of plant for salt’s tolerance.

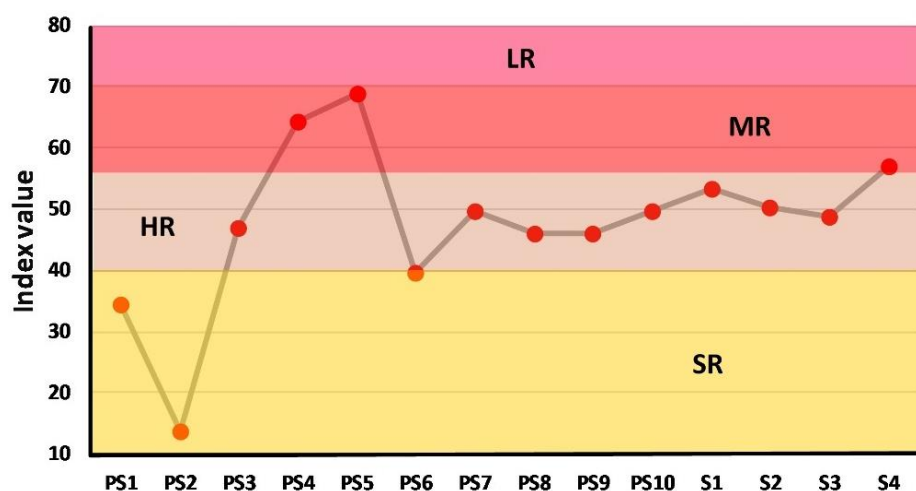


Figure 77. Results of IWQI in the study area

Table 23 Classifications and characteristics of general IWQI

IWQI	Restrictions	Soil	Plant
[85-100]	No restriction (NR)	Water can be used for almost all types of soil.	No toxicity risk for most plants
[70-85]	Low restriction (LR)	Irrigated soils with a light texture or moderate permeability can be adapted to this range.	high risks for salt sensitive plants
[55-70]	Moderate restriction (MR)	The water in this range would be better used for soils with moderate to high permeability values. Moderate leaching of salts is highly recommended to avoid soil degradation.	Plants with moderate tolerance to salts may be grow
[40-55]	High restriction (HR)	This water can be used in soils with high permeability without compact layers. High frequency irrigation schedule	Suitable with moderate to high tolerance to salts
[0-40]	Severe restriction (SR)	Using this water for irrigation under normal conditions should be avoided.	Only plants with high salt tolerance

VII. Regional hydro-geochemical conceptual model of HJB

A regional model was developed based on the hydrochemical assessment results, including the hydrochemical processes, hydrological processes and groundwater type, that influence the aquifers, integrated into a framework of the 3D geological model HJB (**figures 78**). This integration helps to provide valuable information (hydrological and hydrochemical processes) and understand the spatial hydrochemical evolution of HJB.

Two 2D cross-sections with the distribution of geochemical processes and the hydrochemical facies were used to summarize all processes affecting both aquifers. Laterally, the HJB is subdivided into six hydrogeological layers, which are affected by many faults. Four springs (Ain Soltane, Ain Ouled ben Hassine, Ain Sassi and Ain Djedeat) as superficial system outlets. The main processes occurring in the HJB are cations exchange and mixing processes that reinforce the hypothesis of the aquifer's interconnectivity.

The groundwater recharge in the Hajeb Layoun-Jelma originates from both direct infiltration through floods descending from the mountains, occurring in the Quaternary and the deep aquifer where the Beglia aquifer is exposed at the surface, and vertical leakage, in the south part of the basin, between Beglia aquifer and the Ségui aquifer (Koschel **1980**).

The piezometric map and the water flow direction shown in **figures 78** that the general groundwater flow direction is:

- For the Beglia aquifer, from the west; coming from Mrhilla Mountain (Recharge zone by direct infiltration: Beglia aquifer is exposed at the surface), toward the central part of Hajeb El Layoun where it is divided in two directions: the first discharges at Hajeb Layoun fault and the second at the level of some faults in the north part of Zaouia-Roua Mountain.
- For the shallow aquifer the mean flow direction is west to the east in the south part and two direction flows in the north part: West to the East and south to the north.

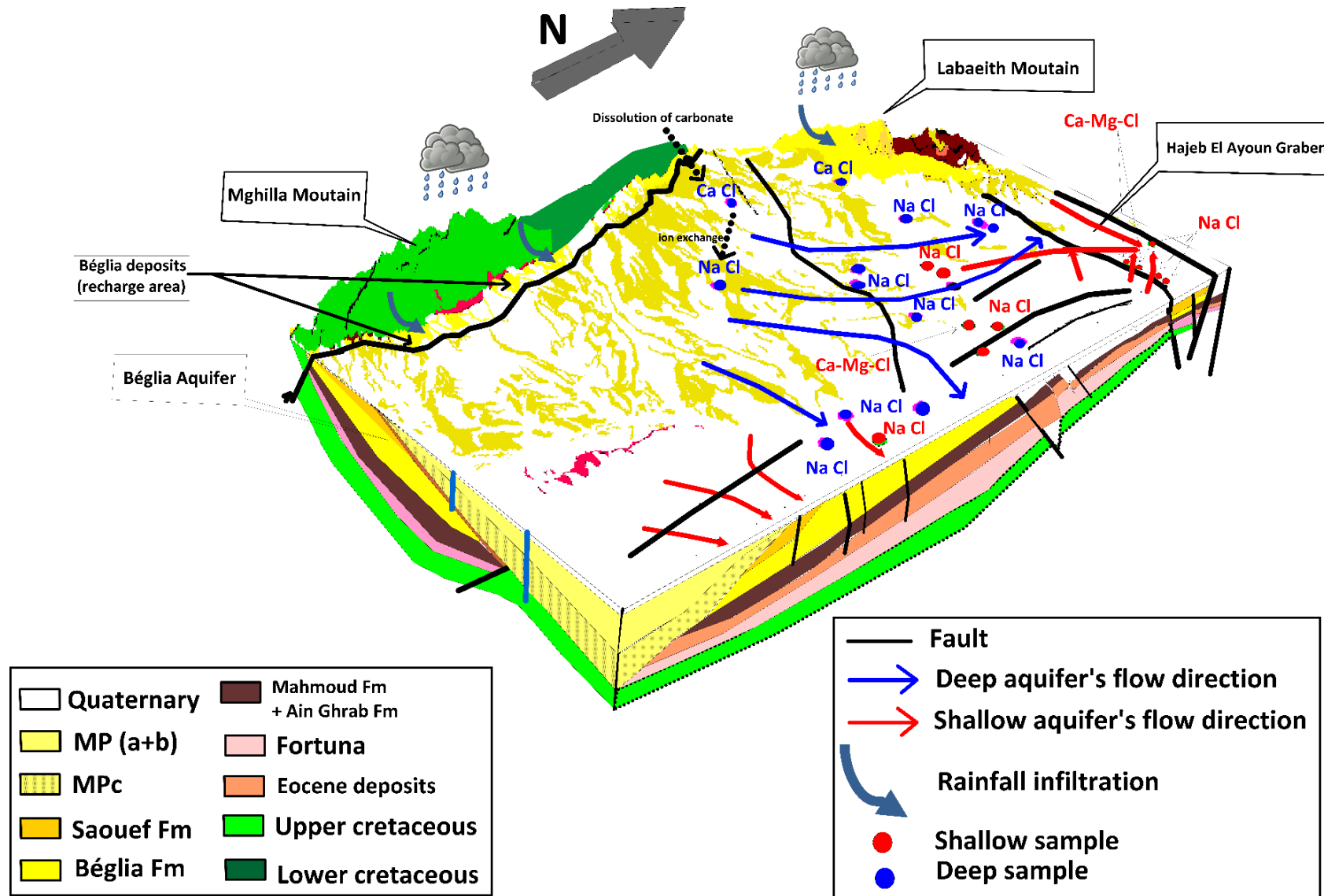


Figure 78. 3D Hydrogeochemical conceptual model

VIII. Discussion

The Hajeb Layoun-Jelma basin is the selected site in this research to provide its actual water quality situation, with highlights on the water chemistry origins and its suitability (drinking and irrigation). The shallow aquifer shows high salinity in most of the water samples (93% of samples have salinity $>1 \text{ g.L}^{-1}$ with one sample exceeding 6 g.L^{-1}) (figures 63b). The deep aquifer has moderate salinity: 21% of samples exceeding 1 g.L^{-1} and the rest (79%) indicate salinity less than 1 g.L^{-1} (figures 63a). Groundwater Salinity pollution is considered common Mediterranean problems; it is seen in recent investigations conducted in the shallow aquifers in Northeastern Tunisia (Ghouili et al., 2018) and Central-eastern Tunisia (Mnassri et al., 2018). The high level of salt intake in water can cause severe human health problems (Al Nahian et al., 2018).

In this study, based on Gibbs's diagram and the inter-parameters correlation, the high salinity levels in the HJB is related to the natural factors (dissolution of carbonates/gypsum and water evaporation). The anthropogenic factors in HJB also have a strong role in the elevation of the salinity concentration, such as the increasing number of wells (the number of shallow wells increases from 226 in 1974 to 2328 wells in 2018), the low thickness of the vadose zone (from 3 to 20m) and the irrigation practices. The huge quantities of fertilizers impact Na^+ and Cl^- (Mnassri et al., 2018). This is showed by the high correlation between $\text{Na}^+ / \text{Cl}^-$ and salinity in this study (Table 21).

Modern methods such as EWQI, WQI and ImpWQI would confer the best understanding of water suitability. The previously mentioned (see water quality indices section), compared with the evaluation results of different weighting methods, shows that the WQI based CRITIC weighting method (ImpWQI) is feasible HJB's water quality evaluation. Wang et al., (2018) and Zhang et al., (2020) have applied the Improved Water Quality Index method, based on CRITIC weighting, to provide the groundwater's suitability for drinking purposes. Wang et al., (2018) found that the WQI based on CRITIC weighting (ImpWQI), is the realistic method to assess water quality.

As within the HJB, the application of ImpWQI technique shows that: for the shallow aquifer, 14 water samples (Table 21 and figures 74) range between "poor water" and "extremely poor water" and for the deep aquifer the samples range from "excellent water" to "extremely poor water" , for both aquifer the "poor" and "extremely poor" water quality coincides with the Na-Cl water type.

The over-abstraction from HJB, the non-treated sewage rejected, and the irrigation practices lead the degradation of HJB's resources and promote its pollution. To ensure the HJB's sustainability and avoid quality problems, it is necessary to improve the irrigation practices by implementing continuous measures to help farmers adopt the best management practices.

IX. Conclusion

The HJB has an important economic and social status as the first alternative for sustainable agricultural activities and drinking use for Sidi Bouzid, Kairouan (Central Tunisia) and Sfax (Southern coast). The abstraction increases since the mid-1980s and the continuous decline of piezometry cause the degradation of the quality and the quantity of this groundwater.

To assess the water quality of HJB: 28 water-samples were collected in 2017 and analyzed for 11 physicochemical parameters (Temperature, pH, EC, salinity, Na⁺, Ca²⁺, K⁺, Mg²⁺, Cl⁻, HCO₃⁻, and SO₄²⁻).

For both aquifers (the MPQ and Beglia aquifers), the order of the abundance of major cations is Na>Mg>Ca>K and anions is Cl>HCO₃>SO₄. The dominant hydrochemical facies for the shallow aquifer and springs is Na-Cl and Ca-Mg-Cl, for the deep aquifer, the geochemical facies are Na-Cl, Ca-Mg-Cl and Ca-Cl.

The WQI and the EWQI indicate that most shallow and deep samples present excellent to medium water type and only 7% present poor water. The ImpWQI presents the logic index, which indicates 100% and 57% extremely poor water for the shallow and the deep samples, respectively, which coincide with the Na-Cl water type. The water quality evaluation for irrigation uses was performed by assembling various geochemistry methods (SAR, TH, % Na, PI, MH, KR, EC). The results indicate that the shallow samples show quality less than the deep one (unsuitability according to EC :79%). The lousy irrigation practices, the low thickness, and the vadose zone's high permeability play a strong role in the infiltration of pollutants and reach HJB's shallow aquifer.

Chapter II: Recharge estimation and groundwater flow modeling of HJB

I. *Recharge estimation*

1. Thematic maps

Five thematic maps were generated (pixel size=30m) using ArcGIS software based on the water holding capacity, rates assigned for each subfactor.

1.1 Slope gradient

The slope is one of significant factors that directly influence aquifer recharge. The slope determines the degree of infiltration and the runoff; the low slope (flat surface) can hold the water inside the aquifer, increasing the groundwater recharge, whereas the high slope (steep) increases the runoff and decreases the groundwater recharge. The slope of HJB has been made in percentage based on the DEM. The slope has been ranged into four classes ([Figure 79a](#)).

The Slope varied between less than 1 % to more than 10 % ([Table 24](#)). Mountainous Sloping (<10%) covered 222.4 km² which indicating more runoff and very low infiltration of groundwater. The maximum area of the HJB is in the slopping category (5%<S<10%), it covers an area of 471.6 km². The medium sloping (1–5 %) indicates less amount of runoff and moderately infiltration. It covers an area of 439.1 km². The flat area, which is the more suitable area of recharge, covers an area of 21.69 Km².

1.2 Lithological map

The lithology type plays a significant effect on the aquifer recharge; in fact, the porosity and the permeability varied from lithology to other. The study area is mainly underlain by alluvium and quaternary sediments ([Figure 79b](#)), which are the more favorable regions for groundwater recharge and covering an area of 969 km², then followed by sand and sandstone, also good for groundwater recharge and covering an area of 6 km² and 37 km², respectively. Marl is unfavorable for groundwater recharge and covering an area of 142 km² ([Table 24](#)).

1.3 Soil types factor

The soil type of an area indicates the groundwater holding capacity and infiltration. The study area is mainly underlined by sand, Sandy loam, clay sand, loamy sand, clay loam, and clay. [Figure 79c](#) shows that a significant part of the area is covered by clay loam (743 km²),

which indicates a moderate potentiality of groundwater recharge (**Table 24**).

1.4 Land-use/land-cover factor

The LULC has a significant effect on the amount of recharge. The rated map was generated based on the Lu/Lc map published by the DGRE (2004). The Lu/lc map (**Figure 79d**) shows five major types of land uses: Urban area, bare land, forest, agricultural area and water bodies. The urban area reflects low potentiality of groundwater recharge (5 km²). The bare land indicates a reasonable possibility of groundwater recharge, which extends over an area of 524 km². The forest/agricultural area/water bodies indicate the more favorable area to groundwater recharge (625 km²).

1.5 Drainage density factor

The drainage density “Dd” of an area is an indirect function of lithological formations' permeability. For the HJB, the drainage network was extracted from topographic maps. The Dd values in this study area vary from 0 to 3.29 km/km² (**Figure 79e**). The Dd map shows four classes. The very low drainage density (0-1 km/km²) represents the maximum part of HJB (924 Km²), and it is more favorable for groundwater recharge. Followed by low (1–1.5 km/km²) in an area extending over 174 km² is a favor for groundwater recharge. Medium Dd (1.5–2 km/km²) is present in 46 km². The high Dd (higher than 2 km/km²) covers an area of 10 km².

Table 24 Ranges and its areas of the five factors controlling the recharge potentiality

	Class	Range	Area (Km ²)	Area (%)
LU/LC	Very low	Urban area	5	1%
	Moderate	Bare land	524	45%
	High	Agricultural land /Forest/water bodies	625	54%
Lithology	High	Sand	6	1%
	High	Sandstone	37	3%
	High	Alluvium and quaternary sediments	969	84%
	low	Marl	142	12
Slope	Very low	P >10%	222.4	19%
	moderate	5 < P <10	471.6	41%
	High to moderate	1 < P < 5	439.1	38%
	Very high	P < 1	21.69	2%
Drainage density	Very low	0-1	924	80%
	Low to moderate	1-1.5	174	15%
	Moderate to high	1.5-2	46	4%
	High	>2	10	1%
	Very high	sand	46	4%

Soil	High	Sandy loam/clay sand/loamy sand	105	9%
	Moderate	Clay loam	743	64%
	low	clay	256	22%

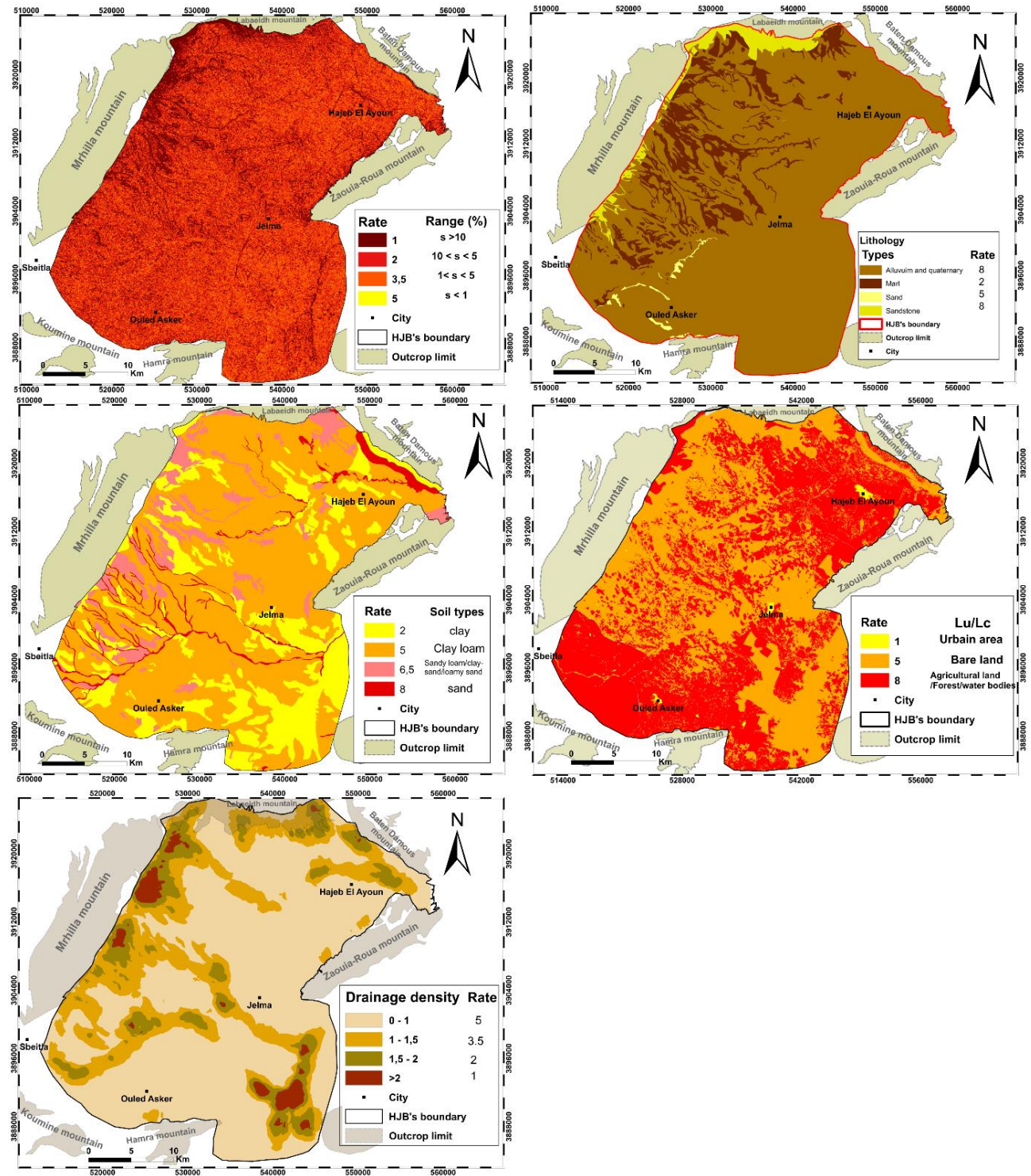


Figure 79. The five factors controlling the recharge potentiality; (a) slope gradient map (in %), (b) lithology map, (c) soil type map, (d) land use/ land cover and map (e) drainage density map

2. Groundwater recharge zones

The HJB was divided into different parts of recharge zones: (1) the shallow aquifer, (2) the exposed deep aquifer and (3) the under-flow aquifers (**Figure 80**). The potential groundwater recharge index was calculated for the three zones by weighted sum of the five rated maps (slope, lu/lc, soil, Dd and lithology).

The results maps (**Figure 81, Figure 82, and Figure 83**) indicate that the groundwater potentiality varies from low to high for the three types of aquifers with different percentages (fig.14). In the three maps, the primary class is the moderate potentiality of recharge, which indicates a percentage equal to 93.82%, 85%, and 84% for the shallow, deep, and under-flow aquifers.

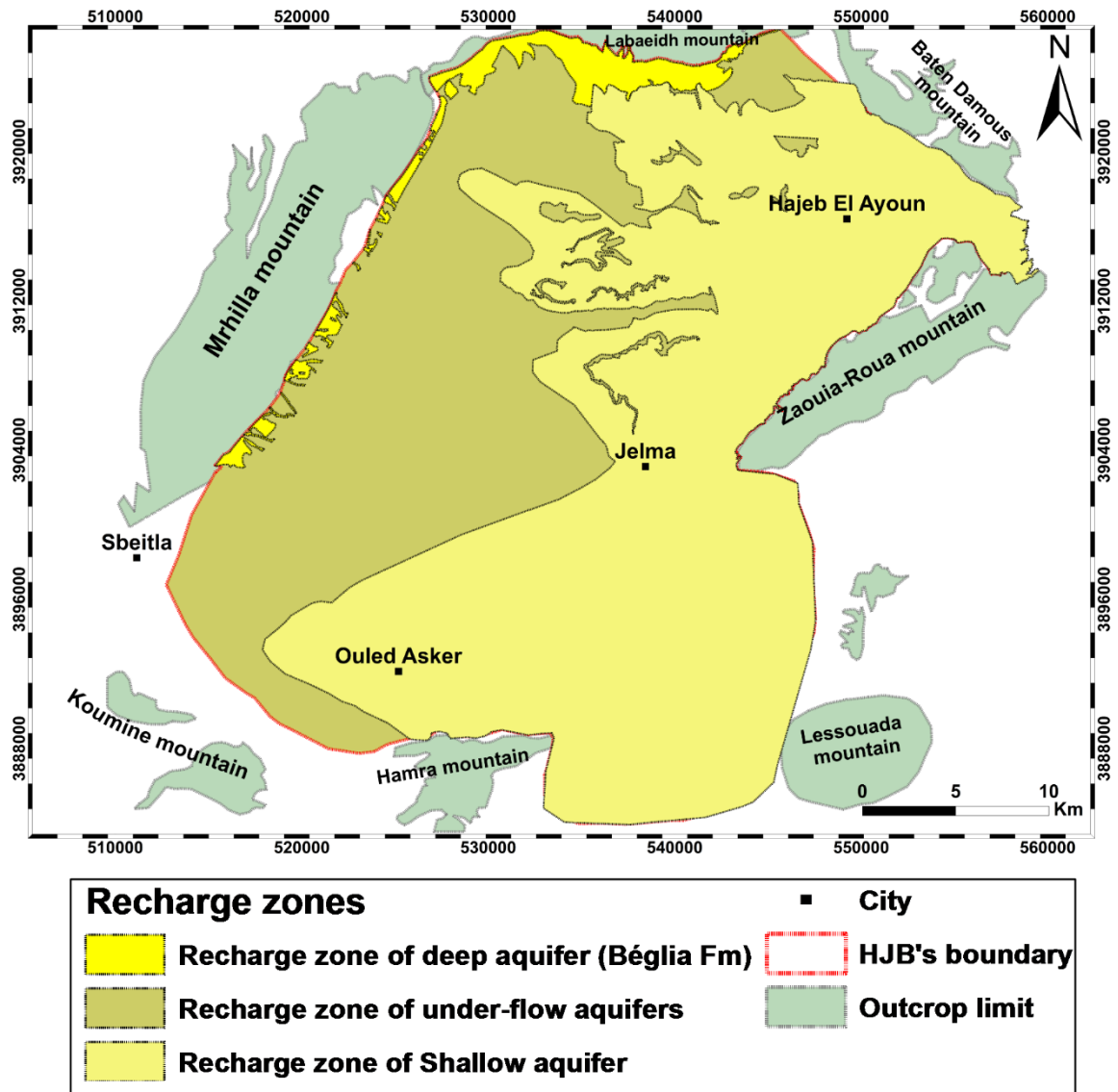


Figure 80. Map of Recharge zones in the HJB

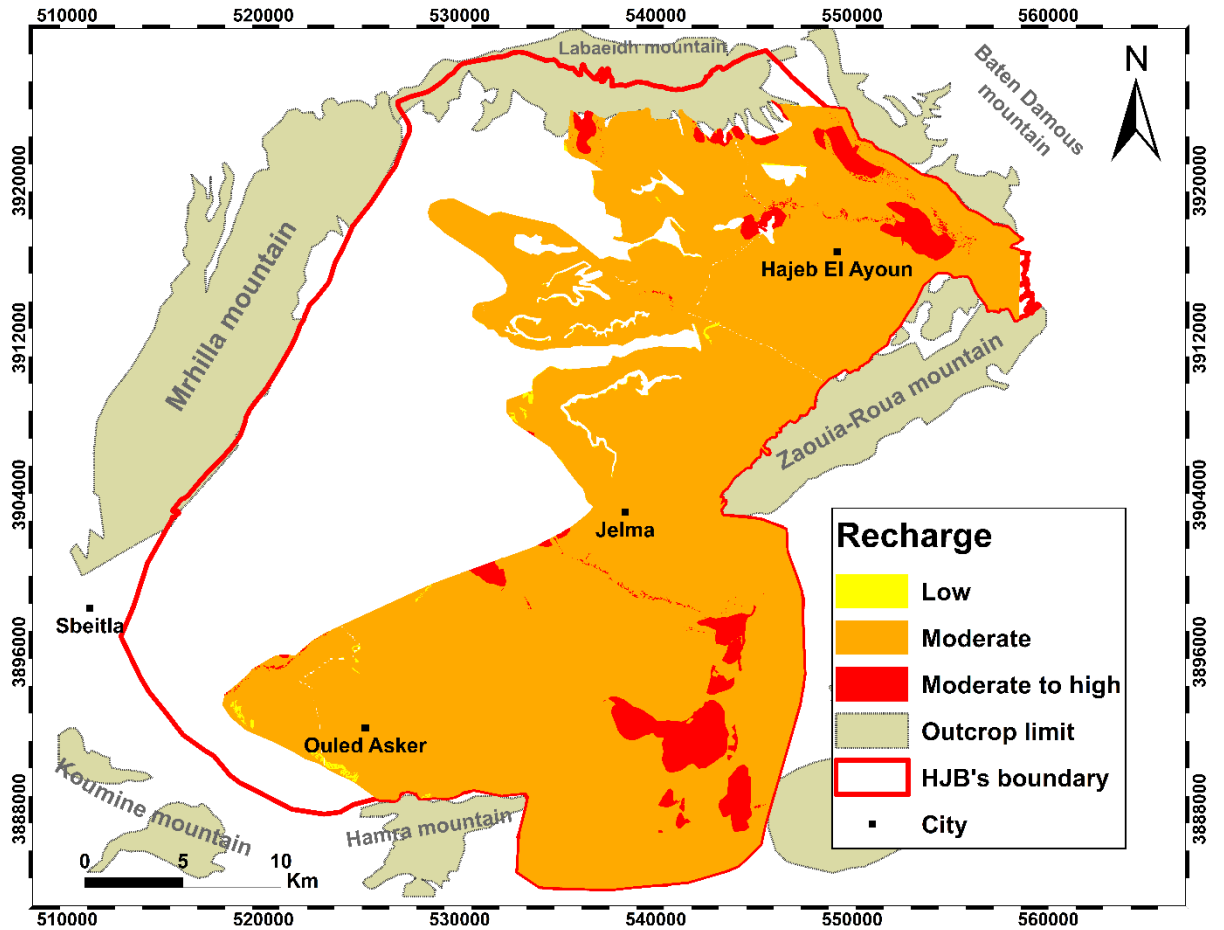


Figure 81. Potential recharge map of the shallow aquifer

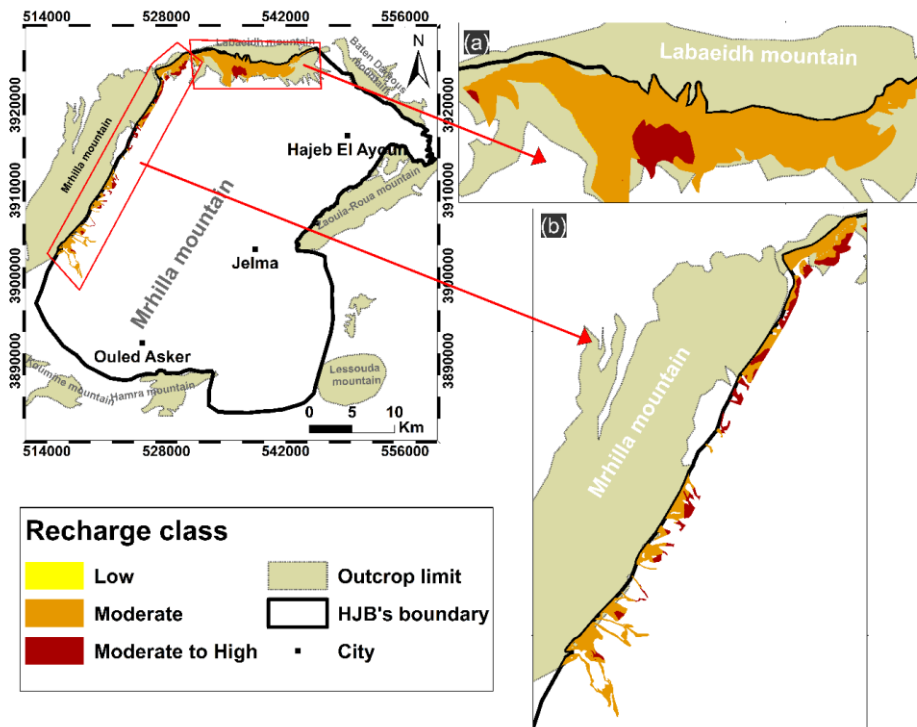


Figure 82. Potential recharge map of the deep aquifer

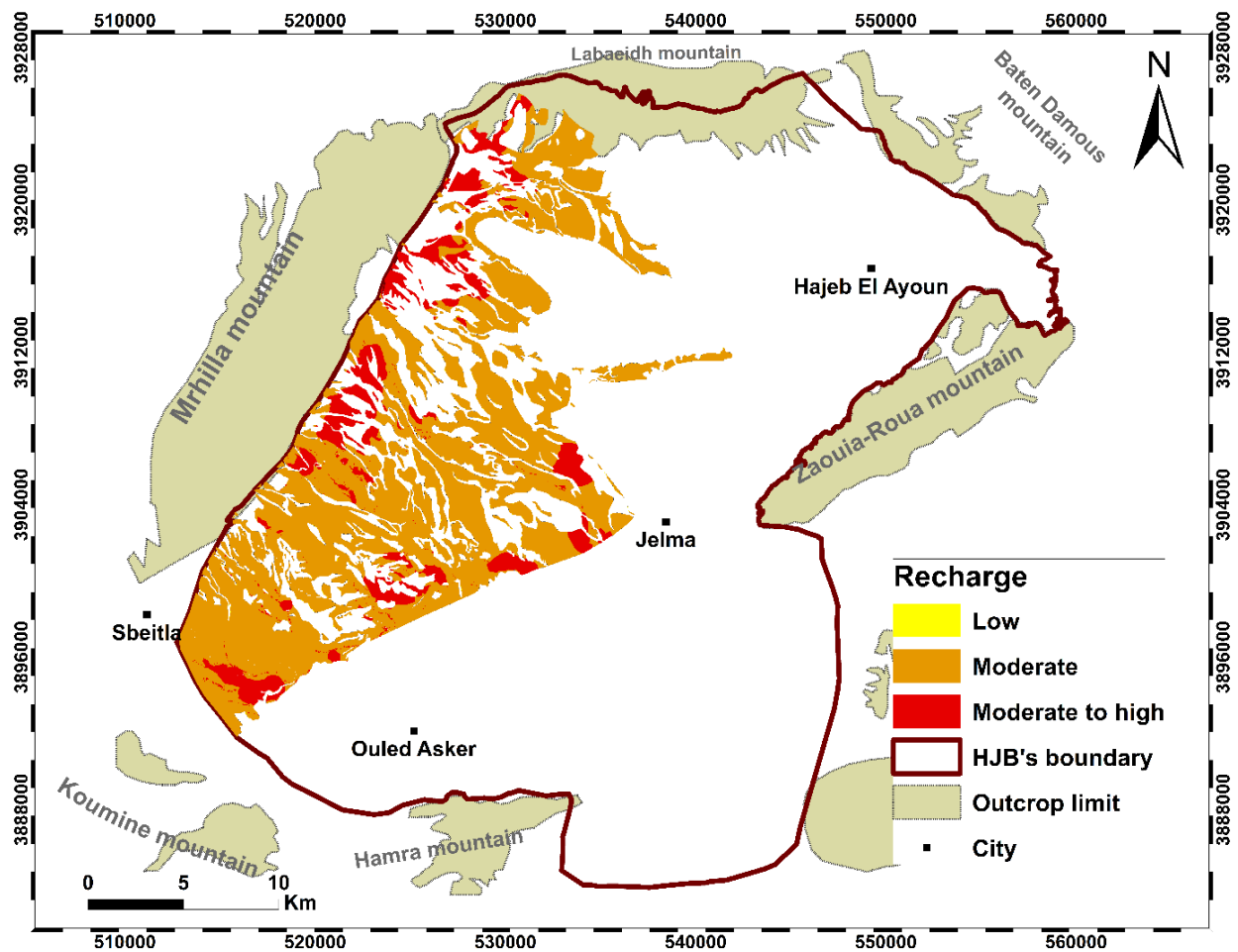


Figure 83. potential recharge map of the under-flow aquifers

3. Recharge estimation

The result of the recharge estimation is showed in [Table 25](#). It indicates that around 15 % of precipitated water in the study area percolates downward to recharge the shallow aquifer and 16.2% of rainfall infiltrates to recharge the deep aquifer. The rest is lost through surface runoff or by evapotranspiration. An insignificant part contributes to the under-flow aquifer's recharge.

Table 25 Recharge estimation of the HJB's aquifers

	V_{inf} (m ³ /year)	L_{inf} (mm/year)	%infiltration
Shallow aquifer	22×10^6	31.5	15%
Deep aquifer	1.19×10^6	34	16.2%
Under-flow aquifers	27.26×10^4	1.1	0.5%

4. Conclusion

To delineate the groundwater potentiality zones of the HJB, GIS-based multi-criteria is used to compute the rates for the classes in the different layers and weights for thematic layers. Five different thematic maps such as lithology, soil, drainage density, slope, and land use/land cover were elaborated in the GIS environment to generate groundwater potentiality zonation of the HJB. The three groundwater potential zones map were obtained by weighted-sum the thematic maps in ArcGIS 10.3. It was indicated that the potential zones in terms of moderate to high, moderate and low zones occupied 94%, 85% and 84% for the shallow, deep and under-flow aquifers, respectively. Finally, only 31.7 % of the total precipitated water (210 mm/year) is infiltrated downward to recharge the HJB. At the same time, the rest is lost either through evapotranspiration or by surface runoff. This method indicates an over estimated recharge.

II. Groundwater modeling

The construction of the model aims to provide a tool to simulate groundwater flow system in HJB for both main aquifers (Shallow and Beglia deep aquifer).

The HJB model was create, under GMS software, using conceptual model approach. The conceptual model approach involves using the GIS tools in the map module to develop a conceptual model of the site being modeled.

The location of sources/sinks, model boundaries, layer parameters (such as hydraulic conductivity), and all other data necessary for the simulation can be defined at the conceptual model level without a grid.

1. Boundary conditions

They generally correspond to recharge areas by direct infiltration of water from rain or runoff, to the natural supply from nearby water tables. They also represent natural outlets and pumping.

The differents data (aquifer limit, wells, wadis, recharge rate, permeability, top and bottom of each layer) were intruduced as coverage derived from GIS shapefiles (**Figure 84**). After the conceptual model was convert to a grid-based numerical model (**Figure 85, 86**). We have adopted a square mesh of 500 m per side, identical throughout the whole area.

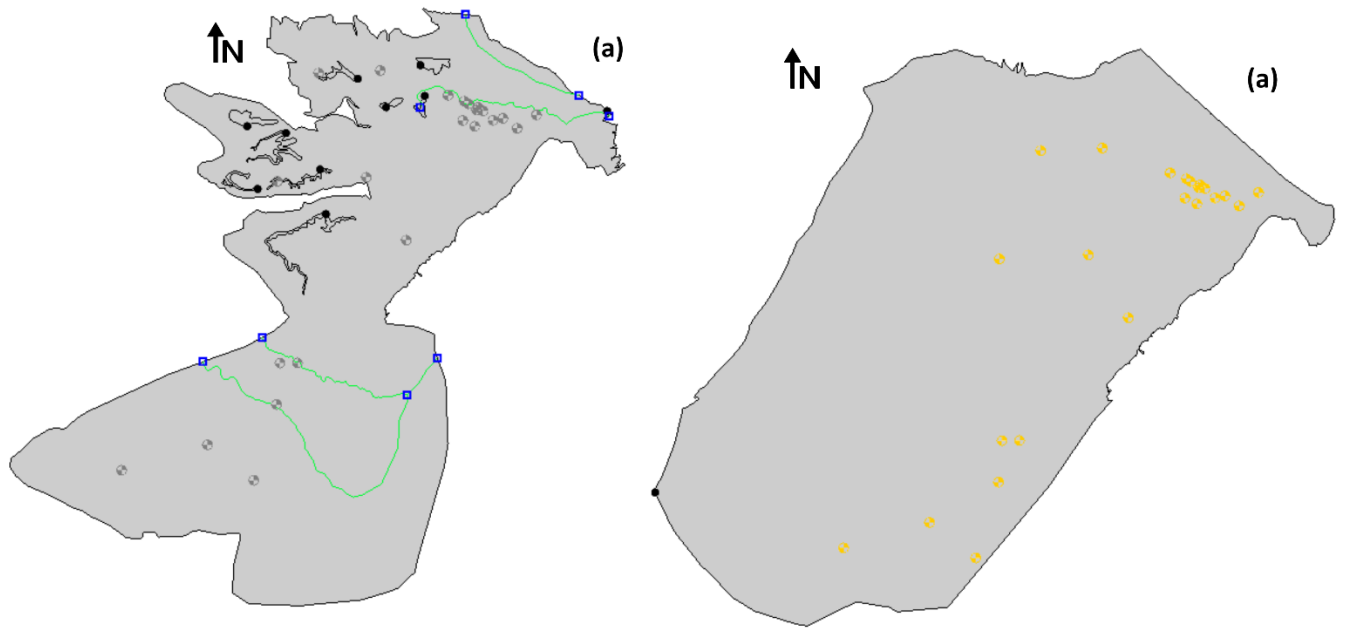


Figure 84. Coverages of the (a) shallow aquifer, (b) deep aquifer

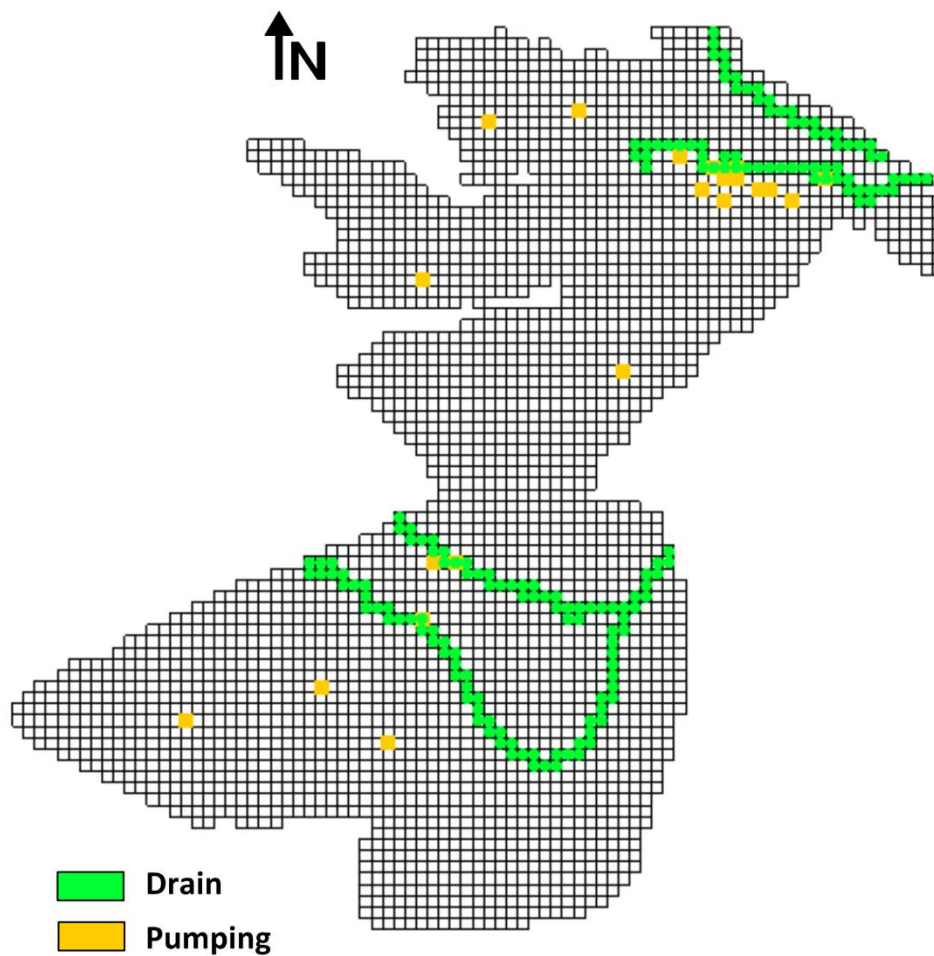


Figure 85 . Grid of the shallow aquifer

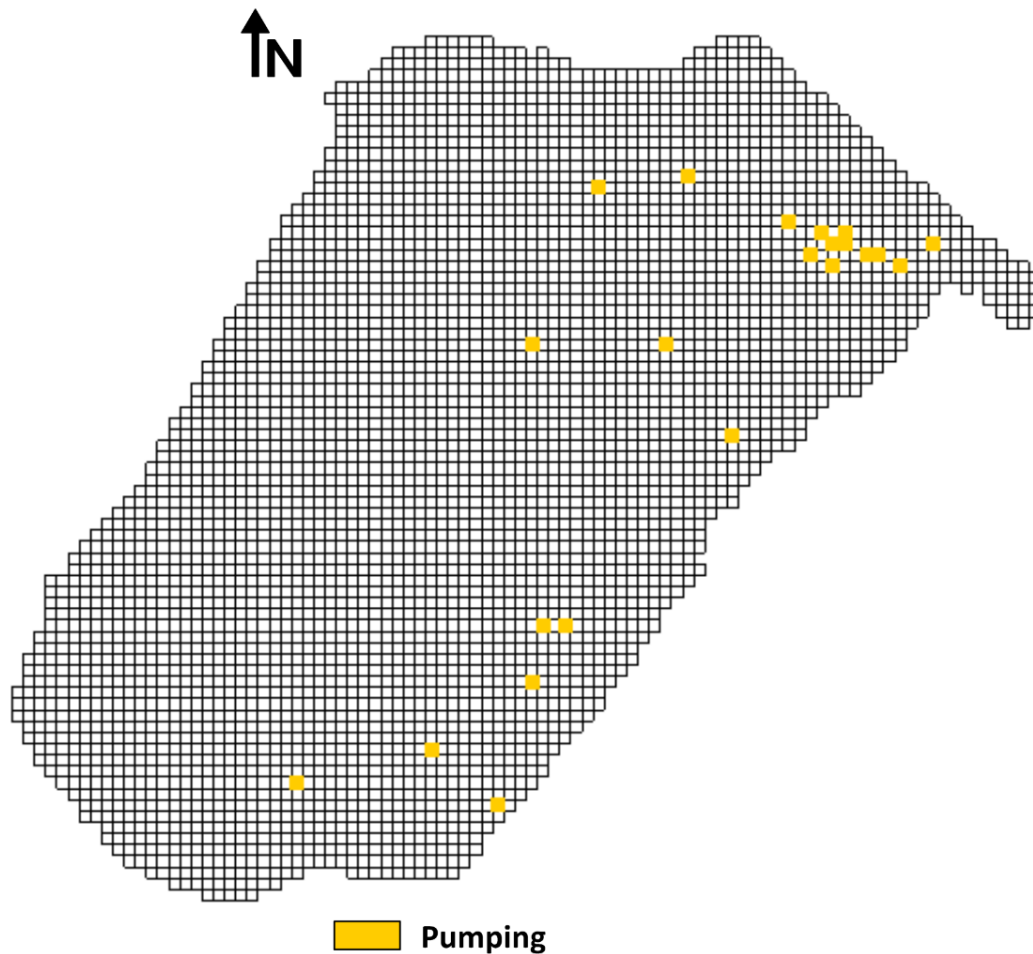


Figure 86. Grid of the deep aquifer

2. Calibration results in steady state

For the two aquifers, the piezometric maps in 1973 (see [Figure 50 and 51](#)), show that the general flow starts west where aquifers are recharged mainly by direct infiltration through floods descending from the mountain ranges. The general groundwater flow direction is west to northeast and southeast. The natural outlets are springs and drainage by down course of wadis in the northeast and losses by evaporation and drainage by wadis in the southeast.

The calculated transmissivities range from 0.0008 to 0.6 m²/s for the deep aquifer and from 0.001 to 0.01m²/s for the shallow aquifer. The high values are located in the North and the low value in the south for both aquifers.

The mean, standard deviation between the calculated and observed piezometric levels in the shallow and deep aquifers is 1.61 m and 1.79 m with a correlation coefficient of 0.9 and 0.8 ([Figure 87](#)). They show a better calibration quality for the shallow aquifer.

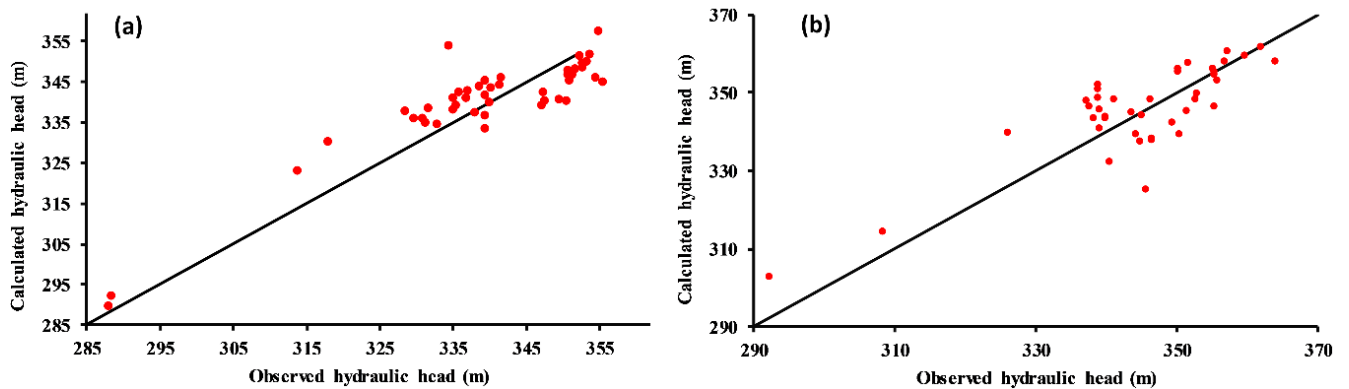


Figure 87. Comparison diagram between the calculated piezometric levels and the measured in steady state (a) shallow aquifer (b) deep aquifer

Comparing the calculated piezometric distributions to the reference maps shows a good concordance in terms of gradient and direction of flow (**Figure 88**).

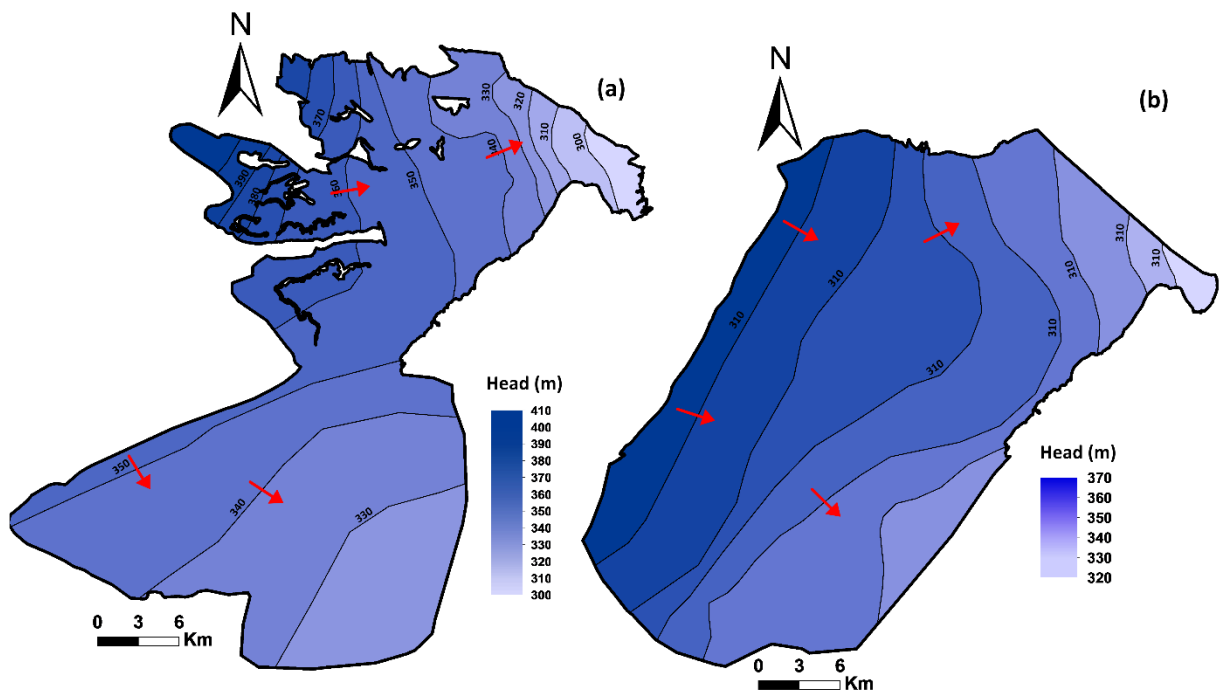


Figure 88. Calculated piezometric maps in the steady state; (a) Shallow aquifer, (b): Deep aquifer (piezometric contour lines in meters).

The calculated water balance indicates that the groundwater recharge is $0.84 \text{ m}^3/\text{s}$ (**Table 26**). The drainage by wadis is $0.343 \text{ m}^3/\text{s}$. In the West part the piezometric level of the shallow aquifer is higher of the deep aquifer which indeed the total exchange flow between aquifers is equal to $0,118 \text{ m}^3/\text{s}$, In the East part, the shallow aquifer is in a recharge situation by the deep aquifer. Furthermore, it is noteworthy that the measured discharge of natural outlets is well reproduced by the model.

The results in the steady state indicate that the basin's renewable resources are equal to 0.84 m³/s distributed as follows: 0.33 m³/s for the shallow aquifer and 0.51 m³/s for the deep aquifer. They are consistent with values published in previous studies. Indeed, the renewable resources assessed by Koschel (1980) are 0.29 m³/s for the shallow aquifer and 0.61 m³/s for the deep aquifer, totalizing 0.9 m³/s. The results of previous modeling studies indicated 0.33 m³/s for the shallow aquifer and 0.51 m³/s for the deep aquifer, and then 0.84 m³/s for the entire basin (Zammouri, 1988). According to DGRE, the basin's renewable resources are equal to 0.8 m³/s with 0.32 m³/s for the shallow aquifer and 0.48 m³/s for the deep aquifer (DGRE 1985).

Table 26 The calculated water balance of the HJB aquifer system, in steady state

Aquifer	Shallow aquifer	Deep aquifer
Inflows (Mm³/year)		
Recharge	10.32	16.15
Exchange between aquifers	8.98	5.27
Total	19.30	21.41
Outflows (Mm³/year)		
Drainage by wadis and evaporation	10.82	-
Pumping	3.21	8.04
Exchange between aquifers	5.27	8.99
Springs	-	4.38
Total	19.30	21.41

3. Transient state

The reproduction of the piezometry trend is taken as calibration criteria. The shallow aquifer presents a good calibration (Figure 89 and 90).

It is considered unconfined over the entire basin; its porosity is equal to 0.2. For the deep aquifer, the calibration quality is less good in some observation wells; the storage coefficient varies between 6×10^{-3} and 8×10^{-3} . It is equal to 0.15 in the recharge area where the aquifer is unconfined.

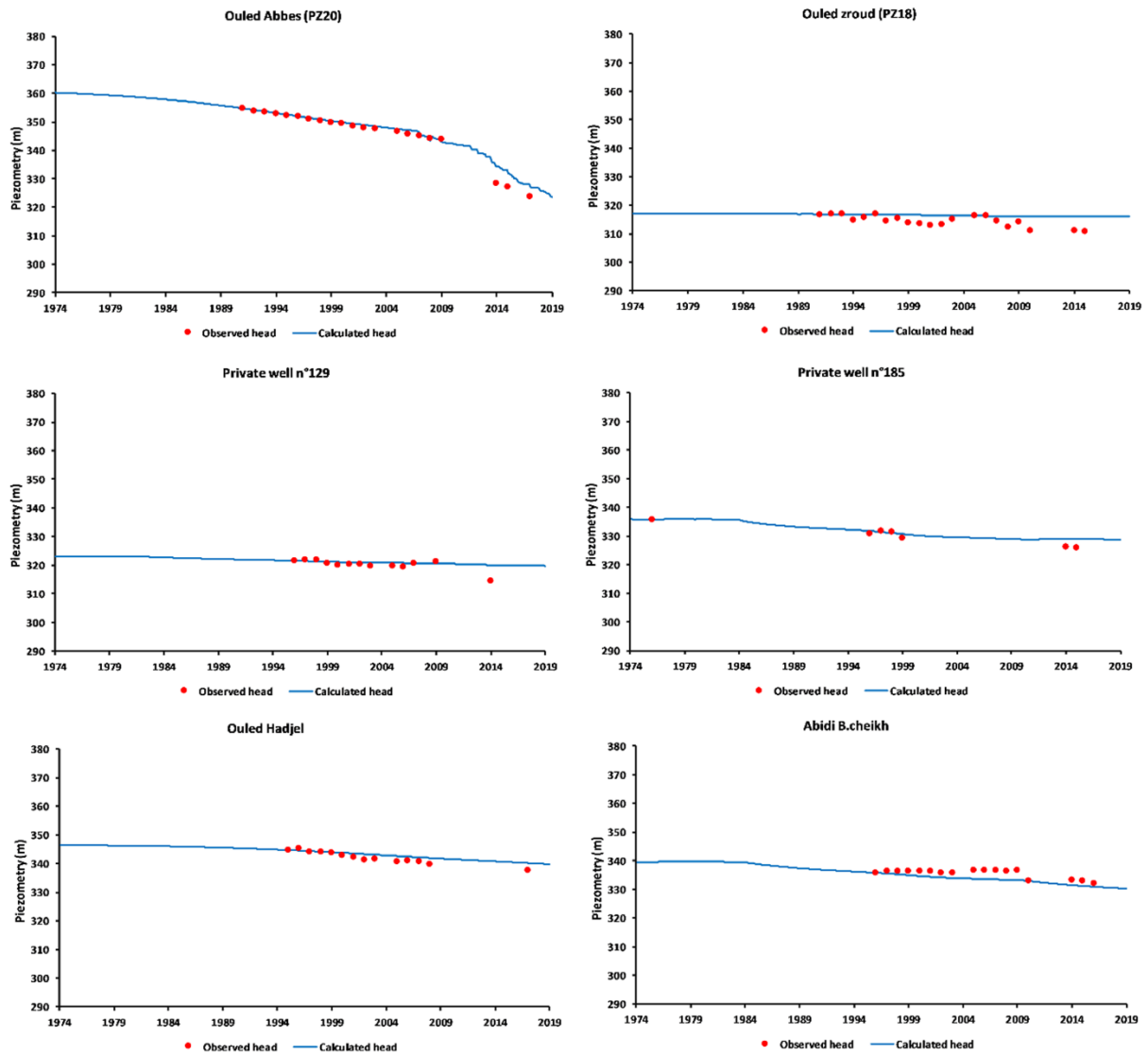


Figure 89. Comparison of the evolution of the calculated and measured hydraulic head in some selected shallow piezometers

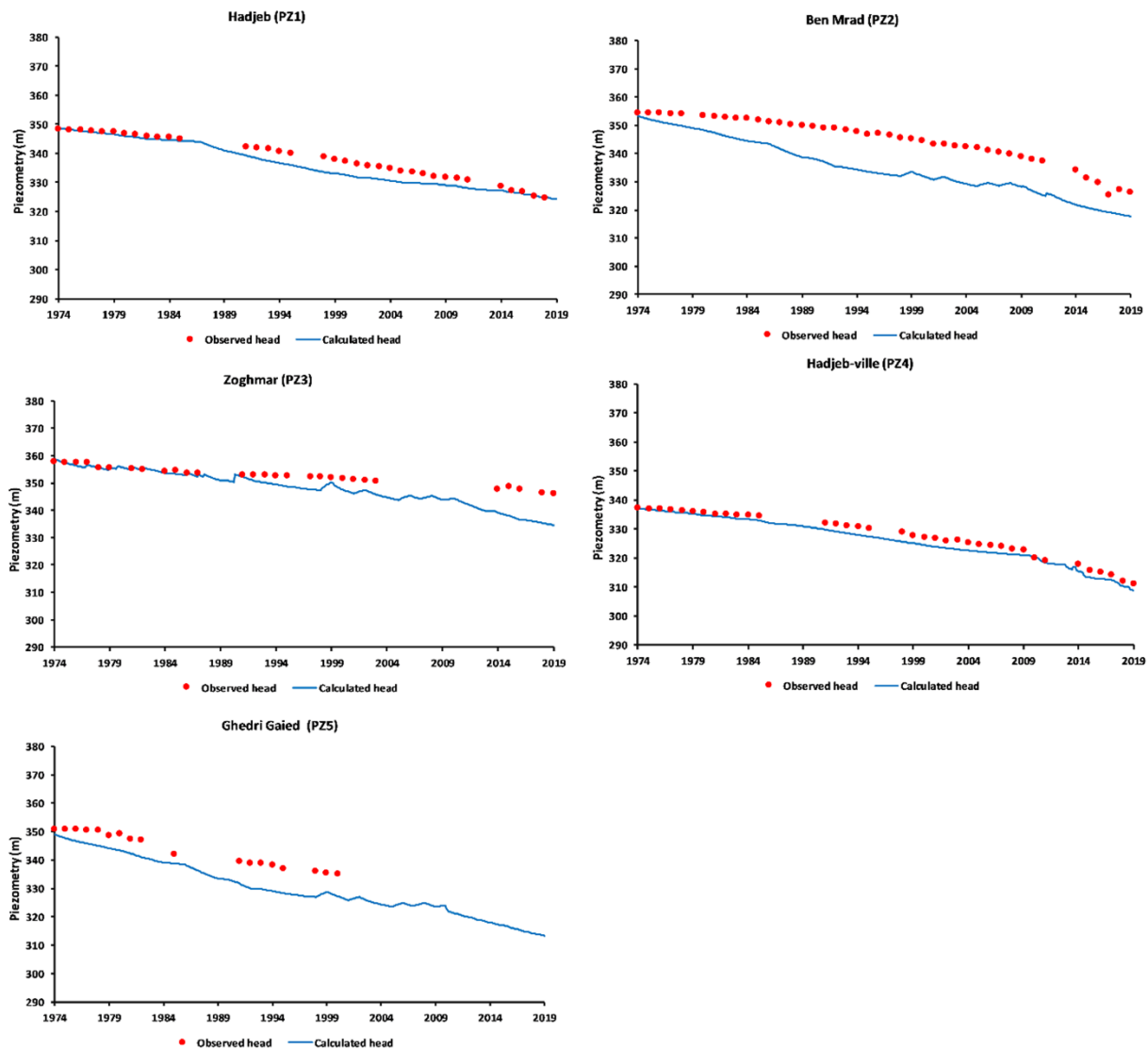


Figure 90. Comparison of the evolution of the calculated and measured hydraulic head in some selected deep piezometers

The calculated water balance analysis indicates that the exploitation increases over the period 1974-2019 was translated by a substantial decrease of the reservoir depletion and a notable decrease of the outflow in the natural outlets of both the shallow and deep aquifers (**Table 27**). The groundwater recharge is calculated to $0.152 \text{ m}^3/\text{s}$ for the shallow aquifer and $0.239 \text{ m}^3/\text{s}$ for the deep aquifer, totalizing $0.391 \text{ m}^3/\text{s}$ for the whole basin. It is lower than the value calculated in steady state. The pluviometry in 2019 is lower than the mean annual pluviometry corresponding to the steady state. The drainage by wadis and losses by evaporation decreased by 37 %, which likely threaten the survival of garaas and sebkhass' ecosystem. The latter is salty marshes located in the southeastern basin.

It is noteworthy that the reservoir depletion is higher in the shallow aquifer despite the similar order of magnitude of withdrawals in the two aquifers. This result shows the strong

hydraulic relation between the phreatic and deep aquifers. The shallow aquifer contributes indirectly to support a part of the pumping in the deep aquifer.

Table 27 The calculated water balance of the HJB aquifer system, in 2019

Aquifer	Shallow aquifer	Deep aquifer
Inflows (Mm³/year)		
Recharge	4.80	7.54
Reservoir depletion	30.12	11.99
Exchange between aquifers	9.84	18.48
Total	44.76	38.01
Outflows (Mm³/year)		
Drainage by wadis and evaporation	5.31	-
Pumping	20.97	28.15
Exchange between aquifers	18.48	9.84
Springs	-	0.015
Total	44.76	38.01

4. Predictive simulations to the year 2050

Considered satisfactory calibrated, the flow model was used to assess the impact of the long-term application of existing and planned extraction projects on groundwater behavior, firstly without considering the effect of climate change. For this purpose, the groundwater simulation model was extended to the year 2050, with various management alternatives modeled.

Three scenarios are carried out. In the scenario S1, a control simulation for the other simulations, present groundwater withdrawals are maintained over the whole basin. In the scenario S2, groundwater extraction in the shallow aquifer is maintained while the deep aquifer extraction is increased linearly to 2050 with an annual increase of 6.6 %. The simulated recharge rates are taken equal to the average annual values over the period 1973-2019. The scenario S2 is compared to those of S1 to determine the effect of withdrawals increasing in the deep aquifer. The extraction increase planned in the deep aquifer is mainly reflected by more extensive reservoir depletion ([Table 28](#)) and a piezometric level lowering varying between 4 and 32 m in 2050 for the shallow aquifer and between 5 and 35 m for the deep aquifer.

In the second stage, the flow model simulates climate change effects on the groundwater behavior. The HJB will be affected by climate change all around the world. The chosen scenario simulated by the HADCM3 model is the average scenario A2 (IPCC 2001). The country was divided into six geographical regions, namely the northwest, northeast, central west, central east, southwest, and southeast, to consider regional variations. The reference period was 1961-

1999, which was marked by strong climate variability. The simulation was conducted for future horizons 2050 (2019-2050). The intense study was based on the analysis of medians deciles, the 1st decile corresponding to the year with the dry season, and the ninth decile is related to the year with the very wet season. According to the HadCM3 model results, the HJB will undergo a precipitation decrease that would reach 11% in 2050 (MARH 2009). Thus, in scenario S3, a recharge decrease reaching 11% in 2050 was simulated to assess the climate change effect. In the scenario S3, the simulated withdrawals are identical to those of the scenario S2.

In scenario S3, the simulated rainfall reduction causes reservoir depletion larger than the calculated value in scenario S2 (Table 28). The calculated piezometric distributions in 2050 indicate that the flow's main directions are maintained for the two aquifers. The piezometric decline will be substantial in the Scenario S3 compared to S1. For the deep aquifer, the additional piezometric lowering in S3 compared to S1 ranges from 20 m to 55 m in 2050. It shows the critical effect of the intensive exploitation planned in this aquifer. In 2050, the additional piezometric decline in the Scenario S3 compared to S2 varies between 1m to 6 m in the shallow aquifer and reaches 8 m in the deep aquifer. An insignificant difference is obtained for the natural outlets discharge confirming that the groundwater recharge decrease will be offset by an ongoing mining in the HJB aquifers' geologic reserves. However, springs will dry up in 2050 in the three scenarios. The comparison of the S2 and S3 results indicates the prevalence of the effect of the withdrawals increase with regard to that of the climate change.

Table 28 The calculated water balance of the HJB aquifer system, in 2050

Scenario	S1	S2	S3
Inflows (Mm³/year)			
Recharge	7.37	7.37	6.55
Reservoirs depletion	43.36	81.40	82.20
Total	50.42	88.78	88.75
Outflows (Mm³/year)			
Drainage by wadis and evaporation	1.36	0.98	0.95
Pumping	49.05	87.80	87.80
Total	50.42	88.78	88.75

5. Conclusion

This part's main objective was to illustrate a numerical simulation methodology for assessing future climate change impacts and increase in withdrawals on Hajeb Jelma aquifers.

The Hajeb El Ayoun Jelma basin is characterized by a semiarid climate with low rainfall and high evapotranspiration. Groundwater resources are the major contributor to the socio-economic development of the basin. The most exploited aquifers in the basin are the deep aquifer (sandstone of the Serravalien) and the shallow aquifer (sands of Mio-Pliocene and Quaternary deposits). From the 80s, the withdrawals exceed the renewable resources, in 2001, it reached 1.66 m³/s while the renewable resources are equal to 0.84 m³/s. GMS software is used in this study to simulate the groundwater flow for the aquifers in Hajeb Jelma basin for both steady and transient conditions to forecast the future changes that occurred under different stresses and to investigate different scenarios to evaluate their effect on the water table.

The flow model developed is composed of two layers representing the shallow and deep aquifers. The model's calibration under steady state and transient conditions yielded results that can be considered satisfactory given the model parameters' data. The model is used to simulate an increase in withdrawals due to the regional socioeconomic. Comparing different scenario results (piezometry and water balance) shows the harmful effect of the increase in withdrawals.

Tunisia is characterized by limited and fragile resources controlled by a constraining climate and erratic precipitations. Currently, most aquifers are overexploited and show signs of deterioration in groundwater quality. According to the Tunisian water management agency, the comparison of the available water resources and the future water needs shows a continuing decline of potential water resources in front of a water demand growing in the next decades. Under the climate change effect, Tunisia would probably experience a continual increase in water demand, mainly due to the rise in temperature, the increase in evaporation and the decrease in rainfall. To overcome this problem, a possible solution would be to stabilize or even reduce water demand in agriculture, which is the main consumer using 80% of water needs. This reduction would be possible by savings in this sector such as carrying out more appropriate pricing and a generalization of localized irrigation techniques.

Chapter III: Vulnerability mapping and Contaminant transport modeling

I. Intrinsic model

1. Mapping the thematic layers

The range of slope has been found between 0 and 64%. Low slope causes an increase in potential vulnerability due to high permeability and low runoff and erosion. Therefore, five rates were assigned (**Figure 91**), the highest rating was assigned with the lowest slope class, and the lowest rating was assigned with a steep slope.

Five soil classes have been found (**Figure 91**): clay loam, sandy clay, sandy loam, loamy sand and sand. The highest rate was assigned to the soil with the highest permeability (sand) and the lowest was assigned to the low soil permeability (clay-loam).

The obtained groundwater depth map was then re-classified into ranges (Fig. 6) according to the SI values (**Table 2**).

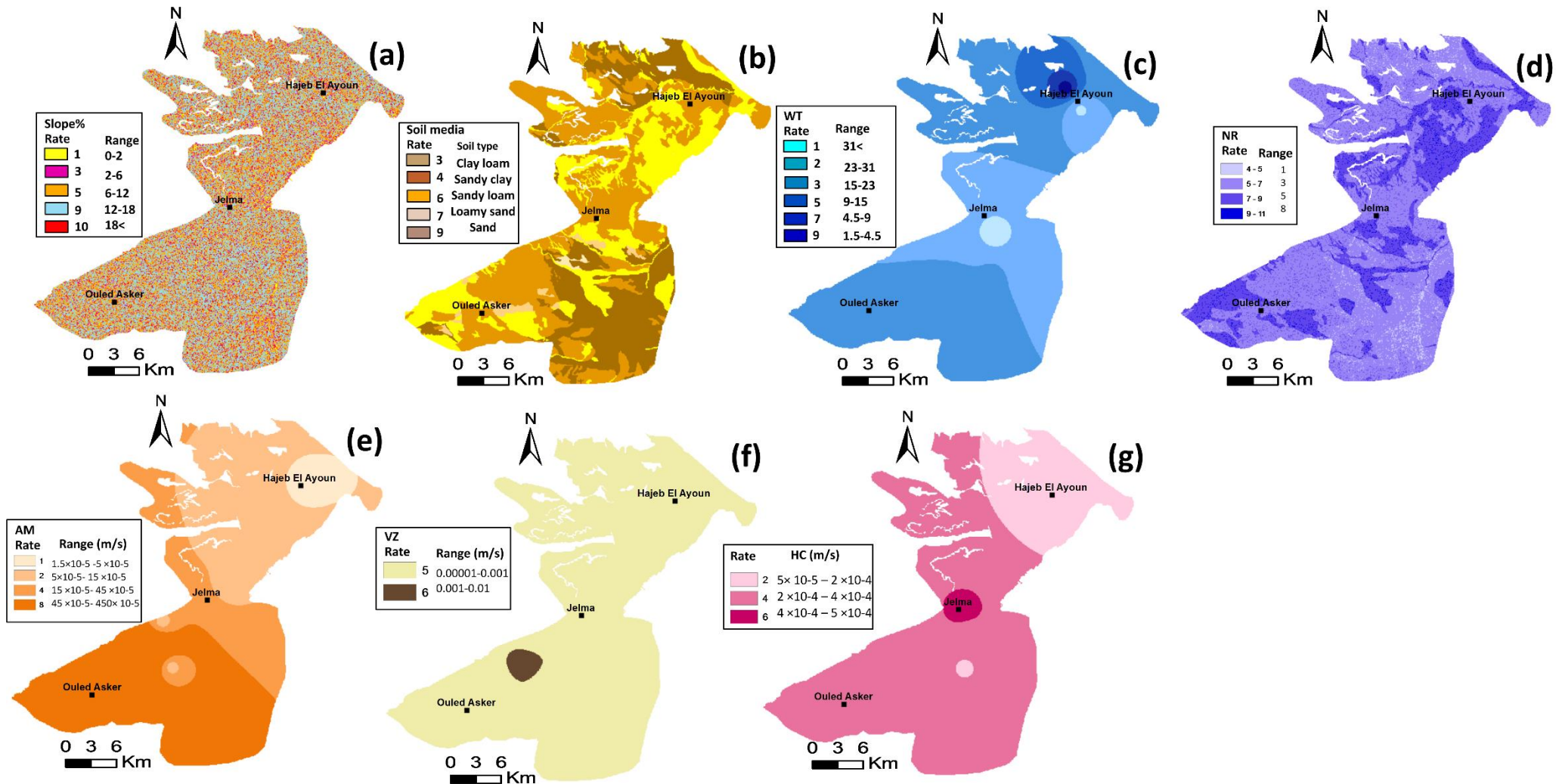


Figure 91. The spatial distribution of rating for the Static parameters ((a) Topography and (b) Soil media) and the Dynamic parameters ((c) water table depth, (d) Net recharge, (e) Aquifer media, (f) vadose zone and (g) hydraulic conductivity) of the shallow aquifer

2. Mapping of the DRASTIC vulnerability (Standard and pesticide)

In the standard model, the DRASTIC index varies from 29 to 111. In order to create the vulnerability map, the index values have been classified into three classes using the quantile classification scheme, i.e., very low, low, and moderate zones (Figure 92). The generated map indicates that low vulnerability zone covers 86.14% of the total study area; however, only 4.58 % is under moderate vulnerable zone.

In the pesticide model, DRASTIC index varies from 64 to 182. Four vulnerability zones have been distinguished as very low, low, moderate and high (Figure 92). The vulnerability map is dominated by “low” vulnerability classes (55.11 %) followed by “moderate” vulnerability classes (42.85 %). The most vulnerable area is located in the north part of the Basin.

The superposition of the DRASTIC maps with the land use map shows that most urban and industrial areas are located in area characterized by moderate vulnerability to industrial and municipal pollutants. However, most agricultural zones are located in areas with high vulnerability, which increases the risk of groundwater contamination by pesticides.

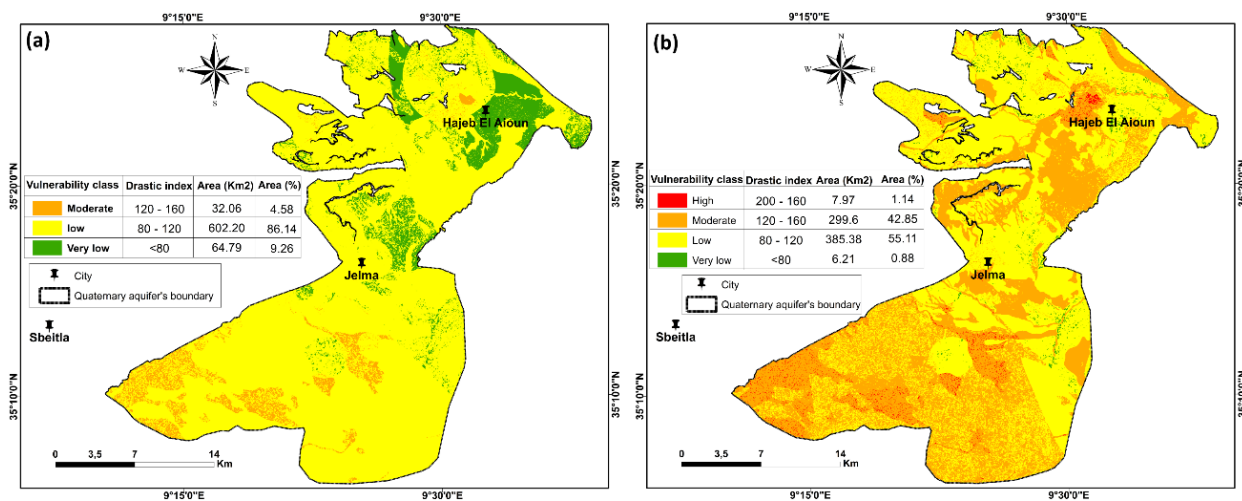


Figure 92. Drastic vulnerability maps: (a) Standard and (b) pesticide

3. Sensitivity of the DRASTIC model

Table 29 shows the statistical summary of the seven rated parameters used in this study to compute the vulnerability index. The comparison of the mean values of parameters reveals that the highest contribution to the vulnerability index is made by topography closely followed by soil media and the vadose zone. The water table, recharge, aquifer media and conductivity

contribute moderately to the vulnerability index. The water table presents the lowest contribution value.

Table 29 Statistical summary of Drastic parameters

	D	R	A	S	T	I	C
Max	9	8	8	9	10	6	6
Min	1	1	1	3	1	5	2
Mean	2.82	3.67	4.83	5.18	7.14	5.01	3.62
SD	0.89	1.26	2.78	2.45	2.36	0.12	0.87

In order to examine the interdependence of the seven rated parameters for the DRASTIC model, a correlation between the parameters were computed (**Table 30**). This analysis indicates that a relatively strong relationship exists between the recharge and the soil media (0.83), between aquifer media and hydraulic conductivity (0.68) and between the impact of the vadose zone and hydraulic conductivity (0.64). The first relationship can be attributed to the porosity of the soil in order to recharge the aquifer.

Table 30 Correlation matrix

	D	R	A	S	T	I	C
D	1						
R	0.11	1					
A	-0.01	-0.02	1				
S	0.05	0.83	-0.06	1			
T	0.16	0.34	0.06	0.08	1		
I	0.37	0.34	0.25	0.25	0.36	1	
C	-0.18	0.08	0.68	0.05	0.11	0.64	1

3.1 Single-parameter sensitivity analysis

The results of the single-parameter sensitivity analysis presented in **Table 31** show that:

- For the standard DRASTIC: The depth to water table and impact of the vadose zone are the most effective parameters in estimating the DRASTIC vulnerability index (weight equal to 5). Effective weights of these parameters (4.04% and 7.23%) are less than their theoretical weights (21.74%). Effective weight of topography (10.12) is more than its theoretical weights. The remaining six parameters, including water depth, net recharge, aquifer media, soil media, vadose zone and hydraulic conductivity represent low effective weights compared to their theoretical weights.
- For the pesticide Drastic: the effective weight of the topography and impact of the vadose zone are more than their theoretical weights.

Table 31 Statistics of single parameter sensitivity analysis

Standard DRASTIC						
Parameter	Theoretical weight	% Theoretical weight	Effective weight			
			Min	Max	Mean	SD
D	5	21.74	1.05	13.43	4.04	1.4
R	4	17.39	1.49	10.12	5.1	1.35
A	3	13.04	0.87	14.28	6.51	3.29
S	2	8.70	3.79	16.98	7.13	2.78
T	1	4.35	1.04	20.93	10.12	3.47
I	5	21.74	4.27	15.62	7.23	1.35
C	3	13.04	1.4	8.33	3.77	0.95
Pesticide DRASTIC						
D	5	19.23	0.73	11.39	2.98	1.07
R	4	15.38	1.23	6.45	3.7	0.81
A	3	11.54	0.6	12.5	4.91	2.7
S	5	19.23	2.88	11.25	5.15	1.72
T	3	11.54	0.81	12.67	7.36	2.3
I	4	15.38	3.08	11.36	5.32	1.07
C	2	7.69	1.23	10.9	3.82	1.17

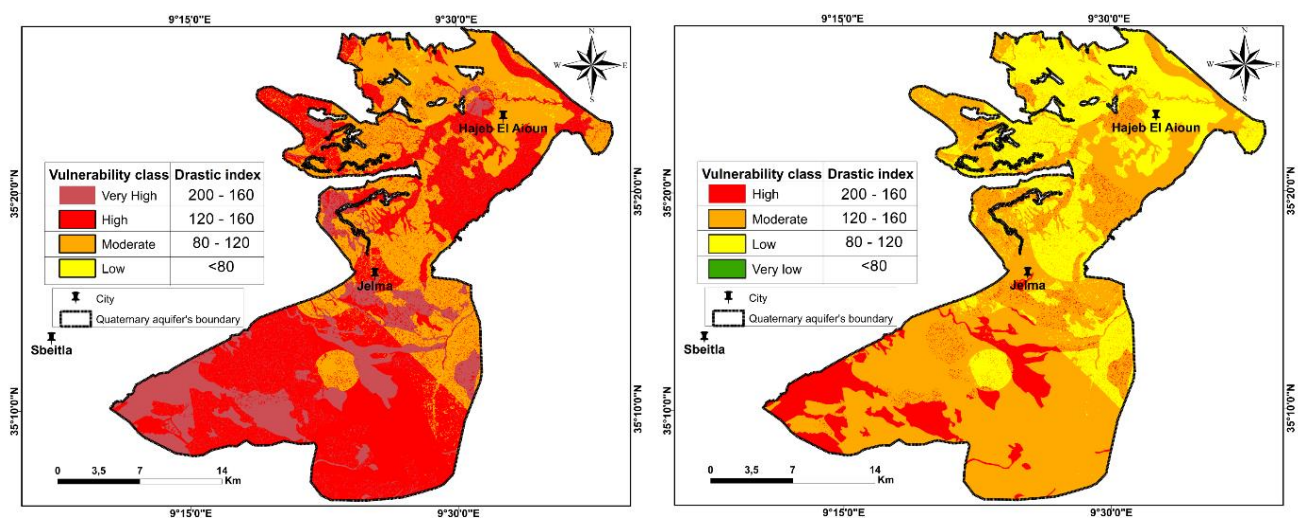


Figure 93. Drastic map using the effective weight: (a) Standard DRASTIC and (b) Pesticide DRASTIC

3.2 Map removal sensitivity analysis

Table 32 Statistics of map removal sensitivity analysis

Standard DRASTIC					Pesticide DRASTIC				
Parameter used	Variation index %				Parameter used	Variation index %			
	Min	Max	Mean	SD		Min	Max	Mean	SD
DRASTIC	0.55	4.56	2.56	2.84	DRASTIC	-0.55	2.83	1.14	2.39

D R A S T	-1.35	4.62	1.64	4.22	D R A S T	-3.08	1.79	-0.65	3.44
D R A S	-3.50	2.62	-0.44	4.32	D R A S	-3.30	-0.17	-1.73	2.21
D R A	-5.20	3.17	-1.01	5.92	D R A	-0.92	3.87	1.48	3.38
D R	-	2.62	-5.10	10.92	D R	-6.87	3.35	-1.76	7.22
	12.83								
R	-8.25	7.62	-0.32	11.22	R	-3.30	8.04	2.37	8.01

Table 33 Statistical summary of one map removal sensitivity analysis

Statistical summary of standard Drastic					
		Mean	Max	Min	SD
D	5	4.04	13.43	6.05	1.40
R	4	5.10	10.12	1.49	1.34
A	3	6.51	14.28	0.87	3.29
S	2	7.13	16.98	2.79	2.78
T	1	10.12	20.93	1.04	3.47
I	5	7.23	15.62	4.27	1.35
C	3	3.77	8.33	1.40	0.95
Statistical summary of Pesticide Drastic					
D	5	2.98	11.39	6.73	1.07
R	4	3.70	6.45	5.23	0.81
A	3	4.91	12.5	0.62	2.7
S	5	5.15	11.25	2.88	1.72
T	3	7.36	12.67	0.81	2.30
I	4	5.32	11.36	3.08	1.07
C	2	3.82	10.9	1.23	1.17

4. Conclusions

In this study, the DRASTIC model of the US Environmental Protection Agency (EPA) was used to assess the aquifer vulnerability of the Shallow aquifer of HJB. The seven DRASTIC parameter maps were prepared and classified in a GIS environment. The vulnerability maps indicated that the dominant vulnerability classes are a low class (55%) followed by the moderate class (43 %) in the pesticide model, and the “low” classes (86 %) in the standard model. A high vulnerability characterizes only 1 % of the study area to pesticide contamination. The superposition of the standard and the pesticide DRASTIC maps with the land use map shows that many agricultural zones are located in the area characterized by “high” to “moderate” vulnerability. The study suggests that these “DRASTIC” maps can be a valuable tool for local authorities for groundwater and land use management. The sensitivity analysis shows that the vulnerability index is susceptible to the removing depth to water and impact of vadose zone in the standard Drastic model and to the net recharge and depth to water in the pesticide Drastic model. Using the effective weight, the vulnerability maps indicated that the dominant vulnerability classes are the High class (64%) in the Standard model and the “moderate” classes (71 %) in the pesticide model.

II. Contaminant transport modeling using MT3DMS

1. Introduction

A hydrodynamic model was developed for HJB. The year 1973 was selected as the steady state; which presented a stable hydrologic and hydrogeological conditions. The transient state was made for 47 years; from 1974 to 2019.

The hydrodynamic model was calibrated, using observed groundwater level, for the both steady and transient states and it had been showed an acceptable result.

The salt transport model in HJB is developed to obtain spatial and temporal distribution of water salinity. The transport model is coupled to the groundwater flow model of the studied aquifer. Indeed, the hydrodynamic model reproduce the spatial distribution of the hydraulic head and thereafter the flow velocity can be calculated to simulate the transport of contaminant in the aquifer by advection, diffusion and dispersion processes in terms of global concentration of salts. For this purpose, the code MT3DMS will be used. The first step is to reproduce the initial conditions by simulating the system behavior on very long time.

2. Model structure and boundary conditions

For the transport model, only the unconfined aquifer was taken into consideration (MPQ Shallow aquifer). The calibrated hydrodynamic model was used as input for the MT3D model.

According to the world health organization, the permissible limit of salinity for water uses is equal to 1 g/l (WHO 2011). In Tunisia, the salinity limit was set as equal to 2 g/l (NT 2013). This difference between both standards reflects the scarcity of freshwater and the required management of Tunisia's water.

In the shallow aquifer of HJB, the water salinity was increased in the last decades. In all the shallow aquifer, the salinity exceeded the WHO limit with an increase general trend.

In this study the salinity was considered as the source of contamination. Salinity data from 1999 to 2019 were used in the calibration of transport model under unsteady-state conditions. The measured salinity distribution in four selected years (1999, 2006, 2013 and 2019) was displayed in Figure 94. The salinity increases from one year to another with exceptional year (2019) which show salinity decrease in some points. This decrease (from 2.2 g/l to 0.5 g/l) reflects the scarcity of laboratory's analysis quality and accordingly the imprecision of the interpolated salinity distribution.

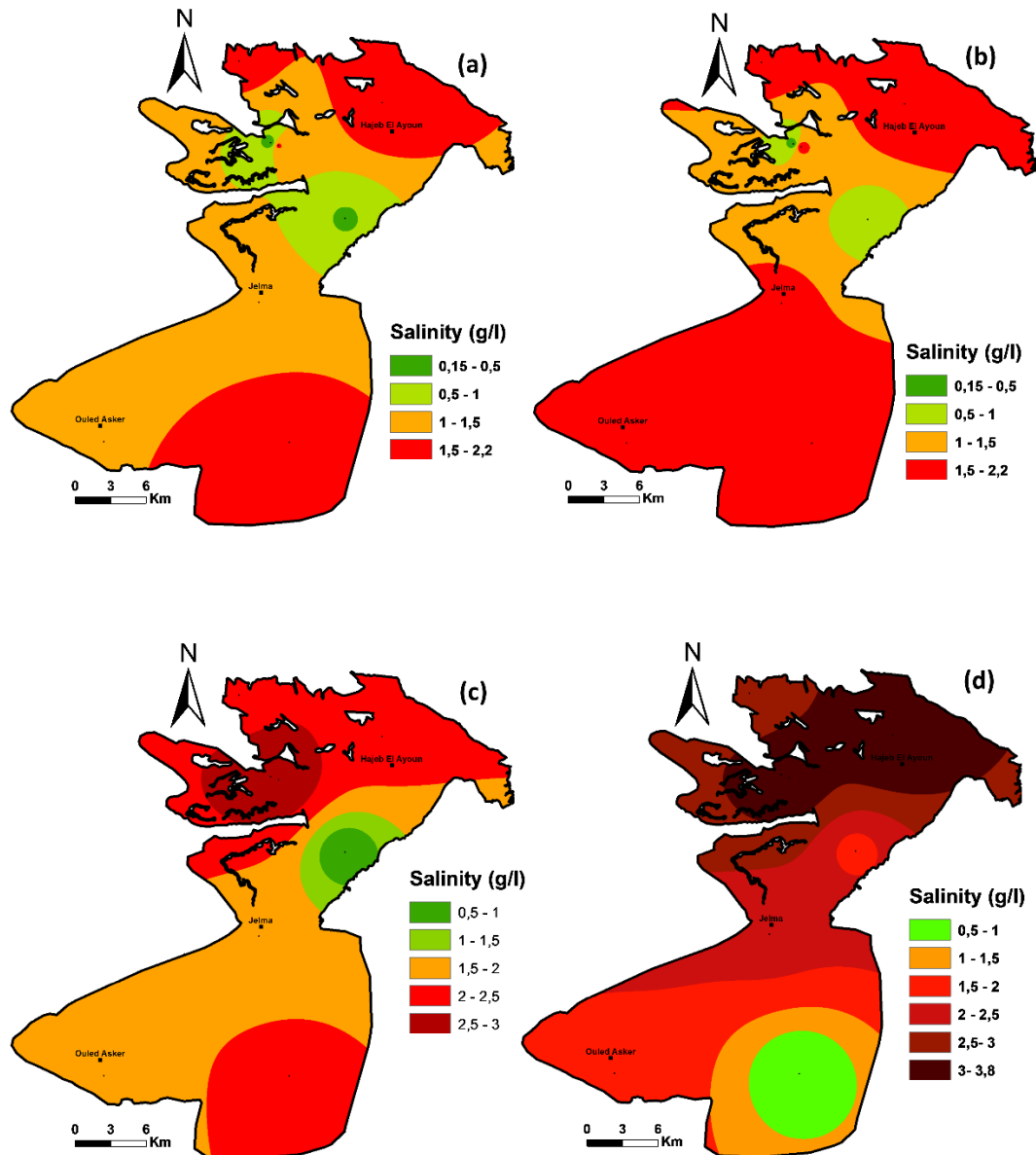


Figure 94. Spatial distribution of measured salinity (in g/l) in four selected years (a) 1999, (b) 2006, (c) 2013 and (d) 2019

3. Results of calibration

In the qualitative model of the HJB; the transport parameters, dispersivity and porosity, were derived from the permeability and lithological characteristics. These parameters were basics to calculate the effective velocity and consequently and to specify groundwater flow by convection and dispersion (Pacheco et al. 2018).

The dispersivity and the porosity were considered as calibration parameters of transport model. There were no measured values of porosity available related to current study area. The effective porosity was attributed according to Castany (1982). We noted that in our case

(unconfined aquifer), the storage was considered to be equivalent to the effective porosity (it varied from 0.1 to 0.3).

For the dispersion, no testing was done for HJB. Therefore, the values of the dispersion coefficients were estimated using a commonly used method based on scaling of targeted study area.

The calibration of the transport model was manually made using the “trial and errors” method, which we tried to represent the general shape of salinity distributions in the study area. The calculated salinity values showed a high correlation index (e.g equal to 0.98 in 1999) with the observed one (Figure 95). Good matches were recorded between the observed and calculated maps (Figure 96).

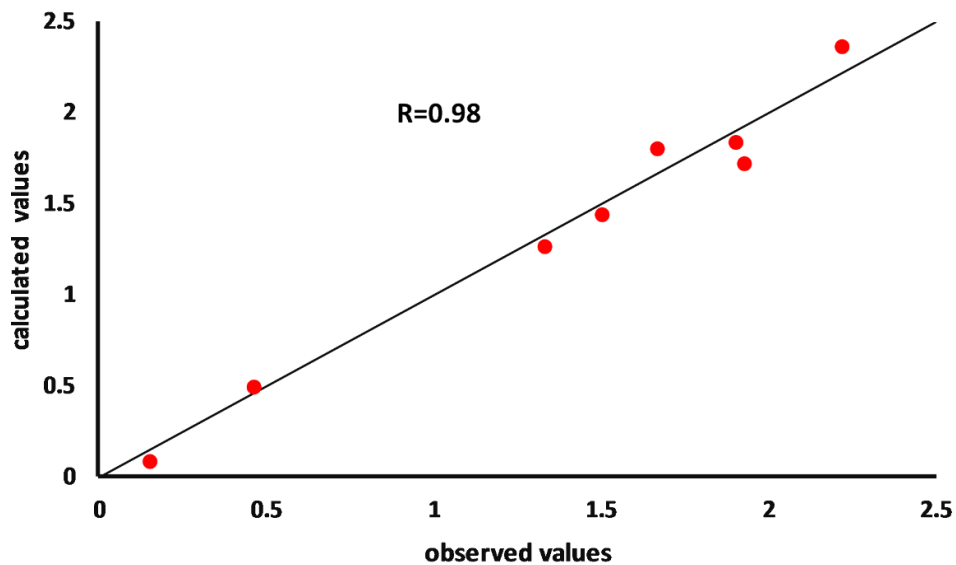


Figure 95. Comparison between salinity observed and calculated values in 1999 (initial condition)

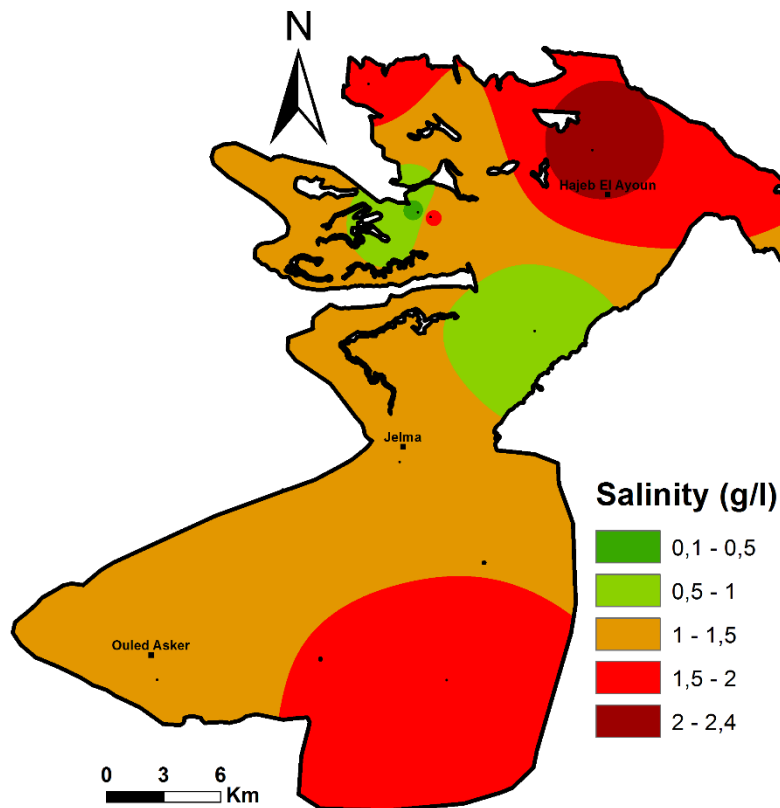


Figure 96. Spatial distribution of calculated salinity (in g/l) in initial condition (1999)

The transport model in the transient state has the same structure as the initial state: the calculated salinity established in 1999, presents the initial condition for the transient state. We conserved the same boundary conditions used in the transient state flow model.

For showing the matching between calculated and measured values of salinity in the shallow aquifer of HJB, over the period 2000-2019, four points with more available data was selected ([Figure 97](#)).

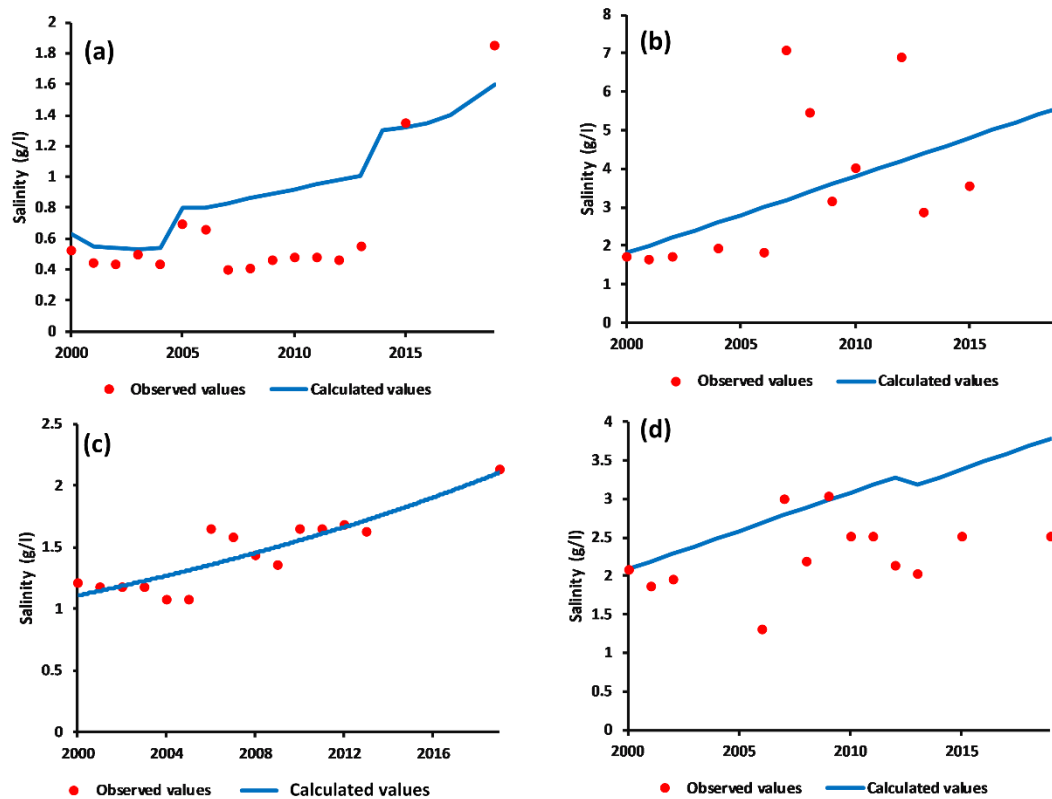


Figure 97. Correlation between the calculated and the measured concentration of salinity (g/l) in the transient state

4. Conclusion

A hydrodynamic model was created using GMS software and calibrated under steady and transient state. The calibrated hydrodynamic model was used as initial conditions of flow for the transport model. A transport models were generated for the salinity pollution. The model was calibrated under long transient state.

The calibrated of the transport model can be used by the water management authorities to simulate the increase in salinity concentration.

Conclusions

The hydrogeological, hydrochemical study of HJB has led to understand the hydrodynamic functioning of the aquifers and contributed to the development of the hydrodynamic and transport models of the aquifer system.

The groundwater hydrochemistry study's main objectives are to determine the water chemistry origins and assess the groundwater suitability for drinking and irrigation purposes. Twenty-eight water samples were collected in 2017 (wet period) from shallow and deep aquifers and analyzed for different physicochemical parameters (temperature, pH, EC, salinity, Na^+ , Ca^{2+} , K^+ , Mg^{2+} , Cl^- , HCO_3^- , and SO_4^{2-}). The shallow aquifer shows high salinity in most water samples (93% > 1 g.l⁻¹). The deep aquifer has moderate salinity (21% of samples exceeding 1 g.l⁻¹).

The results show that both aquifers' water mineralization is controlled by the dissolution of carbonates/gypsum and water evaporation. The drinking water quality assessment shows that 100% and 57% extremely poor water for the shallow and the deep samples, respectively, coincide with the Na-Cl water type. The water quality evaluation for irrigation uses indicates that the shallow samples show quality less good than the deep one and revealed that most samples in the Hajeb Layoun-Jelma basin are not appropriate for irrigation uses.

The recharge rate estimation was made using the multi-criteria method. The results show that the shallow and the deep aquifer receive an average recharge rate, from rainfall, about 31.5 mm/year (infiltration: 15%) and 34 mm/year (16.2%), respectively.

The numerical model was developed using Modflow code under GMS software. The hydrodynamic model system permitted to estimate the hydraulic conductivity distribution. It also allowed estimating abstraction's effect on the water table evolution by two pumping scenarios (2019-2050) (Sc1: constant pumping rates, Sc2: doubled pumping rates). The hydrodynamic models show the continuous water table decrease after 30 years. The simulation of the climate change effect indicated additional drawdown.

The groundwater vulnerability assessment of the shallow aquifer of Hajeb Layoun Jelma basin was made using both intrinsic and simulation models. The DRASTIC model was used as intrinsic tool for identifying the susceptible zones to contamination for the shallow aquifer. The vulnerability maps indicated that the dominant vulnerability classes are the low class (55%)

followed by the moderate class (43 %) in the pesticide model and the “low” class (86 %) in the standard model. A high vulnerability characterizes only 1 % of the study area to pesticide contamination. The superposition of the standard and the pesticide DRASTIC maps with the land use map shows that many agricultural zones are located in the area characterized by “high” to “moderate” vulnerability. The study suggests that these “DRASTIC” maps can be a valuable tool for local authorities for groundwater and land use management.

MTDMS is used to evaluate the transport of salts in the shallow aquifer. The salt transport model results show that the salinization process affects the areas close to the north part's mountains and also is related to the irrigated area.

These investigations could constitute a basis for decision-makers for water resources management and prevent pollution risks.

References

~A~

- **Abbes C (1983)** Etude structurale du Jebel Touila, extrémité septentrionale du chaînon N-S Sidi Khalif-Nara El Houareb. *Thèse Troisième Cycle, Université de Tunis II, Tunisie, 121 p.*
- **Abbes C (2004)** Structurations et évolutions tectono-sédimentaires Mésozoïques et Cénozoïques, associées aux accidents reghmatiques, à la jonction des marges Téthysienne et nord-Africaine (Chaîne Nord-Sud, Tunisie centrale). Thèse ès Sciences, Université Tunis El Manar, Tunisie, 440 p.
- **Abdeslam I, Chemseddine F, Djabri L (2017)** Application of drastic method for drastic method for determining the vulnerability of an alluvial aquifer: Morsott - El Aouinet north east of the of Algeria: using arcgis. *Environment Energy Procedia*, 308–317
- **Adimalla N (2019)** Groundwater quality for drinking and irrigation purposes and potential health risks assessment: a case study from semi-arid region of south india. *Expo Health* 11: 109-123. <https://doi.org/10.1007/s12403-018-0288-8>.
- **Aller L, Bennet T, Leher J.H (1987)** A Standardized System for Evaluating Ground Water Pollution Potential Using Hydrogeological Settings. EPA 600/2-87- 035
- **Allouche F. (1997).** Etude géologique du secteur compris entre les Jebels Bouzer et Rhéouis (Axe Nord-Sud-Tunisie centrale). Inventaire et cartographie
- **Ameur M, Hamzaoui–Azaza F, Gueddari M (2016)** Nitrate contamination of Sminja aquifer groundwater in Zaghouan, northeast Tunisia: WQI and GIS assessments. *Desalin Water Treat* 57:1-11. <https://doi.org/10.1080/19443994.2015.1137495>
- **Ameur M, Hamzaoui-Azaza F, Gueddari M (2016)** Nitrate contamination of Sminja aquifer groundwater in Zaghouan, northeast Tunisia: WQI and GIS assessments. *Desalin Water Treat* 57:1–11. <https://doi.org/10.1080/19443994.2015.1137495>
- **Amouri m. (1994).** Etude hydrogéologique du système aquifère de Sidi Bouzid. Rapport de Direction Générale des Ressources en Eau (DGRE), 45p+annexes. Des matériaux utiles des Jebels Kebar et Merfag. Thèse de Doctorat, Université de France-Comté-France, 411p.
- **Anderson M. P., Woessner W.W (1992)** *Applied groundwater modeling. Simulation of flow and advective transport.* Academic Press, INC. Harcourt Brace Jovanovich, Publishers, 381p.
- **Aouiti S, Hamzaoui Azaza F, El Melki F, Hamdi M, Celico F, Zammouri M (2021a)** Groundwater quality assessment for different uses using various water quality indices in semi-arid region of central Tunisia. *Environ Sci Pollut Res.* <https://doi.org/10.1007/s11356-020-11149-5>
- **Aouiti S., Hamzaoui-Azaza F., Zammouri M., Hamdi M., Celico F. (2021b)** Water Quality Assessment of the Shallow and Deep Aquifers of Hajeb Layoun-Jelma Basin (Central Tunisia). In: Ksibi M. et al. (eds) *Recent Advances in Environmental Science from the Euro-Mediterranean and Surrounding Regions* (2nd Edition). EMCEI 2019. Environmental Science and Engineering. Springer, Cham. https://doi.org/10.1007/978-3-030-51210-1_264
- **Archamault J, Castany G, Roulais M, Degallier R, Azzouz A (1951)** Carte géologique du sbiba 1/50.000.
- **Archamault J, Decrocq J, Roulais M, Degallier R (1949)** Carte géologique du Djebel Mghilla 1/50.000
- **Archamault J, Castany G, Schoeller H (1947)** Carte géologique du Hajeb Layoun 1/50.000.

- **Asadi P, Ataie-Ashtiani B, and Beheshti A (2017)** Vulnerability assessment of urban groundwater resources to nitrate: the case study of Mashhad, Iran. *Environmental Earth Sciences* 76. DOI: 10.1007/s12665-016-6357-z
- **Asadi E, Isazadeh M, Samadianfard S, Ramli M.F, Mosavi A, Nabipour N, Shamsirband S, Hajnal E, Chau K.W (2020)** Groundwater quality assessment for sustainable drinking and irrigation. *Sustainability* 12, 177. <https://doi.org/10.3390/su12010177>
- **Ayadi M (2002)** Etude structurale et évaluation pétrolière de l’alignement Labaeid- Koudiat el Beida-Bledel Gounna (Tunisie Centrale). Mém. DEA. Fac. Sc., Univ. Tunis El Manar, Tunis. Tunisia. (In French)

~B~

- **Babiker I. S., Mohamed A. A., Hiyama T., Kato K (2005)** A GIS based DRASTIC model for assessing aquifer vulnerability in Kakamigahara Heights, Gifu Prefecture, central Japan”, *Science of the Total Environment*, vol. 345, p. 127– 140.
- **Barbieri M, Ricolfi L, Vitale S, Muteto PV, Nigro A, Sappa G (2019)** Assessment of groundwater quality in the buffer zone of Limpopo National Park, Gaza Province, Southern Mozambique. *Environ Sci Pollut Res* 26: 62-77. <https://doi.org/10.1007/s11356-018-3474-0>
- **Bazimenyera, J.D.D. and Tang, Z (2008)** A GIS-based DRASTIC model for assessing groundwater vulnerability in shallow aquifer in Hangzhou-Jiaxing-Huzhou Plain, China. *Research Journal of Applied Sciences*, 3(8): 550–559.
- **Bedir M., Bobier C (1987)** Les grabens de Mahdia et Sidi Chérif (Tunisie orientale). Dynamique des fossés oligo-miocènes induits au toit d’anticlinaux Crétacés-éocènes par les jeux, au Néogène, de décrochement Est-Ouest et Nord-Sud. *Bulletin des Sciences Géologiques*. France, t: III, n°6, pp.1143-1151
- **Bedir M (1995)** Mécanismes géodynamiques des bassins associés aux couloirs de coulissements de la marge atlasique de la Tunisie. *Sismo-stratigraphie, sismo-tectonique et implications pétrolières*. Thèse de Doctorat d’Etat Es-Sciences, Faculté des sciences de Tunis, Université de Tunis II, 417 p.
- **Ben Ayed N (1986)** Evolution tectonique de l’avant pays de la chaîne alpine de Tunisie du début du Mésozoïque à l’actuel. Thèse ès Sciences, Université du Paris-sud, Orsay, France, 347 p
- **Bear J., Beljinb M. S., Rosse R. R (1992)** *Ground Water Issue: Fundamentals of Ground-Water Modeling*. EPA/540/S-92/005.
- **Bear J (1993)** *Modeling flow and contaminant transport in fractured rocks*, Academic Press. San Diego, 37p.
- **Benzarti R (2002)** Synthèse biostratigraphique du permis Jelma. Rapport Inédit, SEREPT, Tunis, GN3833, 37 p.
- **Ben Jemiaa M (1986)** Evolution tectonique de la zone des failles Trozza-Labaeid Tunisie centrale, Université de Paris-Sud centre d’Orsay, 162p.
- **Biely A., Rakus M (1972)** Analyse critique des données sur l’âge du salifère en Tunisie septentrionale. *Notes Serv. Géol. Tunisie*, 38, pp. 35-48.
- **Bismuth H (1984)** Les unités lithostratigraphiques du Miocène en Tunisie orientale. Journées sur les nomenclatures et classifications stratigraphiques en Tunisie, Tunis, 19-20 janvier.
- **Blondel T. J. A (1991)** Les séries à tendance transgressives marines du Miocène inférieur à moyen de Tunisie centrale. Thèse de Doctorat, Uni de Genève, 409 pp.

- **Boukadi N., Zargouni F (1991)** Sur l'interférence des directions structurales dans l'Atlas de Tunisie. L'exemple du noeud tectonique des Jebels M'rghila-Labeïd. Comptes Rendus de l'Académie des Sciences de Paris, France, 312, II, pp. 529-534.
- **Boukadi N (1994)** Signification géométrique et cinématique des noeuds et des zones d'interférences structurales au contact de grands couloirs tectoniques. Thèse de Doctorat d'Etat. Université de Tunis II, 249p.
- **Bouaziz S (1995)**. Etude de la tectonique cassante dans la plate-forme et l'Atlas sahariens (Tunisie méridionale), évolution des paléochamps de contraintes et implication géodynamiques. Thèse ès Sciences, Université, Tunis II, Tunisie, 485 p.
- **Burollet P. F (1956)** Contribution à l'étude stratigraphique de la Tunisie centrale. Annale des mines et de la géologie, 345p.
- **Burollet P.F., et Byramjee R (1974)** Réflexion sur la tectonique globale. Exemples sircains et méditerranéens. Notes et Mémoires de la Compagnie française de Pétrole, _ n 11, P.71-120.

~C~

- **Castany G (1956)** Notice explicative de la carte géologique 1/50.000 de Sbiba (Feuille n° 69). Service des Mines, de l'Industrie et de l'Energie, Tunis, 24 p.
- **Castany G (1967)** *Traité pratique des eaux souterraines*. Ed Dunod, Paris, 2ème édition, 1967, 661p.
- **Castany G (1982)** *Principe et méthodes de l'hydrogéologie*. Université Pierre Marie Curie (ParisVI).
- **Celico F, Rotigliano E (2002)** Saline groundwater problems in the Gaza Strip: causes and integrative management solutions. Bollettino. Soc. Geol. It 121:139–146.
- **Celico F, and G Naclerio (2005)** Verification of a DRASTIC-based method for limestone aquifers. Water International, 30: 530-537
- **Celico F, Petrella E and Naclerio G (2008)** Updating of a DRASTIC-based method for vulnerability assessment in carbonate aquifers. Water International. 32, 475-482
- **Celico, F., Celico, P., De Vita, P., Piscopo, V (2000)** Groundwater flow and protection in the Southern Apennines (Italy). Hydrogeology 4, 39–47.
- **Chadha D.K (1999)** A proposed new diagram for geochemical classification of natural waters and interpretation of chemical data. Hydrogeology J 7: 431-439. <https://doi.org/10.1007/s100400050216>
- **Chiang W.H, Kinzelbach W (1998)** Processing *Modflow*. « *A simulation System Modelling Groundwater Flow and Pollution* »327 pp.
- **Chihi L (1984)** Etude tectonique et microtectonique du graben de Kasserine (Tunisie centrale) et des structures voisines : Jebel Selloum et Jebel Maargaba. Thèse de l'Université Paris-Sud. 116p.
- **Chihi L., BEN AYED N (1991)** Le rôle de la fracturation précoce sur la distribution des récentes le long du décrochement de Kasserine. Annales Tectonic, vol. V, n° 1, pp. 64-73.
- **Chihi L (1995)** Les fossés néogènes à quaternaires de la Tunisie et de la mer pélagienne :leur signification dans le cadre géodynamique de la méditerranée centrale. Thèse ès Sciences, Université Tunis II, Tunisie, 324 p.
- **Civita M (1994)** Aquifer Vulnerability maps to pollution, Pitagora Ed., Bologna

- **Civita M., De Maio M (1997)** SINTACS un sistema parametrico per la valutazione e la cartografia della vulnerabilità degli acquiferi all'inquinamento. Metodologia et Automatizzazione. Pitagora Ed., Bologna: Italia, 191 pp.
- **Creuzot G., OUALI J (1989)** Extension diapirisme et compression en Tunisie centrale, le Jebel lessouda. Revue Géodynamique, v. 4, n. 1, pp. 39-48.
- **Condesso de Melo MT (2018)** Groundwater quality assessment of the Takelsa phreatic aquifer (Northeastern Tunisia) using geochemical and statistical methods: Implications for aquifer management and end-users. Environ Sci Pollut 25 : 36306–36327. <https://doi.org/10.1007/s11356-018-3473-1>

~D~

- **Daher, W; Pistre, S; Kneppers, A; Bakalowicz, M; Najem, W (2011)** Karst and artificial recharge: Theoretical and practical problems: A preliminary approach to artificial recharge assessment. *Journal of Hydrology*. <https://doi.org/10.1016/j.jhydrol.2011.07.017>.
- **Dassi L (2004)** Etude hydrogéologique, hydrochimique et isotopique du système aquifère du bassin de Sbeitla (Tunisie centrale). Thèse de Doctorat, Faculté des Sciences de Sfax, 187p.
- **DGRE (1973–2019)** Situation de l'exploitation des nappes phréatiques et profondes de 1973 à 2019. Direction Générale des Ressources en Eau. Tunisia.
- **DGRE (1973-2018)** Piezométrie des nappes phréatiques et profondes de 1973 à 2018. Direction Générale des Ressources en Eau. Tunisia.
- **DGRE (1968-2017)** Annuaire pluviométriques du Kairouan, Sidi Bouzid et Kasserine.
- **DGRE (2017)** Annuaire des qualités des eaux 2017. Direction Générale des Ressources en Eau. Tunisia.
- **DGRE (2015)** Annuaire des qualités des eaux 2015. Direction Générale des Ressources en Eau. Tunisia.
- **DGRE (1996-2006)** Annuaire des qualités des eaux de 1996 à 2006. Direction Générale des Ressources en Eau. Tunisia.
- **DGRE (2018)** Situation de l'exploitation des nappes phréatiques et profondes en 2018. Direction Générale des Ressources en Eau. Tunisia.
- **Dhahri F, Tanfous D, Gabtni H, Boukadi N (2015)** Structural and geodynamic study in central Tunisia using field and geophysical data: new structural interpretation of the N–S axis and associated Atlasic structures. Int J Earth Sci (Geol Rundsch) 104:1819–1835. <https://doi.org/10.1007/s00531-015-1159-1>
- **Dlala M (1995)** Evolution géodynamique et tectoniques superposés en Tunisie : implications sur la tectonique récente et la sismicité. Thèse de doctorat ès-science, Université de Tunis II, Faculté des sciences de Tunis, 389 p.
- **Doneen LD (1964)** Notes on water quality in agriculture. Water Science and Engineering Paper 4001, California, Department of Water Sciences and Engineering, University of California.

~E~

- **Eaton F.M (1950)** Significance of carbonates in irrigated waters. Soil Science, 69, 123–134.
- **El Bihery M.A (2009)** Groundwater flow modeling of Quaternary aquifer Ras Sudr, Egypt Environmental Geology, vol. 58, p. 1095–1105.

- **El Ghali A (1993)** Néotectonique et évolution tectono-sédimentaire associées aux jeux de la faille de Sbiba-Kairouan du crétacé supérieur à l'actuel, Tunisie centrale. Thèse 3ème cycle, Univ. Tunis II, 251 p.
- **Emberger, L (1955)** Une classification biogéographique des climats. Recueil, travaux de laboratoire géo-zoologique, Faculté des sciences. Service botanique. Montpellier, 7, 3-43.

~F~

- **FAO. (1967)** La défense des terres cultivées contre l'érosion hydraulique. Rome, Italie: FAO. 202p.
- **Farhat H (1978)** Contribution à l'étude hydrogéologique de la cuvette de Maknassy (Tunisie). Thèse de Doctorat en Sciences de la Terre. Université de Bordeaux, 200p.
- **Focazio MJ, Kolpin DW, Barnes KK, Furlong ET, Meyer MT, Zaugg SD, Larry B, Thurman ME (2008)** A national reconnaissance for pharmaceuticals and other organic wastewater contaminants in the United States—II) Untreated drinking water sources. *Sci Total Environ.* 402(2):201–216
- **Foster S (1987)** Fundamental Concept in Aquifer Vulnerability, Pollution Risk and Protection Strategy, In: W. Van Duijvenbooden and H. G. Van Waegeningh, Eds., *Vulnerability of Soil and Groundwater to Pollutions.* Committee on Hydrogeological Research, Hague, p. 69-86.
- **Fournie D (1978)** Nomenclature lithostratigraphique des séries du Crétacé supérieur au Tertiaire en Tunisie. *Bulletin des Centres de Recherches d'Exploration-Production, Elf- Aquitaine*, v. 2, pp. 97-148.

~G~

- **Gaaloul N, Cheng AH-D (2003)** Hydrogeological and Hydrochemical Investigation of Coastal Aquifers in Tunisia-Crisis in Overexploitation and Salinization. Second International Conference on Saltwater Intrusion and Coastal Aquifers-Monitoring, Modeling, and Management. Merida, Mexico, March 30-April 2, 2003
- **Gassara A (1980)** Contribution à l'étude hydrogéologique du bassin de Horchane-Braga (Sidi Bouzid). Thèse de Doctorat, Université Pierre et Marie Curie, France, 89p+annexes.
- **Ghali A and Batik P (1922)** Carte géologique du Debel Trozza 1/50.000.
- **Ghouili N, Hamzaoui-Azaza F, Zammouri M, Zaghrarni MF, Jarraya Horriche F, Condesso de Melo MT (2018)** Groundwater quality assessment of the Takelsa phreatic aquifer (Northeastern Tunisia) using geochemical and statistical methods: Implications for aquifer management and end-users. *Environ Sci Pollut Res.* <https://doi.org/10.1007/s11356-018-3473-1>
- **Gibbs RJ (1970)** Mechanism controlling world water chemistry. *Science* 170(1088) :1090
- **Gleick, P.H (1993)** *Water in Crisis: A Guide to the World's Fresh Water Resources*
- **Goldscheider N., Klute M., Sturm S (2000)** "The PI method – a GIS-based approach to mapping groundwater vulnerability with special consideration of karst aquifers", *Zeitschrift für Angewandte Geologie*, vol. 46(3), p. 157–166.
- **Gordon, C., Cooper, C., Senior, C.A., Banks, H., Gregory, J.M., Johns, T.C., Mitchell, J.F.B., Wood, R.A (2000)** The simulation of SST, sea ice extents and ocean heat transports in a version of the Hadley Centre coupled model without flux adjustments. *Climate Dynamics* 16: 147-168.

~H~

- **Hajjem A (1999)** Etude sur l'hydrogéologie de la plaine de Bled Regueb, rapport de la Direction Générale des Ressources en Eau (DGRE), 50p.
- **Hajri, J (2013)** Climat et ressources en eau en Tunisie. Proc. XXVIth AIC Colloquy: 261-266. Cotonou, Benin. www.aic2013.uac.bj/IMG/pdf/hajri_p261-266.pdf. (In French)
- **Haller P (1983)** Structure profonde du Sahel tunisien. Interprétation géodynamique. Thèse 3ème cycle, Univ. Université de Franche-Comté, 162 p.
- **Hamzaoui-Azaza F, Ketata M, Bouhlila R, Gueddari M, Riberio L (2011)** Hydrogeochemical characteristics and assessment of drinking water quality in Zeuss–Koutine aquifer, southeastern Tunisia. *Environ Monit Assess* 18: 159-174. <https://doi.org/10.1007/s10661-010-1457-9>
- **Hamzaoui-Azaza F, Tlili-Zrelli B, Bouhlila R, and Gueddari M (2013)** An integrated statistical methods and modeling minerals-water interaction to identifying hydrochemical processes in groundwater in southern Tunisia. *Chemical Speciation and Bioavailability*, 25: 165–178. DOI: 10.3184/095422913X13785679075430
- **Hamzaoui-Azaza F, Ameer M, Chaouch R, Cheikha L, Gueddari M, José Joel R (2020)** Assessment of groundwater quality based on GIS and geochemical methods: Coastal aquifer of Bouficha (north-eastern Tunisia). *J Coast Conserv*. 24, 45. <https://doi.org/10.1007/s11852-020-00762-8>
- **Haouchine, A et al. (2011)**. Cartographie de la recharge potentielle des aquifères en zone aride. Cas de la plaine d'eloutaya, Biskra-Algérie, *euro journal* 45,4. p.1-13.
- **Hlaiem A (1999)** Halokinesis and structural evolution of the major features in eastern and southern Tunisian Atlas. *Tectonophysics*, 306, pp. 79-95.
- **Horriche, F.J., Benabdallah, S. (2020)**. Assessing Aquifer Water Level and Salinity for a Managed Artificial Recharge Site Using Reclaimed Water. *Water J*, 12, 341.
- **Hossein Rezaei, Moghaddam Mahsa, Nakhostin Rouhi, Subir Sarkar, Tohid Rahimpour (2018)** Groundwater vulnerability assessment using the DRASTIC model under GIS platform in the Ajabshir Plain, southeast coast of Urmia Lake, Iran. *Arabian Journal of Geosciences*. 11:575
- **Hounslow AW (1995)** Water quality data. Analysis and interpretation. Lewis, New York
- **Hussein, A.A., Govindu, V., Nigusse, A.G.M (2017)** Evaluation of groundwater potential using geospatial techniques. *Appl Water Sci* 7, 2447–2461. <https://doi.org/10.1007/s13201-016-0433-0>.

~|~

- **Iglesias A, Garrote L, Flores F, Moneo M (2007)** Challenges to manage the risk of water scarcity and climate change in the Mediterranean. *Water Resour Manag* 21(5):227–288
- **INS (2014)** Recensement Général de la Population et de l'Habitat 2014. <http://www.ins.tn/fr>
- **INM (1972-2016)** Institut National de la Météorologie, Tableaux climatiques mensuels. Archive INM pour la période de 1974-2008. Stations Kairouan, Sidi Bouzid et Sbeitla.
- **Islam A.R.MT, Ahmed N, Bodrud-Doza Md, Chu R (2017)** Characterizing groundwater quality ranks for drinking purposes in Sylhet district, Bangladesh, using entropy method, spatial autocorrelation index, and geostatistics. *Environ Sci Pollut Res* 24: 26350. <https://doi.org/10.1007/s11356-017-0254-1>

~J~

- **Jallalia D, Lachaal F, Andoulsi M, Zouaghi T, Hamdi M, Bedir M (2015)** Hydro-geophysical and geochemical investigation of shallow and deep Neogene aquifer systems in Hajeb Layoun-Jilma-Ouled Asker area, Central Tunisia. *J Afric Earth Sci* 110: 227-244. <https://doi.org/10.1016/j.jafrearsci.2015.06.016>
- **Jarray H, Zammouri M, Ouessar M, Zerrim A, and Yahyaoui H (2017)** GIS based DRASTIC Model for Groundwater Vulnerability Assessment: Case Study of the Shallow Mio-Plio-Quaternary Aquifer 1 (Southeastern Tunisia), *Water Resources*. 44(4):595–603, ISSN 0097-8078
- **Jha, M.K., Chowdhury, A., Chowdary, V.M., Peiffer, S (2006)** Groundwater management and development by integrated remote sensing and geographic information systems: prospects and constraints. *Water Resour. Manag.* 21 (2), 427e467.

~K~

- **Kadri, A et ben ayed (1990)** Evolution tectono-sédimentaire du bassin oriental de kassrine au crétacé (aptien-campanien) : exemple des jebels koumine, hamra et lessouda (tunisie centrale). Notes du service géologique de Tunisie N°56, pp 101-116. (In French)
- **Kadri A and Ben Haj Ali M (1993)** Carte géologique du Sbeitla 1/50.000.
- **Kelly WP (1951)** Alkali soils-their formation, properties and reclamation. Reinhold Publ, New York
- **Khazri D, and Gabtni H (2015)** Geophysical contribution in the characterization of deep-water tables geometry (Sidi Bouzid, Central Tunisia). *Int J Geophys.* 16 p
- **Khessibi M (1978)** Etudes géologiques du secteur de Maknassy-Mezzouna et du Jebel Kébar (Tunisie centrale). Thèse Troisième Cycle, Université Claude Bernard, Lyon, France, 175 p.
- **Khomsi S., Bedir M., Ghazi Ben Jemia M (2004)** Mise en évidence d'un nouveau front de chevauchement dans l'Atlas tunisien oriental de Tunisie par sismique réflexion. Contexte structural régional e rôle du Trias salifère. *Compte Rendues de l'Académie des Sciences du Paris*, t.336, pp. 1401-1408.
- **Koschel R (1980)** Etude hydrogéologique de la nappe de Hajeb el Aioun –Jelma –Ouled Asker. Proj. Coop. Tech. Tuniso-allemande. N°6520/7. Division des ressources en eau. Minist. Agric. Tunis. Tunisia. 245p. (In French)
- **Kumar, C.P (2012)** Assessment of Groundwater Potential. *International Journal of Engineering and Science*, 1, 64-79. <http://www.theijes.com/papers/v1-i1/L011064079>.
- **Kumar C (2002)** Ground water flow models. Technical report, National Institute of Hydrology. Roorkee.
- **Kumar C. P (2001)** “Common Ground Water Modelling Errors and Remediation”, *Journal of Indian Water Resources Society*, vol. 21 (4), p. 149-156.

~L~

- **Le Treut, H (2010)** Modèles climatiques : certitudes, incertitudes perspectives. Institut Pierre Simon Laplace, Institut de recherche en sciences de l'environnement. <http://www.clermont.inra.fr/urep/accae> (In French)
- **Ligavha-Mbelengwa L, Gomo M (2020)** Investigation of factors influencing groundwater quality in a typical Karoo aquifer in Beaufort West town of South Africa. *Environ Earth Sci* 79, 196. <https://doi.org/10.1007/s12665-020-08936-1>
- **Lodwick WA, Monson W, Svoboda L (1990)** Attribute error and sensitivity analysis of map operations in geographical information systems : suitability analysis. *Int. J. Geogr. Inf. Syst.* 4(4):413–428.

- **Longley, Paul A., Michael F. Goodchild, David J. Maguire, and David W. Rhind (2015)** Geographic Information Science and Systems. New York, NY: Wiley.

~M~

- **Mamou A (1981)** Etude hydrogéologique du bassin versant de Sebkhath En Noual. Bureau de l'Inventaire et des Recherches Hydrologique (B.I.R.H.), 37p+Annexes.
- **Mansouri R (1980)** Contribution à l'étude hydrogéologique de la plaine de Sebkhath El Bhira (Sud-Ouest de Kairouan). Thèse de Doctorat en Sciences de la Terre, Université de Bordeaux-France, 107p.
- **Margat J (1968)** "Groundwater Vulnerability to Contamination," Bases de la Cartographie. Doc. 68 SGC 198 HYD, BRGM, Orleans. (In French).
- **MARH (2009)** Eau et adaptation au changement climatique, expérience tunisienne. Tunis. Tunisia. (In French)
- **Matmati MF, Kadri A, Ouali J (1992)** Carte géologique du Jbel Lassouda 1/50.000.
- **Mckee, T.B., N.J. Doesken et J. Kleist (1993)** The relationship of drought frequency and duration to time scale. In: Proceedings of the Eighth Conference on Applied Climatology, Anaheim, California, du 17 au 22 janvier 1993. Boston, American Meteorological Society. p.179–184.
- **Medina-Gomez I, Herrera-Silveira JA (2003)** Spatial characterization of water quality in a karstic coastal lagoon without anthropogenic disturbance: A multivariate approach. Coastal and Shelf Science 58 : 455-465. [https://doi.org/10.1016/S0272-7714\(03\)00112-4](https://doi.org/10.1016/S0272-7714(03)00112-4)
- **Meireles, A., Andrade E. M., Chaves L., Frischkorn, H., and Crisostomo, L. A (2010)** "A new proposal of the classification of irrigation water", Revista Ciência Agronômica, Vol. (41), No. (3), pp. 349-357.
- **Mnassri S, Dridi L, Lucas Y b, Schäfer G, Hachicha M, Majdoub R (2018)** Identifying the origin of groundwater salinisation in the Sidi El Hani basin in central-eastern, Tunisia. *J Af Earth Sc* 147 : 443-449. <https://doi.org/10.1016/j.jafrearsci.2018.07.004>
- **Moghari SM, Ebrahimi K, Azarnivand A (2015)** Groundwater quality assessment with respect to fuzzy water quality index (FWQI): an application of expert systems in environmental monitoring. *Environ Earth Sci* 74 :7229–7238. <https://doi.org/10.1007/s12665-015-4703-1>
- **M'RABET A (1981)** Stratigraphie, sédimentation et diagenèse carbonatée des séries du Crétacé inférieur de la Tunisie centrale. Thèse Doctorat d'Etat Es Sciences, Université de Paris Sud, Centre d'Orsay, 540p.
- **Muheeb M, Awawdeh Rasheed, A Jaradat (2009)** Evaluation of aquifers vulnerability to contamination in the Yarmouk River basin, Jordan, based on DRASTIC method. *Arab J Geosci.* 3 :273–282
- **Murthy, K.S.R. (2000).** Ground water potential in a semi-arid region of Andhra Pradesh-a geographical information system approach. *IJRS*, 21 (9), 1867–1884. doi :10.1080/014311600209788.

~N~

- **Napolitano P, Fabbri AG (1996)** Single-parameter sensitivity analysis for aquifer vulnerability assessment using DRASTIC and SINTACS. In : Proceedings of the Vienna conference on HydroGIS 96: Application of geographic information systems in hydrology and water resources management, IAHS Pub, No. 235, pp 559–566

- **Neshat A, Pradhan B, Dadras M (2014)** Groundwater vulnerability assessment using an improved DRASTIC method in GIS/ Resources, Conservation and Recycling 86 (2014) 74–86.
- **NT (2013)** Norme Tunisienne NT 09-14, Relative à la qualité des eaux de boisson. Rapport du laboratoire SONEDE.

~O~

- **Ouali J (1984)** Structure et évolution géodynamique du chaînon Nara-Sidi Kralif (Tunisie centrale). Thèse Doct. 3ème cycle, Univ. Rennes I, 120 p.
- **Ouali J (2007)** Importance du réseau réghmatique dans la tectonogenèse de la Tunisie atlasique à travers l'étude de l'axe Nord-Sud. Thèse ès Sciences, Université Tunis El Manar, Tunisie, 399 p.
- **Ouda B (2000)** Paléo-hydrologie isotopique du bassin de Maknassy (Tunisie centrale) pendant le Quaternaire récent. Thèse de Doctorat, Faculté des Sciences de Tunis, 234p.

~p~

- **Parkhurst DL, Appelo C.A.J (1999)** A computer program for speciation, batch - reaction, one - dimensional transport and inverse geochemical calculations. USGS.
- **Piper AM (1944)** A graphic procedure in the geochemical interpretation of water analyses. Trans Am Geophys Union 25:914–923
- **Piscopo G (2001)** Groundwater Vulnerability Map, Explanatory Notes, Castlereagh Catchment. NSW Department of Land and Water Conservation

~R~

- **Rabhi M (1999)** Contribution à l'étude stratigraphique et analyse de l'évolution géodynamique de l'axe Nord-Sud et des structures avoisinantes (Tunisie centrale). Thèse Doctorat (PhD) Université Tunis II, Tunisie, 217 p.
- **Ragunath HM (1987)** Groundwater, 2nd edn. Wiley Eastern Ltd, New Delhi.
- **Richard LA (1954)** Diagnosis and improvement of saline and alkaline soils. Agricultural, Handbook 60. US Department of Agriculture, Washington, DC, p 160.
- **Ricolfi L, Barbieri M, Muteto P.V, Nigro A, Sappa G, Vitale S (2020)** Potential toxic elements in groundwater and their health risk assessment in drinking water of Limpopo National Park, Gaza Province, Southern Mozambique. Environ Geochem Health 42: 2733–2745. <https://doi.org/10.1007/s10653-019-00507-z>
- **Rouabhia A, Fehdi C, Baali F, Djabri L (2008)** Impact of human activities on quality and geochemistry of groundwater in the Merdja area, Tebessa, Algeria. Environ Geol DOI 10.1007/s00254-008-1225-0
- **Rouabhia A., Baali F., Fehdi CH.; Kherici N., Anddjabri L (2009)** “Hydrochemical and isotopic investigation of a sandstone aquifer groundwater in a semiarid region, El Ma El Abiod, Algeria”, Environmental Geology, , vol. 57 (8), p. 1699–1705.
- **Ross M., Parent M., Martel R., Lefebvre R (2004)** “Towards seamless interactions between geologic models and hydrogeologic applications”, Geological Models for Groundwater Flow Modeling Workshop, 49th annual

Meeting Geological Association of Canada, Mineralogical Association of Canada, St. Catherines, Ontario, Canada.

~S~

- **Saidi S (2006)** Etude de la vulnérabilité des ressources hydriques du bassin Hajeb-Jilma (Tunisie centrale). Mastère de la Faculté des Sciences de Sfax, Université de Sfax, 121p.
- **Schnebelen N., J.P. Platel, Y. Lenindre et D. Baudry (2002)** Gestion des eaux souterraines en Aquitaine Année 5. Opération sectorielle. Protection de la nappe de l'oligocène en région bordelaise. Cartographie de la vulnérabilité à la pollution. Bureau de recherches géologiques et minières, RP-51178-FR, France, 75 p.
- **Secunda S, Collin ML, Melloul AJ (1998)** Groundwater vulnerability assessment using a composite model combining DRASTIC with extensive agricultural land use in Israel's Sharon region, Israel. *J. Environ. Manag.* 54:39–57
- **Shakoor, A., Khan, Z.M., Farid, H.U. et al (2020)** Delineation of regional groundwater vulnerability using DRASTIC model for agricultural application in Pakistan. *Arab J Geosci* 13, 195. <https://doi.org/10.1007/s12517-020-5161-y>.
- **Shrestha S, John D, Vishnu P (2016)** Assessment of groundwater vulnerability and risk to pollution in Kathmandu Valley, Nepal. *Science of the Total Environment* 556 (2016) 23–35
- **Smida H (2008)** Apports des Systèmes d'Informations Géographiques (SIG) pour une approche intégrée dans l'étude et la gestion des ressources en eau des systèmes aquifères de la région de Sidi Bouzid (Tunisie centrale). PhD thesis, Faculté des sciences de Sfax, Université de Sfax, 283p (In French)
- **Soyer C. and Tricart P (1989)** Tectonique d'inversion en Tunisie centrale, le chaînon atlasique Segdal-Boudinar. *Bulletin de la Société Géologique de France*, 8 (4), 829-836.
- **Stempvoort, V.D., EWERT, L. and WASSENAAR, L (1993)** Aquifer Vulnerability Index: A GIS-compatible method for groundwater vulnerability mapping. *Canadian Water Resour. Jour.*, v.18/1, pp.25-37.
- **Su F, Wu J, He S (2019)** Set pair analysis (SPA)-Markov chain model for groundwater quality assessment and prediction: a case study of Xi'an City, China. *Hum Ecol Risk Assess* 25: 158-175. <https://doi.org/10.1080/10807039.2019.1568860>

~T~

- **Tanfous D (2007)** Sismostratigraphie et sismotectonique du Jurassique dans l'atlas centro-meridional de la Tunisie. Thèse de Doctorat 3ème cycle. Université Tunis El Manar II, Faculté des Sciences, 239 p.
- **Tanfous D., Gabtni H., Azaiez H., Soussi M., Bedir M (2010)** Integrated gravity and seismic investigations over the Jebel Es Souda-Hmaeima structure: implication for basement configuration of the eastern frontal fold and thrust belt of Tunisian Atlasic Mountains.
- **Thebti S, Jellalia D, Azaiez H, Bédir M (2018)** Basin structuring and hydro-geophysical characterization of Upper Cretaceous and Eocene fractured deep carbonate reservoirs in the Hajeb Layoun-Jelma-Ouled Asker area (Central Tunisia). *Arab J Geosci* 11, 107. <https://doi.org/10.1007/s12517-018-3445-2>.
- **Todd DK (1980)** Groundwater hydrology, 2nd edn. Wiley, New York

- **TOUATI M. A (1985)** Etude géologique et géophysique de la concession de Sidi Itayen en Tunisie orientale, Sahel de Sfax. Histoire géologique du bassin et évolution de la fracturation et des structures du Crétacé au plio-quaternaire. Thèse Doct. 3ème cycle, Univ. Paris VI, 255 p.
- **Touhami I, Chirino E, J.M. Andreu, J.R. Sánchez, H. Moutahir, J. Bellot (2015)** Assessment of climate change impacts on soil water balance and aquifer recharge in a semiarid region in south east Spain. *J. Hydrol.*, 527, pp. 619-629, [10.1016/j.jhydrol.2015.05.012](https://doi.org/10.1016/j.jhydrol.2015.05.012)
- **Touir ET Al (1989)** Biostratigraphie et sédimentologie des séquences du Jebel Mghilla-Tunisie centrale. *Géologie Méditerranéenne*, t.XVI, n. 2, pp.55-66.
- **TURKI M. M (1985)** Polycinématique et contrôle sédimentaire associé sur la cicatrice Zaghouan-Nebhana. 2ème sujet témoignage de déformations synsédimentaires pré-tectoniques (Trias-Crétacé) en Tunisie. Thèse ès Sciences, Université Tunis, 252 p.

~U~

- **UN (1967)** Hydrogeologic map of Lebanon. Carte hydrogéologique du Liban au 1/100000 me, United Nations, Beyrouth, Lebanon.
- **United Nations (1977)** Report of the United Nations water conference. United Nations Publications, New York, Mar del Plara.
- **USGS (2010)** <http://ga.water.usgs.gov/edu/2010/gallery/global-water-volume.html>
- **USSL (US Salinity Laboratory) (1954)** Diagnosis and improvement of salinity and alkaline soil. USDA Handbook no. 60, Washington.

~W~

- **Wang S, Huang T, Chen H, Liu M, Xue H (2018)** Application of fuzzy comprehensive evaluation model-based CRITIC weighting in water quality evaluation. *Hydropower Energy Sci* 36(06) :48-51
- **WHO (2011)** Guidelines for drinking-water quality: fourth edition incorporating the first addendum. ISBN 978-92-4-154995-0564
- **Wilcox LV (1955)** Classification and use of irrigation water, circular 969. Washington, DC, USA.
- **Wu J, Li P, Qian H (2011)** Groundwater quality in Jingyuan plain, a semi-humid area in northwest China. *E-J Chem* 8(2):787–793. <https://doi.org/10.1155/2011/163695>

~Z~

- **Zammouri, M (1988)** Modèle de simulation des nappes de Hajeb el Aioun –Jelma-Oule Asker. DGRE, Tunis.
- **Zammouri M (2007)** Cours en principes des modèles de simulation de nappes d'eau souterraine, ESIER, Mjez El Bab. 36 p.
- **Zammouri M, Jarraya-Horriche F, Odo B. O, Benabdallah S (2013)** Assessment of the effect of a planned marina on groundwater quality in Enfida plain (Tunisia). *Arab J Geosci* 7: 1187-1203. <https://doi.org/10.1007/s12517-012-0814-0>
- **Zargouni F (1985)** Tectonique de l'Atlas méridional de Tunisie, évolution géométrique et cinématique des structures en zone de cisaillement. Thèse de l'Université de Strasbourg, 304p.

- **Zghal I (1994)** Etude microbiostratigraphique du Crétacé inférieur de la Tunisie du Centre Ouest. Thèse 3ème Cycle, Université Tunis II, Tunisie, 393 p.
- **Zhang Q, Xu P, Qian H (2020)** Groundwater Quality Assessment Using Improved Water Quality Index (WQI) and Human Health Risk (HHR) Evaluation in a Semi-arid Region of Northwest China. *Expo Health* 12: 487-500. <https://doi.org/10.1007/s12403-020-00345-w>
- **Zheng C., Wang P. P (1999)** MT3DMS: A Modular Three-Dimensional Multispecies Transport Model for Simulation of Advection, Dispersion, and Chemical Reactions of Contaminants in Groundwater Systems; Documentation and User's Guide. U.S. Army Engineer Research and Development Center Contract Report SERDP-99-1, Vicksburg, MS, 202 p.
- **Zitouni L (1997)** Evolution géodynamique des bassins mésozoïques de subsurface des régions de Sidi Aïch-Majoura (Tunisie centrale), sismostratigraphie, sismotectonique et implications pétrolières. Thèse Doctorat (PhD), Université Tunis II, Tunisie, pp 320, 335.
- **Zouaghi T (2002)** Identification et répartition des séquences et des faciès sismiques des dépôts de l'Albien-Sénonien en Tunisie centro-méridionale (Région de Gafsa-Sidi Bou Zid). Diplôme d'Etudes Approfondies, Université Tunis El Manar, Tunisie, 161 p.
- **Zouaghi T., Bedir M., Inoubli M. H (2005)** Structuration profonde des dépôts de l'Albien- Maastrichtien en Tunisie centrale : nouvelle limite de l'archipel de Kasserine et implications géodynamiques. *Comptes Rendus Geoscience*, v. 337, pp. 685-693.
- **Zouaghi T., Inoubli M. H., Bedir M (2007)** Contribution of seismic velocities to the structural and the lithostratigraphic studies: Salt-intruded corridor ceiling and Lower Turonian Beida Anhydrite deposits outline in Central-Southern Atlas of Tunisia. *Comptes Rendus Geoscience*, v. 339, pp. 13-23.
- **Zouaghi T (2008)** Distribution des séquences de dépôt du Crétacé (Aptien- Maastrichtien) en subsurface : rôle de la déformation tectonique, l'Halocinèse et évolution géodynamique (Atlas central de Tunisie). Thèse de Doctorat, Faculté des sciences de Tunis, 341p.
- **Zouari H (1995)** Evolution géodynamique de l'Atlas centro-méridional de la Tunisie, stratigraphie, analyse géométrique, cinématique et tectono-sédimentaire. Thèse ès Sciences, Université Tunis II, Tunisie, 278 p.
- **Zouari K (1998)** Etude isotopique et hydrochimique des systèmes multicouches de Gafsa et de Hajeb Layoun– Jilma. Rapport final de coopération scientifique et technique. Projet AIEA. Code: TUN/8/012, 70p.

Appendices

List of appendices

Appendix 1 Annual rainfall (from 1968 to 2017) at the seven rain gauge stations in HJB	1
Appendix 2 Wells characteristics	3
Appendix 3: Water level historics and abstraction.....	5
- Appendix 3.1: Water level historics	
- Appendix 3.2: Water abstraction	
Appendix 4: Field trip and laboratory materials.....	11
- Appendix 4.1: <i>laboratory materials</i>	
- Appendix 4.1: Pumping test (August 2019)	
- Appendix 4.2: Field trip	
- Appendix 4.3: laboratory analysis	
Appendix 5 Top, Bottom and thikness of aquifers.....	4

Liste of Publications

Arciles

<p>[1] Aouiti, S., Hamzaoui Azaza, F., El Melki, F., Hamdi, M., Celico, F., Zammouri, M. Groundwater quality assessment for different uses using various water quality indices in semi-arid region of central Tunisia. <i>Environ Sci Pollut Res.</i> https://doi.org/10.1007/s11356-020-11149-5</p>	IF= 4.223
---	------------------

Book chapter

<p>[1] Aouiti, S., Hamzaoui Azaza, F., Zammouri, M., Hamdi, M., Celico, F. Water Quality Assessment of the Shallow and Deep Aquifers of Hajeb Layoun-Jelma Basin (Central Tunisia). https://doi.org/10.1007/978-3-030-51210-1_264</p>
<p>[2] Aouiti, S., Hamzaoui Azaza, F., El Melki, F., Hamdi, M., Celico, F., Zammouri, M. Assessment of groundwater abstraction for irrigation practices using FAO-CROPWAT model and GIS: Case study of Hajeb Layoun-jelma basin (Central Tunisia)</p>
<p>[3] Aouiti, S., Troudi, N., Hamzaoui Azaza, F., Hamdi, M., Celico, F., Zammouri, M. Irrigation Water Quality Index (IWQI) for evaluation of groundwater suitability in the agricultural domain: case of Hajeb Layoun Jelma Basin (Central Tunisia)</p>

Congress

Oral presentation	
Eau et Terre 4 (Algeria, 16-18 May 2016)	<p>[1] Aouiti, S et Zammouri, M. Evaluation de l'impact du changement climatique sur l'etat des ressources en eau souterraine du bassin de Hajeb El Ayoun-Jelma (Tnunsie Centrale).</p>
AGIC2019 (Hammamet)	<p>[2] Aouiti, S., Hamzaoui Azaza, F., Zammouri, M., Celico, F., Hamdi, M. Vulnerability assessment using combined remote sensing and GIS. Case study of the shallow aquifer of Hajeb Layoun-Jelma basin (Central Tunisia).</p>
EMCEI 2019 (Sousse, 10-13 Octobre)	<p>[3] Aouiti, S., Hamzaoui Azaza, F., Zammouri, M., Hamdi, M., Celico, F. Water quality assessment of the shallow and deep aquifers of Hajeb Layoun-Jelma basin (Central Tunisia)</p>
WEN 2020 (online, 2-4 december)	<p>[4] Aouiti, S., Hamzaoui Azaza, F., El Melki, F., Hamdi, M., Celico, F., Zammouri, M. Assessment of groundwater abstraction for irrigation practices using FAO-CROPWAT model and GIS: Case study of Hajeb Layoun-jelma basin (Central Tunisia)</p>
EMCEI 2021	<p>[5] Aouiti, S., Troudi, N., Hamzaoui Azaza, F., Hamdi, M., Celico, F., Zammouri, M. Irrigation Water Quality Index (IWQI) for evaluation of groundwater suitability in the agricultural domain: case of Hajeb Layoun Jelma Basin (Central Tunisia).</p>
Poster	
AGIC2019 (Hammamet)	<p>[1] Aouiti, S., Hamzaoui Azaza, F., Zammouri, M., Celico, F., Hamdi, M. Pollution potential assessment using GIS-based DRASTIC model in the shallow aquifer of Hajeb Layoun-Jelma basin (Central Tunisia).</p>

Appendix 1 Annual rainfall (from 1968 to 2017) at the seven rain gauge stations in HJB

Hydrologic year	Station						
	HAJ EB EL AYOUN DEL	CEBALA DELEGATION	NEGADA	OUM LADHAM	Jelma Her	JEL MA AGRO COMBINA	Jbel Mrhilla
1968	229.3	-	-	162.3	-	-	-
1969	1297.5	-	-	629.8	731.9	-	-
1970	190.6	-	-	124.5	16.5	-	-
1971	255.3	-	-	211.6	207.8	-	-
1972	399.9	-	-	-	-	-	-
1973	276.3	-	-	273.0	174.8	-	-
1974	-	-	-	-	231.6	-	-
1975	198.1	-	-	400.8	289.9	-	-
1976	-	-	230.9	-	272.1	242.3	-
1977	191.3	-	170.0	195.8	180.3	264.7	-
1978	256.2	-	269.8	226.1	261.6	231.1	-
1979	263.2	-	-	260.5	193.6	248.1	-
1980	157.6	-	130.5	132.8	103.1	126.5	-
1981	-	-	200.9	-	153.0	120.0	-
1982	255.3	-	190.7	146.9	197.9	190.3	-
1983	292.3	-	155.5	157.4	198.9	203.4	-
1984	332.2	-	235.8	-	253.5	222.1	-
1985	192.9	-	246.8	207.5	168.6	132.6	-
1986	295.1	-	197.7	177.5	197.0	117.0	-
1987	158.9	-	114.7	97.0	149.0	95.0	-
1988	-	-	149.3	153.1	154.4	185.5	-
1989	531.8	-	336.6	387.2	371.0	368.5	-
1990	278.7	-	240.0	196.0	257.4	251.8	-
1991	452.0	-	-	297.9	315.0	254.5	-
1992	352.8	252.2	187.1	243.0	221.6	257.9	-

1993	242.6	158.5	150.8	143.4	158.8	141.8	-
1994	348.7	169.0	161.8	203.2	143.5	148.7	-
1995	612.6	324.0	330.7	251.1	248.6	247.7	86.5
1996	234.5	-	133.6	104.3	-	140.4	358.5
1997	512.0	263.5	124.1	-	285.4	-	157.7
1998	276.0	206.0	242.3	204.5	161.4	229.8	281.5
1999	264.5	-	208.0	170.9	210.4	215.9	227.8
2000	173.0	53.0	100.5	99.3	111.4	84.0	151.0
2001	231.0	148.0	183.5	139.4	217.0	255.4	133.2
2002	348.0	247.5	266.5	247.1	346.4	361.1	195.9
2003	340.5	-	328.7	205.7	367.4	428.7	376.4
2004	346.0	298.0	165.9	180.6	178.8	203.1	258.5
2005	396.5	300.5	266.5	241.0	281.1	230.8	130.9
2006	343.0	247.0	250.6	232.0	288.1	-	327.5
2007	194.5	47.5	-	46.0	166.6	-	-
2008	372.8	255.0	311.0	255.5	315.3	288.5	75.5
2009	205.4	181.0	225.3	173.0	192.3	150.1	438.1
2010	504.9	223.0	419.3	85.5	-	257.8	194.5
2011	216.8	197.0	178.5	-	123.7	169.9	495.8
2012	151.0	166.0	196.3	-	191.5	203.0	-
2013	339.5	396.5	346.0	331.1	389.8	217.0	99.7
2014	259.0	266.5	223.7	273.9	261.5	228.0	294.3
2015	189.5	147.5	123.8	168.7	135.0	21.5	176.3
2016	-	193.6	-	-	-	277.0	135.5
2017	-	268.0	-	-	217.5	-	259.1

Appendix 2 Wells characteristics

N°IRH	Creation date	X (UTM)	Y(UTM)	Total depth	Screen	Transmissivity (m²/s)
17847/4	janv-85	526712.954	3904785.772	550	385-432	0.49*10-3, 0.78*10-3
18971/4	avr-91	539678.986	3915710.609	300	218-290	3.05×10-3, 4.8 ×10-3, 6.4×10-3
19798/4	juil-91	536763.842	3888355.112	230	118-178	
19214/4	juil-93	544347.309	3922170.641	381	280-370	0.63×10-3,1.43×10-3,1.78×10-3
14925/4	mai-74	539638.091	3915710.428	287	194-270	1×10-3, 1.32×10-3
18306/4	avr-86	544727.086	3908601.222	152	110-140	2.2×10-2,2.14×10-2,2.26×10-2
18060/4	déc-87	534993.019	3922528.516	266	183.3-243	0.58×10-2, 0.73×10-2, 0.96×10-2
17442/4	oct-81	529655.538	3918467.09	333	287-327	1.35×10-2
18823/4	janv-90	523485.25	3903376.67	800	654-719.5	3.92×10-3, 3.41×10-3, 5.35×10-3
19053/4	août-91	529841.225	3910936.289	535	467-527	
10417/4	févr-63	547 561.936	3 918 305.302	182	111.8-183.3	
15984/4	juil-77	537 240.353	3 902 585.594	268	148-248.14	3.05×10-2, 4×10-2
14008/4	déc-71	548 266.800	3917628.944	200	143-192	6.8 10-2
19038/4	mai-93	543131.045	3919873.007	340	232-304	2.04×10-2, 1.04×10-2
16641/4	févr-81	547 024.747	917 892.308	200	140-195	1.04×10-2, 1.08×10-2, 1.57×10-2
17690/4	mars-82	546805.777	3918029.856	220	175-208	2.2×10-2, 1.85×10-2, 1.57×10-2
18561/4	mai-88	538844.986	3919450.795	380	292-352	1.11×10-2, 1.35×10-2, 1.79×10-2
17822/4	sept-83	542 279.204	906 190.176	172	106-150.47	7.02×10-2, 7.21×10-2, 7.24×10-2
17790/4	oct-83	540 096.078	3 903 224.508	300	86.91-152.24	3.83×10-2,5.58×10-2, 3.86×10-2
10923/4	déc-68	549 921.076	3 917 247.681	169	111.5-163.5	
10928/4	mai-64	550 591.351	3 916 613.841	194	147-182	
7621/4	janv-53	520 836.977	3 895 535.020	697	405.8-423.5	
11758/4	janv-67	549 737.546	3 920 801.501	170	76-147	
11767/4	févr-67	553 520.649	3 916 993.175	283	107-204	
9156/4	mai-54	542 969.090	3 919 967.946	520	251-323.7	

10418/4	nov-62	549 355.763	3 916 203.672	120	38-90	
18848/4	mai-90	524211.031	3892149.841	240	152-227	2.12×10-3, 4.83×10-3, 6.74×10-3
19577/4	sept-98	525050.907	3912014.741	716	621-673.4	
17791/4	oct-83	519915.401	3892471.802	200	160-192	2.6 10-2 , 3.66 10-2
3590/4		549 604.052	3 917 204.408	300	75-88	
5336/4	mars-46	548 664.760	3 917 900.926	323	66.51-120	
5336 b/4	déc-61	548 659.200	3 917 900.384	125	75-85, 90-100, 110-125	
19507/4	févr-97	552469.087	3915477.622	150	44.8-50.4, 89.6- 90.2,90.2-123.8	
18741/4	oct-87	557 992.734	3 914 893.143	141	102.3-125.2	
16244/4	1978	547 024.748	917 892.309			
7024/4	janv-51	536 014.176	3 912 502.693	788	303-365	
15980/4	août-77	541 474.309	3 906 162.342	177	122-162	
3396/4	nov-74	536993.018	3902314.046	300	55.6-79.5	
7809/4	juin-53	542 022.274	3 912 781.357	160	95-156	
16247/4	févr-79	548620.845	3 917997.501	239	108.6-188.8	1.95×10-2 , 1.69×10-2 , 2.44×10-2
18914/4	sept-89	519 909.658	3 892 289.076	200	160-190	
13272/4	juin-69	544 725.936	3 908 546.579	170	100-140	
13740/5	déc-71	536 171.285	3 900 265.375	446	80-144	
18529/4	déc-86	550 533.414	3 916 412.269	196	145-181	3.5×10-2,3.7×10-2,4.2×10-2
19049/4	mai-91	546 735.584	3 917 796.261	250	160-237	
6648/4	août-42	549 572.288	3 917 495.160	91.23	67.48-89.27	
10009/4	sept-62	538 804.137	3 919 796.939	396	293-346	
17737/4	oct-83	539744.04	3910270.955	650	597-646	3.76×10-2, 5.49×10-2,5.44×10-2

Appendix 3: Water level historics and abstraction

Appendix 3.1: Water level historics

Beglia aquifer

	PZ.1	PZ.2	PZ.3	PZ.4	PZ.5	PZ 24 Lassouda	pz ouled hadjel	PZ10
Altitude	359.93	362.98	432.06	351.29	384.09	378	397.2	353
Screen	90-115	204-224	115-170	60-79.8	123-138			
X(UTM)	545616.800	539111.400	531663.300	549486.600	540849.800	540897.820	543645.840	536331.190
Y(UTM)	3914804.000	3915413.000	3916573.000	3916618.000	3904759.000	3909776.620	3905353.290	3915302.300
1973	350.61	353.37	356.03	343.49	350.89			
1974	350.26	353.04	356.98	343.29	350.93			
1975	350.08	352.94	356.55	343.08	350.95			
1976	350.04	352.89	356.52	343.09	350.91			
1977	349.89	352.63	356.48	342.87	350.79			
1978	349.49	352.42	354.69	342.46	350.71			
1979	349.35		354.74	342.32	348.91			
1980	348.99	352.04		341.75	349.27			
1981	348.62	351.71	354.17	341.16	347.52			
1982	347.93	351.42	354.05	341.16	347.21			
1983	347.63	350.93		340.87				
1984	347.63	350.48	353.26	340.87	344.07			
1985	346.93	350.21	353.62	340.66	342.09			
1986	346.558333	349.779167	352.830833	340.685833	343.005			
1987	346.1525	349.416667	352.561667	339.7025	342.155833			
1988	345.5125	348.933333	352.281667	339.05	341.113333			
1989	344.819167	348.395	352.198333	338.65	340.3275			
1990	344.64	348.205		338.59				
1991	344.23	347.64	352.175	338.095	339.53			
1992	344.035	347.42	352.05	338.16	339.23			

Appendix 3: Water level historics and abstraction

Appendix 3.1: Water level historics

1993	343.545	346.95	351.95	337.3	338.915			
1994	342.805	346.175	351.775	337.01	338.405			
1995	342.08	345.44	351.755	336.47	336.995			344.05
1996	341.96	345.535		336.405				
1997	341	344.83	351.4	335.7	336.2			
1998	340.74	344.1	351.195	334.99	336.075			343.8
1999	339.875	343.745	350.88	333.955	335.425			342.66
2000	339.335	343.165	350.705	333.175	335.27			
2001	338.5	341.915	350.25	332.9				341.565
2002	337.675	341.665	349.94	331.92				340.435
2003	337.535	341.295	349.875	332.29				340.155
2004	336.95	340.89		331.54				339.835
2005	335.93	340.665		330.78				339.21
2006	335.62	339.445		330.48				338.43
2007	335.06	338.935		330.195				337.9
2008	334.19	338.31		329.315				336.94
2009	333.66	337.465		328.98		361.225	381.425	336.485
2010	332.615	336.275		328.045		361.105	380.31	334.91
2011	332.205	335.67		327.75		360.845	379.785	335.125
2012								
2013								
2014	328.815	332.54	346.81	325.24				331.61
2015	327.27	329.63	347.68	323.935				330.495
2016	327.08	328.13	346.835	323.73				329.545
2017	325.4	323.82		322.19				328.3
2018	323.23	325.58	345.46	320.47				326.8

Appendix 3: Water level historics and abstraction

Appendix 3.1: Water level historics

 Shallow aquifer

N° puits	PZ12	PZ15	PZ16	PZ17	PZ18	PZ20	PZ21	PZ22	PZ23	PZ24	Pz24	PZ25	pz felta	Pépinière	PzNouail 2
		13976/4	13977/4	13978/4	18318/4	18727/4	19495/4	19479/4	19976/4	18977/4	19577/5	20057/5			
X															
Y															
Elevation	443	346	309	302	305	346	336	326	363	355	321	351	326		
1973	423.97	342.39	299.37	293.17											
1974			299.32												
1975	424.89	342.34	299.4	293.66											
1976	425.01	342.35	299.6	294.35											
1977	425.06	342.07	299.09	293.18											
1978	425.01	341.91	298.28	292.36											
1979	424.84	341.74	298.02												
1980	424.8	341.71	297.7												
1981		341.18	297.3	291.02											
1982		341.06	297	290.22											
1983															
1984		340.76		289.8											
1985		340.83	295.94	290.55											

Appendix 3: Water level historics and abstraction

Appendix 3.1: Water level historics

1986		340.925 833	296.15	290.401 667										
1987		340.498 571		289.516 667	288.64	331.07	326.1	314.35						
1988			295.154 167		288.665 833	330.94 25	325.550 833	314.161 667						
1989				288.55	289.367 5	330.28 25	324.415	313.915						
1991					293.01	329.71 5	323.35	313.275	349.6 2	336.4 05				
1992					292.29	328.98 5	322.57	313.055	349.2 5	336.1 05				
1993					292.29	328.67	321.985	312.89	349.0 1	335.8 75				
1994					290.125	327.93	321.04	312.14	348.4 5	335.1 3				
1995					290.92	327.25	320.515		347.7 55	334.8		339.8		
1996					292.185	327.07 5	320.625		347.7 1	334.7 5		340.4 6		
1997					289.69	326.14 5	318.74		347.1 5	333.6 95		339.1 35		
1998					290.49	325.52	318.33		347.1 7	332.9 65		339.2 1		
1999					289.17	324.79 5	318.145		346.3 05	332.2 65		339.0 05		
2000					288.725	324.57 5			346.0 05	331.5 4		338.0 3	310.3 95	
2001					288.085	323.51 5	315.99		344.7 75	329.8 95		337.3 15	309.5 85	4.92

Appendix 3: Water level historics and abstraction

Appendix 3.1: Water level historics

2002					288.61	322.89 5	315.615		344.1 75	329.5 4		336.4 8	308.5 5	5.555	
2003					290.355	322.53	317.185		344.1 25	329.2 85	306.7 2	336.6 5	309.4 5	5.555	46.25 5
2004														6.42	46.62
2005					291.69	321.9	316.03				293.5 2	335.6 7	307.9 9	7.06	47.32 5
2006					291.41	320.76	315.03			327.2 2	293.5 2	336.0 6	307.7 7	7.32	47.33
2007					289.645	320.15	314.01			326.4 65	304.8 75	335.9	307.3 45	7.75	48.1
2008					287.405	319.41	314.01				304.3 4	334.9 25	306.1 05	8.37	48.78
2009					289.39	318.88	311.77			325.6 6			306.4 15	8.48	49.09 5
2010					286.445	317.81 5	309.05			324.4 85			304.2	9.605	49.88 5
2011														9.815	50.28 5
2014					287.02	314.35 5				321.8			303.9		
2015					286.67	313.18							302.4 15		
2016													299.8 25		
2017						310.45						327.7	295.3 85		
2018										330.2 5			293.3 5		

Appendix 3: Water level historics and abstraction

Appendix 3.2: Water abstraction

	Year	1973	1980	1985	1990	1995	2000	2005	2010	2015	2018	2019
Deep aquifer	Wells		14	17	20	22	25	46	57	74	137	137
	Exploitation (10 ⁶ m ³)	6.83	10.03	14.54	15.3	19.06	21.2	26.4	27.1	28.4	33.4	28.15
	Ressources	27.8	27.8	27.8	27.8	27.8	27.8	27.8	27.8	27.8	27.8	27.8
	Taux d'exploitation(%)	24.5683453	36,08	52,3	55,04	68,56	76,26	95,5	97,48	102,2	120.143885	101.258993
Shallow aquifer	Wells	226	450	821	1359	1621	1866	2313	2314	2332	2444	2446
	Exploitation (10 ⁶ m ³)	3.5	4.59	8.64	14.3	17.05	19.63	20.36	21.97	22.15	20.94	20.96
	Ressources	15	15	15	15	15	15	15	15	15	15	15
	Taux d'exploitation(%)		30,6	57,6	95,33	113,66	130,86	135,7	144,9	147,6	139.6	139.733333
	Total	10.33	14.62	23.18	29.6	36.11	40.83	46.76	49.07	50.55	54.34	

Appendix 4: Field trip and laboratory materials

Appendix 4.1 : laboratory materials



Appendix 4: Field trip and laboratory materials

Appendix 4.2: Pumping test measurements (August 2019)

Shallow well: Monji Rachdi (Q=3L/S , Depth= 12 m, Mrg=20 cm and SL=8.6)					
Drawdown		Recovery			
Time (minutes)	SL (m)	Time (minutes)	SL(m)		
1	8.62	1	9.09	42	8.84
2	8.64	2	9.09	43	8.8
3	8.65	3	9.09	44	8.8
4	8.67	4	9.085	45	8.7
5	8.69	5	9.08	47	8.7
7	8.71	6	9.07	48	8.6
9	8.73	7	9.065		
11	8.75	8	9.06		
13	8.78	9	9.05		
15	8.8	10	9.04		
17	8.82	11	9.03		
19	8.85	12	9.02		
21	8.87	13	9.01		
23	8.88	14	9		
25	8.9	15	8.99		
27	8.92	16	8.97		
29	8.94	17	8.97		
31	8.96	18	8.96		
33	8.98	19	8.95		
35	8.99	20	8.95		
37	9.01	21	8.94		
39	9.03	22	8.94		
41	9.03	23	8.94		
43	9.04	24	8.93		
45	9.05	25	8.93		
47	9.06	26	8.92		
49	9.07	27	8.92		
51	9.08	28	8.91		
53	9.09	29	8.91		
55	9.1	30	8.9		
57	9.1	31	8.9		
63	9.11	32	8.89		
		33	8.89		
		34	8.88		
		35	8.87		
		36	8.87		
		37	8.865		
		38	8.86		
		39	8.86		
		40	8.85		
		41	8.85		

Appendix 4: Field trip and laboratory materials

Appendix 4.2: Pumping test measurements (August 2019)

Shallow well: Faiza ben mokhtar ($Q=4L/S$, Depth (m) = 14, Mrg=20 cm and SL=8.5)					
Drawdown		Recovery			
Time (minutes)	SL (m)	Time (minutes)	SL (m)		
1	8.57	1	9.87	36	9.22
2	8.6	3	9.81	37	9.21
3	8.67	4	9.8	38	9.2
4	8.72	5	9.75	39	9.1
5	8.79	6	9.74	40	9.15
6	8.84	7	9.71	41	9.1
8	8.89	8	9.7	42	9
10	8.95	9	9.68	43	8.98
12	9	10	9.66	44	8.86
14	9.06	11	9.64	45	8.83
15	9.11	12	9.62	46	8.76
16	9.18	13	9.6	47	8.67
17	9.23	14	9.59	48	8.6
18	9.29	15	9.54	49	8.5
19	9.42	16	9.48		
20	9.42	17	9.48		
21	9.51	18	9.47		
22	9.6	19	9.46		
23	9.7	20	9.45		
24	9.8	21	9.43		
25	9.86	22	9.39		
26	9.92	23	9.38		
		24	9.37		
		25	9.37		
		26	9.36		
		27	9.34		
		28	9.32		
		29	9.31		
		30	9.3		
		31	9.28		
		32	9.26		
		33	9.25		
		34	9.24		
		35	9.23		

Appendix 4: Field trip and laboratory materials
Appendix 4.2: Pumping test measurements (August 2019)

Appendix 4.3 : *Field trip*



Appendix 4.4 laboratory analysis

n	Nom	T (°C)	PH	C25°C	Salinity	O ₂	Na ⁺	Ca ²⁺	Mg ²⁺	K ⁺	Cl ⁻	HCO ₃ ³⁻	SO ₄ ²⁻
1	F1	21.3	7.23	1746	0.8	6.43	6.96	2	4.36	0.15	9.78	2.1	0.33
2	F2	18.5	7.14	1680	0.8	6.8	6.57	1.89	4.24	0.15	7.61	4.1	0.27
3	F3	23.5	7.23	1667	0.7	5.09	6.02	1.97	3.65	0.12	8.7	2.05	0.21
4	F4	24.3	7.15	1803	0.8	6.55	6.29	2.01	0.04	0.13	5.78	1.58	0.37
5	F5	20.8	7.26	3170	1.7	4.87	13.42	2.78	10.1	0.19	20.65	1.55	2.19
6	F6	24.6	7.52	1888	0.8	6.23	6.43	1.93	4.25	0.19	10.87	1.05	0.26
7	F7	21.1	7.66	2420	1.2	7.44	9.75	2.38	5.53	0.26	14.13	2.53	0.15
8	F8	14	7.9	1149	0.5	10.37	5.37	1.55	2.45	0.11	8.7	1.58	0.28
9	F9	13.1	8.45	1187	0.4	9.33	1.88	1.1	2.43	0.11	5.43	0.53	0.13
10	F10	28.5	7.8	1287	0.4	6.4	5.2	1.12	1.92	0.33	7.61	1.58	0.18
11	F11	20.5	7.98	393	0.2	7.6	0.76	1.09	0.79	0.06	2.35	0.53	0.1
12	F12	18.5	8.04	608	0.1	7	1.05	1.05	1.55	0.08	2.32	1	0.15
13	F13	22.1	7.78	966	0.3	6.07	2.96	0.29	2.45	0.09	4.35	1.05	0.23
14	F14	26.7	7.6	1792	0.7	5.65	6.01	1.93	3.95	0.13	9.78	2.1	0
15	S1	14.4	7.96	1825	1.3	12.5	8.16	2.25	7.6	0.51	9.81	5	1.98
16	S2	10.3	8.12	3130	1.4	8.9	9.94	3	8.52	0.18	17.04	2.1	1.42
17	S3	24.8	7.7	2630	1.3	7.4	11.24	2.08	4.74	0.3	15.22	2.1	0.17
18	S4	15.3	7.7	1879	1	7.2	8.85	2.26	5.18	0.15	13.04	1.05	0.63
19	PS1	16.4	7.63	3200	2	9.67	16.46	2.7	7.18	0.45	25	0.53	0
20	PS2	18.2	7.75	9770	6.5	9.43	46.74	3.52	10.7	0.12	49.82	3.55	1.93
21	PS3	21.3	7.74	2620	1.1	11.2	12.38	2.06	5.74	0.13	9.78	3.75	4.9
22	PS4	15.8	8.24	2270	1.3	9.72	7.98	2.5	6.51	0.12	16.7	1.05	0.1
23	PS5	17.6	8.05	1544	0.7	9.73	6.2	1.89	3.44	0.14	9.61	1.58	0.03
24	PS6	22.4	7.78	4070	2.2	5.73	18.88	2.52	12.2	0.24	26.09	3.65	0.94
25	PS7	18.4	7.75	2970	1.7	6.6	14.32	2.63	7.8	0.29	20.65	1.05	0.04
26	PS8	24.4	7.68	2860	1.4	7.67	11.4	2.3	7.03	0.23	14.13	3.98	0.9
27	PS9	17.5	8.12	2440	1.4	9.48	12.38	2.27	6.64	0.21	16.3	4.05	0.07
28	PS10	18.7	8.03	2740	1.5	9.88	11.69	2.42	6.86	0.18	15.13	1.9	2.28

Appendix 5 Top, Bottom and thickness of aquifers

Wells	X(UTM)	Y(UTM)	Elevation	Layer
17442	529655.54	3918467.09	485	1
17442	529655.54	3918467.09	455	2
17442	529655.54	3918467.09	255	3
17442	529655.54	3918467.09	158	4
17442	529655.54	3918467.09	152	4
17598	539538.09	3919852.37	378	1
17598	539538.09	3919852.37	315	2
17598	539538.09	3919852.37	78	3
17598	539538.09	3919852.37	-122	4
17598	539538.09	3919852.37	-192	5
17598	539538.09	3919852.37	-274	5
17212	541534.19	3913475.23	348	1
17212	541534.19	3913475.23	338	2
17212	541534.19	3913475.23	208	3
17212	541534.19	3913475.23	-152	4
17212	541534.19	3913475.23	-244	5
17212	541534.19	3913475.23	-325	5
17737	539744.04	3910270.96	370	1
17737	539744.04	3910270.96	365	2
17737	539744.04	3910270.96	280	3
17737	539744.04	3910270.96	-276	4
17737	539744.04	3910270.96	-290	4
17847/4	526712.95	3904785.77	430	1
17847/4	526712.95	3904785.77	425	2
17847/4	526712.95	3904785.77	130	3
17847/4	526712.95	3904785.77	-122	3
18060	534993.02	3922528.52	420	2
18060	534993.02	3922528.52	413	3
18060	534993.02	3922528.52	170	4

18060	534993.02	3922528.52	154	4
18823	523485.25	3903376.67	425	1
18823	523485.25	3903376.67	414	2
18823	523485.25	3903376.67	-221	3
18823	523485.25	3903376.67	-310	4
18823	523485.25	3903376.67	-321	5
18823	523485.25	3903376.67	-375	5
17706	542273.06	3911629.99	365	2
17706	542273.06	3911629.99	277	3
17706	542273.06	3911629.99	-75	4
17706	542273.06	3911629.99	-155	5
17706	542273.06	3911629.99	-235	5
18306	544727.09	3908601.22	385	1
18306	544727.09	3908601.22	373	2
18306	544727.09	3908601.22	275	3
18306	544727.09	3908601.22	230	3
19105	550824.63	3911412.07	391	6
19105	550824.63	3911412.07	229	6
19049	546735.58	3917796.26	345	1
19049	546735.58	3917796.26	330	2
19049	546735.58	3917796.26	188	3
19049	546735.58	3917796.26	98	4
19049	546735.58	3917796.26	90	4
14008	548266.80	3917628.94	356	1
14008	548266.80	3917628.94	339	2
14008	548266.80	3917628.94	213	3
14008	548266.80	3917628.94	156	4
14008	548266.80	3917628.94	146	4
3412	552804.26	3913096.64	375	6
3412	552804.26	3913096.64	149	6

16247	548620.85	3917997.50	308	1
16247	548620.85	3917997.50	287	2
16247	548620.85	3917997.50	252	3
16247	548620.85	3917997.50	89	4
16247	548620.85	3917997.50	69	4
10928	550591.35	3916613.84	349	1
10928	550591.35	3916613.84	319	2
10928	550591.35	3916613.84	225	3
10928	550591.35	3916613.84	210	4
10928	550591.35	3916613.84	203	5
10928	550591.35	3916613.84	155	5
11767	553520.65	3916993.18	295	1
11767	553520.65	3916993.18	250	2
11767	553520.65	3916993.18	190	3
11767	553520.65	3916993.18	20	4
11767	553520.65	3916993.18	2	4
19214/4	544347.31	3922170.64	370	1
19214/4	544347.31	3922170.64	338	2
19214/4	544347.31	3922170.64	166	3
19214/4	544347.31	3922170.64	-11	3
18850/4	530893.02	3891621.65	360	1
18850/4	530893.02	3891621.65	345	2
18850/4	530893.02	3891621.65	209	3
18850/4	530893.02	3891621.65	28	3
18848/4	524211.03	3892149.84	403	1
18848/4	524211.03	3892149.84	323	2
18848/4	524211.03	3892149.84	260	3
18848/4	524211.03	3892149.84	168	4
18848/4	524211.03	3892149.84	163	4
19798/4	536763.84	3888355.11	345	1

19798/4	536763.84	3888355.11	297	2
19798/4	536763.84	3888355.11	217	3
19798/4	536763.84	3888355.11	162	4
19798/4	536763.84	3888355.11	115	4
11578/4	530680.44	3891589.02	360	1
11578/4	530680.44	3891589.02	330	2
11578/4	530680.44	3891589.02	233	3
11578/4	530680.44	3891589.02	192	4
11578/4	530680.44	3891589.02	110	5
11578/4	530680.44	3891589.02	10	5
10426/4	531291.16	3894766.63	355	1
10426/4	531291.16	3894766.63	350	2
10426/4	531291.16	3894766.63	295	3
10426/4	531291.16	3894766.63	219	4
10426/4	531291.16	3894766.63	195	5
10426/4	531291.16	3894766.63	107	6
10426/4	531291.16	3894766.63	-90	6
19053	529841.23	3910936.29	440	2
19053	529841.23	3910936.29	-19	3
19053	529841.23	3910936.29	-95	3
18971	539678.99	3915710.61	355	1
18971	539678.99	3915710.61	329	2
18971	539678.99	3915710.61	158	3
18971	539678.99	3915710.61	55	3
13539/4	534219.82	3895557.85	341	1
13539/4	534219.82	3895557.85	321	2
13539/4	534219.82	3895557.85	181	3
13539/4	534219.82	3895557.85	19	6
13539/4	534219.82	3895557.85	-71	6
18795/5	536840.19	3899277.50	345	1

18795/5	536840.19	3899277.50	321	2
18795/5	536840.19	3899277.50	254	3
18795/5	536840.19	3899277.50	163	4
18795/5	536840.19	3899277.50	93	5
18795/5	536840.19	3899277.50	32	6
18795/5	536840.19	3899277.50	-136	6
15980/4	541474.31	3906162.34	384	1
15980/4	541474.31	3906162.34	381	2
15980/4	541474.31	3906162.34	246	3
15980/4	541474.31	3906162.34	222	4
15980/4	541474.31	3906162.34	207	4
13994/4	540261.85	3903182.92	359.87	1
13994/4	540261.85	3903182.92	317.872	2
13994/4	540261.85	3903182.92	257.87	3
13994/4	540261.85	3903182.92	195.87	4
13994/4	540261.85	3903182.92	151.87	5
13994/4	540261.85	3903182.92	54.87	6
13994/4	540261.85	3903182.92	-40.13	6
7621/4	520836.98	3895535.02	438	1
7621/4	520836.98	3895535.02	416.5	2
7621/4	520836.98	3895535.02	104.8	3
7621/4	520836.98	3895535.02	-155	4
7621/4	520836.98	3895535.02	-196	5
7621/4	520836.98	3895535.02	-259	5

*Groundwater quality assessment for
different uses using various water quality
indices in semi-arid region of central
Tunisia*

**Soumaya Aouiti, Fadoua Hamzaoui
Azaza, Fetheddine El Melki, Monji
Hamdi, Fulvio Celico & Mounira
Zammouri**

**Environmental Science and Pollution
Research**

ISSN 0944-1344

Environ Sci Pollut Res
DOI 10.1007/s11356-020-11149-5



Your article is published under the Creative Commons Attribution license which allows users to read, copy, distribute and make derivative works, as long as the author of the original work is cited. You may self-archive this article on your own website, an institutional repository or funder's repository and make it publicly available immediately.



Groundwater quality assessment for different uses using various water quality indices in semi-arid region of central Tunisia

Soumaya Aouiti^{1,2} · Fadoua Hamzaoui Azaza¹ · Fetheddine El Melki³ · Monji Hamdi⁴ · Fulvio Celico² · Mounira Zammouri¹

Received: 19 May 2020 / Accepted: 5 October 2020
© The Author(s) 2020

Abstract

The Hajeb Layoun-Jelma basin, located in the central Tunisia, is the principal source of water supply for Sidi Bouzid and Sfax region. The over-abstraction from this groundwater, since 1970, and the intensive agriculture activities led to the degradation of the water quantity and quality. The quality evaluation for this groundwater is very important tool for sustainable development and decision for water management. A total of 28 groundwater samples, from shallow, springs, and deep aquifers, were collected, storage and analyzed to evaluate its quality suitability for domestic and agriculture purposes using geographic information system and geochemical methods. For the both aquifers, the abundance of cations: $\text{Na} > \text{Mg} > \text{Ca} > \text{K}$, and of anions in the order: $\text{Cl} > \text{HCO}_3 > \text{SO}_4$. The dominant hydrochemical facies, for the shallow aquifer and springs, are Na-Cl and Ca-Mg-Cl; for the deep aquifer, the geochemical facies are Na-Cl, Ca-Mg-Cl, and Ca-Cl. The comparison of the major parameters and the chemical data with the World Health Organization standards and the national standards indicate that this groundwater is suitable for drinking, except in some samples, with high salinity concentrations. The water quality was assessed, for drinking uses, using “water quality index,” “entropy,” and “improved water quality index.” The results mentioned that the improved water quality index is the best method which indicated that the poor water quality coincide with the Na-Cl water type. The entropy method and the water quality index present the optimistic methods. The irrigation suitability assessment was made using various parameters (SAR, TH, % Na, PI, MH, KR, EC). The results revealed that the majority of samples in Hajeb Layoun-Jelma basin are not appropriate for irrigation uses.

Keywords Drinking and irrigation suitability · Quality · WHO · Tunisian standard · Quality indices · Hajeb Layoun-Jelma basin

Introduction

Water is the principal component in the earth which supports the life of all living. Groundwater is a very important source of water, specifically in the semi-arid and arid region. It supports all types of uses (drinking, irrigation, and industrial) (Hamzaoui-Azaza et al. 2020). However, groundwater is threatened by severe problems caused by natural/anthropogenic factors, such as the extensive agricultural activities, the marine intrusion, the population growth, and the industrial development (Zammouri et al. 2013). This factor engendered a degradation in the quality and the quantity of groundwater in many countries: for example, Ameer et al. (2016) found that the water quality, in the northeast Tunisia, is at poor level due to the nitrate pollution that originate from the excessive use of nitrate-rich fertilizers. Adimalla (2019) conducted a study on the effect of the rapidly urban activities (South India) on water quality and the human health risk

Responsible editor: Xianliang Yi

✉ Soumaya Aouiti
soumaya.aouiti@fst.utm.tn

¹ Faculty of Sciences of Tunis, Sedimentary Environments, Oil Systems and Reservoir Characterization Laboratory, University of Tunis El Manar, UR11 ES15, 2092 Tunis, Tunisia

² Department of Chemistry, Life Sciences and Environmental Sustainability, University of Parma, Parco Area delle Scienze 157a, 43124 Parma, Italy

³ Faculty of Sciences of Tunis, Geodynamics, Geonumerics and Geomaterials Laboratory, University of Tunis El Manar, Lab3G, 2092 Tunis, Tunisia

⁴ Commissariat Régional au Développement Agricole (CRDA), Sidi Bouzid, Tunisia

related to the nitrate and the fluoride pollution. Mnassri et al. (2018) demonstrate that the sources of the groundwater salinization (central-eastern Tunisia), which the salinity exceeding 6 g L^{-1} , originate from an anthropogenic/natural factors (dissolution of halite, precipitation of carbonate coupled with the dissolution of gypsum, evaporation, and intensive irrigation practices), and Ligavha-Mbelengwa and Gomo (2020) conducted a work investigated of factors influencing the water quality (South Africa), and it indicated that both anthropogenic and natural factors are controlling the groundwater quality of this site.

The water quality has a strong relation with the health risk (Ricolfi et al. 2020); for this, the water quality evaluation is very important and widely studied in many regions around the world (Barbieri et al. 2019; Su et al. 2019; Asadi et al. 2020).

Various methods are used for the water quality evaluation; for drinking uses, we cited the following: the “Water quality index” (WQI) (Ghouili et al. 2018), “the Entropy water quality index” (Islam et al. 2017), “the improved water quality index” (Wang et al. 2018; Zhang et al. 2020), the fuzzy logic method coupled with WQI (Moghari et al. 2015). For the irrigation uses, the evaluation of water quality is based on classic indices such as the electrical conductivity “EC,” the percent sodium “Na%,” alkalinity hazard “SAR,” and Kelly ratio “Kr.”

In Africa and specifically in Tunisia, which groundwater is practically the main water’s source in many regions, the evaluation of water quality was taking, recently, many attentions by the hydrogeologists which show that various regions are facing a decline in groundwater quality (Ghouili et al. 2018; Mnassri et al. 2018; Hamzaoui-Azaza et al. 2020).

The Hajeb Layoun-Jelma basin (HJB), which is the subject of this study, is located in central Tunisia. It is extending for over 1380 km^2 which corresponds to 0.8% of the national territory and has about 172,003 inhabitants (INS 2014), which correspond to approximately 1.54% of the Tunisian population and which was 50,306 inhabitants in 1972 (Koschel 1980). The population growth (more than three times) plays a strong effect in the water request and has a big effect on water resources. The HJB aquifer system is of importance to the economic activity of both the southern and the central part of Tunisia. The water of the deep aquifer is transported to the Sfax city located at 180 km far away from the HJB. During the last decades, the HJB presented a development of agriculture activities, which is based on the uses of fertilizers and pesticides for improving agricultural production. This development has affected significantly pressure on groundwater resources: the water extraction increases for the both aquifers (shallow and deep aquifer) from 14.8×10^6 in 1973 to $58.45 \times 10^6 \text{ m}^3$ in 2018 with almost 2328 shallow wells and 137 deep wells (DGRE 1973–2018a). These human activities have putted increasing pressure on groundwater quality of these aquifers.

In order to check the safety of HJB’s water, 28 water samples collected from shallow and deep aquifers tapping the HJB have been interpreted using statistical and geochemical methodologies to wholly understand the patterns of groundwater quality distribution. The principal aims of this research is to study the groundwater hydrochemistry and identify the purposes of water use of the HJB for either human consumption, irrigation using combined through GIS, or geochemical methods.

Study area

Site description

The Hajeb Layoun-Jelma basin located in the north-east central part of Tunisia. It is, approximately, located between $x = 35^\circ 00' 00''$, $y = 8^\circ 30' 00''$, and $x = 35^\circ 30' 00''$, $y = 9^\circ 00' 00''$ and extending for over 1380 km^2 . It comprises three regions (Sidi Bouzid, Kairouan, and Kasserine) with different occupied area; the maximum area of HJB is covered by the Sidi Bouzid region (Fig. 1). The HJB present a wide NE-SW directed syncline surrounded by various mountains; it is bordered to the north by the Labaieith mountain, to the south by the Hamra mountain, to the east by the Zaouia-Roua mountain, to the west by the Mrhilla mountain, to south-east by the Lessouda mountain, and to the south-west by the Koumine mountain (Fig. 1). The maximum altitude of HJB is 1384 m.

The HJB is characterized by semiarid climate, January presents the coldest month (mean temperature $\approx 11.8^\circ \text{C}$), and the hottest is August (mean temperature $\approx 29.4^\circ \text{C}$). The mean annual precipitation in Hajeb Layoun-Jelma basin, over the period 1972–2017, is 230 mm. The irrigation practices and the drinking supply for three regions (Sidi Bouzid, Kairouan, and Kasserine) are maintained by the water of HJB. The National Water Supply and Distribution Company (S.O.N.E.D.E) transport the water of the HJB to Sfax (Fig. 1), which is used for drinking purposes.

Geology and hydrogeology

The study area presents a geology series from Triassic to Quaternary with the missing of the Jurassic series (Fig. 2) (Koschel 1980; Jallalia et al. 2015; Thebti et al. 2018). The HJB is a collapse pan filled by Neogene and Quaternary deposits closed by anticlines (Fig. 2a).

The HJB is composed by multilayer aquifer system (Fig. 2b) (Jallalia et al. 2015; Thebti et al. 2018). The HJB is structured by various aquifer layers: the Cretaceous, the Miocene, and the Mio-Plio-Quaternary aquifers which coincide with the following local formations (from the bottom to the top):

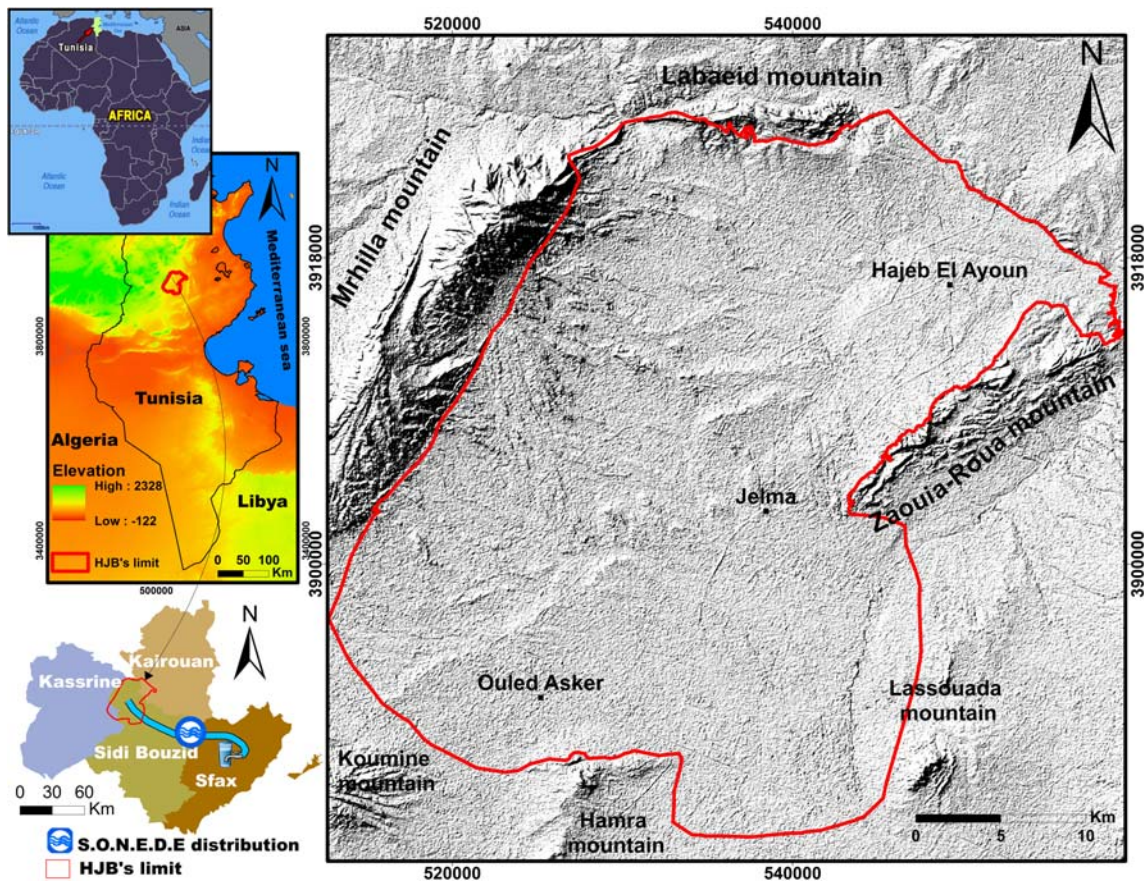


Fig. 1 Location and elevation of the HJB

Abiod, El Gueria, Ain Grab, Beglia, Segui, and Quaternary deposits. The Beglia aquifer is usually confined, due to the superimposition of the clayey Saouaf formation. However, in HJB's southern part, this aquiclude has been eroded, therefore allowing the Beglia formation to be closer to Mio-Plio-Quaternary aquifers, with an interposition of a lateritic layer (Koschel 1980). Due to the lateral discontinuity of the lateritic layer, somewhere, the Mio-Plio-Quaternary and the Beglia aquifers can interact from the hydraulic point of view (Koschel 1980).

Abstraction and piezometry

The Hajeb Layoun-Jelma basin is composed by two main aquifers (the most exploited aquifers); the shallow aquifers (Mio-Plio-Quaternary) and the first deep aquifer which coincide with the Beglia local formation.

The HJB's shallow aquifer is drilled by 2328 wells and the deep one is captured by 137 wells (DGRE 2018). The most of deep wells are located in Labaidh region, Ben Mrad region, and Felta and El Soud region. The total abstraction of HJB, in 2018, is equal to $58.45 \times 10^6 \text{ m}^3$; however, the total renewable resources are equal to $42.8 \times 10^6 \text{ m}^3$ which indicate a deficit of $15.65 \times 10^6 \text{ m}^3$ (DGRE 2018). For the shallow aquifer, in

2018, the resources are calculated by DGRE equal to $15 \times 10^6 \text{ m}^3$ and the abstraction equal to $20.94 \times 10^6 \text{ m}^3/\text{year}$ which indicate an abstraction of 140% with deficit equal to $5.94 \times 10^6 \text{ m}^3$. This over-abstraction engendered the decrease of the water quality. In fact, in the last decades, the water salinity of the shallow aquifer was increased from 0.5 to 1 g/l (DGRE 2018). This over-exploitation is manifested by the increase of the number of wells (Fig. 3a): in 1974, 226 shallow wells tapped the shallow aquifer with an extraction rate equal to $7.94 \times 10^6 \text{ m}^3/\text{year}$; in 2018, the number of wells increased to attend 2328 wells extracting a volume equal to $20.94 \times 10^6 \text{ m}^3/\text{year}$ (Fig. 3a) (DGRE 1974–2018).

The Beglia aquifer presents a good quality in many regions of HJB, which is transported, by S.O.N.E.D.E, to supply by drinking water the Sidi Bouzid and Sfax government. The S.O.N.E.D.E exploitation, of Beglia aquifer, exceeded $20 \times 10^6 \text{ m}^3/\text{year}$ (DGRE 2018). The total abstraction of this aquifer is equal to $33.4 \times 10^6 \text{ m}^3$ in 2018 (Fig. 3b) which indicate an abstraction of 120% (resources equal to $27.8 \times 10^6 \text{ m}^3$).

This over-exploitation of the both aquifers resulted in the decrease of the piezometric levels (Fig. 3c and d). For the shallow aquifer, the average yearly piezometric decline, over the period 1973–2018, equals to 0.4 m/year (DGRE 1973–

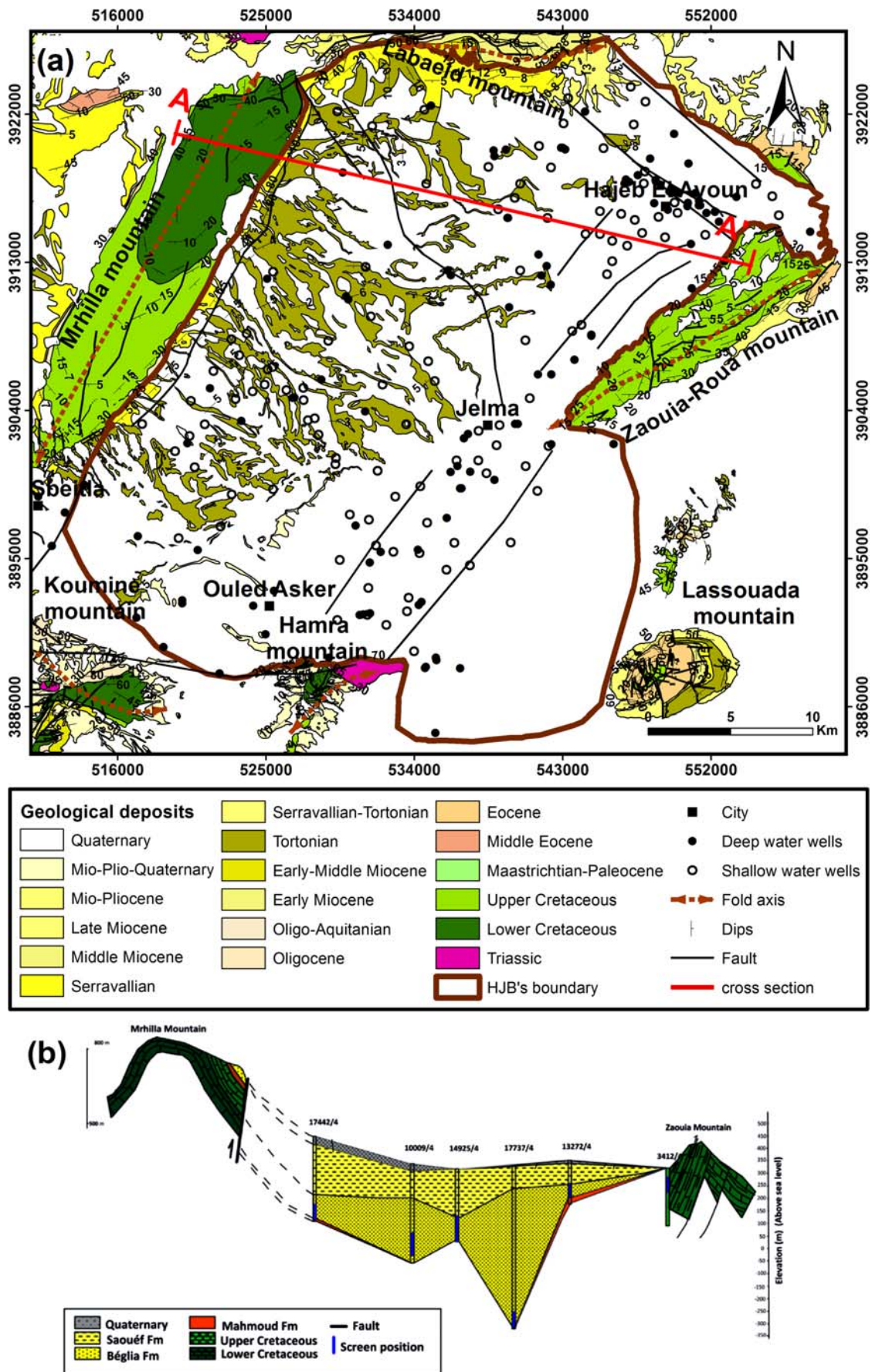


Fig. 2 a Geologic map of HJB and b cross-section showing the principal formations in HJB (based on Jallalia et al. 2015)

2018b) (Fig. 3c). For the deep aquifer, from 1973 to 2018, the over-exploitation resulted in a high total decline of piezometric levels, average equal to 29.9 m (Fig. 3d) (DGRE 1973–2018b), which signify that this aquifer has a yearly piezometric decline equal to 0.7 m/year (Fig. 3d).

For the deep aquifer, the main groundwater flow direction is from the west coming from Mrhilla Mountain (Recharge zone), toward the central part of Hajeb Layoun where groundwater is divided in two parts: the first discharges at Hajeb Layoun fault and the second at the level of some faults in the north part of Zaouia-Roua Mountain (Fig. 4). The discharge areas are manifested by springs. For the shallow aquifer, the main flow direction is from the east to the west in the south part and two direction flows in the north part: east to the west and south to the north (Fig. 4).

Land use

The land use/land cover map of Hajeb Layoun-Jelma basin, published by DGRE in 2004, shows that the main type of agriculture is the irrigated and non-irrigated annual crops of olive (Fig. 5); these types of crops need high amounts of water with the use of huge quantities of fertilizers as well as to increase production, which influence on groundwater quality. Urban areas are also a potential source of pollution: in fact, the non-treated sewage

rejected, by the ONAS (National Sanitation Office), in the natural environment of Hajeb Layoun-Jelma basin, which is estimated to an average of 400 m³ by day (DGRE 2017) can have a long-term influence on groundwater resources.

Materials and methods

Samples collection and analysis

In February 2017, a total of 28 samples were taken from wells in Hajeb Layoun-Jelma basin (humid period): 14 samples from the Beglia aquifer, 10 from the shallow aquifer (from depth of approximately 10–50 m), and 4 from springs (Fig. 5). In field, in order to avoid residual water’s influence, each well was pumped, for at least 30 min, until steady-state chemical conditions were obtained. According to the standard procedures given by Eaton (1950), the samples of HJB were collected using pre-cleaned and rinsed (distilled water and water sample) polyethylene bottles (1 L). The physical parameters (including temperature (T), pH, and electrical conductivity (EC)) were measured in the field (under minimal atmospheric contact) using handheld analyzing kits, which was calibrated first in the laboratory using standard solutions before use. After sampling, samples were labeled, taken to the

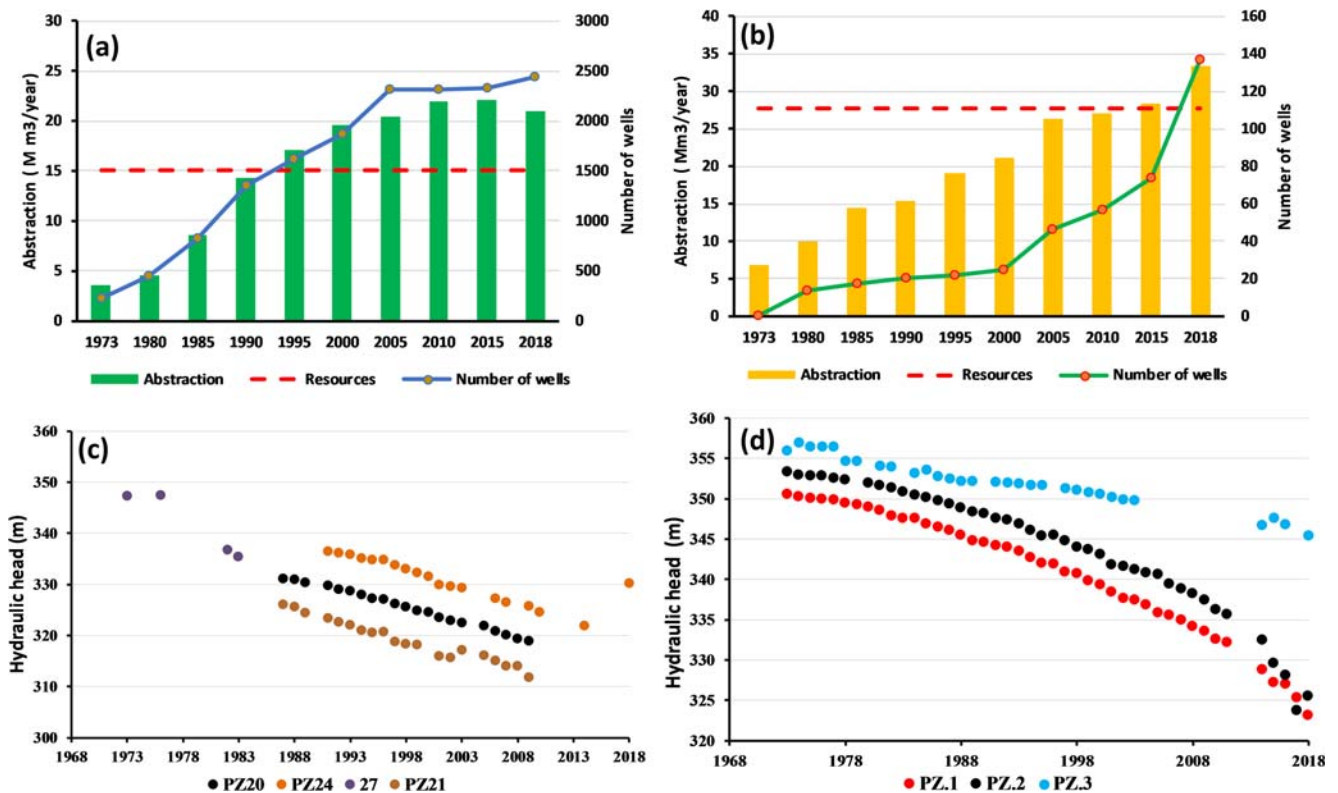


Fig. 3 Evolution of groundwater abstraction and number of wells. **a** Shallow aquifer. **b** Deep aquifer and the decline of the piezometric level. **c** Shallow aquifer. **d** Deep aquifer

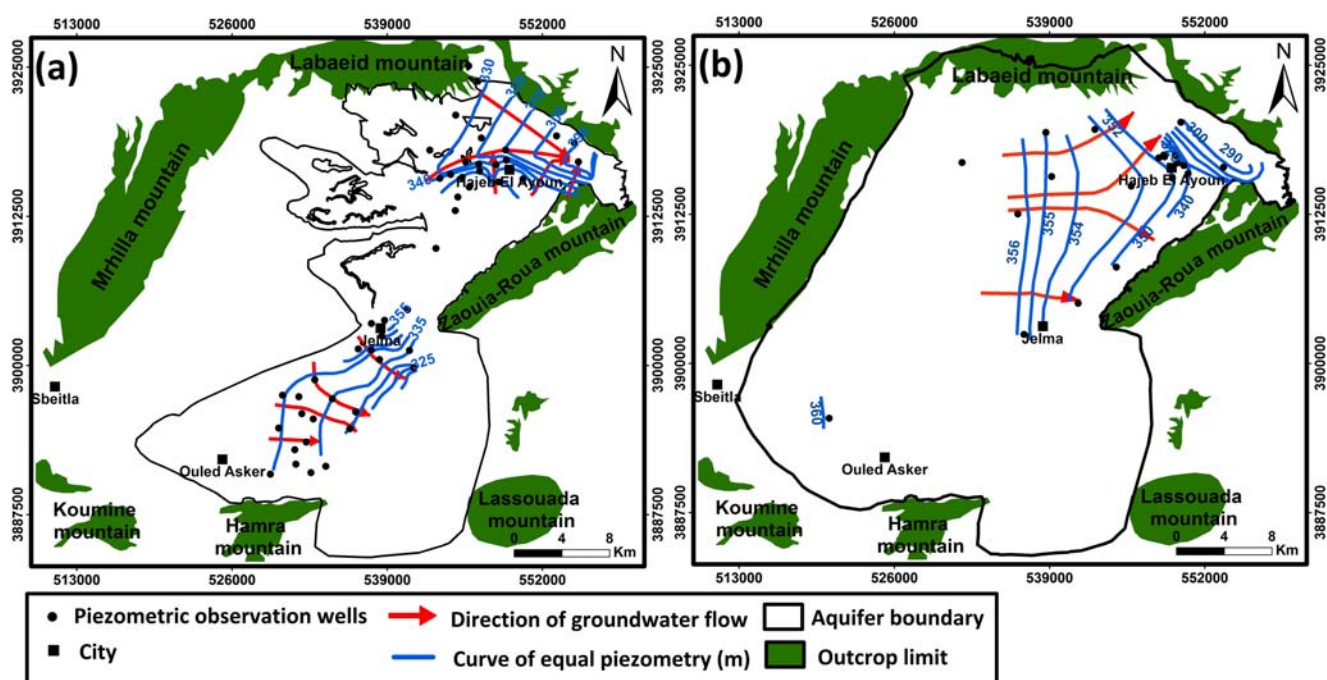


Fig. 4 Piezometric maps. a Shallow and b deep aquifers

laboratory, and stored below 4 °C. The chemical-analyzed parameters include major anions and cations (sodium (Na⁺), potassium (K⁺), calcium (Ca²⁺), magnesium (Mg²⁺), chloride (Cl⁻), bicarbonates (HCO₃⁻), and sulfate (SO₄²⁻)).

In order to validate the analysis results, the charge balance errors (%E) was calculated, for all samples, using the following formula:

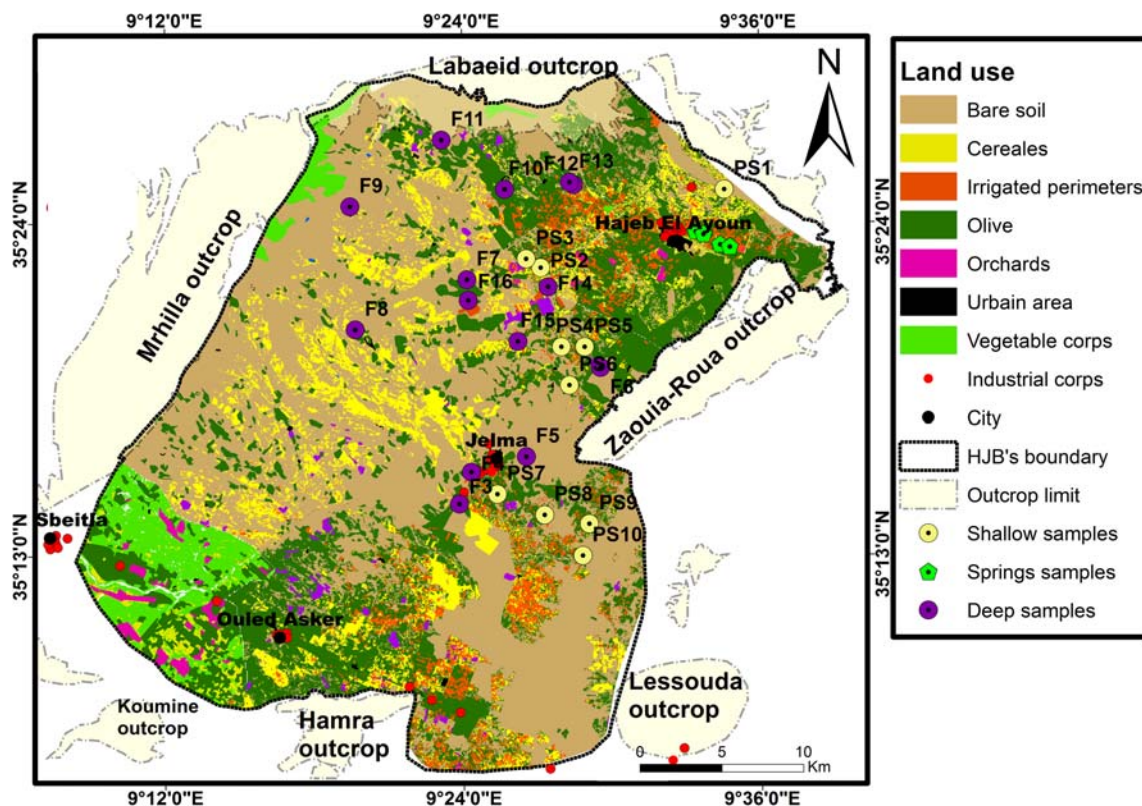


Fig. 5 Land use map of HJB extracted from the agriculture map obtained from Regional Direction of Agriculture Development of Sidi Bouzid (CRDA-Sidi Bouzid)

$$\%E = \frac{\sum C - \sum A}{\sum C + \sum A} \quad (1)$$

where C is cations in meq/l and A is anions in meq/l.

The charge balance error checking of HJB’s samples showed that the results of analysis are judged perfectly (average %E ≈ 1.59% < 5%)

Hydrochemical characterization

Conventional methods

The identification of hydrochemical processes, for the both aquifers of HJB (shallow and deep), was obtained by constructing several diagrams such as Piper diagram (Piper 1944) and Chadha diagram (Chadha 1999).

Origin of mineralization

Different reactions can be derived from the water-rock interaction, then defining the chemical water type. To understand the chemical processes, we have elaborated the correlation matrix, and also, we have established some correlations between selected major ions. These correlations can help to analyze the primary reactions that have formed current water chemistry and identify the origin of groundwater mineralization.

The Gibbs’ diagram (Gibbs 1970) was also used to understand the main mechanisms governing groundwater chemistry.

Multivariate statistical analysis

In the geochemical study, the separate study of each variable is an important phase in the analysis of chemical behavior, but it is often insufficient. Therefore, the data should be analyzed taking into account their multidimensional nature (Hamzaoui-Azaza et al. 2011).

Multivariate statistical analysis (MSA) is a multidimensional analysis widely used to identify the sources of solutes in a groundwater system and to well understanding of water quality. It allows the comparison of all samples of water and the identification of their different solutes’ origin (Hamzaoui-Azaza et al. 2011). MSA was chosen to determine the inter-data relationships of the HJB’s samples. In total, 12 physico-chemical parameters were analyzed in 28 samples collected in 2017; these variables (pH, EC, salinity, O₂, Na⁺, Ca²⁺, Mg²⁺, K⁺, Cl⁻, HCO₃⁻, and SO₄²⁻) were successfully used in principal component analysis. The parameters used in MSA referred to different units of measurement (meq/l, us/cm...), so their values should be standardized; we have used the following transformation function (Medina-Gomez and Herrera-

Silveira 2003):

$$Z = (X - \mu) / \sigma \quad (2)$$

where Z is the standardized value, X the original value of the measured parameter, μ the mean of the variable, and σ the standard deviation.

Water quality assessment

Drinking use

Standards of drinking

In order to maintain the human health, the World Health Organization (WHO) has set limit values not to be exceeded if want to respect international standards of consumption. Also, all countries, of the world, do not follow the same standards; each country has defined their propriety standards of drinking water quality, some adopt their own standards, and others choose those recommended by the WHO (2011). Tunisia has fixed national standards (NT.09.14) for the potability of the water. The difference between the Tunisian standards and WHO limits reflects the required management of water in Tunisia.

Drinking index

The assessment of suitability for drinking purpose, in HJB, was evaluated using three indices: water quality index (WQI), entropy water quality index (EWQI), and improved water quality index (ImpWQI).

Water quality index

The WQI method is frequently used to assess the drinking water’s quality (Ghouili et al. 2018; Asadi et al. 2020).

The calculation of WQI is based on the standards suggested for uses, where 9 groundwater quality parameters are considered: pH, EC, HCO₃⁻, Cl⁻, SO₄²⁻, Ca²⁺, Mg²⁺, Na⁺, and K⁺. For computing the WQI, weights (wi) are assigned for each parameter: the weight of “5” has been attributed to five parameters: EC, Mg²⁺, Na⁺, Cl⁻, and SO₄²⁻ due to their major role in quality assessment. A minimum weight equal to “1” has been given to HCO₃⁻ and k⁺ since their less significant role in quality evaluation and medium weights of 2 and 3 has been assigned to Ca²⁺ and pH.

The WQI is computing on following up the Eqs. (3), (4), and (5):

$$RWi = \frac{wi}{\sum_{i=1}^n wi} \quad (3)$$

$$Q_i = \frac{C_i}{S_i} \times 100 \tag{4}$$

$$WQI = \sum R W_i \times Q_i \tag{5}$$

where w_i is the weight for each parameter, $R W_i$ relative weight for each parameter, n number of parameters, C_i concentration of parameter i (each water sample, (mg/L)), and S_i drinking use’s standard (WHO 2011).

The ranges of water quality were determined according to the WQI; we have classified the water samples according the ranges of WQI values (Table 1). Spatial distribution of WQI values were prepared using a weighted inverse-distance interpolation (IDW) technique.

Entropy water quality index

The EWQI is widely applied to assess the drinking water’s quality (Wu et al. 2011; Islam et al. 2017).

For computing the EWQI, according to Islam et al. (2017), when m water samples ($i = 1, 2, \dots, m$) are taken to evaluate the quality and each sample is analyzed for “ n ” parameters ($j = 1, 2, \dots, n$), the following steps have been followed:

In the first step, eigenvalue matrix, A , was constructed as follows:

$$A = \begin{pmatrix} A_{11} & A_{12} & \dots & \dots & A_{1n} \\ A_{21} & A_{22} & \dots & \dots & A_{2n} \\ A_{31} & A_{32} & \dots & \dots & A_{3n} \\ \dots & \dots & \dots & \dots & \dots \\ A_{m1} & A_{m2} & \dots & \dots & A_{mn} \end{pmatrix} \tag{6}$$

After, matrix A is converted into a standard-grade matrix B (Eq. (8)) using Eq. (7).

$$\begin{cases} B_{ij} = \frac{A_{ij} - A_{ij \min}}{A_{ij \max} - A_{ij \min}} & \text{for efficiency type parameters} \\ B_{ij} = \frac{A_{ij \max} - A_{ij}}{A_{ij \max} - A_{ij \min}} & \text{for cost type parameters} \end{cases} \tag{7}$$

Table 1 Classification of groundwater quality based on WQI, EWQI, and ImpWQI

Index	< 50	50–100	100–150	150–200	> 200
Rank	1	2	3	4	5
Water quality	Excellent	Good	Medium	Poor	Extremely poor

$$B = \begin{pmatrix} B_{11} & B_{12} & \dots & \dots & B_{1n} \\ B_{21} & B_{22} & \dots & \dots & B_{2n} \\ B_{31} & B_{32} & \dots & \dots & B_{3n} \\ \dots & \dots & \dots & \dots & \dots \\ B_{m1} & B_{m2} & \dots & \dots & B_{mn} \end{pmatrix} \tag{8}$$

Then, the entropy weight (W_j), for each parameter, is calculated as follows:

$$W_j = \frac{1 - e_j}{\sum_{i=1}^m (1 - e_j)} \tag{9}$$

where

$$e_j = \frac{1}{Ln \ m} \sum_{i=1}^m P_{ij} \ln(P_{ij}) \tag{10}$$

and

$$P_{ij} = \frac{1 + B_{ij}}{\sum_{i=1}^m (1 + B_{ij})} \tag{11}$$

The rating quality is calculated for the n parameters ($j = 1, 2, \dots, n$) for all the samples, using the concentration of parameter j (C_j) and the standard limit (S_j), using the following formula:

$$q_j = \frac{C_j}{S_j} \times 100 \tag{12}$$

In this study, the rating quality is calculated based on the WHO standard (2011).

Finally, the EWQI is calculated as follows:

$$EWQI = \sum_{j=1}^m W_j \times q_j \tag{13}$$

Improved water quality index

The ImpWQI is widely used for assessing the drinking water quality (Zhang et al. 2020). For computing the ImpWQI, the first step is to determinate the weights of the different used parameters. Firstly, the data was normalized to eliminate the units’ influence. To calculate the weight of parameters, the CRITIC weighting (Zhang et al. 2020) was used (Eq. (14)–(16)).

The ImpWQI, for each sample, are calculated on following up these equations:

$$C_{ij} = \frac{\sum (a_{ij} - \bar{a}_{ij}) (b_{ij} - \bar{b}_{ij})}{\sqrt{\sum (a_{ij} - \bar{a}_{ij})^2 \times \sum (b_{ij} - \bar{b}_{ij})^2}} \tag{14}$$

$$F_j = \frac{1}{E_j} \sum_{i=1}^m (1 - c_{ij}) \tag{15}$$

$$W_j = F_j / \sum_{j=1}^m F_j \tag{16}$$

$$q_j = \frac{a_{ij}}{S_j} \times 100 \tag{17}$$

$$\text{ImpWQI} = \sum_{j=1}^m W_j \times q_j \tag{18}$$

where a_{ij} and b_{ij} are the original and the normalized data value, respectively, \bar{a}_{ij} and \bar{b}_{ij} the average of a_{ij} and b_{ij} , respectively, F_j the information amount of the j th parameter, ξ_j standard deviation of the j th parameter, c correlation coefficient, m total number of parameter, and W_j the weight of the j th parameter. q_j is the rating of the j th parameter and S_j the standard limit of the j th parameter (WHO 2011).

The obtained results from the three drinking indices were classified into five classes (Table 1).

Irrigation suitability assessment Different ionic parameters (in meq/l) were used to assess the irrigation water quality in HJB basing on various indices such as TH (total hardness) (Todd 1980), EC (electrical conductivity ($\mu\text{s}/\text{cm}$)), SAR (alkalinity hazard) (Richard 1954), Na% (percent sodium) (Wilcox 1955), MH (magnesium hazard) (Raghunath 1987), KR (Kelley ratio) (Kelly 1951), and PI (permeability index) (Doneen 1964) (Eqs. (19)–(24)):

$$\text{TH} = 2.5 \times \text{Ca} + 4.1 \times \text{Mg} \tag{19}$$

$$\%Na = 100 \times \frac{\text{Na} + \text{K}}{\text{Ca} + \text{Mg} + \text{Na} + \text{K}} \tag{20}$$

$$\text{SAR} = \frac{\text{Na}}{\sqrt{(\text{Ca} + \text{Mg})/2}} \tag{21}$$

$$\text{PI} = 100 \times \frac{\text{Na} + \sqrt{\text{HCO}_3^-}}{\text{Na} + \text{Mg} + \text{Ca}} \tag{22}$$

$$\text{Kr} = \frac{\text{Na}}{\text{Ca} + \text{Mg}} \tag{23}$$

$$\text{Mh} = \frac{\text{Mg}}{\text{Ca} + \text{Mg}} \tag{24}$$

GIS analysis

A GIS database was developed to make useful tools from available data to greater understand the functioning of HJB. Under ArcGis 10.3, a database has been established including the inventory of all deep and shallow wells implemented in different aquifers and their main characteristics (localization, year of creation, borehole depth) and

historical data (rainfall, piezometry, and withdrawals). The thematic maps, such as piezometric maps, geological maps, land use, and distribution maps of some parameters such as salinity and quality indices of study area, were obtained from 1:50000 scale and were georeferenced under the UTM coordinate system. The coordinate of each well was measured by using, in the field, a global positioning system (GPS). The spatial distribution of different indices such as salinity, WQI, EWQI, and ImpWQI were obtained by the IDW method.

Results and discussion

The steps followed, in this research, are resumed in Fig. 6.

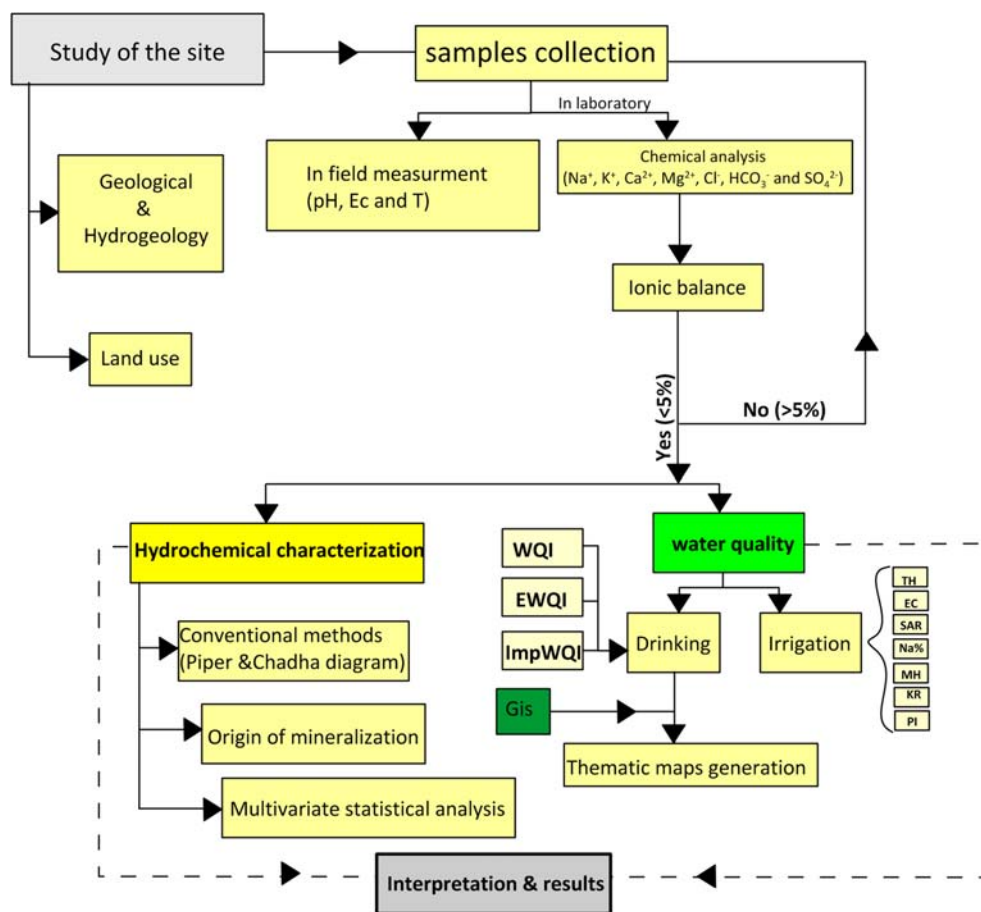
Hydrochemical data

A statistical view of hydrochemical parameters (min, max, and standard deviation) is given in Table 2. The pH data ranged from 7.15 to 8.45 and 7.63 to 8.24 for the shallow and the deep samples, respectively. These results show that the both aquifers have a pH close to neutrality with a slight tendency toward the basic composition. The temperatures are characterized by heterogeneous values varying from 10.3 to 24.8 °C and 13.1 to 30.2 °C for the shallow and the deep samples, respectively. The temperature of water depends on the well depth, with an average value and standard deviation equal to 17.9 °C and 3.97 °C, for the shallow and springs samples, and equal to 22.8 °C and 4.96 °C for the deep samples. For the shallow and springs samples, the electrical conductivity values vary from 1544 to 9770 $\mu\text{s}/\text{cm}$ with a mean of 2685 $\mu\text{s}/\text{cm}$. For the deep samples, the EC varies from 393 to 3960 $\mu\text{s}/\text{cm}$ with a mean of 1729 $\mu\text{s}/\text{cm}$.

For the both type of samples (shallow/springs and deep), the chemical analysis indicated that the abundance order of the major cations is $\text{Na} > \text{Mg} > \text{Ca} > \text{K}$. For the shallow and springs samples, the concentration of major cations, Na^+ , Ca^{2+} , Mg^{2+} , and K^+ , are ranged from 142.6 to 1075, 37.8 to 70.4, 41.8 to 148.23, and 4.68 to 19.89 mg/l with a mean value of 265.54, 47.2, 84.38, and 7.61 mg/l, respectively. For the deep samples, the cations, Na^+ , Ca^{2+} , Mg^{2+} , and K^+ , are ranged from 17.48 to 459.31, 5.8 to 55.6, 0.47 to 117.67, and 2.34 to 15.6 mg/l with a mean value of 138.35, 37.7, 35.53, and 4.88 mg/l, respectively. The order of abundance of anion is $\text{Cl}^- > \text{HCO}_3^- > \text{SO}_4^{2-}$. The abundance of these cations and anion is derived from a mineralization process, which can be natural or anthropogenic.

The groundwater salinity shows a wide variation from 100 to 1800 mg/l with a mean value equal to 700 mg/l and from 700 to 6500 mg/l with a mean value equal to 1400

Fig. 6 Flow chart showing the methodology applied in the HJB's water evaluation



mg/l for the deep and the shallow aquifers, respectively. The distribution of the salinity presented in Fig. 7 reveals that in the shallow, aquifer has high soluble salts in the totality of samples (one sample, salinity < 1 and 13 samples, salinity > 1 g l⁻¹ with one sample exceeding 6 g l⁻¹) (Fig. 7). The deep aquifer has moderate salinity: 3 samples exceeding 1 g l⁻¹ and the rest (11 samples) indicate salinity less than 1 g l⁻¹. The high salinity values would be related to the leaching of salts from soils, the use of fertilizers in agriculture activities, or/and return flow from irrigation water (Mnassri et al. 2018). This hypothesis is confirmed

by analyzing the samples that are taken from wells located in the irrigated perimeters (see Fig. 5).

Groundwater mineralization processes

Correlation of parameters

The correlation matrix of the shallow and springs samples indicated that the contents of sodium, magnesium, chloride, and calcium are high positively correlated with salinity (Table 3(a)). These positive correlations indicate the

Table 2 Statistical summary of the physical and chemical parameters of HJB samples (ionic contents in mg/l)

		T (°C)	PH	EC	Salinity	Na ⁺	Ca ²⁺	Mg ²⁺	K ⁺	Cl ⁻	HCO ³⁻	SO ⁴ ²⁻
Deep	Min	13.10	7.15	393	0.10	17.48	5.80	0.47	2.34	82.36	32.33	4.80
	Max	30.20	8.45	3960	1.80	459.31	55.60	117.67	15.60	935.43	154.33	105.12
	SD	4.96	0.35	961.82	0.52	117.60	13.09	29.16	3.89	240.49	37.09	32.80
Shallow /springs	Min	10.30	7.63	1544	0.70	142.60	37.80	41.80	4.68	341.16	32.33	1.44
	Max	24.80	8.24	9770	6.50	1075.02	70.40	148.23	19.89	1768.61	305.00	235.20
	SD	3.97	0.20	2014.12	1.41	230.09	8.38	27.55	4.71	368.03	87.15	65.05

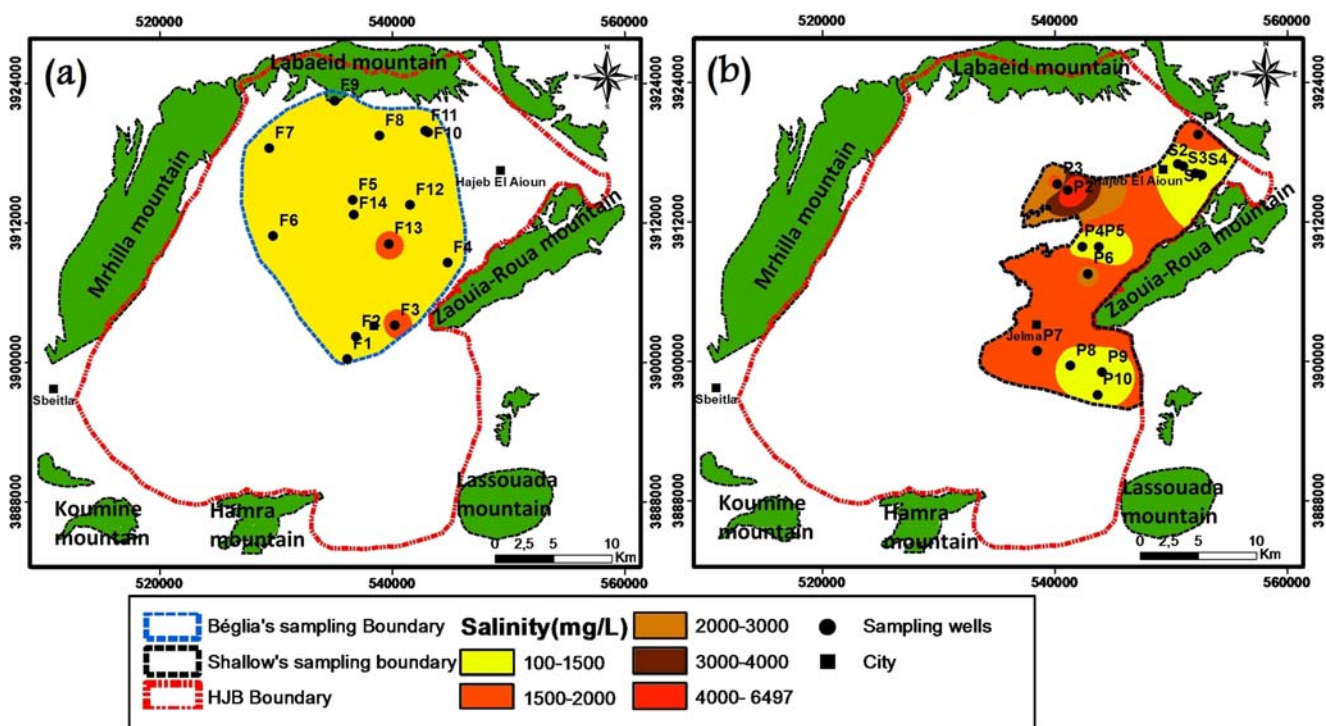


Fig. 7 Spatial distribution of salinity. a Deep and b shallow aquifer. The map was plotted using the IDW method

continuous addition of these ions along groundwater flow path. Therefore, these elements contribute to the groundwater mineralization. The concentration of Cl^- is correlated with Na^+ with a correlation index of 0.95, indicating that the halite dissolution may be the important reaction affecting the water chemistry. The electrical conductivity also shows a perfect positive correlation with Na^+ ($R = 0.98$), Ca^{2+} ($R = 0.82$), salinity ($R = 0.98$), Cl^- ($R = 0.95$), and moderately positive correlation with Mg^{2+} ($R = 0.67$).

The matrix of the deep samples (Table 3(b)) indicates that EC shows a high correlation (positive) with salinity ($R = 0.98$), Na^+ ($R = 0.97$), and Cl^- ($R = 0.96$) and moderately positive correlation with Ca^{2+} , Mg^+ , K^+ , and HCO_3^- with correlation value equal to 0.77, 0.75, 0.72, and 0.61, respectively. Na^+ also shows a high correlation index (positive) with all the major ions except SO_4^{2-} . The high correlation observed between some parameters suggests the extent of interdependence and also suggests that these ions may be derived from a common source.

Identification of water-rock interaction

To understand the main mechanisms governing groundwater chemistry, Gibbs' diagrams have been used. The weight ratios of ratio I: ($Na^+/(Na^++Ca^{2+})$) and ratio II: ($Cl^-/(Cl^- + HCO_3^-)$) are plotting as a function of total dissolved solids (TDS), representing Gibbs' diagrams. This diagram is used to identify the origin of dissolved constituents, such as rock weathering dominance, precipitation dominance, and

evaporation dominance or by combination of these influences (Gibbs 1970). According to the Gibbs' diagrams (Fig. 8), the data indicates that the chemical composition's HJB samples are governed by evaporation and rock weathering. The importance of evaporation processes and rock weathering are also confirmed by the calculation of Hounslow ratio (Cl^-/Σ anions) which indicates, for the both aquifers, two chemical sources: evaporate or brine water sources (ratios > 0.8 and TDS > 500) and rock weathering (ratios < 0.8) (Hounslow 1995).

A plot of Ca^{2+} and SO_4^{2-} shows that for the shallow samples (Fig. 9a), one sample below the line 1:1 (PS 3) indicates a deficit in Ca^{2+} , suggesting carbonate precipitation; two samples (PS10 and S1) are close to the bisector line (1:1), indicating that gypsum is the source of calcium, while the majority of samples are located above the dissolution straight line and indicated an excess in Ca^{2+} , suggesting carbonate dissolution (Fig. 9a). For the deep samples, two samples (F11 and F14) are close to the bisector line (1:1), indicating that gypsum is a source of calcium, while the majority of the water samples are located above the dissolution straight line and indicated an excess in Ca^{2+} , suggesting carbonate dissolution (Fig. 9a).

Evaporation process is also a major process in controlling the groundwater's chemistry. The both type of samples (shallow/springs and deep) represented in Fig. 9b are very close to the bisector line (1:1) of sodium against chloride's plot, suggesting that in these wells, salinity is controlled by halite dissolution.

Table 3 Pearson correlation matrix of HJB. (a) Shallow wells/springs, and (b) deep wells. Italics indicates significant 50% confidence level

	T (°C)	PH	EC	Salinity	Na ⁺	Ca ²⁺	Mg ²⁺	K ⁺	Cl ⁻	HCO ₃ ⁻	SO ₄ ²⁻
(a)											
T (°C)	1										
PH	-0.53	1									
EC	0.08	-0.26	1								
Salinity	0.03	-0.24	<i>0.98</i>	1							
Na ⁺	0.12	-0.33	<i>0.98</i>	<i>0.98</i>	1						
Ca ²⁺	-0.34	-0.05	<i>0.82</i>	<i>0.82</i>	<i>0.77</i>	1					
Mg ²⁺	-0.02	-0.11	<i>0.65</i>	<i>0.63</i>	<i>0.63</i>	<i>0.72</i>	1				
K ⁺	-0.05	-0.28	-0.22	-0.14	-0.16	-0.08	0.09	1			
Cl ⁻	0.02	-0.26	<i>0.95</i>	<i>0.95</i>	<i>0.95</i>	<i>0.86</i>	<i>0.69</i>	-0.11	1		
HCO ₃ ⁻	0.25	0	0.20	0.20	0.21	-0.04	0.34	0.13	0.03	1	
SO ₄ ²⁻	0.07	-0.10	0.17	0.12	0.16	0.01	0.12	-0.19	-0.05	0.47	1
(b)											
T (°C)	1										
PH	-0.53	1									
C25°C	0.47	-0.52	1								
Salinity	0.39	-0.55	<i>0.98</i>	1							
Na+	0.49	-0.49	<i>0.97</i>	<i>0.95</i>	1						
Ca2+	0.26	-0.65	<i>0.77</i>	<i>0.82</i>	<i>0.70</i>	1					
Mg2+	0.14	-0.36	<i>0.75</i>	<i>0.80</i>	<i>0.70</i>	<i>0.69</i>	1				
K+	0.59	-0.21	<i>0.72</i>	<i>0.65</i>	<i>0.77</i>	0.38	0.40	1			
Cl-	0.40	-0.40	<i>0.96</i>	<i>0.95</i>	<i>0.97</i>	<i>0.71</i>	<i>0.80</i>	<i>0.75</i>	1		
HCO3-	0.42	-0.57	<i>0.61</i>	<i>0.58</i>	<i>0.62</i>	<i>0.61</i>	0.40	<i>0.56</i>	<i>0.58</i>	1	
SO42-	0.07	-0.30	0.37	0.46	0.32	0.45	<i>0.60</i>	-0.02	0.34	-0.08	1

According to scatter diagrams (Fig. 9c), the groundwater mineralization is controlled, in addition to minerals dissolution, by ion exchange with clay minerals present in the aquifers and also reverse ion exchange.

The indicator of carbonate and silicate weathering is confirmed by the (Ca²⁺+Mg²⁺) against (HCO₃⁻ + SO₄²⁻) scatter diagrams in Fig. 9d showing that:

- The shallow and springs samples are distributed at the left and the right part of the 1:1 (line). One sample indicating the abundance of SO₄²⁻ + HCO₃⁻ by 54% over Ca²⁺+Mg²⁺ is a sign of silicate weathering. The most of samples located in the left part of the 1:1 (line) indicates that the water samples are related to carbonate rock.

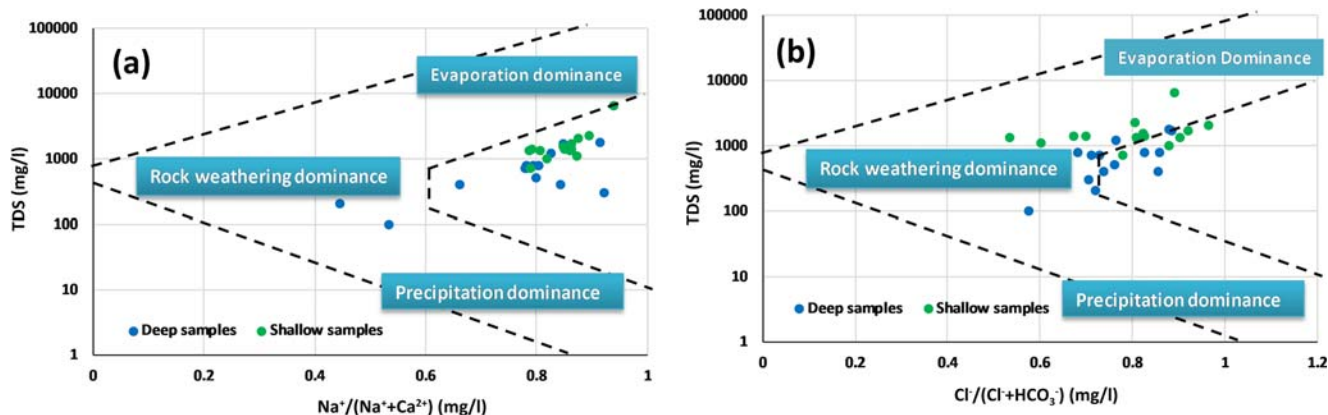


Fig. 8 Gibbs' diagrams of the shallow and deep aquifers of HJB. **a** Ratio I vs. TDS and **b** ratio II vs. TDS

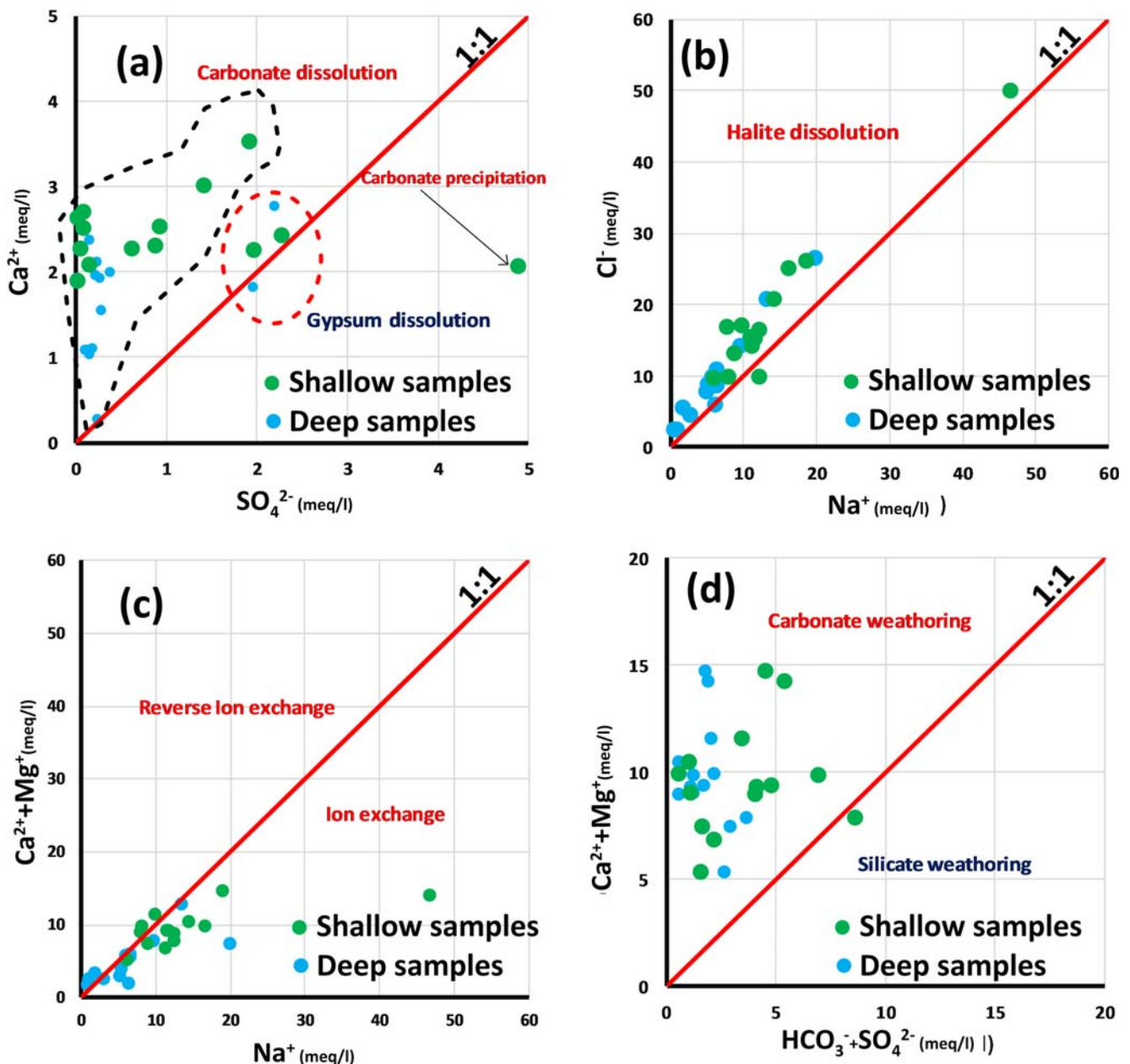


Fig. 9 a Plot of SO_4^{2-} against Ca^{2+} . b Plot of Na^+ against Cl^- . c Plot of Na^+ against $(\text{Ca}^+ + \text{Mg}^+)$ in meq/l in shallow and deep aquifer water samples. d Plot of $(\text{HCO}_3^- + \text{SO}_4^{2-})$ against $(\text{Ca}^{2+} + \text{Mg}^{2+})$ in meq/l in shallow and deep aquifer water samples.

- The deep samples are distributed at the left part of the 1:1 (line) indicating a weathering of carbonates which represents the main source of bicarbonate ion.

Hydrochemical water type

Considering the piper trilinear plot (Figs. 10 and 11), we can distinguish three major groundwater groups for the deep aquifer: Na-Cl, Ca-Mg-Cl, and Ca-Cl and two water type for the shallow aquifer: Na-Cl and Ca-Mg-Cl. For the deep aquifer; the first group (Ca-Cl) type waters are highly mineralized.

They represent the northwest part of Beglia aquifer (recharge zone). The high Ca^+ concentration in the northwest part of Beglia aquifer is derived from dissolution of carbonate present in the cretaceous of Dj Mghilla. The second water type is Na-Cl; it presents 78% of samples for the deep aquifer and also for the shallow aquifer. The Na cation is derived from the ion exchange with the clay of the adjacent layer (Saouaf formation). Two much closed wells, in the deep aquifer, present two different water type (Na-Cl and Ca-Mg-Cl); the Na-Cl water type presents 78% of samples while Ca-Mg-Cl is present only in one sample. Based on the screen position of wells, we can detect that the well corresponding to the Ca-Mg-Cl water type

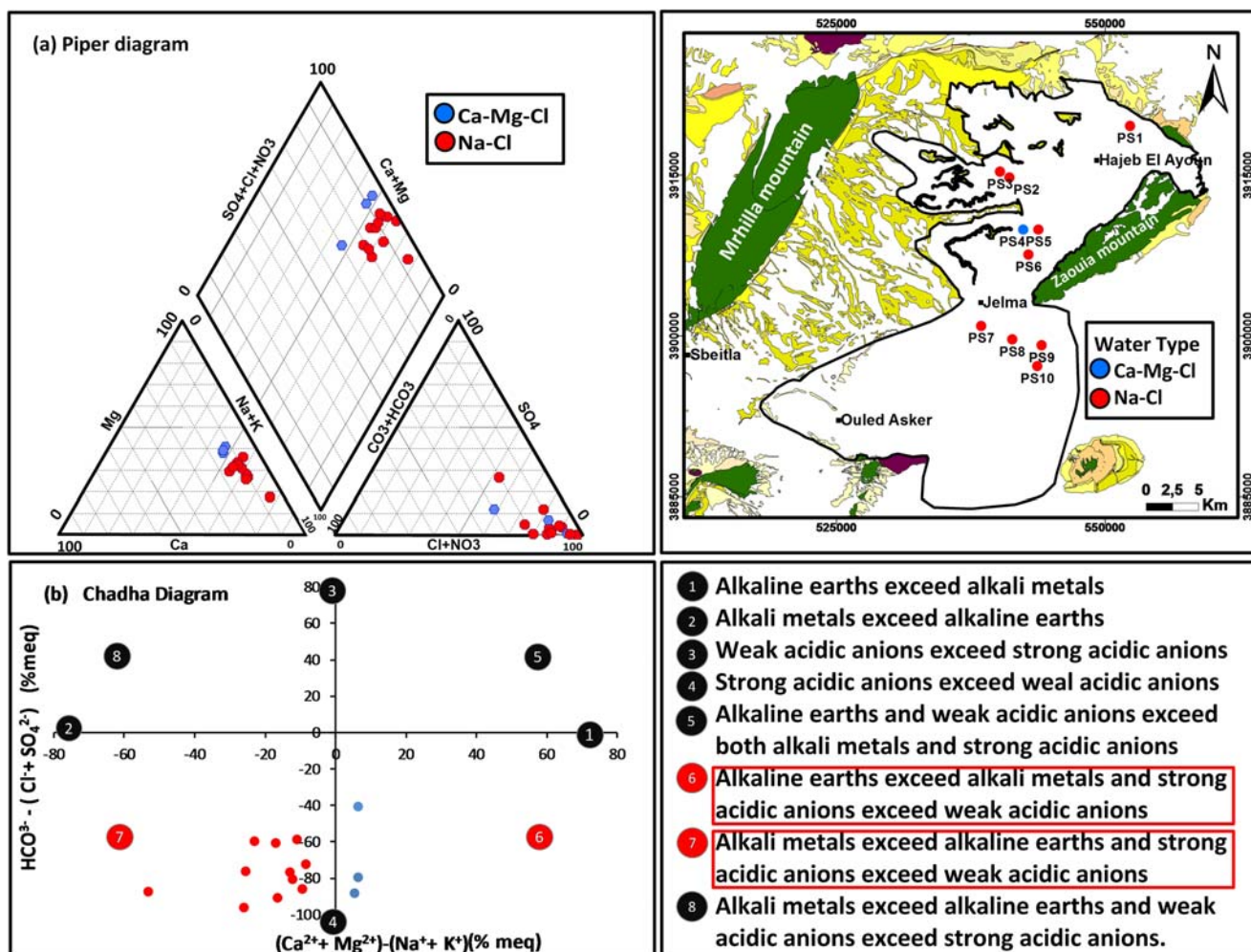


Fig. 10 a Piper diagram and b Chadha diagram of the shallow samples

presents very different screen position; so, we can conclude that Beglia aquifer presents vertical water-type stratification.

The chemical data of shallow/springs and deep samples, collected from the studied area, are plotted in the Chadha diagram presented in Figs. 10 and 11. All the samples fall in fields 6 and 7, and this means that “alkaline earths exceed alkali metals and strong acidic anions exceed weak acidic anion” and “Alkali metals exceed alkaline earths and strong acidic anions exceed weak acidic anions.”

Multivariate statistical analyses

Principal component analysis was achieved for the two aquifers separately: a dataset of 28 samples (14 deep samples and 14 shallow and springs samples) and 12 physico-chemical elements to determine relationships between major elements and also physical parameters. Table 4 shows the eigenvalues, the percentage of variance, associated with each other, and the cumulative percentage.

The results of the analysis presented in Fig. 12 reveal that the first three factors illustrate approximately 78%, of total variance, for the shallow and springs samples and 86% for the deep samples. For the shallow and springs samples, the first factor is responsible for about 48%, of total variance, and is well represented by salinity, Na⁺, EC, Mg, Ca²⁺, and Cl⁻. These elements ensure the mineralization of the shallow aquifer’s water. Consequently, component “1” is defined as the salinity component representing the weathering of halite and evaporate minerals. Component “2” is represented by O₂, SO₄²⁻, and HCO₃⁻. Additional 12.25%, of total variance, was explained in F3 and was represented by K⁺, O₂, and pH.

For the deep samples, the first factor is responsible for about 63.11%, of total variance, and is well represented by Mg²⁺, salinity, Na⁺, K⁺, Ca²⁺, HCO₃⁻, Cl⁻, and EC; this component is defined as the salinity component representing the weathering of halite and evaporate minerals. Component 2 is represented by SO₄²⁻ defined as a factor of sulfates. The third

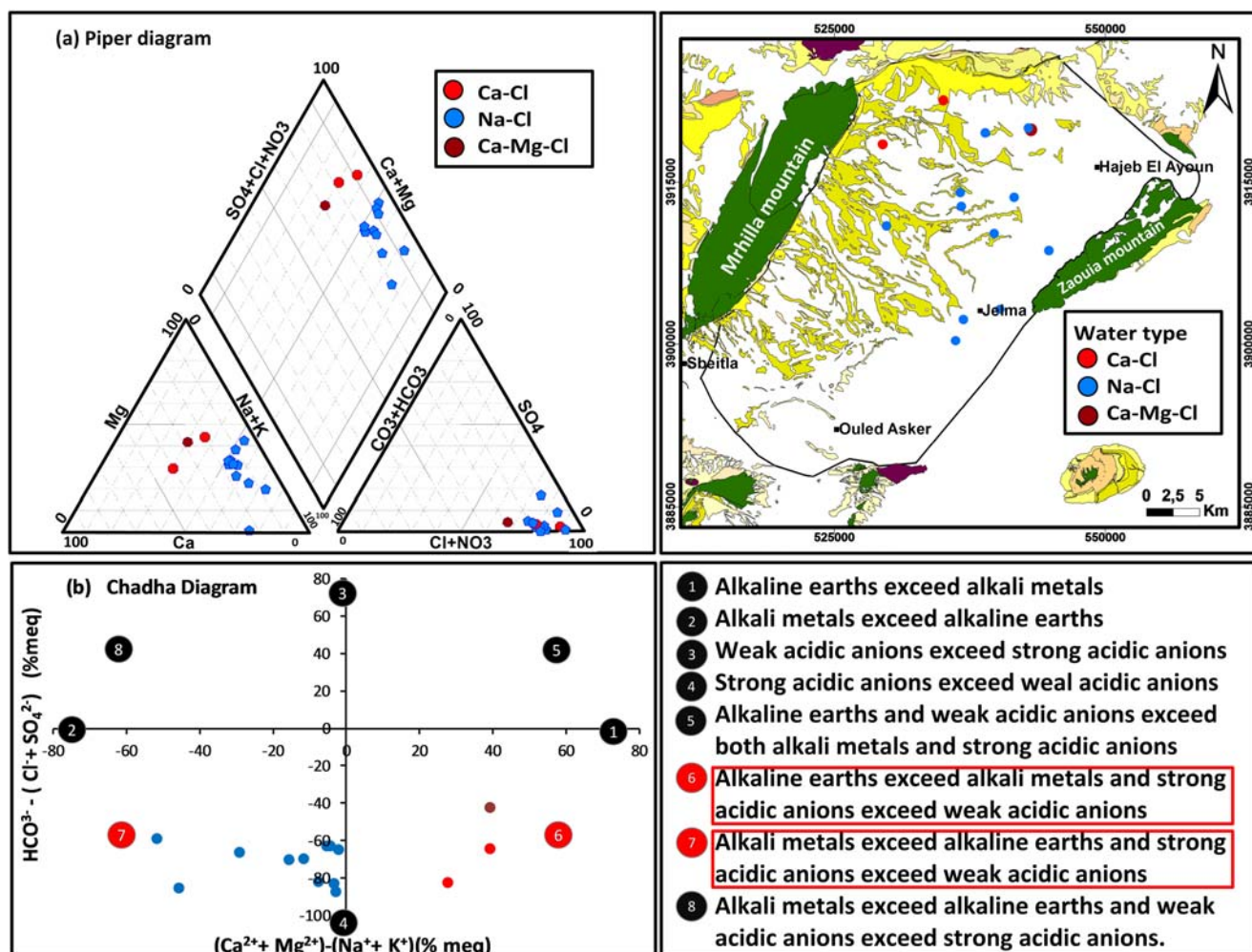


Fig. 11 a Piper diagram and b Chadha diagram of the deep samples

component represents 10.85%, of total variance, was explained in F3, and was represented by O₂ and pH.

Water quality

Drinking use

Standard limits The physical (pH and EC (μs/cm)) and chemical parameters (K⁺, Ca⁺, Mg⁺, Cl⁻, SO₂⁻, Na⁺, HCO₃⁻/in mg/l) were compared with the world’s standard (WHO 2011) and

Table 4 Variance explained by the first three principal components

Component	Eigenvalues	% total variance	% cumulative
Shallow samples	1 5.34	48.55	48.55
	2 1.92	17.45	66
	3 1.34	12.25	78.25
Deep samples	1 6.94	63.11	63.11
	2 1.39	12.64	75.76
	3 1.19	10.85	86.61

- 1 Alkaline earths exceed alkali metals
- 2 Alkali metals exceed alkaline earths
- 3 Weak acidic anions exceed strong acidic anions
- 4 Strong acidic anions exceed weak acidic anions
- 5 Alkaline earths and weak acidic anions exceed both alkali metals and strong acidic anions
- 6 Alkaline earths exceed alkali metals and strong acidic anions exceed weak acidic anions
- 7 Alkali metals exceed alkaline earths and strong acidic anions exceed weak acidic anions
- 8 Alkali metals exceed alkaline earths and weak acidic anions exceed strong acidic anions.

the national standard (NT 2013). As show in Fig. 13, all samples ($n = 28$) respect the maximum permissible limit, for the both WHO and NT standards, for the pH, the potassium (K⁺), the calcium (Ca⁺), the magnesium (Mg⁺), the bicarbonates (HCO₃⁻), and the sulfates (SO₂⁻). For the electrical conductivity (EC), the limit given by the WHO (1500 μs/cm) is not respected by all the shallow samples and the most of deep samples (58%). For the chlorides (Cl⁻), all the shallow samples exceeded the WHO limit (250 mg/l) and 29% of the shallow samples exceeded the national limit (600 mg/l). For the deep aquifer, 9 samples (64%) exceeded the WHO limit and two samples (14%) exceeded the national limit (600 mg/l). For the sodium (Na⁺) parameter, the permissible value given by the WHO (200 mg/l) was respected only by four samples (29%) in the shallow aquifer and exceeded by three samples (21%) from the deep one. In all collected samples, only one physical parameter and two major ions (one cation and one anion) not respect the WHO and NT limit in the most of samples. In the total, only 15% of samples respect the permissible limits, of all physico-chemical parameter, given by the WHO, which can affect the human health.

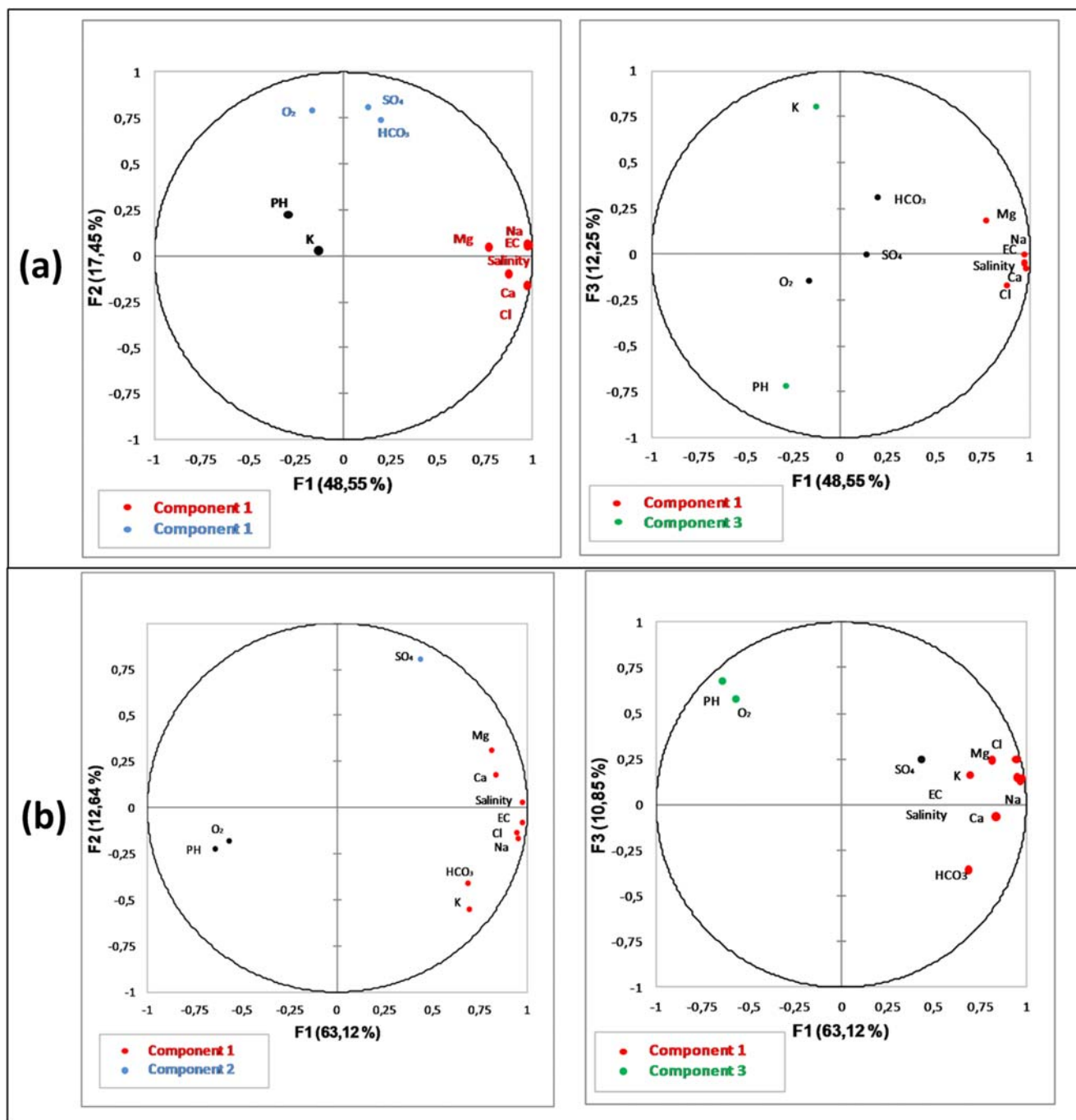


Fig. 12 Projection of the variables in the first, second, and third factorial plan (principal component analysis) (a) including all shallow and springs samples in HJB and (b) deep samples in HJB

Water quality indices

The evaluation of water quality, of HJB, for drinking uses was effectuated using three quality indices: EWQI, WQI, and ImpWQI.

The WHO standards were selected to calculate the quality rating scale (Q). The WQI ranged from 64.41 to 328.64 for the shallow aquifer and from 22 to 155.61 for the deep aquifer. It shows four classes of both aquifers (Table 5), extended from

“good” to “extremely poor” for the shallow aquifer and from “excellent” to “poor” for the deep one. For the EWQI, the index value ranged from 55.29 to 248.41 for the shallow aquifer and from 22 to 122.8 for the deep aquifer. It shows three classes of both aquifers (Table 5, extended from “good” to “extremely poor” for the shallow aquifer and from “excellent” to “Medium” for the deep one. For the ImpWQI, the value ranged from 178.69 to 1011 for the shallow aquifer and from 43.93 to 475.6 for the deep aquifer. It shows various classes of

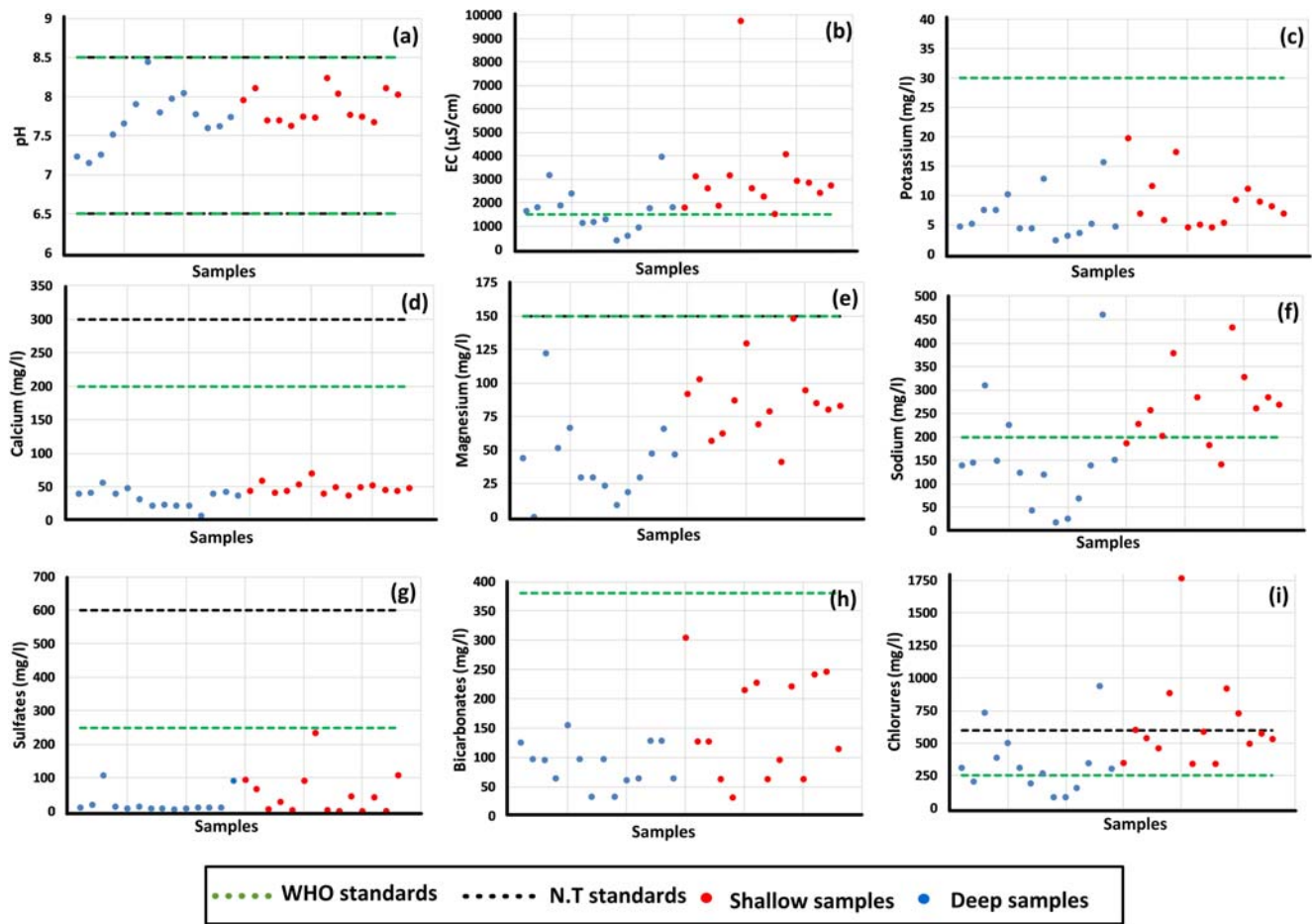


Fig. 13 Comparison of major ion concentration (in mg/l) and physical parameters in HJB with the WHO standards and Tunisian norms (NT 09–14). a pH, b EC ($\mu\text{S}/\text{cm}$), c K^+ , d Ca^{2+} , e Mg^{2+} , f Na^+ , g SO_4^{2-} , h HCO_3^- , and i Cl^-

both aquifers (Table 5), extended from “poor” to “extremely poor” for the shallow aquifer and from “excellent” to “poor” for the deep one.

A correlation was effectuated between the physico-chemical parameters, used in the calculation of the indices, and the three indices (Table 6). For the both aquifers, the three indices (ImpWQI, EWQI, and WQI) present a negative low correlation with the pH, a low correlation with sulfates (SO_4^-), and a strong correlation with the major physico-chemical

parameters (EC , Na^+ , Ca^{2+} , Mg^{2+} , Cl^- , HCO_3^-) except in the shallow aquifer the potassium K^+ and the bicarbonates HCO_3^- present a low correlation value with the three indices (Table 6). The correlation values are related to the parameter’s weight which is given in WQI method and calculated in the two indices (ImpWQI and EWQI). For the both types of samples (shallow/deep), the three indices indicate very similar correlation values but the EWQI indicate the high values with very negligible differences with the two other indices.

Table 5 Classification of shallow and deep samples quality based on EWQI, WQI, and ImpWQI

Index		< 50	50–100	100–150	150–200	> 200
Water quality		excellent	Good	Medium	Poor	Extremely poor
EWQI	% shallow aquifer	-	79%	14%	-	7%
	% deep aquifer	50%	36%	14%	-	-
WQI	% shallow aquifer	-	36%	50%	7%	7%
	% deep aquifer	29%	57%	7%	7%	-
ImpWQI	% shallow aquifer	-	-	-	7%	93%
	% deep aquifer	7%	14%	22%	-	57%

Table 6 Correlation between the various water quality indices (ImpWQI, EWQI, and WQI) and physico-chemical parameters for the deep and shallow aquifer

	Index	pH	EC	Na ⁺	Ca ²⁺	Mg ²⁺	K ⁺	Cl ⁻	HCO ³⁻	SO ₄ ²⁻
Deep aquifer	WQI	- 0.47	0.99	0.98	0.76	0.82	0.73	0.99	0.59	0.42
	EWQI	- 0.47	0.99	0.98	0.76	0.81	0.75	0.99	0.62	0.40
	ImprWQI	- 0.46	0.99	0.98	0.76	0.81	0.75	0.99	0.62	0.40
Shallow aquifer	WQI	- 0.29	0.99	0.99	0.84	0.7	- 0.16	0.97	0.2	0.16
	EWQI	- 0.33	0.99	0.99	0.83	0.72	- 0.12	0.97	0.24	0.17
	ImprWQI	- 0.27	0.99	0.98	0.85	0.69	- 0.16	0.99	0.13	0.07

Figure 14 shows the water quality index values calculated by the three proposed indices (WQI, ImpWQI, and EWQI) in the deep and shallow aquifers. The indices showed similar results, regarding EWQI and WQI. The ImpWQI indicate the higher index values; for the shallow samples, the ImpWQI indices are ranged from 178.69 to 1011 which indicate poor to extremely poor water quality. For the deep samples, the ImpWQI indicated that the samples with Na-Cl water type indicate the low water quality then the other water types.

The spatial distribution of the water quality based on the three indices (EWQI, WQI, and ImpWQI) is shown in Fig. 15.

For the both aquifers, the ImpWQI method shows the best result; it indicates that the Na-Cl water type coincides with the poor, and the extremely poor water quality and the two other indices (WQI and EWQI) indicate good to poor water types. These results reflect the effect of the parameter’s weight in the calculation of the water quality index.

Irrigation purposes

The collected samples were assessed for irrigation uses using different indices; the results are illustrated in the Table 7. According the TH (total hardness) values, all samples of the both aquifers present a soft water (TH < 75).

The EC values of HJB are ranked into various categories for the both aquifers (shallow and deep aquifer). For the deep aquifer, 79% of samples present good to permissible

water quality and 21% of samples indicated a doubtful water class (samples with Na-Cl water type). For the shallow aquifer, 21% of samples are permissible; 79% of samples present doubtful to unsuitable water class (including samples with Na-Cl water type). The %Na indicated that only 71% shallow samples are permissible for irrigation; the %Na of samples with Na-Cl water type varies from 54.3 to 76.71 indicating permissible to doubtful water quality. For the deep samples, three samples (F7, F9, and F10) present a good water class which coincide with the Ca-Cl and Ca-Mg-Cl water type; 58% (Na-Cl water type) indicate permissible water for irrigation, and three samples (Na-Cl water type; F2, F8, and F13) indicate a doubtful water class. The SAR values for HJB samples are ranked into two groups; for the both aquifers, all samples have a low degree of alkalinity hazards (2 < SAR < 10), except three samples with a high alkalinity hazards (10 < SAR < 18). Based only on the SAR values, the samples of HJB are distributed on two water classes (“excellent” to “good”) and its can be utilized for most types of soil. According the calculated values of MH (magnesium hazard) and the PI (permeability index), all samples of the shallow, springs, and deep aquifers are unsuitable for irrigation. The calculated values of Kr show that the groundwater samples of HJB, with Na-Cl water type, are more than 1, indicating moderate to unsuitable water quality for irrigation uses. Based on the seven estimated indices, the most

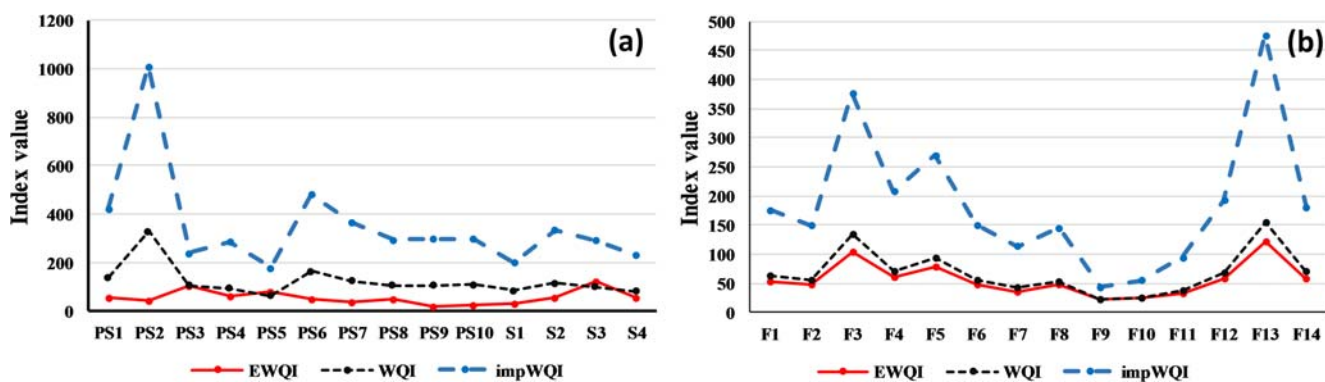


Fig. 14 Comparison of the results of the WQI, ImpWQI, and EWQI indices using the WHO standard in (a) shallow aquifer and (b) Deep aquifer

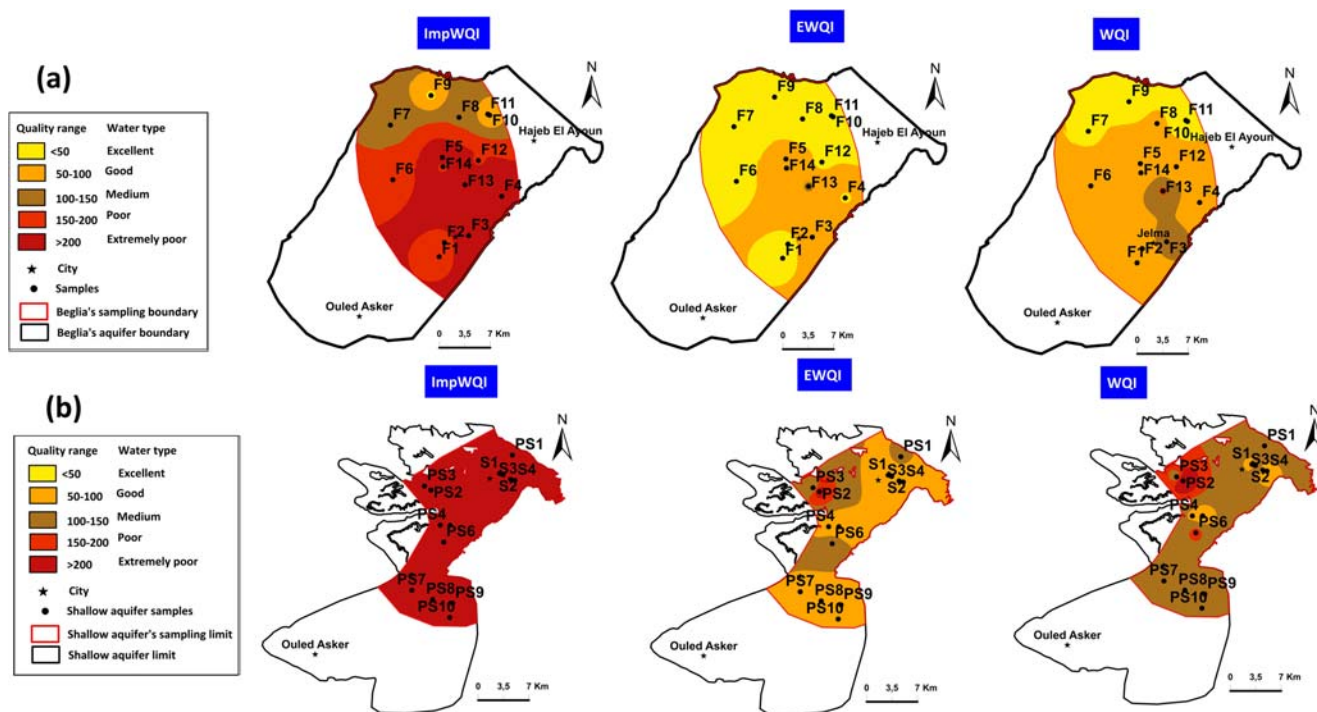


Fig. 15 Distribution of the three indices (ImpWQI, EWQI, and WQI) based on WHO standard in (a) deep aquifer and (b) shallow aquifer

of HJB’s samples are unsuitable for irrigation uses which the shallow samples present an irrigation quality less than the deep samples, and it is due to the shallow aquifer position, the thickness of the vadose zone which has a strong effect on the pollutants infiltration.

WILCOX and USSL classification

The %Na vs. EC values for HJB’s samples were plotted in the Wilcox graphical diagram of irrigation water (Wilcox 1955). The diagram shows that 10 samples present a water quality permissible to doubtful (Na-Cl water type), 3 samples are classed under good to permissible (Ca-Cl and Na-Cl water type), 13 samples are doubtful to unsuitable (Na-Cl water type), and 2 samples are excellent to good (Ca-Cl and Ca-Mg-Cl water type) (Fig. 16a).

The SAR vs. EC values for groundwater samples of HJB were plotted in the USSL diagram of irrigation water (Fig. 16b). Based on USSL diagram (USSL 1954), the water samples show five categories; “C2-S1” (medium salinity with low sodium), “C3-S1” (high salinity with low sodium), “C4-S2” (very high salinity with medium sodium), “C3-S2” (high salinity with medium sodium), and “C4-S3” (very high salinity with high sodium). Based on the combination between EC and SAR, in USSL diagram, HJB have only two deep samples suitable for irrigation (F9 and F10) (medium salinity with low sodium) which coincide with Ca-Cl and Ca-Mg-Cl water type.

Discussion

The Hajeb Layoun-Jelma basin is the selected site in this research in order to provide its actual water quality situation, with highlights on the water chemistry origins and its suitability (drinking and irrigation). The shallow aquifer shows high salinity in most of the water samples (93% of samples has salinity > 1 g l⁻¹ with one sample exceeding 6 g l⁻¹) (Fig. 7b). The deep aquifer has moderate salinity: 21% of samples exceeding 1 g l⁻¹ and the rest (79%) indicate salinity less than 1 g l⁻¹ (Fig. 7a). Groundwater salinity pollution is considered as common Mediterranean problems; it is seen in recent investigations conducted in the shallow aquifers in Northeastern Tunisia (Ghouili et al. 2018) and central-eastern Tunisia (Mnassri et al. 2018). The high level of intake salt in water can cause a serious human health problem (Al Nahian et al. 2018).

In this study, based on Gibbs’s diagram and the inter-parameters correlation, the high salinity levels in the HJB are related to the natural factors (dissolution of carbonates/gypsum and water evaporation). The anthropogenic factors in HJB have also a strong role in the elevation of the salinity concentration such as the increasing number of wells (the number of shallow wells increase from 226 in 1974 to 2328 wells in 2018), the low thickness of the vadose zone (from 3 to 20 m), and the irrigation practices. The huge quantities of fertilizers have an impact on the increasing of rates of Na⁺ and Cl⁻ (Mnassri et al. 2018). This is showed by the high correlation between Na⁺/Cl⁻ and salinity in this study (Table 3).

Table 7 Irrigation quality indices of Hajeb Layoun-Jelma aquifers

Range	Reference	Classification	Shallow + springs samples		Deep samples	
			Number of samples	% of samples	Number of samples	% of samples
Total hardness (TH)						
< 75	Todd (1980)	Soft	All samples	100%	All samples	100%
75–150		Moderately hard	-	-	-	-
150–300		Hard	-	-	-	-
> 300		Very hard	-	-	-	-
EC (µs/cm)						
< 250	Richard (1954)	Excellent	-	-	-	-
250–750		Good	-	-	2	14%
750–2000		Permissible	3	21%	9	65%
2000–3000		Doubtful	7	50%	1	7%
> 3000		Unsuitable	4	29%	2	14%
Percent sodium (Na%)						
< 20	Wilcox (1955)	Excellent	-	-	-	-
20–40		Good	-	-	3	21%
40–60		Permissible	10	71%	8	58%
60–80		Doubtful	4	29%	3	21%
> 80		Unsafe	-	-	-	-
Alkalinity hazard (SAR)						
< 10	Richard (1954)	Excellent	All samples except PS2	93%	All samples except F13	93%
10–18		Good	1	7%	1	7%
18–26		Doubtful	-	-	-	-
> 26		Unsuitable	-	-	-	-
Magnesium hazard (MH)						
> 50	Raghunath (1987)	Unsuitable	All samples	100%	All samples	100%
< 50		Suitable	-	-	-	-
Permeability index PI						
< 25	Doneen (1964)	Suitable	-	-	-	-
25–75		Moderate	-	-	-	-
> 75		Unsuitable	All samples	100%	All samples	100%
Kelley ratio (KR)						
< 1	Kelly (1951)	Suitable	3	21%	3	21%
1–2		Moderate	10	72%	10	72%
> 2		Unsuitable	1	7%	1	7%

The use of modern methods such as EWQI, WQI, and ImpWQI would confer the best understanding of water suitability. Based on the previously mentioned (see the “Water quality indices” section), compared with evaluation results of different weighting methods, it shows that the WQI-based CRITIC weighting method (ImpWQI) is feasible in the HJB’s water quality evaluation. Wang et al. (2018) and Zhang et al. (2020) have applied the improved water quality index method, based on CRITIC weighting, to provide the groundwater’s suitability for drinking purposes. Wang et al. (2018) found that the WQI based on CRITIC weighting (ImpWQI) is the realistic method to assess water quality. As

within the HJB, the application of ImpWQI technique shows that for the shallow aquifer, 14 water samples (Table 5 and Fig. 9) range between “poor water” and “extremely poor water,” and for the deep aquifer, the samples range from “excellent water” to “extremely poor water,” for the both aquifer, the “poor” and “extremely poor” water quality coincide with the Na-Cl water type.

The over-abstraction from HJB, the non-treated sewage rejected, and the irrigation practices lead the degradation of HJB’s resources and promote its pollution. To ensure the HJB’s sustainability and avoid the quality problems, it is necessary to improving the irrigation practices by the

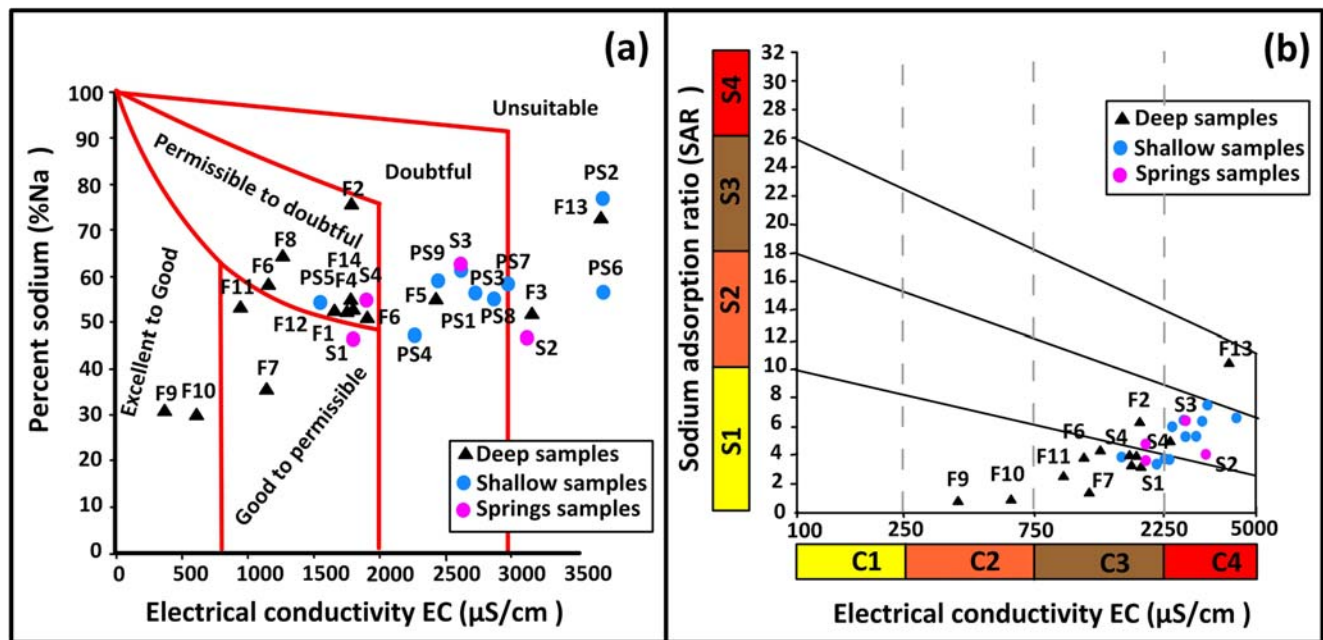


Fig. 16 a Sodium percentage vs. EC values plot for water quality classification (Wilcox diagram 1955) and b USSL classification of HJB samples

implementing of a continuously measures to help farmers to adopt the best management practices.

Conclusion

The HJB has an important economic and social status as a first alternative for sustainable agricultural activities and drinking use for Sidi Bouzid, Kairouan (central Tunisia), and also Sfax (southern coast). The abstraction increases since the mid-1980s and the continuous decline of piezometry make the degradation of the quality and the quantity of this groundwater. To assess the water quality of HJB, 28 water samples were collected in 2017 and analyzed for 11 physico-chemical parameters (temperature, pH, EC, salinity, Na^+ , Ca^{2+} , K^+ , Mg^{2+} , Cl^- , HCO_3^- , and SO_4^{2-}). For the both aquifers (the MPQ and Beglia aquifers), the order of the abundance of major cations is $\text{Na} > \text{Mg} > \text{Ca} > \text{K}$ and anions are $\text{Cl} > \text{HCO}_3 > \text{SO}_4$. The dominant hydrochemical facies, for the shallow aquifer and springs, are Na-Cl and Ca-Mg-Cl; for the deep aquifer, the geochemical facies are Na-Cl, Ca-Mg-Cl, and Ca-Cl. The WQI and the EWQI indicate that most shallow and deep samples present excellent to medium water type and only 7% presents poor water. The ImpWQI present the logic index which indicates 100% and 57% extremely poor water for the shallow and the deep samples, respectively, which coincide with Na-Cl water type. The water quality evaluation for irrigation uses was performed by assembling various geochemistry methods (SAR, TH, % Na, PI, MH, KR, EC). The results indicate that

the shallow samples show quality less than the deep one (unsuitability according EC, 79%). The bad irrigation practices, the low thickness, and the high permeability of the vadose zone play a strong role in the infiltration of pollutants and reach to the HJB’s shallow aquifer.

Availability of data and materials The datasets used and analyzed during the current study are available from the corresponding author on reasonable request.

Authors’ contributions Soumaya Aouiti was responsible for the lead, conceptualization, investigation, methodology, formal analysis, and manuscript redaction. Fadoua Hamzaoui-Azaza was responsible for conceptualization, formal analysis, and visualization. Fetheddine El Melki was responsible for conceptualization and geological part validation. Monji Hamdi was responsible for conceptualization and investigation. Fulvio Celico was responsible for conceptualization, validation, and supervision. Mounira Zammouri was responsible for conceptualization, validation, and supervision. All authors read and approved the final manuscript.

Funding Open access funding provided by Università degli Studi di Parma within the CRUI-CARE Agreement.

Compliance with ethical standards

Competing interests The authors declare that they have no competing interests.

Ethics approval and consent to participate Not applicable.

Consent for publication Not applicable.

Open Access This article is licensed under a Creative Commons Attribution 4.0 International License, which permits use, sharing, adaptation, distribution and reproduction in any medium or format, as long as

you give appropriate credit to the original author(s) and the source, provide a link to the Creative Commons licence, and indicate if changes were made. The images or other third party material in this article are included in the article's Creative Commons licence, unless indicated otherwise in a credit line to the material. If material is not included in the article's Creative Commons licence and your intended use is not permitted by statutory regulation or exceeds the permitted use, you will need to obtain permission directly from the copyright holder. To view a copy of this licence, visit <http://creativecommons.org/licenses/by/4.0/>.

References

- Adimalla N (2019) Groundwater quality for drinking and irrigation purposes and potential health risks assessment: a case study from semi-arid region of south india. *Expo Health* 11:109–123. <https://doi.org/10.1007/s12403-018-0288-8>
- Al Nahian M, Ahmed A, Lazar AN, Hutton CW, Salehin M, Streatfield PK (2018) Drinking water salinity associated health crisis in coastal Bangladesh. *Elem Sci Anth*:6. <https://doi.org/10.1525/elementa.143>
- Ameur M, Hamzaoui-Azaza F, Gueddari M (2016) Nitrate contamination of Sminja aquifer groundwater in Zaghuan, northeast Tunisia: WQI and GIS assessments. *Desalin Water Treat* 57:1–11. <https://doi.org/10.1080/19443994.2015.1137495>
- Asadi E, Isazadeh M, Samadianfard S, Ramli MF, Mosavi A, Nabipour N, Shamshirband S, Hajnal E, Chau KW (2020) Groundwater quality assessment for sustainable drinking and irrigation. *Sustainability* 12:177. <https://doi.org/10.3390/su12010177>
- Barbieri M, Ricolfi L, Vitale S, Muteto PV, Nigro A, Sappa G (2019) Assessment of groundwater quality in the buffer zone of Limpopo National Park, Gaza Province, Southern Mozambique. *Environ Sci Pollut Res* 26:62–77. <https://doi.org/10.1007/s11356-018-3474-0>
- Chadha DK (1999) A proposed new diagram for geochemical classification of natural waters and interpretation of chemical data. *Hydrogeol J* 7:431–439. <https://doi.org/10.1007/s100400050216>
- DGRE (2018) Situation de l'exploitation des nappes phréatiques et profondes en 2018. Direction Générale des Ressources en Eau, Tunisia
- DGRE (1973–2018a) Situation de l'exploitation des nappes profondes de 1973 à 2018. Direction Générale des Ressources en Eau, Tunisia
- DGRE (1973–2018b) Piezométrie des nappes phréatiques et profondes de 1973 à 2018. Direction Générale des Ressources en Eau, Tunisia
- DGRE (1974–2018) Situation de l'exploitation des nappes phréatiques de, (1974) à 2018. Direction Générale des Ressources en Eau, Tunisia
- DGRE (2017) Annuaire des qualités des eaux 2017. Direction Générale des Ressources en Eau, Tunisia
- Doneen LD (1964) Notes on water quality in agriculture. Water Science and Engineering Paper 4001. Department of Water Sciences and Engineering, University of California, California
- Eaton FM (1950) Significance of carbonates in irrigated waters. *Soil Sci* 69:123–134
- Ghouili N, Hamzaoui-Azaza F, Zammouri M, Zaghrami MF, Jarraya Horriche F, Condesso de Melo MT (2018) Groundwater quality assessment of the Takelsa phreatic aquifer (northeastern Tunisia) using geochemical and statistical methods: implications for aquifer management and end-users. *Environ Sci Pollut* 25:36306–36327. <https://doi.org/10.1007/s11356-018-3473-1>
- Gibbs RJ (1970) Mechanism controlling world water chemistry. *Science* 170(1088):1090
- Hamzaoui-Azaza F, Ketata M, Bouhlila R, Gueddari M, Riberio L (2011) Hydrogeochemical characteristics and assessment of drinking water quality in Zeuss–Koutine aquifer, southeastern Tunisia. *Environ Monit Assess* 18:159–174. <https://doi.org/10.1007/s10661-010-1457-9>
- Hamzaoui-Azaza F, Ameur M, Chaouch R, Cheikha L, Gueddari M, José Joel R (2020) Assessment of groundwater quality based on GIS and geochemical methods: coastal aquifer of Bouficha (north-eastern Tunisia). *J Coast Conserv* 24:45. <https://doi.org/10.1007/s11852-020-00762-8>
- Hounslow AW (1995) Water quality data. Analysis and interpretation. Lewis, New York
- INS (2014) Recensement Général de la Population et de l'Habitat 2014. <http://www.ins.tn/fr>
- Islam ARMT, Ahmed N, Md B-D, Chu R (2017) Characterizing groundwater quality ranks for drinking purposes in Sylhet district, Bangladesh, using entropy method, spatial autocorrelation index, and geostatistics. *Environ Sci Pollut Res* 24:26350–26374. <https://doi.org/10.1007/s11356-017-0254-1>
- Jallalia D, Lachaal F, Andoulsi M, Zouaghi T, Hamdi M, Bedir M (2015) Hydro-geophysical and geochemical investigation of shallow and deep Neogene aquifer systems in Hajeb Layoun-Jilma-Ouled Asker area, Central Tunisia. *J Afr Earth Sci* 110:227–244. <https://doi.org/10.1016/j.jafrearsci.2015.06.016>
- Kelly WP (1951) Alkali soils-their formation, properties and reclamation. Reinhold Publ, New York
- Koschel R (1980) Etude hydrogéologique de la nappe de Hajeb el Aioun –Jelma –Ouled Asker. Proj. Coop. Tech. Tuniso-allemande. N°6520/7. Division des ressources en eau. Minist. Agric. Tunis, Tunisia 245p. (In French)
- Ligavha-Mbelengwa L, Gomo M (2020) Investigation of factors influencing groundwater quality in a typical Karoo aquifer in Beaufort West town of South Africa. *Environ Earth Sci* 79:196. <https://doi.org/10.1007/s12665-020-08936-1>
- Medina-Gomez I, Herrera-Silveira JA (2003) Spatial characterization of water quality in a karstic coastal lagoon without anthropogenic disturbance: a multivariate approach. *Coast Shelf Sci* 58:455–465. [https://doi.org/10.1016/S0272-7714\(03\)00112-4](https://doi.org/10.1016/S0272-7714(03)00112-4)
- Mnassri S, Dridi L, Lucas YB, Schäfer G, Hachicha M, Majdoub R (2018) Identifying the origin of groundwater salinisation in the Sidi El Hani basin in central-eastern, Tunisia. *J Afr Earth Sci* 147: 443–449. <https://doi.org/10.1016/j.jafrearsci.2018.07.004>
- Moghari SM, Ebrahimi K, Azarnivand A (2015) Groundwater quality assessment with respect to fuzzy water quality index (FWQI): an application of expert systems in environmental monitoring. *Environ Earth Sci* 74:7229–7238. <https://doi.org/10.1007/s12665-015-4703-1>
- NT (2013) Norme Tunisienne NT 09-14, Relative à la qualité des eaux de boisson. Rapport du laboratoire SONEDE
- Piper AM (1944) A graphic procedure in the geochemical interpretation of water analyses. *Trans Am Geophys Union* 25:914–923
- Ragunath HM (1987) Groundwater, 2nd edn. Wiley Eastern Ltd, New Delhi
- Richard LA (1954) Diagnosis and improvement of saline and alkaline soils. Agricultural, Handbook 60. US Department of Agriculture, Washington, DC, p 160
- Ricolfi L, Barbieri M, Muteto PV, Nigro A, Sappa G, Vitale S (2020) Potential toxic elements in groundwater and their health risk assessment in drinking water of Limpopo National Park, Gaza Province, Southern Mozambique. *Environ Geochem Health* 42:2733–2745. <https://doi.org/10.1007/s10653-019-00507-z>
- Su F, Wu J, He S (2019) Set pair analysis (SPA)-Markov chain model for groundwater quality assessment and prediction: a case study of Xi'an City, China. *Hum Ecol Risk Assess* 25:158–175. <https://doi.org/10.1080/10807039.2019.1568860>
- Thebti S, Jellalia D, Azaiez H, Bédir M (2018) Basin structuring and hydro-geophysical characterization of Upper Cretaceous and Eocene fractured deep carbonate reservoirs in the Hajeb Layoun-Jelma-Ouled Asker area (Central Tunisia). *Arab J Geosci* 11:107. <https://doi.org/10.1007/s12517-018-3445-2>
- Todd DK (1980) Groundwater hydrology, 2nd edn. Wiley, New York

- USSL (US Salinity Laboratory) (1954) Diagnosis and improvement of salinity and alkaline soil. USDA Hand Book no. 60, Washington
- Wang S, Huang T, Chen H, Liu M, Xue H (2018) Application of fuzzy comprehensive evaluation model based CRITIC weighting in water quality evaluation. *Hydropower Energy Sci* 36(06):48–51
- WHO (2011) Guidelines for drinking-water quality-4th ed. Geneva. World Health Organization. p 564
- Wilcox LV (1955) Classification and use of irrigation water, circular 969. Washington, DC, USA
- Wu J, Li P, Qian H (2011) Groundwater quality in Jingyuan plain, a semi-humid area in northwest China. *E-J Chem* 8(2):787–793. <https://doi.org/10.1155/2011/163695>
- Zammouri M, Jarraya-Horriche F, Odo BO, Benabdallah S (2013) Assessment of the effect of a planned marina on groundwater quality in Enfida plain (Tunisia). *Arab J Geosci* 7:1187–1203. <https://doi.org/10.1007/s12517-012-0814-0>
- Zhang Q, Xu P, Qian H (2020) Groundwater quality assessment using improved water quality index (WQI) and human health risk (HHR) evaluation in a semi-arid region of northwest China. *Expo Health* 12:487–500. <https://doi.org/10.1007/s12403-020-00345-w>

Publisher's note Springer Nature remains neutral with regard to jurisdictional claims in published maps and institutional affiliations.

Water Quality Assessment of the Shallow and Deep Aquifers of Hajeb Layoun-Jelma Basin (Central Tunisia)



Soumaya Aouiti, Fadoua Hamzaoui-Azaza, Mounira Zammouri, Monji Hamdi, and Fulvio Celico

Abstract The assessment of the groundwater quality is an important way to ensure its sustainability for various uses. In this study, the suitability of groundwater for irrigation and drinking uses was assessed by determining the water quality index, sodium adsorption ratio, electrical conductivity, Kelly's ratio, and sodium percentage values of water samples. The results show that not all the groundwater in Hajeb Layoun-Jelma Basin can be used for irrigation. According to World Health Organization guidelines and the national standards, the major parameter data of drinking water indicate that the majority of the analyzed samples of groundwater in the area are suitable for drinking.

Keywords Groundwater quality · Shallow and deep aquifers · Sustainability · Irrigation · Drinking water · Hajeb layoun-jelma

1 Introduction

Groundwater is essentially vital for human consumption and agricultural purposes in any region. The assessment of groundwater quality has become a necessary and important task for present and future groundwater quality management. The aim of the present study is to assess suitability of groundwater for both drinking and irrigation purposes in the Hajeb Layoun-Jelma Basin. Assessment is based on computed water quality index values and four parameters of irrigation quality, namely, Electrical

S. Aouiti (✉) · F. Hamzaoui-Azaza · M. Zammouri
Faculty of Sciences of Tunis, Oil Systems and Reservoir Characterization Laboratory, University of Tunis El Manar, Sedimentary environments, LR18 ES07, 2092 Tunis, Tunisia
e-mail: soumaya.aouiti@fst.utm.tn

M. Hamdi
University of Sfax, 3029 Sfax, Tunisia

S. Aouiti · F. Celico
Department of Chemistry, Life Sciences and Environmental Sustainability, University of Parma, Parco Area delle Scienze 157a, 43124 Parma, Italy

© The Editor(s) (if applicable) and The Author(s), under exclusive license to Springer Nature Switzerland AG 2021

1663

M. Ksibi et al. (eds.), *Recent Advances in Environmental Science from the Euro-Mediterranean and Surrounding Regions (2nd Edition)*, Environmental Science and Engineering, https://doi.org/10.1007/978-3-030-51210-1_264

Conductivity (EC), Sodium Absorption Ratio (SAR), Sodium percentage (%Na), and Kelly Ratio (KR).

2 Materials and Methods

2.1 Study Area

The Hajeb Layoun-Jelma Basin (HJB) is located in the northeast central part of Tunisia, between north latitudes $35^{\circ} 08' 00''$ and $35^{\circ} 27' 00''$ and east longitudes $9^{\circ} 06' 00''$ and $9^{\circ} 39' 00''$. It covers an area of approximately 1140 km^2 and the population was estimated at 172,003 inhabitants in 2014, which corresponds to approximately 1.54% of the Tunisian population. The HJB area, which is characterized by semiarid climate, shows a grabben-like structure that is filled with Neogene and Quaternary deposits sediments, and is surrounded by anticlines (Fig. 1).

The geological structure of the HJB shows a major northeast-southwest direction that is typical of the main direction of Atlasic folds in northeastern Algeria and Tunisia. Previous hydrostratigraphic and hydrogeophysical studies [1, 2] reveal a multilayer aquifer system. The main wells used for irrigation and human purposes

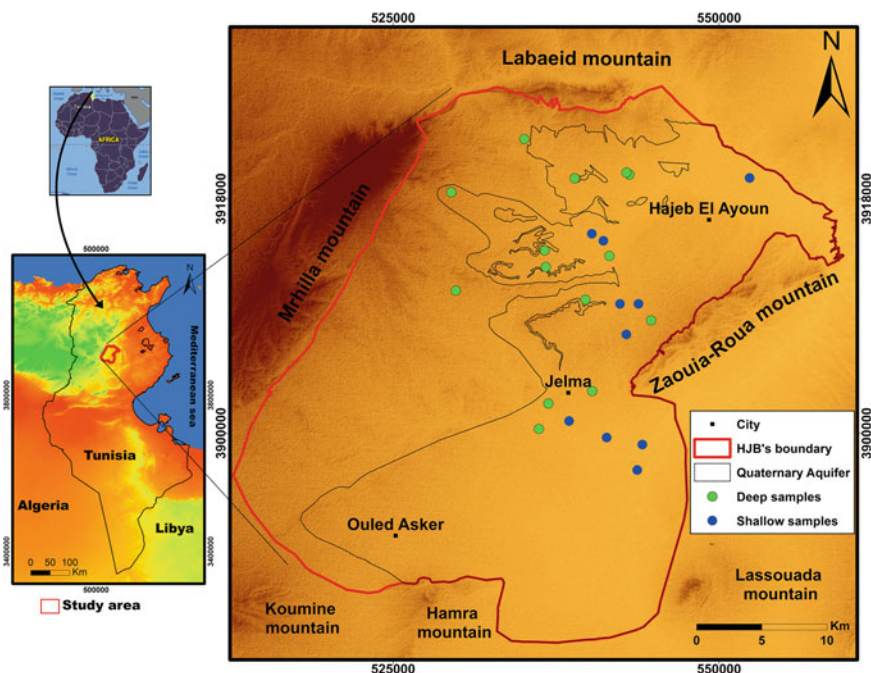


Fig.1 Geographic location of the study area and sampling location

are drilled into both the shallow Mio-Plio-Quaternary aquifer system (MPQ) and the deep Béglia formation aquifer. During the last decades, the over-exploitation induced a progressive groundwater head lowering throughout the study area. The decrease in hydraulic head goes from 2 to 17 m in the deeper aquifers and from 3 to 11 m in the shallower one [3].

From the hydrogeological point of view, the main flow direction in Béglia aquifer is from the west, coming from Mrhilla Mountain (Recharge zone) toward the central part of Hajeb El Ayoun. In this area, it becomes divided into two parts: the first discharges at Hajeb El Ayoun fault and the second at the level of some faults in the north part of Zaouia-Roua Mountain. The discharge parts are manifested by springs. For the shallow aquifer, the mean flow direction is east to the west.

3 Sampling and Water Quality

The present study is based on 28 groundwater samples that were collected in February 2017 (wet period); they are distributed over the two aquifers (Fig. 1). Polyethylene bottles (1L) were washed with distilled water and rinsed with the water sample before collection according to the protocol of standard methods for the examination of water and wastewater [4].

A statistical summary of hydrochemical parameters with (min, max, and standard deviation values) is given in Table 1. For both types of samples (shallow and deep), the chemical analysis indicates that the order of abundance of the major cations is $Na^+ > Mg^{2+} > Ca^{2+} > K^+$ and the order of abundance of anion is $Cl^- > HCO_3^- > SO_4^{2-}$. The abundance of these cations and anions is derived from a mineralization process.

The assessment of suitability for drinking purpose was evaluated by Water Quality Index (WQI). The calculation of WQI is based on the standards suggested for uses, using the formula 1 and 2, where 9 groundwater quality parameters (Ph, EC, Ca^{2+} , Mg^{2+} , Na^+ , K^+ , HCO_3^- , Cl^- , and SO_4^{2-}) are considered. Four parameters of irrigation quality, namely, EC, SAR, %Na, and KR, were calculated.

WQI is calculated using the following equation:

$$WQI = \sum RWi \times Qi \tag{1}$$

where

$$Qi = (Ci/Si) * 100 \tag{2}$$

$$RWi = \frac{wi}{\sum_{i=1}^n wi} \tag{3}$$

and Rwi: relative weight,

Table 1 Statistical summary of the physical and chemical parameters of HJB samples (ionic contents in mg/l)

	T (°C)	PH	EC	Salinity	Na ⁺	Ca ²⁺	Mg ²⁺	K ⁺	Cl ⁻	HCO ³⁻	SO ₄ ²⁻
Deep	Min	13,10	393	0,10	17,48	5,80	0,47	2,34	82,36	32,33	4,80
	Max	30,20	3960	1,80	459,31	55,60	117,67	15,60	935,43	154,33	105,12
	SD	4,96	961,82	0,52	117,60	13,09	29,16	3,89	240,49	37,09	32,80
Shallow	Min	10,30	1544	0,70	142,60	37,80	41,80	4,68	341,16	32,33	1,44
	Max	24,80	9770	6,50	1075,02	70,40	148,23	19,89	1768,61	305,00	235,20
	SD	3,97	2014,12	1,41	230,09	8,38	27,55	4,71	368,03	87,15	65,05

W_i : weight for each parameter,
 C_i : concentration of each chemical parameter (mg/L) for each water sample, and
 S_i : permissible limit of water for drinking uses [5].

4 Results

The calculation of the WQI for the shallow aquifer indicates that the highest quality (good water) presents 2% of groundwater samples. The water samples within permissible, doubtful, and unsuitable for drinking purposes are, respectively, 85%, 5%, and 3% of groundwater samples. The permissible and doubtful water qualities can be used for drinking, but after treatment and conventional disinfection. However, the water “unsuitable for drinking purposes” should only be used for aquaculture, irrigation, and industrial purposes.

The WQI results of the deep aquifer show two major water quality types: excellent and good, and are classified as high quality. In this aquifer, poor water quality represents only 17% (Fig. 2).

The results of the water quality for irrigation uses show that:

- The SAR values for HJB samples show two water classes: “excellent” and “good.” For both aquifers, the samples show low degree of alkalinity hazards ($2 < SAR < 10$), except for three samples with a high alkalinity hazards ($10 < SAR < 18$). Based on the SAR values, all water samples are suitable for irrigation and this water can be used for most types of soil.

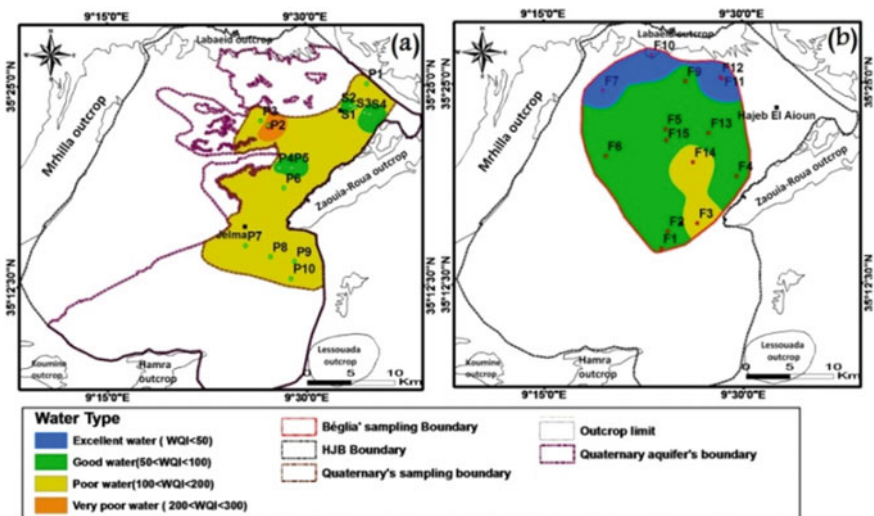


Fig.2 Classification of the water quality based on the values of WQI: a shallow and b: deep aquifer

- The EC values of HJB show three classes for both shallow and deep aquifers. In the deep aquifer, two water samples are good, ten samples show permissible water and two water samples indicate a doubtful water class. In the shallow aquifer, two water samples are unsuitable, three samples present permissible water, and nine water samples indicate a doubtful water class.
- The Na (%) indicates that all samples from shallow aquifer are permissible for irrigation. In the deep aquifer, only three samples show a good water class, 58% indicate permissible water for irrigation, and three samples indicate a doubtful water class.
- According to the KR values, the majority of groundwater samples (78%) from both aquifers are greater than 1, indicating an unsuitable water quality for irrigation.

5 WILCOX and USSL Classification

The Na (%) versus EC values were plotted in the Wilcox graphical diagram of irrigation water [6]. The water quality diagram for irrigation and domestic purposes shows four water classes: permissible to doubtful (10 samples), good to permissible (3 samples), doubtful to unsuitable (13 samples), and excellent to good (2 samples) (Fig. 3a). The SAR versus EC values were plotted in the USSL graphical diagram [7] of irrigation water (Fig. 3b). The water quality shows five categories: C2-S1 (medium salinity with low sodium), C3-S1 (high salinity with low sodium), C4-S2 (very high salinity with medium sodium), C3-S2 (high salinity with medium sodium), and C4-S3 (very high salinity with high sodium).

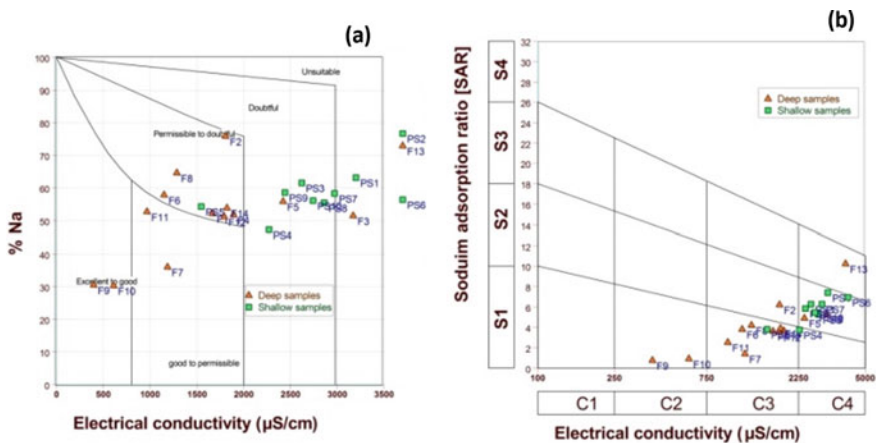


Fig. 3 a Sodium percentage versus EC value plot for water quality classification; **b** USSL classification of HJB samples

6 Conclusions

The HJB has a significant economic and social status as a first alternative for sustainable agricultural activities and drinking source for the region of Sidi Bouzid, Kairouan, and also Sfax located in the southern coast. The abstraction increases since the mid-1980s and the continuous decline of piezometry contributes largely to the degradation of both the quality and the quantity of groundwater. In order to show the water quality, 28 water samples were collected in 2017 and analyzed for 11 physico-chemical parameters (temperature, pH, EC, Na^+ , Ca^{2+} , K^+ , Mg^{2+} , Cl^- , HCO_3^- , and SO_4^{2-}). The water quality index shows that the majority of the samples from the shallow aquifer exhibit poor water quality. In the deep aquifer, the majority of the samples show good to excellent water type, only 14% exhibit poor water quality. In order to assess the water quality for irrigation, the various geochemical data (SAR, Na (%), PI, MH, KR, and EC) obtained from the groundwater samples, from both the shallow and deep aquifers of the HJB, indicate that groundwater should be treated before its use for irrigation purposes.

References

1. Jallalia, D., Lachaal, F., Andoulsi, M., Zouaghi, T., Hamdi, M., Bedir, M.: Hydro-geophysical and geochemical investigation of shallow and deep Neogene aquifer systems in Hajeb Layoun-Jilma-Ouled Asker area, Central Tunisia. *J. Afr. Earth Sc.* **110**, 227–244 (2015)
2. Thebti, S., Jellalia, D., Azaiez, H, Bédir, M., : Basin structuring and hydro-geophysical characterization of Upper Cretaceous and Eocene fractured deep carbonate reservoirs in the Hajeb Layoun-Jelma-Ouled Asker area (Central Tunisia). *Arab. J. Geosci.* **11**, 107 (2018)
3. DGRE: Annuaire piézométriques des nappes phréatiques et profondes de 1972 à 2016. Direction Générale des Ressources en Eau. Tunisia (1972–2016)
4. APHA., : Standard methods for the examination of water and wastewater, 19th edn. American public Health Association, Washington, DC (1995)
5. WHO.: Guidelines for drinking-water quality: fourth edition incorporating the first addendum (2017). ISBN 978-92-4-154995-0564
6. Wilcox, L.V.: Classification and use of irrigation water, circular 969. DC, USA, Washington (1955)
7. USSL: Diagnosis and improvement of saline and alkali soils. USDA, Handbook (1954)

1 **Assessment of groundwater abstraction for irrigation**
2 **practices using FAO-CROPWAT model and GIS: Case**
3 **study of Hajeb Layoun-Jelma basin (Central Tunisia)**

4 Soumaya Aouiti^{1,2}, Fadoua Hamzaoui Azaza¹, Fetheddine Melki³, Monji Hamdi⁴,
5 Fulvio Celico², Mounira Zammouri¹

6 ¹ Laboratory of Sedimentary Basins and Petroleum Geology
7 (SBPG), LR18 ES07, Geology Department, Faculty of Sciences of
8 Tunis, University of Tunis El Manar, Tunis 1060, Tunisia

9 ² Department of chemistry, Life Sciences and Environmental Sustainability, University of Par-
10 ma, Parco Area delle Scienze 157a, 43124 Parma, Italy

11 ³ University of Tunis El Manar, Faculty of Sciences of Tunis, Geodynamics, Geonumerics and
12 Geomaterials Laboratory, Lab3G, 2092, Tunis, Tunisia

13 ⁴ Commissariat Régional au Développement Agricole (CRDA), Sidi Bouzid, Tunisia
14 Corresponding author: Soumaya Aouiti

15 E-mail: soumaya.aouiti@fst.utm.tn ORCID: 0000-0001-9827-0970

16 **Abstract.** The assessment of groundwater abstraction is an important tool to
17 ensure its sustainability and management. This study aimed to assess the
18 groundwater abstraction for irrigation during the hydrological year 2016-2017,
19 using GIS, and to compare it with the water abstraction estimated by the Tuni-
20 sian water management authority. This land use map allowed us to extract the
21 different irrigated crops and to calculate the Irrigation Water Requirements
22 (IWR). The results showed that the groundwater pumping volume is approxi-
23 mately 34.29 Mm³. This volume is 2.7 times higher than that published by the
24 Tunisian water management authority which is equal to 12.7 Mm³. This signifi-
25 cant difference (21.59 Mm³) is caused by the increasing number of illegal wells
26 (digging wells without permission from water management authorities).

27 **Keywords:** Irrigation, Abstraction, Crop water requirement, Hajeb Layoun-Jelma
28 basin, evapotranspiration

29 **1 Introduction**

30 In the semi-arid and arid region, which the groundwater resources are the main source
31 of water, the agricultural intensification caused the groundwater over-exploitation.
32 The estimation of the crop water requirements is very important for improving the
33 irrigation practices and, consequently, the groundwater resources sustainability re-
34 quires an excellent estimation of water abstraction.

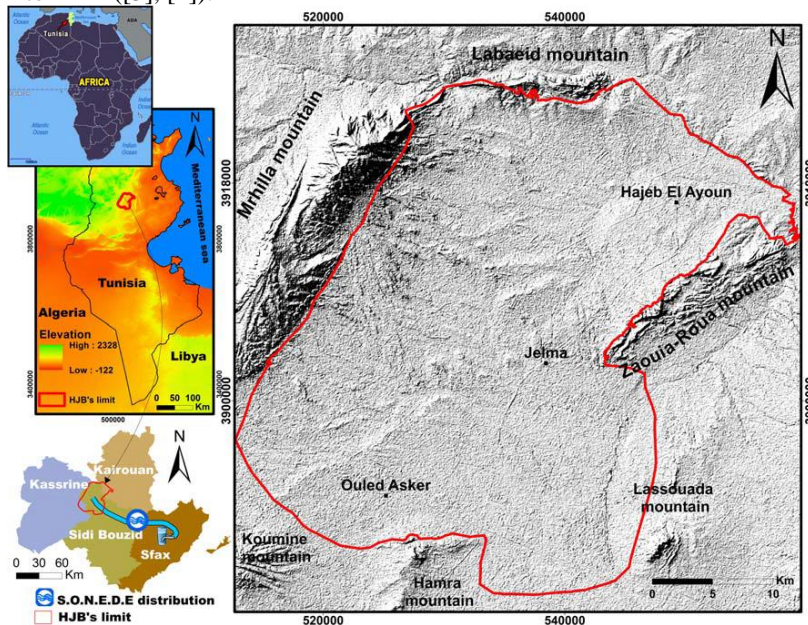
35 The Hajeb layoun Jelma basin, which is the study site in this work, located in the
 36 Northeast part of central Tunisia, covers 1350 km², is the main source of water for
 37 many regions. The use of this groundwater resources for irrigation is considered as
 38 the key asset of agricultural development in Hajeb Layoun, Jelma and Ouled Asker
 39 regions. The over-exploitation of this groundwater, since 1970, and the intensification
 40 of the agriculture activities led to the degradation of the water quantity and quality, so
 41 the quantity evaluation for this groundwater is an important tool for sustainable de-
 42 velopment and decision for water management.

43 2 Materials and Methods

44 2.1. Study area

45 The Hajeb Layoun-Jelma basin (HJB) is located in the northeast central part of Tuni-
 46 sia, between 35°08'00" N and 35°27'00" N and 9°06'00" E and 9°39'00"E, With an
 47 area of approximately 1350 km². The Hajeb Layoun-Jelma basin, which is character-
 48 ized by semiarid climate, shows a syncline structure, surrounded by anticlines, which
 49 is filled with Neogene and Quaternary deposits (fig.1).

50 Previous studies ([1], [2]) reveal a multilayer aquifer system. The main wells used
 51 for irrigation are drilled into the shallow Mio-Plio-Quaternary aquifer (MPQ). The
 52 over-exploitation induced a progressive groundwater head lowering throughout the
 53 study area, during the last decades. The decrease in shallow hydraulic head goes from
 54 3 m to 11 m ([3], [4]).

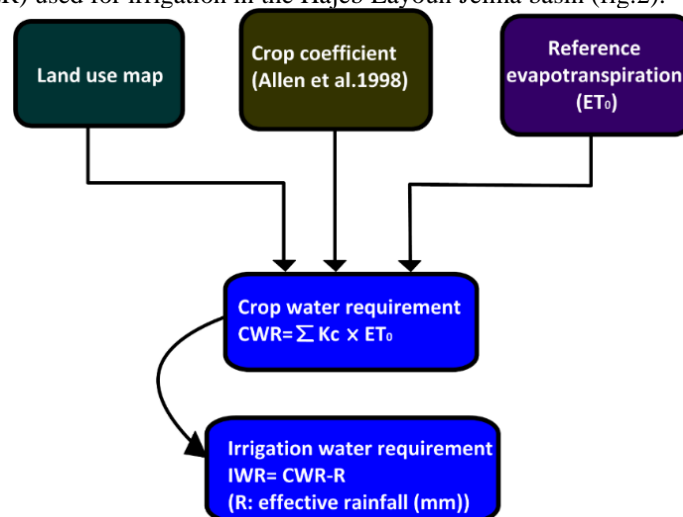


55
56 **Fig. 1.** Geographic location of the study area

57 2.2. assessment of pumped volume

58 This work aims to assess the groundwater volumes pumped for irrigation during the
59 hydrological year 2016-2017, using CROPWAT 8 model which is given by the Unit-
60 ed Nations' Food and Agriculture Organization' (FAO) [5], and to compare it with
61 the pumped volumes published by the water management direction.

62 The different irrigated crops were extracted from the land use map using ArcGIS
63 software. The meteorological data (Temperature, Humidity, sun hours and wind-
64 speed), the irrigated crops types and its occupied areas allowed us to calculate the
65 Irrigation Water Requirements (IWR) of each crop. The Penman-Monteith method
66 was used to estimate the reference evapotranspiration (ET_0). Crop coefficients (K_c)
67 from the phenomenological stages of each crop, given by FAO [6], were applied to
68 adjust and estimate the actual evapotranspiration. The estimation of the pumped vol-
69 ume was determined after subtracting the Crop Water Requirements from efficient
70 rainfall (ER) used for irrigation in the Hajeb Layoun Jelma basin (fig.2).



71
72

Fig. 2. Methodology adopted for the present study

73 3 Results

74 Table 1 represents the calculated values of IWR, from the land use map, for the dif-
75 ferent crops.

76

Table 1. Water requirement for the different crops of HJB

	Area (km ²)	ETc	IWR
Olive	310	692.1	538.3
Cereals	136.2	543.5	462.2
Vegetables corps	60	474.7	408.1
orchard	19.36	692.1	538.3

77 The results showed that the estimated groundwater pumping volume is equal
 78 to 34.29 Mm³. This volume is 2.7 times higher than the value published by the water
 79 management direction which is equal to 12.7 Mm³.

80 **4 Discussion**

81 The estimated groundwater pumping volume is equal to 34.29 Mm³. The significant
 82 difference, between the estimated and the published value, (21.59 Mm³) is caused by
 83 the increasing number of illegal wells (digging wells without permission from water
 84 management authorities).

85 In fact, in 2018, the water management authorities have announced that more than
 86 2500 illegal wells are detected in all Sidi Bouzid region and its pumped volume is
 87 estimated at 49 Mm³.

88 This over-estimated volume may be due to the absence of water metering at many
 89 shallow wells and the use of the dug wells by several farmers. This over-exploitation,
 90 by the illegal wells, will engendered, in the nearest future, the exhaustion of this ba-
 91 sin.

92 **5 Conclusions**

93 The water resources management in the HJB needs reliable knowledge on water re-
 94 sources and requirements. An estimation of water abstracted from the groundwater is
 95 thus a crucial issue for a sustainable water resource.

96 This work aimed at providing an estimate of aquifer abstraction due to irrigation in
 97 the HJB during the hydrological year 2016-2017. A simple approach was used.

98 The estimated groundwater abstraction volume is equal to 34.29 Mm³. This volume
 99 is 2.7 times higher than the value published by the water management direction which
 100 is equal to 12.7 Mm³. This significant difference is caused by the increasing number
 101 of illegal wells (digging wells without permission).

102 The present study presents a helpfull tool for the water management direction for
 103 developing more reliable strategies to groundwater abstraction's manage.

104 **References**

- 105 1. Jallalia D, Lachaal F, AndoulsiM, Zouaghi T, HamdiM, Bedir M (2015) Hydro-
 106 geophysical and geochemical investigation of shallow and deep Neogene aquifer systems
 107 in Hajeb Layoun-Jilma-Ouled Asker area, Central Tunisia. *J Afr Earth Sci* 110:227–244.
 108 <https://doi.org/10.1016/j.jafrearsci.2015.06.016>
 109 2. Thebti S, Jellalia D, Azaiez H, Bédir M (2018) Basin structuring and hydro-geophysical
 110 characterization of Upper Cretaceous and Eocene fractured deep carbonate reservoirs in
 111 the Hajeb Layoun- Jelma-Ouled Asker area (Central Tunisia). *Arab J Geosci* 11:107.
 112 <https://doi.org/10.1007/s12517-018-3445-2>
 113 3. Aouiti, S., Hamzaoui Azaza, F., El Melki, F. *et al.* Groundwater quality assessment for dif-
 114 ferent uses using various water quality indices in semi-arid region of central Tunisia. *Envi-
 115 ron Sci Pollut Res* (2020). <https://doi.org/10.1007/s11356-020-11149-5>

- 116 4. Aouiti S., Hamzaoui-Azaza F., Zammouri M., Hamdi M., Celico F. (2021) Water Quality
117 Assessment of the Shallow and Deep Aquifers of Hajeb Layoun-Jelma Basin (Central Tu-
118 nisia). In: Ksibi M. et al. (eds) Recent Advances in Environmental Science from the Euro-
119 Mediterranean and Surrounding Regions (2nd Edition). EMCEI 2019. Environmental Sci-
120 ence and Engineering. Springer, Cham. https://doi.org/10.1007/978-3-030-51210-1_264
121 5. FAO., 2009. Cropwat 8.0 for windows user guide. Rome, Italy.
122 6. Allen R G., Pereira L S., Raes D., Smith M., 2006. Crop Evapotranspiration-Guidelines for
123 Computing Crop Water Requirements-FAO Irrigation and Drainage FAO 56.

1 **Irrigation Water Quality Index (IWQI) for evaluation of**
2 **groundwater suitability in the agricultural domain: case**
3 **of Hajeb Layoun Jelma Basin (Central Tunisia)**

4 Soumaya Aouiti^{1,2}, Nizar Troudi¹, Fadoua Hamzaoui Azaza¹, Monji hamdi³, Fulvio
5 Celico², Mounira Zammouri¹

6
7 ¹Sedimentary Basins and Petroleum Geology Laboratory (LR18ES07), Faculty of Sciences
8 University of Tunis El Manar Tunis Tunisia

9 ²Department of chemistry, Life Sciences and Environmental Sustainability, University of
10 Parma, Parco Area delle Scienze 157a, 43124 Parma, Italy

11 ³University of Sfax, 3029 Sfax, Tunisia

12 Corresponding author: Soumaya Aouiti

13 E-mail: soumaya.aouiti@fst.utm.tn ORCID: 0000-0001-9827-0970

14 **Abstract.** Groundwater is vital for human uses in many regions of the world, espe-
15 cially in arid and semi-arid regions. The groundwater's quality assessment has become
16 necessary for the present and the future of groundwater quality management. The Hajeb
17 layoun Jelma basin, located in the Northeast part of central Tunisia, covering an area
18 equal to 1350 km². The Hajeb Layoun Jelma basin has a significant economic and social
19 influence as a first alternative for sustainable agricultural activities and drinking re-
20 source for many regions. The quality evaluation of this groundwater can help setting
21 recommendations to protect the soil and the crops. This study aims to assess the ground-
22 water quality for irrigation proposes using the Irrigation Water Quality Index (IWQI)
23 to better understand its fields of use. To this aim, 14 shallow wells' samples were col-
24 lected in February 2017 (wet season), to present the EC, Na⁺, HCO₃⁻, Cl⁻, and SAR
25 results, which are the five parameters used in the IWQI. The results show that the IWQI
26 ranged from 13.72 to 68.77. The majority of samples fall within the 4th class (High
27 Restriction) (57.14 %) which indicates that the plants have moderate to high tolerance
28 to salts in soils with high permeability without compact layers. Based on the obtained
29 results, it is recommended to avoid grow salt-sensitive plants to increase the agricultural
30 productivity in the Hajeb Layoun Jelma basin.

31 **Keywords:** Groundwater quality, Sustainability, irrigation, IWQI, Hajeb Layoun Jelma
32 basin, central Tunisia.

33 **1 Introduction**

34 Groundwater is essentially vital for human consumption and agricultural purposes
35 in many regions of the world, especially in arid and semi-arid regions ([1], [2] and [3]).
36 The groundwater's quality assessment has become a necessary and an important task
37 for the present and the future of groundwater quality management. The Hajeb layoun

38 Jelma basin, located in the Northeast part of central Tunisia, covering an area equal to
39 1350 km². The Hajeb Layoun Jelma basin has a significant economic and social influ-
40 ence as a first alternative for sustainable agricultural activities and drinking resource
41 for the region of Sidi Bouzid, Kairouan and Sfax located in the southern coast. The use
42 of these groundwater resources for irrigation is a key asset in agricultural development
43 in Hajeb Layoun, Jelma and Ouled Asker regions. The over-exploitation of this ground-
44 water, since 1970, and the intensification of the agriculture activities led to the degra-
45 dation of the water quantity and quality; therefore, the quality evaluation of this ground-
46 water can help setting recommendations to protect the soil and the crops. This study
47 aims to assess the groundwater quality for irrigation proposes in the Hajeb Layoun
48 Jelma basin using the Irrigation Water Quality Index (IWQI).

49 **2 Materials and Methods**

50 **Study area**

51 The Hajeb Layoun-Jelma basin (HJB) is located in the Northeast part of central Tunisia.
52 It is, approximately, located between $x = 35^{\circ}00'00''$, $y = 8^{\circ}30'00''$ and $x = 35^{\circ}30'00''$, $y =$
53 $9^{\circ}00'00''$ (Figure 1). Three economically underdeveloped regions cover the study area:
54 Hajeb Layoun, Jelma, and Sbeitla, which belong to three different governments: Kairou-
55 ouan, Sidi bouzid and Kasserine. The HJB is located at an elevation ranging from 234
56 to 1384 m. It presents a wide NE-SW directed syncline around by various mountains.

57 The study area has a semi-arid climate; January present the coldest month (mean
58 temperature $\approx 11.8^{\circ}\text{C}$), and the hottest is August (mean temperature $\approx 29.4^{\circ}\text{C}$). The
59 mean annual rainfall in the HJB, over the period 1968–2017, is equal to 241.8 mm.

60 Previous hydrostratigraphic and hydrogeophysical studies [1], [2] reveal a multilayer
61 aquifer system. The main wells used for irrigation and human purposes are drilled into
62 both the shallow (MPQ) and the first deep aquifer. The over-abstraction induced a pro-
63 gressive groundwater head lowering throughout the study area, during the last decades.
64 The decrease in hydraulic head goes from 2 m to 17 m in the deeper aquifers, and from
65 3 m to 11 m in the shallow one [1].

66 The assessment of groundwater quality is an important step to ensure its sustainabil-
67 ity for various uses. In this study, the suitability of groundwater for irrigation uses was
68 assessed by determining the irrigation water quality index (IWQI).

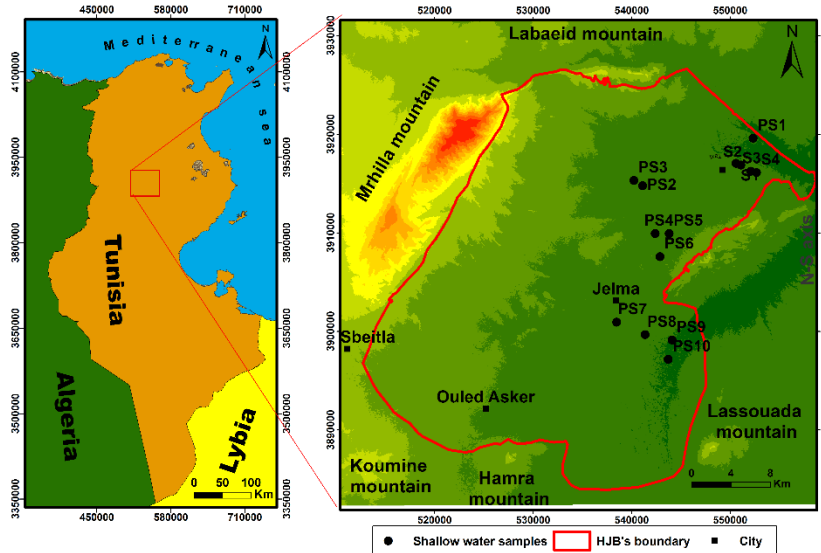


Fig. 1. Location map of the study area

69

70

71 Sampling and water quality

72 The present study is based on 14 shallow samples that were collected in February 2017
 73 (wet periode) (Fig.1). Polyethylene bottles (1L) were washed with distilled water and
 74 rinsed with the water sample before collection according to the protocol of standard
 75 methods for the examination of water and wastewater [1].

76 A statistical summary of hydrochemical parameters with (min, max and standard
 77 deviation values) is given in Table 1. For all the samples, the chemical analysis, indi-
 78 cated that the order of abundance of the major cations is $Na > Mg > Ca > K$ and the order
 79 of abundance of anion is $Cl > HCO_3 > SO_4$. The abundance of these cations and anion is
 80 derived from a mineralization process [1].

81 **Table1.** Statistical summary of the physical- chemical parameters of shallow samples
 82 (ionic contents in mg/l).

	T (°C)	PH	EC	Salinity	Na ⁺	Ca ²⁺	Mg ²⁺	K ⁺	Cl ⁻	HCO ³⁻	SO ₄ ²⁻
Min	10,30	7,63	1544	0,70	142,60	37,80	41,80	4,68	341,16	32,33	1,44
Max	24,80	8,24	9770	6,50	1075,02	70,40	148,23	19,89	1768,61	305,00	235,20
SD	3,97	0,20	2014,12	1,41	230,09	8,38	27,55	4,71	368,03	87,15	65,05

83

84 The computing of IWQI is composed by two steps [4]. The first step consisted of the
 85 parameters selection, taking into account the preponderant water 's use, in this case,
 86 irrigation. In the second step, the individual quality measures (qi) of each variable were
 87 calculated.

88 IWQI is calculated using the following equation:

89

$$IWQI = \sum qi \times Wi \quad (1)$$

90 With $q_i = Q_{imax} - ((X_{ij} - X_{inf}) \times Q_{iamp}/X_{amp})$ (2)

91 where q_{imax} : maximum value of q_i for the class;

92 x_{ij} : observed value for the parameter n;

93 x_{inf} : parameter value corresponding to the lower limit of the class;

94 q_{imax} : the maximum value of q_i for the class;

95 x_{amp} : the class amplitude to which the parameter belongs;

96 In order to evaluate x_{amp} , of the last class of each parameter, the upper limit was the
97 highest value determined in the physical-chemical of the water samples [4].

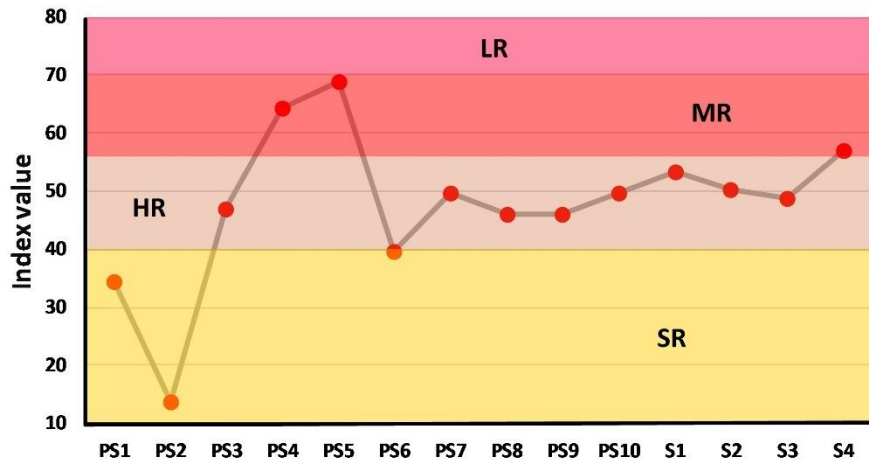
98 **Table 2.** Parameter limiting values for q_i computing [5]

q_i	EC	SAR	Na	Cl	HCO ₃
85-100	200<EC<750	2<SAR<3	2<Na<3	1<Cl<4	1<HCO ₃ <1.5
60-85	750<EC<1500	3<SAR<6	3<Na<6	4<Cl<7	1.5<HCO ₃ <4.5
35-60	1500<EC<3000	6<SAR<12	6<Na<9	7<Cl<10	4.5<HCO ₃ <8.5
0-35	EC<200	SAR<2	Na<2	Cl<1	HCO ₃ <1
	Or EC>3000	Or SAR>12	Or Na>9	Or Cl>10	Or HCO ₃ >8.5
Wi	0.211	0.189	0.204	0.194	0.202

99 3 Results

100 Figure 2 shows results of IWQI in the study area and it is varying from severe restriction
101 (SR) to moderate restriction (MR) according to Table 3 [4]. The areas with high re-
102 striction water quality cover 57.14% of total samples. This category is suitable for irri-
103 gation with moderate to high tolerance to salts.

104 The rest of the study area, which is about 43% fall within the “severe to moderate
105 restriction” categories. These categories of groundwater should be used only with the
106 soil have high permeability and some constrains in type of plant for salt’s tolerance.



107
108
109

Fig. 2 Results of IWQI in the study area

Table 3. Classifications and characteristics of general IWQI [4].

IWQI	re- restrictions	Soil	Plant
[85-100]	No re- striction (NR)	Water can be used for almost all types of soil.	No toxicity risk for most plants
[70-85]	Low re- striction (LR)	Irrigated soils with a light texture or moderate permeability can be adapted to this range.	high risks for salt sensitive plants
[55-70]	Moderate restriction (MR)	The water in this range would be better used for soils with moderate to high permeability values. Moderate leaching of salts is highly recommended to avoid soil degradation.	Plants with moderate tolerance to salts may be grow
[40-55]	High re- striction (HR)	This water can be used in soils with high permeability without compact layers. High frequency irrigation schedule	Suitable with moderate to high tolerance to salts
[0-40]	Severe re- striction (SR)	Using this water for irrigation under normal conditions should be avoided.	Only plants with high salt tolerance

110 4 Conclusions

111 The HJB has a significant economic and social status as a first alternative for sus-
 112 sustainable agricultural activities and drinking resource for many regions. The abstraction
 113 increases since the mid-1980s and the continuous decline of piezometry contribute
 114 largely to the degradation of both the quality and the quantity of groundwater. In order
 115 to assess the water quality, 14 water samples were collected in 2017 and analyzed for
 116 12 physicochemical parameters. The irrigation water quality index shows that most of
 117 collected samples should be used only with the soil have high permeability and some
 118 constrains in type of plant for salt's tolerance.

119 References

- 120 1. Aouiti, S., Hamzaoui Azaza, F., Zammouri, M., Hamdi, M., Celico, F. Recent Advances in
 121 Environmental Science from the Euro-Mediterranean and Surrounding Regions (2nd Edition),
 122 1663-1669 (2021). https://doi.org/10.1007/978-3-030-51210-1_264
- 123 2. Aouiti, S., Hamzaoui Azaza, F., El Melki, F. *et al.* Groundwater quality assessment for dif-
 124 ferent uses using various water quality indices in semi-arid region of central Tunisia. *Envi-*
 125 *ron Sci Pollut Res* (2020). <https://doi.org/10.1007/s11356-020-11149-5>
- 126 3. Troudi, N., Hamzaoui-Azaza, F., Tzoraki, O. *et al.* Assessment of groundwater quality for
 127 drinking purpose with special emphasis on salinity and nitrate contamination in the shallow
 128 aquifer of Guenniche (Northern Tunisia). *Environ Monit Assess* **192**, 641 (2020).
 129 <https://doi.org/10.1007/s10661-020-08584-9>
- 130 4. Meireles, A., Andrade E. M., Chaves L., Frischkorn, H., and Crisostomo, L. A. (2010): "A
 131 new proposal of the classification of irrigation water", *Revista Ciência Agronômica*, Vol.
 132 (41), No. (3), pp. 349-357.
- 133 5. AYERS, R. S. and WESTCOT, D. W. (1985). "Water quality for agriculture". FAO Irriga-
 134 tion and Drainage Paper No. (29), Rev. (1), U.N. Food and Agriculture Organization, Rome.

Abstract

Groundwater is the main water source in all the world and especially in the arid and semi-arid regions. The Hajeb Layoun Jelma basin is the principal source of water supply for Sidi Bouzid and Sfax region. In the last decades, pollution is considered a common groundwaters problem, representing a severe and harmful threat to the water resources. In this context, this work has been taken place. The Hajeb Layoun-Jelma basin is the selected site. The main objectifs is to provide its actual water quality and quantity situation. This research aims to perform a geochemical view of the two principal aquifers, implement a numerical mode to control the basin, and assess the vulnerability to the shallow aquifer's pollution using different models.

The groundwater hydrochemistry study's main objectives are to determine the water chemistry origins and assess the groundwater suitability for drinking and irrigation purposes. Twenty-eight water samples were collected in 2017 (wet period) from shallow and deep aquifers and analyzed for different physicochemical parameters (temperature, pH, EC, salinity, Na^+ , Ca^{2+} , K^+ , Mg^{2+} , Cl^- , HCO_3^- , and SO_4^{2-}). The shallow aquifer shows high salinity in most water samples (93% $> 1 \text{ g.l}^{-1}$). The deep aquifer has moderate salinity (21% of samples exceeding 1 g.l^{-1}). The results show that both aquifers' water mineralization is controlled by the dissolution of carbonates/gypsum and water evaporation. The drinking water quality assessment shows that 100% and 57% extremely poor water for the shallow and the deep samples, respectively, coincide with the Na-Cl water type. The water quality evaluation for irrigation uses indicates that the shallow samples show quality less than the deep one and revealed that most samples in the Hajeb Layoun-Jelma basin are not appropriate for irrigation uses. The recharge rate estimation was made using the multi-criteria method. The results show that the shallow and the deep aquifer receive an average recharge rate, from rainfall, about 31.5 mm/year (infiltration: 15%) and 34 mm/year (16.2%), respectively. The numerical model was developed using Modflow code under GMS software. The hydrodynamic model system permitted to estimate the hydraulic conductivity distribution. It also allowed estimating abstraction's effect on the water table evolution by two pumping scenarios (2019-2050) (Sc1: constant pumping rates, Sc2: doubled pumping rates). The hydrodynamic models show the continuous water table decrease after 30 years.

The groundwater vulnerability assessment of the shallow aquifer of Hajeb Layoun Jelma basin was made using both intrinsic and simulation models. The DRASTIC model was used as intrinsic tool for identifying the susceptible zones to contamination for the shallow aquifer. The vulnerability maps indicated that the dominant vulnerability classes are a low class (55%) followed by the moderate class (43 %) in the pesticide model and the “low” classes (86 %) in the standard model. A high vulnerability characterizes only 1 % of the study area to pesticide contamination. The superposition of the standard and the pesticide DRASTIC maps with the land use map shows that many agricultural zones are located in the area characterized by “high” to “moderate” vulnerability. The study suggests that these “DRASTIC” maps can be a valuable tool for local authorities for groundwater and land use management.

MTDMS is used to evaluate the transport of salts in the shallow aquifer. The salt transport model results show that the salinization process affects the areas close to the north part's mountains. The high salinity concentration is related to the irrigated area. These investigations could constitute a basis for decision-makers for water resources management and prevent pollution risks.

Key words: Geochemistry, Recharge, Vulnerability, Groundwater flow modeling, Transport modeling, Hajeb Layoun Jelma basin, Central Tunisia.